
UNIVERSITY OF BIRMINGHAM

# Development of an In-Situ Oil Conversion Process to Generate Clean Hydrogen

By

Thomas James Lopeman

A thesis submitted to the University of Birmingham

For the degree of

DOCTOR OF PHILOSOPHY

School of Chemical Engineering

College of Engineering and Physical Sciences

University of Birmingham

December 2023

## ABSTRACT

There are huge reserves of heavy oil throughout the world that can be energy intensive to recover. Improving the energy efficiency of the recovery process and developing novel methods of cleaner recovery will be essential for the transition from traditional fossil fuel usage to net-zero. In-situ combustion (ISC) is a less used technique, with Toe-to-Heel Air Injection (THAI) and CAtalytic PRocessing In-Situ (CAPRI) being specialised novel versions of traditional ISC. They utilise a horizontal producing well and in the case of CAPRI, a catalyst. This project aims to investigate the impact that injected steam has on both the THAI and CAPRI processes for the purpose of in-situ heavy oil upgrading and will help to bridge the gap between the extant laboratory research and the unknown commercial potential. This thesis also presents a novel method for modelling the THAI-CAPRI method using CMG STARS, proposing an in-situ hydrogen production reaction scheme. THAI and CAPRI experimental-scale models were run under three conditions: dry, pre-steam and constant steam. Starting from a reservoir API (a measure of a hydrocarbon liquid's density compared to water) of 10.5°, THAI reached an average API of ~16 points, observing no increase in API output with the use of steam injection. A decreased API output by ~0.7 points during constant steam injection was achieved due to a high temperature oxidation (HTO) dominant environment. This decreases reactant availability for thermal cracking. CAPRI dry run reached an API of 20.40 points and achieved increased API output for both pre-steaming (~21.17 points) and constant steaming (~22.13 points). The mechanics for this increased upgrading were discussed, and catalytic upgrading, as opposed to thermal cracking was shown to be the reason for the increased upgrading. Both processes produce similar cumulative oil (~3150 $cm^3$) during dry and pre-steamed runs, only increasing to ~3300 $cm^3$ with the constant steam injection during THAI and 3500 $cm^3$ for CAPRI.

This thesis also investigates the possibility and extent of hydrogen generation during Toe-to-Heel Air Injection (THAI) applied to heavy oil via reservoir simulation. This was achieved by incorporation of hydrogen reactions such as coke gasification, forward and reverse water gas shift into the THAI model for ISC processes in heavy oil reservoirs. This enabled the interaction between components and reactions to be assessed. The reservoir simulation model was history matched using field data from the Kerrobert THAI field pilot; it successfully incorporated hydrogen reactions, showing good agreement. The inclusion of coke gasification reactions resulted in hydrogen production but reduced oil rates due to temperature decrease and increased gas saturation. Forward water-gas shift (FWGS) had negligible impact on oil production, due to reduced competition with cracking and oxidation reactions. Combined coke gasification and FWGS increased hydrogen production and slightly reduced oil rates. Reverse water-gas shift (RWGS) had minimal impact on hydrogen fraction. This thesis emphasises the importance of hydrogen reactions in the THAI model and their influence on the THAI process. It provides valuable insights for optimising THAI projects and underscores the role of reaction scheme choice in history matching.

## ACKNOWLEDEMENTS

I would like to acknowledge both Professor Joe Wood and the Natural Environment Research Council (NERC), Centre for Doctoral Training (CDT) in Oil & Gas for providing me with the opportunity to undertake this PhD at the School of Chemical Engineering, University of Birmingham, in addition to the opportunities to complete external training schemes for both my personal and professional development.

I would further express my gratitude towards Professor Gary Leeke, for his support and constructive feedback and support throughout my studies.

I am forever grateful to my friends and family who supported me through my studies, with special thanks to Kayley Parslow, my mother Gillian Lopeman, and my late father Patrick Lopeman, who always thoroughly encouraged me throughout my education.

CONTENTS

## LIST OF FIGURES

LIST OF TABLES

## GENERAL NOMENCLATURE

3D = Three Dimensional

2D = Two Dimensional

API = In the context of this thesis API stands for API gravity, a measure of a petroleum liquid's density compared to water, determining its relative heaviness or lightness.

BHP = Bottom Hole Pressure

CAPRI = Catalytic PRocess In-situ

CSS = Cyclic Steam Stimulation

EOR = Enhanced Oil Recovery

HTO = High Temperature Oxidation

HUO = Heavy Upgraded Oil

ISC = In-Situ Combustion

$K_h$ = Absolute Horizontal Permeability

$K_v$ = Absolute Vertical Permeability

LTO = Low Temperature Oxidation

OOIP = Original Oil In Place

PIHC = Pre-Ignition Heating Cycle

SAGD = Steam Assisted Gravity Drainage

THAI = Toe-to-heel Air Injection

## EQUATION VARIABLES NOMENCLATURE

$Ad_i$: A term related to additional porosity or an external parameter affecting the porosity of the medium.

$c_i$: Specific parameter or concentration related to some component or condition.

$HA_{CV}+HA_{CD}$: Heat accumulation or depletion terms in the control volume.

$HL_o$, $HL_v$, $HL_c$: Heat loss or gain terms associated with oil, some parameter, and some other parameter respectively.

$H_{rk}$: Enthalpy change due to reaction k.

$H_w$, $H_o$, $H_g$: Enthalpies of water, oil, and gas respectively.

$i_k$: Parameter or value related to reaction k and component i.

K = permeability

$K_r$ = relative permeability

$K\Delta T$: Change in temperature across the volume.

$q_{wk}$, $q_{ok}$, $q_{gk}$: Specific heat production rates of water, oil, and gas respectively in well layer k.

Ri is the source/sink term for species i

$s_{ki}$: Represents a specific condition or value associated with reaction k and component i.

$S_w$, $S_o$, $S_g$: Saturation terms representing the volume fraction of each fluid phase in the porous medium.

$M_w$, $M_o$, $M_g$: Mass transfer coefficients associated with water, oil, and gas respectively.

$T_w$, $T_o$, $T_g$: Thermal conductivities associated with water, oil, and gas respectively.

$U_r$: Internal energy of the rock matrix or reservoir rock.

$U_s$: Internal energy related to solid components.

$U_w$, $U_o$, $U_g$: Internal energy terms of water, oil, and gas respectively.

V: Volume of the porous medium or control volume.

$w_i$, $x_i$, $y_i$: Component fractions or concentrations of a specific component within the water, oil, and gas phases respectively.

$Y_i$ is the mass fraction of species i

$\frac{\partial}{\partial t}$: Partial derivative with respect to time, indicating the rate of change of the following expression over time.

$\sum_{k=1}^{n_r}$: Summation over nr terms or reactions.

$\frac{\partial}{\partial t}$: Partial derivative with respect to time, indicating the rate of change of the following expression over time.

$\frac{\partial \phi}{\partial x}$ = potential gradient

$\mu$ = viscosity

$\delta_{iw}$: Delta term, representing a specific condition or value related to components in water.

$\Delta\phi_w$, $\Delta\phi_o$, $\Delta\phi_g$: Changes in porosity for water, oil, and gas phases.

$\rho_w$, $\rho_o$, $\rho_g$: Densities of water, oil, and gas respectively.

$\rho_w q_{wk}$, $\rho_o q_{ok}$, $\rho_g q_{gk}$: Terms related to the specific production rates of components $w_i$, $x_i$, $y_i$ in well layer k.

$\phi D_{wi}$, $\phi D_{o}i$, $\phi D_{gi}$: Diffusion coefficients for component i in water, oil, and gas phases respectively.

$\phi_f$: Fluid porosity, representing the fraction of pore space occupied by fluids.

$\phi_v$: Void porosity, representing the fraction of the pore space not occupied by fluids.

# CHAPTER 1. INTRODUCTION

## 1.1 Background

The exploration and extraction of hydrocarbon reserves has been an integral aspect of global energy production, yet the evolution towards cleaner energy sources poses a critical challenge. The transition from fossil oils to sustainable alternatives, particularly via the hydrogen economy, necessitates innovative approaches in the oil and gas sector. This PhD project, a part of the NERC CDT in Oil and Gas, endeavoured to confront this challenge by addressing the conversion of various oil reserves into upgraded oil and hydrogen as a more sustainable energy source.

The significance of this research was underscored by the imminent shift in energy demands, prompting a move away from traditional fossil fuels towards cleaner energy solutions (Dudley, 2018). Despite the prevalence of reserves like light oil, heavy oil, bitumen, shale gas, and shale oil—predominantly found in Canada, Venezuela, and partially depleted reservoirs in the North Sea—there exists a pressing need to explore and devise methodologies for both their in-situ upgrading and conversion into hydrogen (Kapadia et al., 2011). This paradigm shift demands a concentrated effort to minimise environmental impact while effectively harnessing these reserves for the growing net-zero and hydrogen economy.

This project was supported by the NERC CDT in Oil and Gas, offering a platform for comprehensive training, and fostering interdisciplinary skills essential for addressing complex challenges in the oil and gas domain. Collaborations with esteemed institutions, including the University of Nottingham, reinforced this research effort through the provision of background numerical models and simulation training. Additionally, the project benefited from prior expertise and a 15-year engagement of the Birmingham-

Nottingham team in developing in-situ recovery methods, particularly focusing on heavy oil extraction using THAI-CAPRI (Toe-to-Heel Air Injection and its catalytic add-on CAPRI).

## 1.2 Study Aims

The primary objectives of this research encompassed distinct sections, each focusing on key research areas aimed at achieving specific goals within the study. The breakdown of the study into these components was essential to comprehensively address the complex challenges associated with the conversion of oil reserves into hydrogen while minimising environmental impact.

The main aim of the study was to develop comprehensive THAI and THAI-CAPRI reservoir simulations using CMG STARS. These simulations were modelled at two distinct scales: laboratory scale and field scale. Addressing these scales posed unique challenges, as each necessitated specific considerations and factors for accurate representation. The simulations aimed to capture in-situ oil upgrading and hydrogen generation reactions within the reservoir, accounting for the differences in scale and their implications on the behaviour of the hydrogen plume.

Another crucial aspect of the study involved simulating the conversion of oils under well conditions. This task aimed to determine the gas composition resulting from the conversion process. Moreover, it sought to calculate the yield of hydrogen and upgraded oil and quantify the deposition of coke, utilising published reaction kinetics to model these processes accurately.

The study further aimed to optimise in-well conditions and upgrading/gasification technologies. This specific goal involved minimising the production of greenhouse gases

whilst maximising oil upgrading and hydrogen production. The general aims of the project are listed below:

- Creation of laboratory-scale THAI and THAI-CAPRI models in CMG STARS for simulation and comparison of oil upgrading capability
- Utilisation of in-situ hydrogen generation reactions within the laboratory-scale THAI-CAPRI model for comparison against previous hydrogen injection studies
- Creation of a field-scale THAI model in CMG STARS for simulation and investigation into the impact of the addition of hydrogen generation reactions on simulation outputs of THAI models
- Investigation into the potential and optimisation of the THAI process for in-situ hydrogen production

Each of these research components was pivotal in advancing the understanding of in-situ thermal oil upgrading and hydrogen generation from oil reserves and played a significant role in determining the viability, efficiency, and environmental sustainability of the proposed conversion methods. The description of these aims into distinct research segments ensured a systematic and comprehensive approach towards achieving the overarching goal of cleaner hydrogen production from diverse oil reservoirs using THAI technology.

## 1.3 Thesis Outline

There are six chapters in this thesis.

Chapter One outlines the background of the project and the main objectives of the research.

Chapter Two critically surveys the literature of oil thermal upgrading techniques, particularly emphasising the Toe-to-Heel Air Injection (THAI) method, THAI-CAPRI experiments, simulations, field trials, reactions, kinetics, and hydrogen production. It produces prior research findings, encompassing laboratory and field experiments, simulations, and real-world applications of THAI and THAI-CAPRI. The review examines their efficacy in heavy oil recovery and upgrading, analyses reaction kinetics, and explores hydrogen production within these processes, laying the groundwork for subsequent in-depth analyses in Chapters Four and Five.

Chapter Three intricately details the methodology and inputs for CMG STARS simulations, explaining the integration of experimental and field data into the simulation framework. It sheds light on the simulation software, governing equations, and numerical methods for simulation convergence. Also included is a detailed approach to grid independence for simulating THAI and THAI-CAPRI and both laboratory and field scales.

Chapter Four shifts the focus to laboratory-scale simulations investigating THAI and THAI-CAPRI for oil upgrading. Detailed descriptions of these simulations, encompassing scenarios both with and without catalysts, are provided along with analysis and comparative assessments of the outcomes derived from these experiments.

Chapter Five examines the methodology employed for field-scale simulations of THAI, exploring its application for oil upgrading and hydrogen production on a larger scale. Results obtained from these field-scale simulations are presented and thoroughly discussed in terms of their practical implications and feasibility for real-world implementation.

Chapter Six concludes the entire research effort, consolidating the key findings derived from both laboratory and field scale. Furthermore, this section forwards insightful

recommendations for future research paths aimed at advancing the domains of THAI and in-situ hydrogen generation, thereby culminating the thesis with a forward-looking perspective.

# CHAPTER 2. LITERATURE SURVEY

This literature review chapter delves into critical aspects of heavy oil and bitumen extraction and processing. It covers a range of topics, starting with the characteristics of heavy oil and bitumen, and exploring different extraction methods. The focus then shifts to hydrogen production and its relevance in the energy landscape. The chapter investigates innovative recovery techniques, including Toe-to-Heel Air Injection (THAI) and Catalytic THAI (CAPRI), discussing their potential advantages. Furthermore, the application of CMG STARS in the context of THAI is examined, showcasing the role of simulation tools. Lastly, the chapter explores hydrogen generation during In-Situ Combustion (ISC) as a dual-purpose approach for recovery and clean energy production. Through these concentrated analyses, this chapter provides insights into advancements and challenges in the field of heavy oil and bitumen extraction, setting the stage for the subsequent results chapters.

## 2.1 Heavy Oil and Bitumen

Heavy oils are most widely defined by the API gravity, a scale proposed by the American Petroleum Institution which is based on oil relative density. The API parameter defining heavy oils has not been standardised, being classified as an oil below 22.3 API°, equal to or below 20 API° or between 10 API° and 19 API° by the World Petroleum Conference, API and Petrobras respectively. The National Petroleum Agency of Brazil defines heavy oil as 10 API° to 21 API° (Table 1), with anything below 10 API° being classified as extra-heavy oil (Santos et al., 2014). This is concurred by Speight (Speight, 2019) as seen in Table 2. Heavy and extra heavy oils have a very high viscosity, relative to medium and light crudes, with a range of 100 to 10,000 cP, often posing a challenge with production and

transportation (Alvarez et al., 2009). Bitumen and oil sands have a viscosity over >10,000 cP (Hein, 2006).

**Table 2.1.** Table displaying different API° dependent of oil classifications from The National Petroleum Agency of Brazil (Adapted from (Santos et al., 2014).

| Oil Class | °API |
|---|---|
| Light | $^{o}API \geq 31$ |
| Medium | $22 \leq {}^{o}API < 31$ |
| Heavy | $10 \leq {}^{o}API < 22$ |
| Extra-heavy | $^{o}API \leq 10$ |

Heavy oils can be relatively easily found through geophysical techniques such as 2D electrical imaging and resistivity logs. The resulting geo-electrical sections can be interpreted as geological cross-sections, with heavy oils being observed as areas of very high resistance (Meyer et al., 2007). Basin margins are the most frequent exploration locations for heavy oils with the most common plate-tectonic settings for heavy oil and bitumen reservoirs are continental multi-cyclic basin margins, and in continental rifts (Hein, 2017).

In the case of basin margin centric reservoirs, the oil-bearing sediments are found within the foreland basin, where under-thrust crust heats up overlying sediment. Up to 80°C the petroleum is commonly biodegraded (post-migration) over thousands and millions of years by microorganisms. This procedure breaks down hydrocarbons and sulfides, resulting in the formation of dense oils. In areas of significant deterioration, it leads to the creation of bitumen sands. In areas of significant deterioration, it leads to the creation of bitumen sands. In situations where this procedure takes place in oxygen-deprived environments, which is how the majority of the Earth's oil reserves have originated, a substantial by-product in the form of methane is generated. This leads to the discovery of extensive methane reserves alongside deposits of heavy oil and bitumen sands, making the production process more complex but yielding higher benefits (Head et al., 2003).

### 2.1.1 Heavy Oil and Bitumen Deposits and Recovery

Hein (2017) estimates that there are approximately 5600 billion barrels of bitumen and heavy oil, occurring over 70 different countries, with most of the heavy oil being found in Venezuela, and most bitumen being found in Canada. Natural degradation in most cases is biological in nature resulting in relatively shallow reservoirs with geologically young pay-zones when compared to conventional reservoirs (Hein, 2017).

**Table 2.2.** Simplified physical variations between black oil. Tight oil, heavy oil and bitumen sands (Adapted from (Speight, 2019)).

| Crude Type | Characteristics | API Gravity | Mobility in Reservoir | Permeability | Recovery Methods |
|---|---|---|---|---|---|
| Conventional Crude | Mobile in reservoir | > 25° | High | High | Primary Recovery, Secondary Recovery |
| Tight Oil | Similar properties to conventional crude | > 25° | Immobile | Low | Horizontal drilling, Fracturing |
| Medium Crude Oil | Similar properties to conventional crude | 20-25° | High | High | Primary Recovery, Secondary Recovery |
| Heavy Crude Oil | More viscous than conventional crude | 10-20° | Low | High | Secondary Recovery, Tertiary Recovery |
| Extra Heavy Oil | Fluid in reservoir. Similar properties to the properties of tar sand bitumen | $< 10^0$ | Very Low | High | Secondary Recovery, Tertiary Recovery |
| Tar Sand Bitumen | Immobile (solid to near solid) in the deposit | < 10" | Immobile | High | Mining, Steam-assisted gravity drainage, Solvent meth, Extreme heating methods |

Hein (2006) and Hinkle and Batzle (2006) state that over 80% of heavy oil and bitumen deposits are in Venezuela, Canada and the USA (Table 3). This is concurrent with more

recent papers, with around 70% of heavy oil and bitumen deposits being hosted within the same three countries, and other major deposits found in the Middle East, China and Africa (Hein, 2017).

**Table 2.3.** Table displaying locations and respective heavy oil and bitumen deposits (values in billions of boe, BBOE) around the world, with 77% of deposits being found in North and South America (Adapted from (Ahlbrandt, 2002)).

| | Heavy Oil BBOE | Bitumen BBOE |
|---|---|---|
| North America | 35.3 | 530.9 |
| South America | 265.7 | 0.1 |
| Africa | 7.2 | 43 |
| Middle East | 78.2 | 0.0 |
| Asia | 29.6 | 42.8 |
| Russia | 13.4 | 33.7 |
| Western Hemisphere | 301 | 531 |
| Eastern Hemisphere | 128.4 | 119.5 |
| Worldwide | 429.4 | 650.5 |

Karimov, Laman, and Abbuzarli (Karimov et al., 2018) estimate the worldwide safe oil reserves, those being reserves that are economically viable and technically recoverable with current technology and market conditions, to exceed 150 billion tons. OPEC (2018) estimate total reserves to exceed 1497 billion barrels of oil (BBO), making heavy oil and bitumen approximately 72% of the world's total oil reserves, concurred by (Ahlbrandt, 2002; Hart et al., 2013). Meyer and Attanasi (Meyer and Attanasi, 2003) estimate worldwide technically recoverable heavy oil and bitumen resources to be 434.4 BBO and 650.7 BBO respectively, with an average combined recovery factor of 15.5%. The highest recovery factor is seen in North America with 19% and 32% in heavy oil and bitumen respectively. BP's annual review of world energy estimates total production of crude oil in 2017 to be over 93 million barrels per day, with consumption in 2017 to be approximately 98 million barrels per day. This is a positive 9% difference in consumption

when compared to production. This 5% difference has to be met through the use of stored oil from a strategic reserve (e.g., the Strategic Petroleum Reserve, USA) (Kilian and Zhou, 2020). Growth in 2017 approached 1% worldwide, with views for positive net growth over the next 10 years (Dudley, 2018). Brandt et al. (Brandt et al., 2018) state that the price drop in oil over the last decade, from around $110/Bbl in 2014 to <$80/Bbl in 2018 was caused in part by the huge investment by industry into heavy oil and bitumen extraction techniques and technology. This oil surplus was then caused by the low prices and lower up-front expenditure on new plays due to the technology already in place (Brandt et al., 2018; Dudley, 2018), with heavy oil and bitumen aiming to fill the existing gap between consumption rates and production. However, during the 2020 COVID pandemic, oil prices reach all-time lows (<$10/Bbl) not bouncing back to $80/Bbl until early 2022, with late 2022 seeing prices back at >$110/Bbl. According to projections from the Organization of Petroleum Exporting Countries, the trajectory of oil demand is on an upward surge, predicted to rise by a substantial 16.4 million barrels per day (MMBbl/day) from 2015 to 2040. This trajectory is envisioned to culminate in an oil demand of 99.2 MMBbl/day by 2021 (the same as the 2017 figures reported by BP) and a staggering 109.4 MMBbl/day or more by 2040. While conventional light oil production boasts cost-efficiency and swift extraction rates, the relentless growth in energy requirements has sparked a notable shift towards considering heavy oil as a viable solution within the framework of the global energy market (Li et al., 2021).

## 2.2 Extraction Processes

### 2.2.1 Primary and Secondary Recovery

Primary recovery is the initial stage of hydrocarbon production, where natural forces facilitate the recovery process. In this stage, the pressure within the reservoir is higher than the pressure at the bottom of the wellbore. This pressure differential drives the hydrocarbons toward the wellbore and ultimately to the surface. The natural occurrences that aid in pressure maintenance and reservoir displacement include gas drive, water drive, and gravity drainage (Shah et al., 2010). Gas drive refers to the presence of gas in the reservoir, which exerts pressure and helps push the hydrocarbons towards the wellbore. Water drive occurs when water is present in the reservoir, and its movement displaces the hydrocarbons, forcing them towards the wellbore. Gravity drainage relies on the natural tendency of hydrocarbons to rise above water due to their lower density, facilitating their upward movement towards the wellbore (Shah et al., 2010). Following primary recovery, secondary recovery techniques are employed to artificially enhance or assist the primary drives. These techniques involve increasing the pressure within the reservoir through the injection of water or gas into communicable areas of the producing layers. By doing so, the pressure differential in the wellbore is further increased, resulting in improved oil flow and production rates. Secondary recovery methods play a crucial role in extracting a greater volume of hydrocarbons from the reservoir (Pei et al., 2015).

**Table 2.4.** A table displaying various primary and secondary extraction methods and their advantages and disadvantages. Sources within.

| Name | Brief Description | Advantages | Disadvantages | Source |
|---|---|---|---|---|
| Surface Mining | Extraction technique for shallow oil sands | Cost-effective in shallow regions. High recovery rates (up to 90%) | Limited to shallow depths. Time-consuming process | Shah |
| Cold Production | Method for heavy oil reservoirs with low viscosity | Suited for heavy oil reservoirs. Enhanced well contact. Efficient (15% to 70% recovery) | Additional recovery processes often needed for higher rates. Diluents required | Sea, Shah |
| Water Flooding | Secondary technique for declining primary recovery | Economically viable. Increases reservoir pressure. Releases trapped oil within reservoir rock | Requires high-pressure water injection. Limited to certain reservoir conditions | Pei, Miller |
| Cold Heavy-Oil Production with Sand | Modified cold production for heavy oil reservoirs | Enhances heavy oil production. Increases reservoir permeability. Significant production rate improvement | Requires sand erosion. Potential for reservoir damage if not managed properly | Shah, Rangriz Shokri and Babadagl |

### 2.2.2 Tertiary Recovery

Tertiary recovery, also known as enhanced oil recovery (EOR), represents the third stage of hydrocarbon recovery. It involves the extraction of hydrocarbons that remain in the reservoir after primary and secondary recovery methods have been applied. Tertiary recovery employs various techniques that utilise chemicals, heat, and catalysts to enhance production rates. This stage becomes particularly important for reservoirs containing heavy oil and bitumen, which possess high viscosity and require advanced methods to increase the recovery rate when primary and secondary techniques fall short (Shah et al., 2010; Dai and Zhao, 2019). Tertiary techniques encompass thermal recovery methods, wherein the reservoir or specific zones within it are subjected to heat. This heat application serves to enhance the recovery process by reducing viscosity and inducing thermal cracking, among other benefits.

**Table 2.5.** A table displaying various non-thermal tertiary extraction methods and their advantages and disadvantages. Sources within.

| Name | Brief Description | Advantages | Disadvantages | Source |
|---|---|---|---|---|
| Miscible Displacement | Oil displacement method in tertiary recovery. Injects miscible phase (hydrocarbon/non-hydrocarbon) into reservoir. | Maintains reservoir pressure. Displaces oil at microscopic level. | Requires high pressure. | Shah et al., 2010, Dai and Zhao, 2019 |
| CO2 Flooding | Tertiary recovery technique with CO2 injection. Dissolves into heavy oil, reducing viscosity and increasing mobility. | Enhances sweep efficiency. Enables carbon dioxide storage. | Minimum miscibility pressure (MMP) limit. | Bikkina et al., 2016; Gozalpour et al., 2005 |
| N2 Flooding | Injection of nitrogen for miscible flooding. Increases oil volume and mobility. | Economically viable. Widely used for over 50 years. | Higher MMP compared to CO2. Economical but less effective. | Shah et al., 2010, Mogensen and Xu, 2019 |
| Chemical Flooding | Reservoir flooding with chemicals. Decreases interfacial tension and improves sweep efficiency. | Enhances sweep efficiency. Decreases interfacial tension. | Complex chemical management. | Shah et al., 2010, Dai and Zhao, 2019 |
| Polymer Flooding | Injection of polymer solution to displace oil. Increases viscosity, improving sweep efficiency. | Reduces mobility ratio. Minimizes viscous fingering. | Requires careful polymer selection and management. | Amirian et al., 2018 |
| Surfactant Flooding | Tertiary recovery with surfactants. Reduces interfacial tension between oil and water. | Proven recovery enhancement. Enters aqueous and non-aqueous phases. | Dependent on reservoir and hydrocarbon properties. | Shah et al., 2010, Wei et al., 2018 |
| Alkaline Flooding | Creates in-situ surfactant by injecting alkalis. Reduces interfacial tension, aiding oil dispersion. | Reduces interfacial tension. Aids oil dispersion. | Reactivity and chemical compatibility considerations. | Gong et al., 2016 |
| Micellar Flooding | Reservoir flooding with micellar solution. Stable solution enhances surfactant adsorption and reduces tension. | Enhances surfactant adsorption. Balances solution hydrophilicity and hydrophobicity. | Complex formulation. Requires optimal alcohol/salt balance. | Kianinejad et al., 2015, Dai and Zhao, 2019 |
| Alkaline-Surfactant-Polymer (ASP) Flooding | Simultaneous injection of alkaline and synthetic surfactants along with a water-soluble polymer. Creates "petroleum soap" for interfacial tension reduction. | Improves mobility of flood front. Lower injection cost. Reduced surfactant adsorption. | Complex formulation. | Aitkulov and Mohanty, 2016, Shah et al., 2010 |
| Microbial EOR (MEOR) | Utilizes indigenous microbes to enhance oil recovery. Microbes produce materials like surfactants. | Low-cost surfactant production. Biotransformation of heavy oil. | Requires proper microbial conditions. | Shibulal et al., 2018, Al-Sayegh et al., 2017, Shah et al., 2010 |

**Table 2.6.** A table displaying various thermal extraction methods and their advantages and disadvantages. Sources within

| Name | Brief Description | Advantages | Disadvantages | Source |
|---|---|---|---|---|
| Steam Flooding | Continuous injection of steam into reservoir for thermal energy and viscosity reduction of oil. | Enhanced recovery of less viscous oil. | Recovery improvements: 25% to 40%. | Shah et al., 2010, Guo et al., 2016, Dong et al., 2019 |
| Cyclic Steam Stimulation (CSS) | Inject steam into reservoir, alternating soak and production stages. | Low up-front cost. Significant recovery increase. | Recovery enhancement through viscosity reduction. | Trigos et al., 2016 |
| Steam Assisted Gravity Drainage (SAGD) | Inject steam into upper well, heating oil, reducing viscosity. Drains to lower well due to gravity. | Effective viscosity reduction. Gravity-driven drainage. | Requires specific well arrangement. | Rui et al., 2018 |
| In-Situ Combustion | Direct thermal heating of reservoir, cracking heavy oil into lighter hydrocarbons. Facilitates production of less viscous oil. Applicable to various reservoirs. | Effective in-situ heating for enhanced recovery. | Potential limitations in shale formations. | Ahmadi et al., 2015, Kar and Hascakir, 2017, Marfin et al., 2015 |
| Toe-to-Heel Air Injection (THAI) & CAPRI | THAI (Toe-to-Heel Air Injection) is a technique that utilizes a horizontal production well to eliminate gas override. THAI-CAPRI further integrates catalytic upgrading with THAI, aiming to enhance oil recovery. The pelletized catalyst along the producer well enhances oil upgrading, increasing recovery efficiency (Greaves and Xia, 2001a). | THAI offers a reduction in gas override and enhanced oil recovery. THAI-CAPRI combines THAI with in-situ catalytic upgrading, providing the potential for greater recovery improvements. However, both methods require specific well arrangements to be effective. | Specific well arrangement is required for both methods. | Ado et al., 2019, Shah et al., 2010, Greaves and Xia, 2001a, Hart et al., 20 |

## 2.3 Hydrogen Production

Hydrogen is a very important resource for use in the chemical and refining industries and is predicted to play a big role in the future energy market (Rostrup-Nielsen and Rostrup-Nielsen, 2002; Yue et al., 2021). Sato et al. (2003) and Okolie et al. (2021) concur this prediction by stating that hydrogen is expected to be one of the primary sources of energy for electricity, fuel, and other applications within the 21$^{st}$ century. It is an environmentally clean source of energy, as no pollutants are generated. If produced in-situ, it also has the potential to act as both source of energy, and a carbon storage process due to the reactions involved in the production of hydrogen. It is therefore a high priority to find a cheap, efficient process for environmentally friendly hydrogen production to meet future energy demands.

Several technologies exist to produce hydrogen, with the main three processes being hydrogen reforming, electrolysis, and pyrolysis. These three methods, being most developed, meet almost all current hydrogen demand. As of 2017, hydrogen was being produced by natural gas (48%), heavy oils, bitumen, and naphtha (30%) and coal (18%) (Nikolaidis and Poullikkas, 2017), with >4% of hydrogen being generated from electrolysis. As of 2023, the hydrogen being generated from electrolysis is still >5% (Riera et al., 2023). Although membrane reactors also contribute minimally to hydrogen production in newer production schemes and electrolysis is slowly increasing in popularity, fossil fuels remain dominant as the production costs are closely linked to fuel costs.

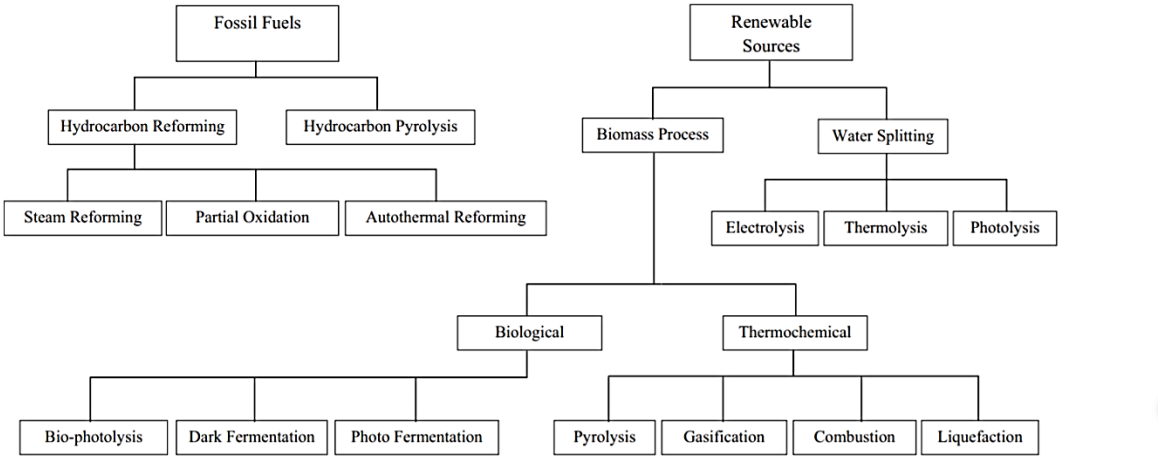


**Figure 2.1.** Flow chart depicting sources of hydrogen production, along with potential reaction processes. Taken from Nikolaidis and Poullikkas (2017).

Kothari et al. (2008) postulate that 96% (with the same breakdown of %'s as presented by (Nikolaidis and Poullikkas, 2017)) of hydrogen is created from hydrocarbon feedstock, with the remaining 4% being indirectly produced by using electricity generated from fossil fuels (electrolysis). This highlights that over the past 15 years, there has been minimal evolution in the hydrogen generation landscape. As a result, there is a pressing need to explore and implement novel approaches for generating hydrogen from existing fossil fuel sources. Demirbaş and Çağlar (1998) state that hydrogen has been suggested to be a convenient, clean-burning fuel, which can ultimately replace the burning of fossil fuels, helping to resolve the political, environmental, and economic impacts associated with their use. For many of the current hydrogen production processes to work, the heavy oil must first be upgraded, turning it into much lighter hydrocarbon compounds such as propylene, ethylene, and most notably methane, which then undergo catalysed steam gasification and dehydrogenation.

### 2.3.1 Hydrocarbon pyrolysis

Pyrolysis of hydrocarbons is a process in which the only source of hydrogen is from the hydrocarbon itself, undergoing thermal decomposition which can be represented by the following general reaction (Nikolaidis and Poullikkas, 2017):

$C_nH_m \rightarrow nC + ½mH_2$ (2.1)

The general reaction simply just splits the hydrocarbon (CH) into its constituent elements. This process, however, is less clearly defined when other elements are involved, such as sulphur and nitrogen, which are often found in crude hydrocarbons. Also complicating this process is that simply pyrolysis is only viable through thermo-catalytic decomposition when light liquid hydrocarbons are involved, as their boiling point is between 50°C and 200°C. For hydrocarbons with chains lengths classified as heavy oil or higher (bitumen etc.), the process consists of two-stages (Nikolaidis and Poullikkas, 2017):

Hydrogasification: $CH_{1.6} + 1.2H_2 \rightarrow CH_4$ (2.2)

Methane cracking: $CH_4 \rightarrow C + 2H_2$ (2.3)

These two reactions can be represented as a whole by the following general reaction:

Overall reaction: $CH_{1.6} \rightarrow C + 0.8H_2$ (2.4)

The pyrolysis process of methane can be represented by the following flow diagram (Nikolaidis and Poullikkas, 2017):

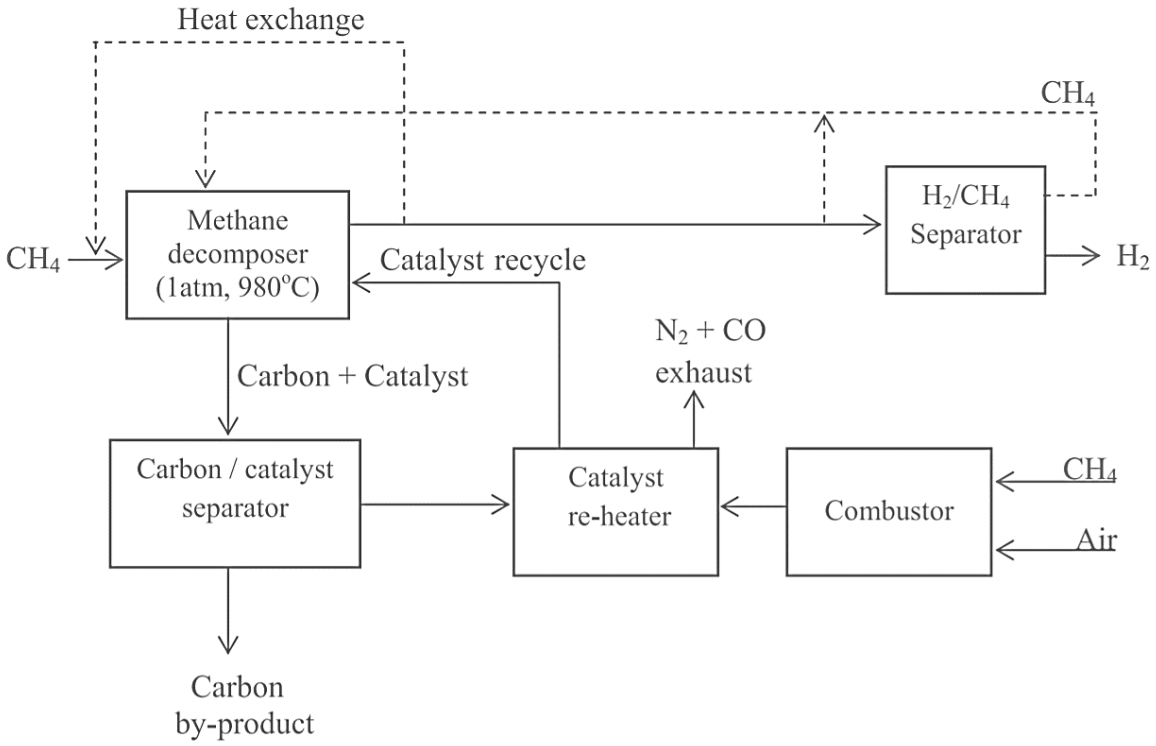


**Figure 2.2.** Flow chart depicting methane pyrolysis process. Taken from Nikolaidis and Poullikkas (2017).

Meng et al. (2008) used catalyst CEP-1 for their experiments in the catalytic pyrolysis, suggesting it to be a specialist catalyst for the process. The catalyst itself was developed by Yi et al. (2002) and its main active component is modified pentasil structure zeolite, containing phosphorous and alkali earth metal. The catalyst has been shown to simultaneously maximise the yield of both ethylene and propylene, both forms of natural gas. The catalyst activates best at reaction temperatures of 560 ℃ to 650 ℃ irrespective of pressure.

### 2.3.2 Hydrogen reforming

Hydrogen reforming is loosely defined as the conversion of hydrocarbons into hydrogen through reforming techniques. Other reactants for the reforming processes can be used; steam reforming (endothermic) and partial oxidation (exothermic). These two reaction mechanisms can be combined, then termed an autothermal reaction (Nikolaidis and Poullikkas, 2017).

### *2.3.2.1 Steam reforming*

Steam reforming (SR) is the principal process for the conversion of hydrocarbons into hydrogen, usually having natural gas as the hydrocarbon fuel. The following set of reactions represent the process:

Steam reforming of methane is very strongly endothermic and due to its reversible nature, it must be carried out according to le Chatelier's principle (Tzanetis et al., 2012). The reaction must be carried out at high temperature, low pressure and a very high steam to methane ratio (Fishtik et al., 2000; Rostrup-Nielsen and Rostrup-Nielsen, 2002). The reaction is carried out this way in order to maximise conversion into hydrogen.

Methane SR: $CH_4 + H_2O \rightarrow CO + 3H_2$ ($\Delta H_{298} = 206.1$ kJmol$^{-1}$) (2.5)

General hydrocarbon reforming: $C_nH_m + nH_2O \rightarrow nCO + (n + ½m)H_2$ (2.6)

The steam then reacts with the produced carbon monoxide to produce carbon dioxide and hydrogen, known as the water-gas shift (WGS) reaction.

WGS reaction: $CO + H_2O \rightarrow CO_2 + H_2$ (2.7)

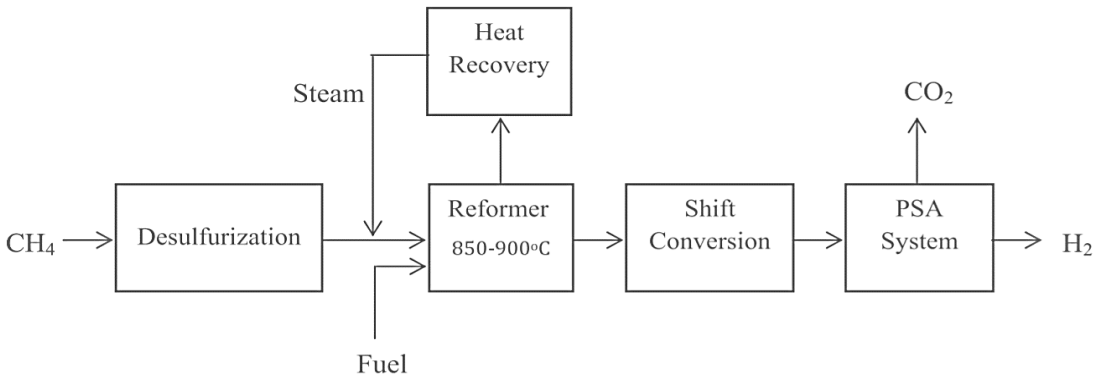


**Figure 2.3.** Flow chart depicting steam reforming process. Taken from (Nikolaidis and Poullikkas, 2017).

The steam and natural gas react at temperatures of 850 °C to 900 °C over a nickel-based catalyst and are then passed through pressure swing adsorption (PSA) which helps to

separate the hydrogen from the other components (carbon oxides). The hydrogen produced can be up to 99.99% pure from these specially designed surface processes (Nikolaidis and Poullikkas, 2017). However, hydrogen generated from in-situ hydrocarbons would likely have a much lower purity (<15%) (Hajdo et al., 1985).

#### *2.3.2.2 Partial oxidation*

Partial oxidation (POX) involves converting steam and hydrocarbons into hydrogen and carbon oxides in the presence of oxygen. The catalytic process, which operates at temperatures around 950 $^{o}$C, can accommodate feedstock from methane to naphtha – both of which can be products from the thermal upgrading and cracking of heavy oils (Greaves and Xia, 2001a; Nikolaidis and Poullikkas, 2017).

Catalytic POX: $C_nH_m + ½nO_2 \rightarrow nCO + ½mH_2$ (2.8)

When the process is performed in the absence of a catalyst it operates at temperatures between 1150 $^{o}$C and 1315 $^{o}$C and can accommodate feedstock that includes methane, heavy oil and coal. POX can be the most effective choice for hydrogen production from feedstock like heavy oil and bitumen (Nikolaidis and Poullikkas, 2017; Chen et al., 2023).

#### *2.3.2.3 Autothermal reforming*

Autothermal reforming (ATR) uses a combination of the two production methods, with the exothermic POX providing heat, and the endothermic SR increasing the total hydrogen yield. The two reactions occur simultaneously and can be represented by the following general reaction and flow chart (Figure 2.4) (Deluga et al., 2004; Nikolaidis and Poullikkas, 2017).

ATR: $C_nH_m + ½\ nH_2O + ¼\ nO_2 \rightarrow nCO + (½n + ½m)H_2$ (2.9)

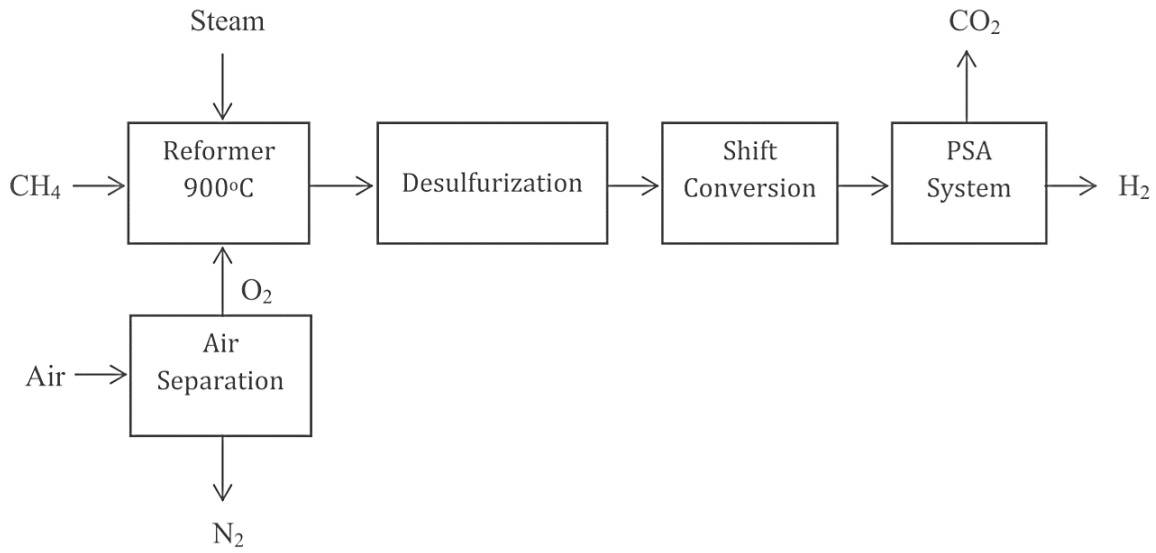


**Figure 2.4.** Flow diagram depicting the autothermal reforming process. Taken from Nikolaidis and Poullikkas (2017).

Using a nickel-based catalyst in this process uses much less oxygen (a lower $O_2/CH_4$ ratio) and the addition of steam helps to adjust the $H_2/CO$ ratio (Chen et al., 2023). The addition of steam in the non-catalytic POX/ATR results in a temperature decrease which slows down the reaction, decreases hydrogen yields and produces carbonic compounds such as soot (Rostrup-Nielsen and Rostrup-Nielsen, 2002).

## 2.4 Toe-to-Heel Air Injection

### 2.4.1 THAI Development History

The development of Toe-to-Heel Air Injection (THAI) emerged as a response to the limitations and economic concerns associated with conventional thermal enhanced oil recovery (EOR) methods. Researchers at the University of Bath in the late 1990s embarked on a quest to devise a cost-effective thermal recovery technique that could improve the efficiency of heavy oil and bitumen production while mitigating the drawbacks of existing methods (Greaves and Xia, 2001b). The core objective of THAI was to optimise heavy oil recovery rates while minimising water and energy consumption and reducing environmental impact. Traditional EOR techniques, such as cyclic steam

stimulation (CSS) and steam-assisted gravity drainage (SAGD), were widely used but posed significant challenges in terms of energy requirements, water usage, greenhouse gas emissions, and groundwater contamination (Singh et al., 2019b). THAI aimed to address these concerns and reform thermal EOR. Unlike conventional steam-based techniques, THAI employed air as the injection medium instead of steam (Greaves and Xia, 2000b).

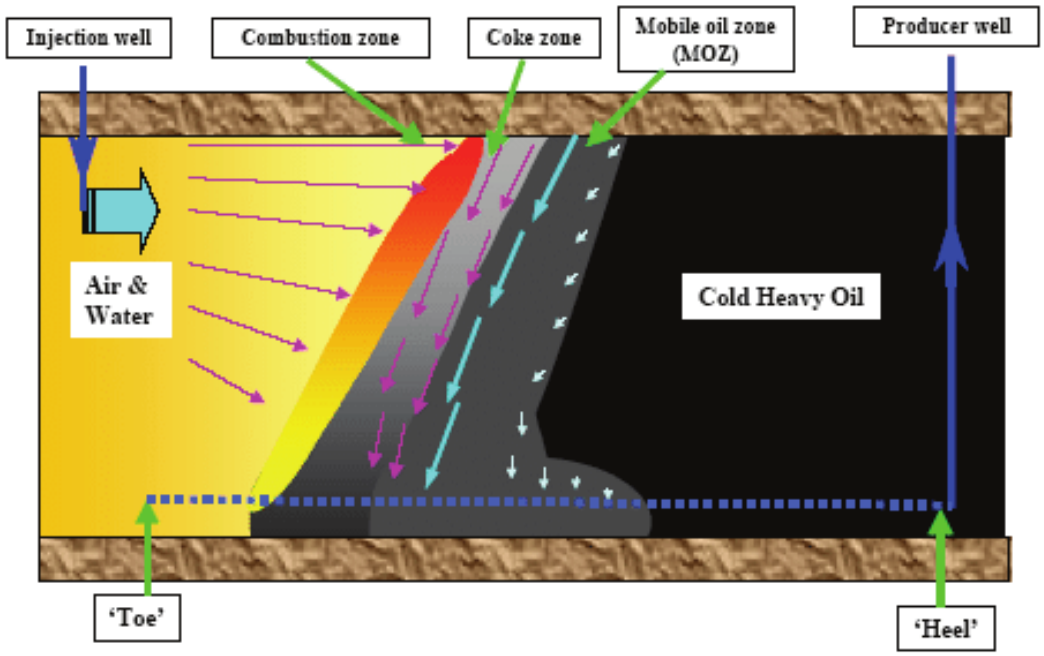


**Figure 2.5.** Schematic of THAI process depicting the various zones generated (Taken from Xia et al. (2003c)).

In THAI, a horizontal well configuration is typically employed, with the "toe" positioned at the lower end of the reservoir and the "heel" at the higher end. Air is injected into the heel, flowing through the reservoir to promote the combustion of oil and generate heat (Figure 2.5). The generated heat reduces the oil viscosity, facilitating its mobilisation and recovery. Additionally, the combustion of oil releases gas, providing the necessary pressure to drive the oil toward the production (Greaves et al., 2000a). Several zones are generated during the process. The combustion zone, located at the front of the reaction, is characterised by high temperatures and oxidation reactions. Here, injected air or

oxygen reacts with the oil, generating heat and combustion gases (Greaves et al., 2008a). Directly behind the combustion zone lies the mobile oil zone, where oil is heated and becomes less viscous, aiding its movement towards the production well (Cao et al., 2009). The coke zone, farther from the combustion front, is where heavier hydrocarbons thermally crack, forming solid coke deposits that can impede fluid flow (Xia et al., 2003c; Greaves et al., 2008b). Separated from the coke zone by a transition region is the steam zone, where injected water vaporises due to the intense heat, leading to steam generation and improved oil mobility through vaporization and pressure enhancement (Turta et al., 2020).

The development of THAI faced numerous challenges and required extensive research and testing. Laboratory studies conducted at the University of Bath demonstrated the feasibility and effectiveness of the THAI process for heavy oil and bitumen recovery from diverse reservoir types (Greaves and Xia, 2001b). These initial findings provided the impetus for further investigation and field trials to validate THAI's potential on a larger scale and will be discussed in detail later on. Field tests were subsequently conducted in Canada, where the THAI process was implemented in oil sands reservoirs. These trials yielded promising results, showcasing increased oil recovery rates compared to conventional steam-based methods. The success of these field trials served as a significant milestone, affirming the viability and potential of THAI as an efficient and sustainable EOR technique (Ayasse et al., 2005; Greaves et al., 2011b; Turta et al., 2023).

The development of THAI was not without its challenges. Achieving optimal combustion control and avoiding excessive burning, which could lead to reservoir damage or premature breakthrough of air or gas to the production well, required meticulous monitoring and operational adjustments. Reservoir heterogeneity, such as variations in

permeability and oil saturation, also presented challenges that necessitated tailored operational strategies (Turta et al., 2018; Ado et al., 2019; Ado, 2021b).

### 2.4.2 THAI advantages

Toe-to-Heel Air Injection (THAI) has emerged as a promising thermal enhanced oil recovery (EOR) technique, offering several advantages over conventional methods. Researchers have further explored and enhanced the THAI process to maximise its potential for increasing oil mobility and production rates (Greaves and Xia, 2004; Hart et al., 2017). By integrating additional upgrading steps, THAI enables the conversion of heavy oil into lighter hydrocarbon types, improving its mobility and facilitating more efficient production (Xia et al., 2003b). One notable advantage of THAI is its reduced water and energy requirements compared to other thermal EOR methods. This aspect is of great significance, as the demand for freshwater resources and energy-intensive processes in traditional EOR methods pose environmental and economic challenges. THAI's reduced water and energy inputs contribute to sustainable oil recovery practices (Greaves et al., 2000b). In terms of environmental impact, THAI offers the advantage of reduced greenhouse gas emissions. As a result of the combustion of heavy oil in the reservoir, the need for external sources of energy is minimised, thereby decreasing the overall carbon footprint associated with the EOR process (Singh et al., 2019a).

Another notable benefit of THAI is its potential to minimise ex-situ treatment and processing. Traditional EOR techniques often require extensive ex-situ treatment and processing steps to upgrade the heavy oil and separate impurities. However, THAI's in-situ combustion and upgrading mechanism reduce the need for complex ex-situ processes, streamlining the overall production and reducing operational costs (Greaves and Xia, 2000a). The displacement of mobilised oil within the reservoir is a critical factor

in determining the efficiency of EOR methods. THAI offers the advantage of shorter displacement, which increases the overall efficiency of the process (Hart, 2014b). This shorter displacement leads to higher levels of connectivity within the mobile oil zone, allowing for improved recovery rates (Xia et al., 2002b).

Furthermore, the coke build-up resulting from the in-situ combustion in THAI aids in sealing the well in produced zones. This phenomenon reduces gas production, allowing for improved control over gas override, which can negatively impact oil recovery rates in conventional EOR methods (Hart, 2014b). The horizontal nature of the wells employed in THAI offers another advantage by reducing gas override. Gas override occurs when the injected gas used for combustion rises to the top of the reservoir, leading to decreased oil production rates. The horizontal configuration of THAI wells helps eliminate this issue, ensuring more efficient recovery and enhancing the overall effectiveness of the process (Greaves et al., 2004b).

The aforementioned advantages of THAI make it an attractive option for thermal EOR applications. The ongoing research and development efforts have focused on refining the process and optimising its performance. For instance, the combination of THAI with in-situ catalytic upgrading, known as THAI-CAPRI, has been proposed as a method to further enhance the upgrading and recovery potential of THAI (Xia et al., 2002c; Hart et al., 2014).

### 2.4.3 Thermal Reactions

High temperatures can induce the chemical upgrading of heavy oils by breaking down chemical bonds and reducing the hydrocarbon chain length through cracking, even in the absence of a catalyst. Thermal cracking primarily affects three main types of bonds within hydrocarbons: carbon-carbon (C-C), carbon-hydrogen (C-H), and carbon-sulfur (C-S)

(Ebrahimi et al., 2008). Gasification refers to the process of converting hydrocarbons into gases such as $CO_2$, CO, and $H_2O$.

The following four reactions facilitate the thermal upgrading of heavy oil (Hart, 2014a):

$$\text{Heavy Oil} \rightarrow \text{Light Oil} + \text{Gas} + \text{Coke} + \text{Absorbed Heat} \quad (2.10)$$

$$\text{Coke} + O_2 \rightarrow H_2O + CO_2/CO + \text{Heat} \quad (2.11)$$

$$\text{Heavy Oil} + O_2 \rightarrow H_2O + CO_2/CO + \text{Heat} \quad (2.12)$$

$$\text{Light Oil} + O_2 \rightarrow H_2O + CO_2/CO + \text{Heat} \quad (2.13)$$

Cracking of C-C bonds at a modest rate without a catalyst requires temperatures of at least 420°C. However, aromatic groups containing C-C and C-H bonds have stronger bonds compared to other hydrocarbon groups due to resonance stabilisation, making them virtually unbreakable below 600°C without a catalyst (Dračínský et al., 2015). Upgrading hydrocarbons at temperatures below 400°C is limited unless a highly active catalyst is introduced to initiate cracking reactions, which are typically referred to as pyrolysis (Shakirullah et al., 2008).

$$\text{Pyrolysis: } CH_{x1} \rightarrow CH_{x2} + \text{Coke } (x2 > x1) \quad (2.14)$$

At lower temperatures, reactions tend towards low-temperature oxidation (LTO), producing oxidised hydrocarbons with higher viscosities that can lead to oil blockage in the downstream region of the reservoir, ahead of the combustion front. When temperatures are sufficiently high, reactions transition into high-temperature oxidation (HTO), producing more gaseous and low-viscosity material (Xia et al., 2002c).

$$\text{LTO: } CH_x + O_2 \rightarrow CH_xO_y \quad (2.15)$$

$$\text{HTO: } CH_x + O_2 \rightarrow CO + CO_2 + H_2O \quad (2.16)$$

The cracking of C-C bonds at temperatures above 420°C is the primary mechanism responsible for the conversion of heavy oil into lighter fractions during thermal processes such as THAI. The cracking reactions break down the long hydrocarbon chains, reducing their viscosity and enhancing their mobility within the reservoir. This allows for better displacement and recovery of the oil. It is important to note that the cracking reactions are influenced by factors such as temperature, pressure, residence time, and the composition of the heavy oil. The temperature plays a critical role in determining the extent and efficiency of cracking. Temperatures of at least 420°C are required to initiate the cracking of C-C bonds at a reasonable rate. However, temperatures above 600°C are necessary to break the strong bonds present in aromatic groups. The presence of catalysts can significantly lower the activation energy required for cracking reactions, enabling them to occur at lower temperatures (Xia et al., 2002c; Hart, 2014a). During the pyrolysis process (Figure 2.6), the hydrocarbon molecules break apart into smaller fragments, resulting in the production of lighter oil fractions and coke. The coke is a solid residue that accumulates in the reservoir and can help seal off wellbores, reducing gas production and improving reservoir pressure maintenance (Hart and Wood, 2018). However, excessive coke formation can lead to reduced permeability and reservoir damage.

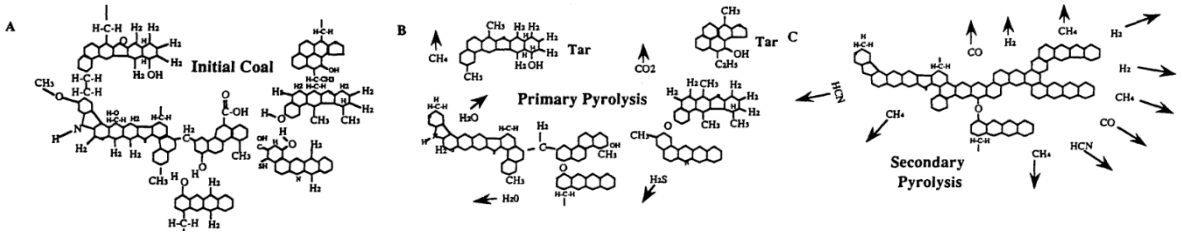


**Figure 2.6.** Sequential stages of Pittsburgh bituminous coal pyrolysis, (A) initial coal, (B) primary pyrolysis, and (C) secondary pyrolysis. Taken from (Hobbs et al., 1993).

In addition to pyrolysis, low-temperature oxidation (LTO) and high-temperature oxidation (HTO) reactions also occur during the thermal upgrading of heavy oil. LTO produces oxidised hydrocarbons with higher viscosities, which can contribute to oil

blocking in the downstream region of the reservoir. On the other hand, HTO reactions generate gaseous components, such as CO, $CO_2$, and $H_2O$, that are more mobile and contribute to improved reservoir sweep efficiency (Greaves et al., 2000a). Understanding the thermal reactions that occur during THAI is crucial for optimising the process and maximising oil recovery. By controlling the temperature and residence time, operators can enhance the cracking reactions while minimising undesirable side reactions like LTO. Additionally, the composition of the heavy oil and the presence of catalysts can also influence the overall efficiency and selectivity of the thermal upgrading process (Ado, 2020b; Turta et al., 2020).

In summary, thermal reactions play a significant role in the upgrading of heavy oils during THAI. Cracking of C-C bonds at elevated temperatures results in the conversion of heavy oil into lighter fractions and gases. Pyrolysis, LTO, and HTO reactions contribute to the overall transformation of the hydrocarbon molecules. By understanding these reactions and their influencing factors, operators can optimise the THAI process to achieve higher oil recovery and minimise undesirable outcomes such as coke formation and oil blocking (Ado, 2020b).

## 2.5 THAI CAPRI

### 2.5.1 Development history of THAI-CAPRI

The development of THAI-CAPRI, a hybrid thermal recovery process, can be traced back to the early 2000s (Greaves and Xia, 2001a; Xia et al., 2002c). It is an innovative combination of the Toe-to-Heel Air Injection (THAI) process and Catalytic Processing In-situ (CAPRI). The aim of this hybrid process is to enhance heavy oil recovery from oil sands and reservoirs while improving energy efficiency and reducing environmental impacts, by incorporating catalytic reactions, such as hydrogenation, through the addition

of a catalyst (Greaves and Xia, 2001a). However, challenges remained in terms of the quality of the produced oil, as it often contained high levels of impurities and had lower market value due to its heavy nature. To address these challenges, the CAPRI concept was integrated with THAI. The catalyst plays a crucial role in promoting the conversion of heavy oil fractions into lighter, more valuable products by increasing the oil API value, reducing impurities, and improving the overall quality of the produced oil (Greaves et al., 2004a). However, as the catalyst is enclosed within an annulus around the horizontal well, the heated, partially upgraded oil flows over the catalyst during production. This process exhibits a dynamic effect, requiring the catalyst to remain active for extended periods. The concern arises because deactivation can be a significant issue for this process, given the high likelihood of the pelleted catalyst pores becoming plugged by coke and impurity deposition (Shah et al., 2011; Hart and Wood, 2018).

The integration of CAPRI with THAI brought several advantages to the process. The addition of a catalyst enables the catalytic reactions necessary for oil upgrading, enhancing the quality of the produced oil (Greaves et al., 2004a; Hart et al., 2013). The catalyst facilitates the conversion of heavy oil components, such as asphaltenes and heavy aromatics, into lighter and more valuable hydrocarbons. This catalytic upgrading occurs in-situ, reducing the need for costly and energy-intensive post-production upgrading processes. The development and optimisation of THAI-CAPRI involved a combination of laboratory experiments and numerical simulation projects (Xia et al., 2002c; Ado et al., 2022a). Laboratory studies were conducted to understand the catalytic reactions, evaluate different catalysts, and assess the effects of various operating conditions on the upgrading performance. These studies provided valuable insights into the behaviour of THAI-CAPRI and aided in the selection and optimisation of the catalyst. Numerical simulation tools played a crucial role in the development of THAI-CAPRI, allowing

researchers to predict and optimise the upgrading performance at various scales. Simulation models were calibrated and validated using laboratory data and field measurements from pilot projects (Ado et al., 2022a; Ado et al., 2022b). The simulation results provided guidance on the design and operation of THAI-CAPRI projects, aiding in catalyst selection, reactor design, and optimisation strategies.

### 2.5.2 THAI-CAPRI operating conditions

The optimisation of operating conditions in the THAI-CAPRI process is crucial for achieving efficient oil upgrading through catalytic reactions. Numerous studies have been conducted to determine the optimal operating parameters, including catalyst type, temperature, and pressure, and their impact on the upgrading performance. Hart et al. (2017) conducted experiments at the laboratory scale using a pelletised Ni-Mo/$Al_2O_3$ catalyst. They investigated the effects of various operating conditions on the upgrading performance and correlated their findings with downhole conditions. Their results indicated that a reaction temperature ranging from 350°C to 425°C, along with 6 grams of catalyst, yielded favourable outcomes in terms of oil upgrading. These findings align with previous research by Hart et al. (2013) that also utilised a similar temperature range.

In the combustion zone of the THAI-CAPRI process, maintaining a sufficiently high temperature is essential for sustaining the high-temperature oxidation (HTO) mode. Greaves et al. (2008b) emphasise that the temperature in the combustion zone needs to be 500°C or higher to ensure effective combustion and maximise hydrocarbon recovery. This high-temperature regime facilitates the desired chemical reactions and helps in the efficient mobilisation and upgrading of heavy oil components. Pressure is another critical factor in optimising THAI-CAPRI operating conditions. Cao et al. (2009) conducted a series of experiments using CMG's WinProp simulation software to investigate the effects

of pressure and temperature on the performance of the THAI-CAPRI process. Their results demonstrated that higher mobile oil ratios, reaching 86%, were achieved at higher pressures and lower temperatures, specifically at 40 bar and 300°C. The selection of pressure conditions influences the balance between oil production, heat transfer, and catalytic reactions within the reservoir. Xia et al. (2002c) suggest that in-situ combustion (ISC) typically requires temperatures ranging from 500°C to 600°C. However, when operating ISC within the THAI process, the suggested temperature range is adjusted to 450°C to 650°C. These temperatures ensure effective in-situ combustion and facilitate the catalytic reactions involved in oil upgrading. Additionally, Xia et al. (2002c) recommend operating at pressures between 30 and 50 bar, which helps to maintain reservoir integrity and ensure efficient oil mobilisation.

It is important to note that the optimal operating conditions may vary depending on specific reservoir characteristics, such as porosity, permeability, and oil composition. Reservoir heterogeneity, including variations in rock properties and fluid distribution, should be considered when determining the appropriate operating conditions for THAI-CAPRI. The optimisation of THAI-CAPRI operating conditions involves a combination of laboratory-scale experiments, numerical simulations, and field-scale studies. Laboratory experiments, such as those conducted by Hart et al. (2017), provide valuable insights into catalyst behaviour and their performance under controlled conditions. These experiments help identify the optimal temperature and catalyst quantity required for efficient oil upgrading. The only field trial of CAPRI was conducted by Petrobank during the Whitesands THAI field pilot. The results of the field trial were, however, inconclusive (Turta et al., 2018).

### 2.5.3 Environmental concerns and THAI-CAPRI

Heavy oil extraction techniques, particularly enhanced oil recovery (EOR) methods that involve the use of chemicals and heat, have raised environmental concerns due to the emission of greenhouse gases and the potential contamination of groundwater with chemicals and heavy metals used in heavy oil treatment (Singh et al., 2019a). Bitumen, the primary component of heavy oil, contains significant amounts of sulfur and heavy metals. When subjected to high-temperature cracking reactions, it can produce acidic and toxic liquids and gases (Morrow et al., 2014). These toxic substances have the potential to seep into groundwater, posing risks to aquifers that supply potable water. Greenhouse gas emissions, particularly $CO_2$, are also associated with heavy oil and bitumen extraction (Soiket et al., 2019). Rosa et al. (2017) note similar environmental concerns with oil production from oil sands.

The THAI-CAPRI process offers a potential solution to mitigate these environmental impacts in several ways. Firstly, compared to other EOR methods, THAI-CAPRI requires less energy input both during the initial phase and throughout production, thereby reducing $CO_2$ emissions (Greaves et al., 2004b). Additionally, surface (ex-situ) refining and catalytic upgrading processes are minimised as these reactions occur within the reservoir during the THAI-CAPRI process. The formation of coke plugging helps reduce the release of toxic gases and liquids that can be by-products of thermal and chemical upgrading of heavy oil (Greaves and Xia, 2000b). Hasan and Rigby (2019a) highlight another environmental benefit of THAI-CAPRI by noting that the produced heavy oil lacks unwanted contaminants such as sulfur, vanadium, and nickel. This aspect contributes to reducing the potential environmental risks associated with the extraction and refining of heavy oil. It is worth noting that while THAI-CAPRI addresses some environmental concerns, it is essential to consider the overall environmental footprint of the process.

Factors such as land disturbance, water usage, and the potential for air emissions during the operation and construction of THAI-CAPRI projects need to be evaluated and mitigated to ensure sustainable and environmentally responsible practices (Singh et al., 2019a).

To further enhance the environmental performance of THAI-CAPRI, ongoing research and development efforts are focused on improving the efficiency of greenhouse gas capture and utilisation technologies. For instance, the utilisation of captured $CO_2$ for enhanced oil recovery or for other industrial purposes can help reduce net emissions and improve the overall environmental profile of the THAI-CAPRI process (Hart, 2014a).

### 2.5.4 THAI-CAPRI reactions

Upgrading reactions play a crucial role in the THAI-CAPRI process by transforming long-chain hydrocarbons into shorter-chained hydrocarbons with lower viscosity, enabling easier production and increased recovery. In addition to viscosity reduction, these reactions can also enhance the quality of the oil through desulfurisation and hydrogenation processes, aiming to achieve the desired hydrogen to carbon ratio of 1.8 (mol/mol) (Chao et al., 2012). Several studies have investigated the utilisation of various reactions to achieve these upgrading objectives.

To prevent catalyst deactivation and optimise the performance of the process, control of coke production is essential. Researchers have explored reaction strategies to mitigate and manage coke formation during the upgrading process (Forzatti and Lietti, 1999). Effective coke mitigation is crucial as coke deposition on the catalyst surface can impede its activity and performance, leading to decreased oil upgrading efficiency. Trimm (1983) also emphasises the significance of controlling coke formation to ensure long-term catalyst stability.

Thermal reactions within the THAI-CAPRI process involve the conversion of heavy hydrocarbons into lighter, more valuable products. Catalysts play a vital role in improving the thermal upgrading of heavy oils by reducing coke formation and enhancing hydrogen uptake (Ferrari et al., 2001). The use of catalysts enables more controlled and selective upgrading reactions, contributing to the production of desired product streams. Trimm (1983) further supports the benefits of catalysts in thermal upgrading processes.

Thermal-catalytic heavy oil upgrading primarily involves two main reactions: carbon rejection and hydrogen addition (Hart, 2014a). Carbon rejection reactions occur due to thermal cracking during the THAI process and are dependent on pressure and temperature conditions. Hydrogenation reactions, on the other hand, involve the use of active transition metals, such as iron, tungsten, nickel, cobalt, and molybdenum, either in metallic or sulfide form, as catalysts (Marafi et al., 2007). These catalysts, known as hydrotreating (HDT) catalysts, facilitate the pyrolysis process by promoting hydrogen addition reactions.

Carbon rejection: $CH_x \rightarrow CH_{x1} + C$ $(x_1 > x)$ (2.17)

Hydrogen addition: $CH_x + H_2 \rightarrow CH_{x1}$ $(x_1 > x)$ (2.18)

The presence of high sulfur content in heavy oils can facilitate the transformation of metal oxide catalysts into sulfide form, which has been reported to exhibit higher catalytic activity compared to the metallic form of the catalyst (Helfensteyn et al., 2003; Marafi et al., 2006). The sulfide form of the catalyst is known to enhance the desulfurisation process, contributing to the production of low-sulfur oil fractions.

### 2.5.5 Laboratory studies of THAI and THAI-CAPRI

CAPRI (Catalytic Processing In-situ) is a catalytic add-on that can be combined with the THAI process (THAI-CAPRI) whereby an industrial hydroprocessing catalyst is packed

along the horizontal producer well. The hydroprocessing catalyst (e.g. alumina-supported cobalt-oxide-molybdenum-oxide ($CoMo/\gamma\text{-}Al_2O_3$) or alumina-supported zinc-oxide-copper-oxide ($ZnCu/\gamma\text{-}Al_2O_3$) (Ado et al., 2022a) facilitates the catalytic upgrading of heated oil through the hydrogenation, hydrotreating and hydrocracking of the heated in-situ heavy oil with in-situ generated hydrogen. THAI-CAPRI was first introduced into literature in the early 2000s (Greaves and Xia; Xia et al.; Greaves and Xia, 2004) and has undergone extensive laboratory testing since. Laboratory testing of THAI-CAPRI on heavy oils show that the addition of a catalyst can increase API upgrading by as much as 5 degrees above that of just THAI (Greaves and Xia; Xia et al.; Greaves and Xia, 2004; Greaves et al.; Greaves et al., 2008b; Hart, 2014a; Hart and Wood, 2018).

In the study conducted by Xia et al. (2002b), the authors investigated the THAI (Toe-to-Heel Air Injection) process as an integrated approach for horizontal wells, enabling the propagation of a stable combustion front through an oil layer. The THAI process operates based on a "short-distance displacement" mechanism, where the oil mobilised ahead of the combustion front is drawn down into the exposed section of the horizontal producer well immediately below. This process leads to the production of thermally cracked heavy oil, contributing to both oil recovery and in-situ upgrading. To examine the dynamics of the THAI process, several 3D combustion cell tests were conducted using Wolf Lake heavy oil with an API gravity of 10.5. The experiments demonstrated consistently stable combustion front propagation through the sandpack at various oil layer thicknesses (0.1m, 0.2m, and 0.4m). The combustion front peak temperature increased with thicker oil layers, reaching 700-800℃. However, increasing the oil layer thickness had minimal impact on oil recovery or the API gravity of the produced oil. Remarkably, the oil recovery remained consistently high, ranging from 80% to 85% of the original oil in place (OOIP). Additionally, the produced oil exhibited a notable increase of 8 API points in gravity and

a significant reduction in viscosity, from 24,400 mPas (20 degrees Celsius) for the original Wolf Lake crude oil to 30 mPas (20 degrees Celsius).

In the study conducted by Tare and Greaves (2002), the authors investigated the effectiveness of the THAI (Toe-to-Heel Air Injection) process as an integrated approach to heavy crude oil recovery and upgrading using horizontal wells. They explored the incorporation of a catalyst layer around the horizontal producer well to create a downhole reactor. Through six catalytic tests, they examined various factors such as catalyst type (NiMo, CoMo), form (extrudate or crushed), and loading. The findings presented by Tare and Greaves (2002) highlighted the stability of the THAI process over a 10-hour period, maintaining average peak combustion temperatures of 500-600 degrees Celsius. Thermal upgrade alone resulted in a significant increase of nearly 10 API points in the produced oil's gravity. The addition of catalytic upgrading (CAPRI) further enhanced the gravity by 4 to 7 API points, demonstrating the potential of this integrated in-situ method to convert heavy crude oil to a lighter, more valuable product directly within the reservoir. Furthermore, the study revealed consistently high oil recoveries (~85% OOIP) and the production of oil with desirable properties, such as a low viscosity of 10 mPas at 20 degrees Celsius. Tare and Greaves (2002) demonstrated the stability of the THAI-CAPRI process when adjusting the air injection rate, and it exhibited improved oil productivity at low water-to-air ratios (WAR$<$1.0). Overall, Tare and Greaves (2002) provide valuable insights into the effectiveness of the THAI-CAPRI process as an efficient and integrated solution for heavy crude oil recovery and upgrading.

Several studies on the catalyst performance during CAPRI have been undertaken at the University of Birmingham. Hart and Wood (2018) investigated the effect of hydrogen on catalyst deactivation. The addition of hydrogen was proven advantageous for oil

upgrading, notably increasing API gravity by 5 degrees compared to the 3 degrees exhibited by nitrogen, especially for oils with an initial API gravity over 13. The impact extended to petroleum distillation yield, with hydrogen at 20 bar pressure yielding 65%, and at 30 bar yielding 71.8%, compared to 40.6% for the original THAI feed oil. Hydrogen also reduces catalyst coking, extending catalyst life and reducing clogging risk. Interestingly, higher hydrogen pressure further reduces coking and slightly improves oil quality. It was found that for every 10-bar increase in hydrogen pressure from 20 bar to 40 bar, a 0.3 API degree increase was observed in the produced oil.

Shah et al. (2011) investigated the impact of operating temperature on catalyst performance. Operating at 500 °C achieved a significant average upgrade of 6.1 °API, but the catalyst's lifespan was limited to 1.5 hours. However, at 420 °C, a more balanced compromise was achieved, yielding an average upgrade of 1.6 °API, occasionally even reaching 3 °API, and extending the catalyst's lifespan to 77.5 hours. Furthermore, it was observed that the CAPRI process displayed relatively limited sensitivity to alterations in gas composition, flow rates, and pressure. This insight suggested that the mechanism driving upgrading reactions might not heavily rely on gas-phase hydrogen or methane dissolution. Through thorough management of temperature and oil flow rates within the in-situ CAPRI process, the potential for additional upgrading compared to the THAI process alone was demonstrated, resulting in the production of more valuable oil with improved transportability characteristics.

## 2.6 STARS for THAI

STARS, the focal simulator, specialises in modelling diverse enhanced recovery methods (steam, solvents, combustion, chemicals) and is an industry leader in accurately simulating kinetic reactions in hydrocarbon recovery. Utilising a grid-based approach, it

solves complex numerical equations, incorporating physical properties to predict fluid behaviour and reservoir performance, aiding engineers in optimising hydrocarbon recovery strategies.

### 2.6.1 Simulation studies of THAI

#### *2.6.1.1 Simulations at laboratory scale*

In this section, laboratory-scale simulations of Toe-to-Heel Air Injection (THAI) technology from the literature are explored in detail. Due to the complex nature of the THAI process and its dependence on various operational parameters, conducting full-scale field pilots can be challenging and expensive. To overcome these limitations, researchers have turned to simulating the extensive laboratory-scale experiments, providing a controlled environment for studying THAI's fundamental mechanisms and optimising its performance. This subsection aims to explore the significance of such simulations and their contributions to understanding THAI technology intricacies. Numerical models used in these simulations are examined. This includes the design of scaled-down THAI reactions, the choice of representative reservoir materials, and the replication of subsurface conditions. Furthermore, delving into the spectrum of measurements and analyses conducted within laboratory-scale experiments includes considerations like temperature profiles, rates of gas and oil production, and characterisation of the combustion front. Through the exploration of laboratory-scale THAI simulations, valuable insights are obtained regarding the behaviour and efficiency of this thermal recovery technique. Such knowledge enhances the understanding of THAI at a fundamental level. It also paves the way for improved design and implementation of this technology in the field.

In their numerical simulation study, Greaves and Xia (2000a) investigate the THAI (Toe-to-Heel Air Injection) process, focusing on two reference physical model experiments using heavy Wolf Lake Oil: one dry combustion test and one wet combustion test. The experiments were conducted in a stable manner, and the authors aimed to determine if this behaviour could be predicted using a numerical model. To create the numerical model, a three-dimensional (3-D) simulation was constructed using the STARS reservoir simulator. The investigation involved four different simulation cases, which were the four iterations of a combination of stable, unstable, wet, and dry combustions. Two model sizes were used, including three base cases with 1000 grid blocks (20 × 10 × 5; x, y, z) and one refined model with 2100 grid blocks (21 × 20 × 10; x, y, z) as seen in Figure 2.7.

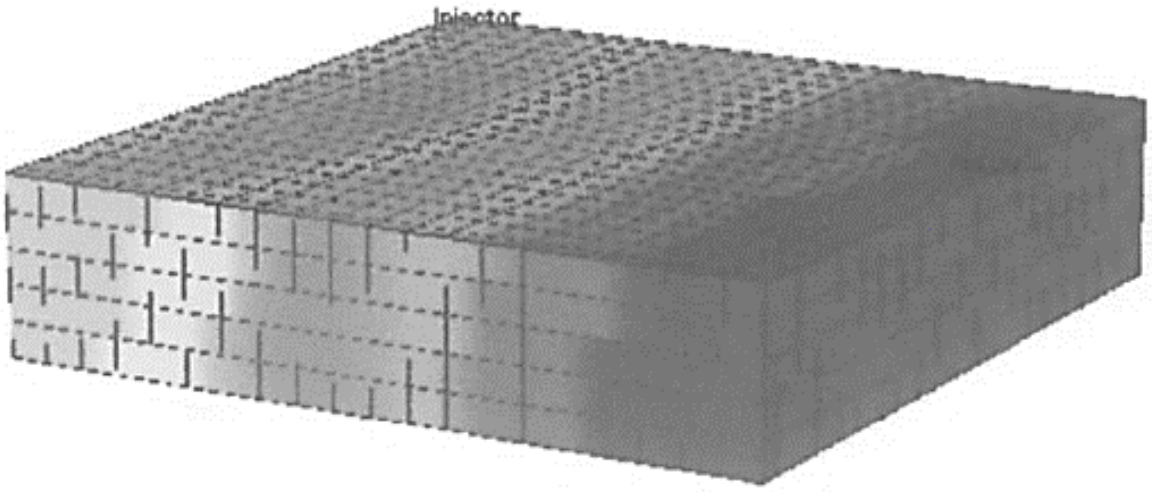


**Figure 2.7.** Grid design for 2100 grid block THAI model from Greaves and Xia (2000a).

The reservoir model consisted of light oil, heavy oil, water, inert gas, oxygen, and coke, with four reaction types: heavy oil cracking, light oil burning, heavy oil burning, and coke burning. The simulation utilised two parallel horizontal wells, one for injection and one for production. Different initial fluid saturations were applied to represent the various phases within the reservoir model, while a constant reservoir temperature of 25°C and

pressure of 290 kPa were maintained. Initially, the predicted results of the numerical model were unstable due to insufficient fuel distribution from the injector well to the horizontal producer well, leading to oxygen breakthrough at the toe of the horizontal well. To address this instability, a sleeve-back modification was introduced to the horizontal well in the dry combustion simulation, resulting in stability. In the wet combustion simulation, the sleeve-back was first used to initiate the process but later removed, maintaining stable combustion front propagation. In a subsequent simulation of the dry combustion experiment, the oil pseudo-component description was enhanced by adding a third component, coke, to match the measured coke residue in the gas-swept zone within the sandpack. The simulation incorporating the coke component yielded a completely stable result, indicating the need for an improved cracking reaction model in the numerical model. The 3-D simulation results demonstrated a highly stable combustion front profile that propagated steadily and completely to the end of the sandpack. The overall oil production from the simulation aligned well with the experimental results, reaching 85% of the original oil in place (OOIP) (Figure 2.8). These findings highlight the numerical model's capability to predict and understand the behaviour of the THAI process. The simulations successfully captured the stable combustion front profile and the high oil production achieved through the THAI process, corroborating the experimental findings. Greaves and Xia (2000a) provide valuable insights into the THAI process, showcasing the potential of numerical simulation in understanding and predicting its behaviour. The study emphasises the importance of achieving stability in the combustion process and highlights the need for an improved cracking reaction model. The results demonstrate the effectiveness of THAI in achieving high oil recovery and a stable combustion front, reinforcing its potential as an advanced in-situ combustion technology for heavy oil recovery.

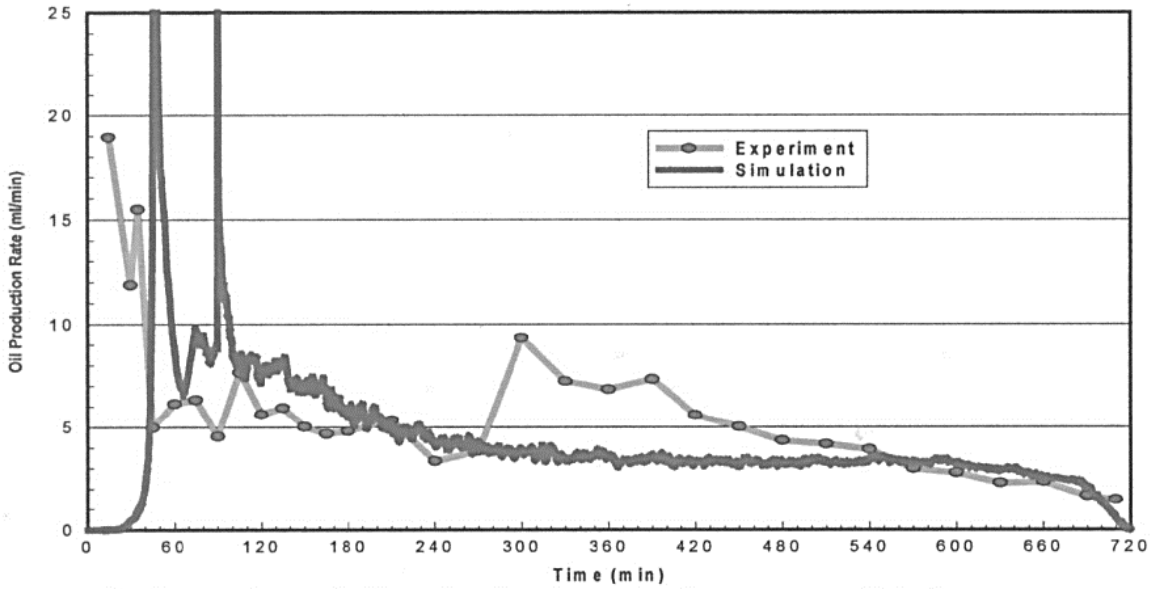


**Figure 2.8.** Simulation matching of lab-experiment for oil rate from Greaves and Xia (2000a).

In a similar manner, Coates and Zhao (2001) conducted a numerical simulation study using the STARS reservoir simulator to investigate the THAI combustion process. Their simulation focused on three groups of reactions: thermal cracking, low-temperature oxidation, and high-temperature oxidation. The thermal cracking reactions involved the conversion of maltenes to asphaltenes, followed by the transformation of asphaltenes into coke and gas. The low-temperature oxidation reactions were similar to cracking reactions but incorporated oxygen on the left-hand side. The high-temperature oxidation reaction entailed the reaction between coke and oxygen to produce water and gas. The study aimed to simulate a lab experiment that had previously been conducted using a cell with dimensions of 40 cm × 20 cm x 10 cm. To achieve computational efficiency, the STARS simulation only modelled half of the cell due to its pattern symmetry. Figure 2.9 shows that the model consisted of 2000 grid blocks (20 x 10 x 10; x, y, z).

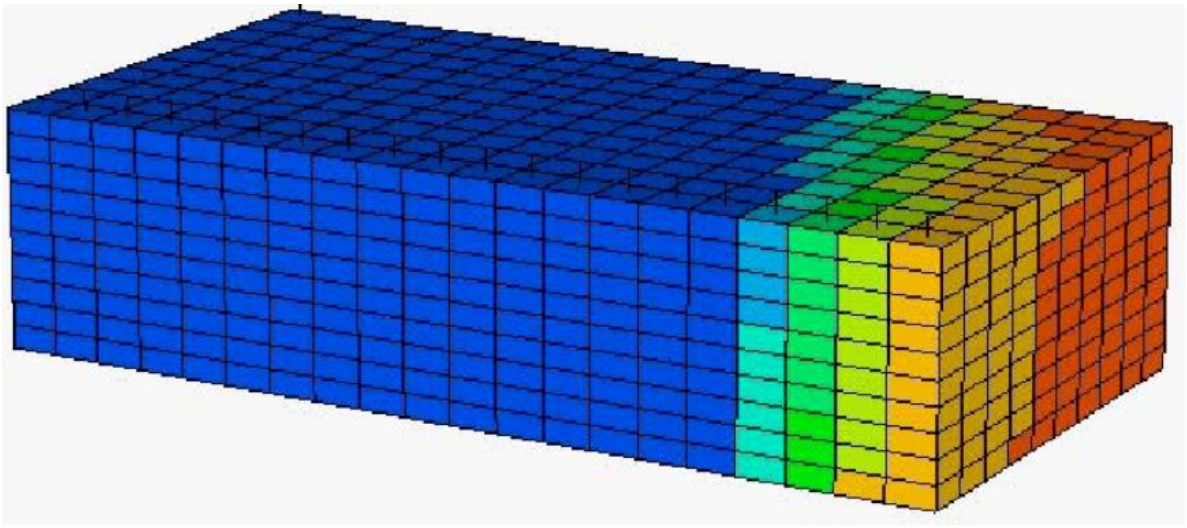

**Figure 2.9.** Diagram of grid block design for lab-scale simulation from Coates and Zhao (2001)

The properties of the heavy oil used in the simulation were based on Lloydminster type heavy oil, which were considered similar enough to the Wolf Lake heavy oil used in the original lab experiment, with the exception of the API gravity, which was known only for the Wolf Lake heavy oil. The findings of the simulation indicated high oil recovery, but the production rates were low. This was attributed to the fact that only the oil immediately ahead of the combustion front was mobilised and produced, with minimal heating or mobilisation of the oil closer to the heel end of the production well. Comparing this study to the previous one by Greaves and Xia (2000a), both studies employed numerical simulations using the STARS reservoir simulator to investigate the THAI process. However, they differed in terms of the reactions considered in the simulation and the specific experimental setups. Coates and Zhao (2001) focused on thermal cracking, low-temperature oxidation, and high-temperature oxidation reactions, while Greaves and Xia (2000a) incorporated heavy oil cracking, light oil burning, heavy oil burning, and coke burning reactions. Furthermore, the two studies used different experimental setups. Greaves and Xia (2000a) conducted physical model experiments with heavy Wolf Lake

Oil, whereas Coates and Zhao (2001) aimed to simulate a previously conducted lab experiment using a smaller cell (Figure 2.10). The grid block configurations also varied, with Greaves and Xia (2000a) utilising 1000 or 2100 grid blocks, and Coates and Zhao (2001) employing 2000 grid blocks. In terms of outcomes, Greaves and Xia (2000a) demonstrated stable combustion front propagation, complete oil recovery, and the need for an improved cracking reaction model. On the other hand, Coates and Zhao (2001) found that although the process at the specific parameters led to high oil recovery, the production rates were low, primarily due to limited mobilisation and heating of the oil towards the heel end of the production well. Both studies contribute to the understanding of the THAI process through numerical simulations. Greaves and Xia (2000a) highlight the stability and high oil recovery achieved through THAI, while Coates and Zhao (2001) emphasise the limitations of the process in terms of oil mobilisation and production rates. These findings provide valuable insights for further optimisation and development of the THAI process for heavy oil recovery.

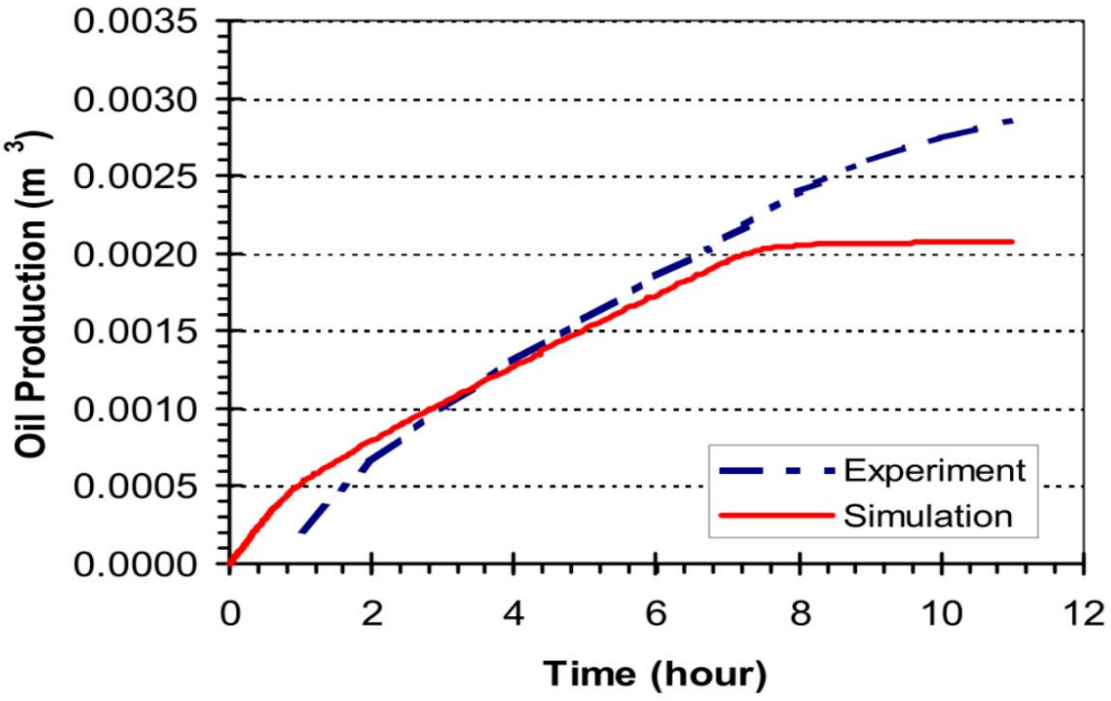


**Figure 2.10.** Simulation matching of lab-experiment for oil production from Coates and Zhao (2001).

### *2.6.1.2 Simulations at field scale*

This section will delve into the realm of field-scale simulations of Toe-to-Heel Air Injection (THAI) technology. Field scale pertains to the spatial scope and measurements used for constructing and implementing simulation models to replicate an actual oil or gas reservoir (Figure 2.11).

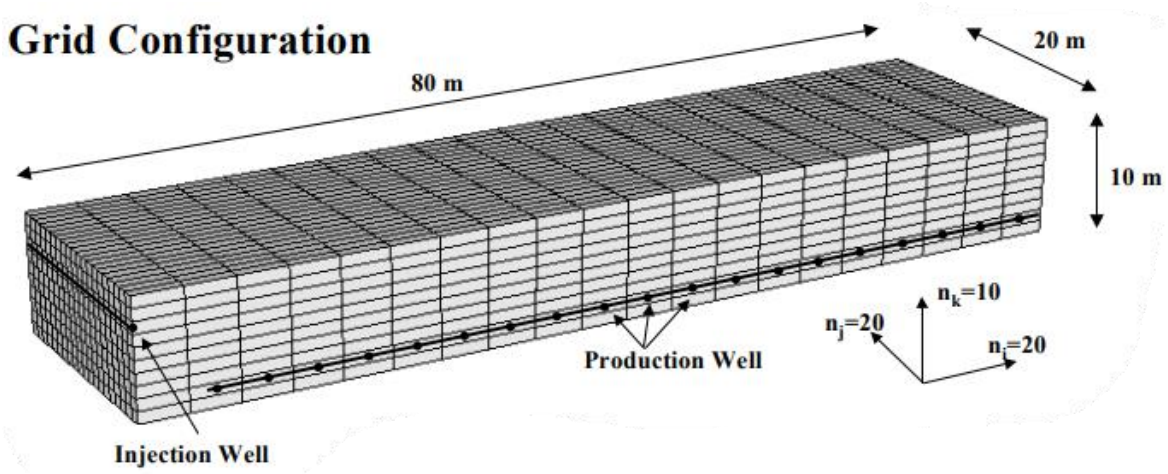


**Figure 2.11.** Example of a field-scale grid block/well model from Coates and Zhao (2001)

While field pilots provide the most accurate representation of real-world conditions, they can be logistically complex, time-consuming, and expensive. To overcome these challenges and gain a deeper understanding of THAI's performance in field settings, researchers have turned to field-scale simulations. This subsection aims to explore the significance of such simulations and their contributions to optimising THAI operations and maximising recovery efficiency. Examining the computational models and reservoir simulators utilised in field-scale THAI simulations allows for the replication of subsurface conditions, fluid flow dynamics, and heat transfer processes. Furthermore, discussing the integration of geologic and reservoir data, encompassing reservoir heterogeneity, fluid properties, and geological structures, guarantees the simulations' accuracy and reliability. Field-scale THAI simulations provide valuable insights into reservoir behaviour, thermal

front propagation, and production performance under different operating conditions. By analysing the results of these simulations, researchers can identify optimal well spacing, injection rates, and production strategies, leading to improved recovery efficiency and economic viability. Furthermore, delving into the challenges and limitations linked to field-scale THAI simulations encompasses considerations such as model calibration, quantification of uncertainty, and the requirement for rigorous validation against real field data. These considerations are crucial in ensuring the reliability and applicability of the simulation results. By harnessing the power of field-scale simulations, we can gain a comprehensive understanding of THAI technology's behaviour in real-world reservoirs. The insights gained from these simulations can inform decision-making processes, guide field operations, and contribute to the continuous advancement and optimisation of THAI as a viable thermal recovery technique.

Kulkarni and Rao (2004) conducted a study to investigate the discrepancies between field-derived correlations and numerical simulation results in the context of the THAI process. Field-derived correlations are empirical relationships established based on observed data from field operations, while numerical simulations involve mathematical models and computational methods to simulate real-world processes. Understanding the differences between these two approaches is crucial for accurately predicting and optimising the performance of the THAI process. The researchers utilised the STARS reservoir simulator to perform numerical simulations and compare the results with field-derived correlations. The objective was to determine the optimal design method for the THAI process by evaluating the agreement between the simulation outcomes and the field data. By identifying any inconsistencies or discrepancies, the study aimed to enhance the reliability and accuracy of the numerical simulations and their predictive capabilities. One of the key areas of focus in the study was the injection of enriched air compared to normal

air and flue gas. Enriched air injection involves modifying the composition of the injected air by increasing the oxygen content. This alteration can affect the combustion characteristics and thermal behaviour of the process, potentially leading to improved oil recovery rates. Through their numerical simulations, Kulkarni and Rao (2004) found that enriched air injection resulted in better oil recovery rates compared to normal air and flue gas injection. The higher oxygen content in enriched air sustained elevated frontal combustion temperatures for a longer duration, enhancing the efficiency of the THAI process. The discrepancies between field-derived correlations and numerical simulation results highlighted by this study indicate the limitations of relying solely on empirical relationships derived from field data. While field-derived correlations provide valuable insights based on real-world observations, they may not capture the complex and dynamic nature of the THAI process accurately. Numerical simulations, on the other hand, offer a more comprehensive and detailed understanding of the underlying physics and mechanisms involved. By comparing the simulation results with field-derived correlations, researchers can identify areas of divergence and gain insights into the factors contributing to the differences (Figure 2.12). Understanding these discrepancies is crucial for advancing the THAI process. By refining the numerical simulation models and improving their agreement with field data, engineers and researchers can develop more accurate predictive tools. This, in turn, enables more effective optimisation of the THAI process design and operational parameters. The findings of Kulkarni and Rao (2004) contribute to the ongoing efforts to bridge the gap between field-derived correlations and numerical simulations, facilitating the development of more reliable and robust techniques for heavy oil recovery using the THAI process.

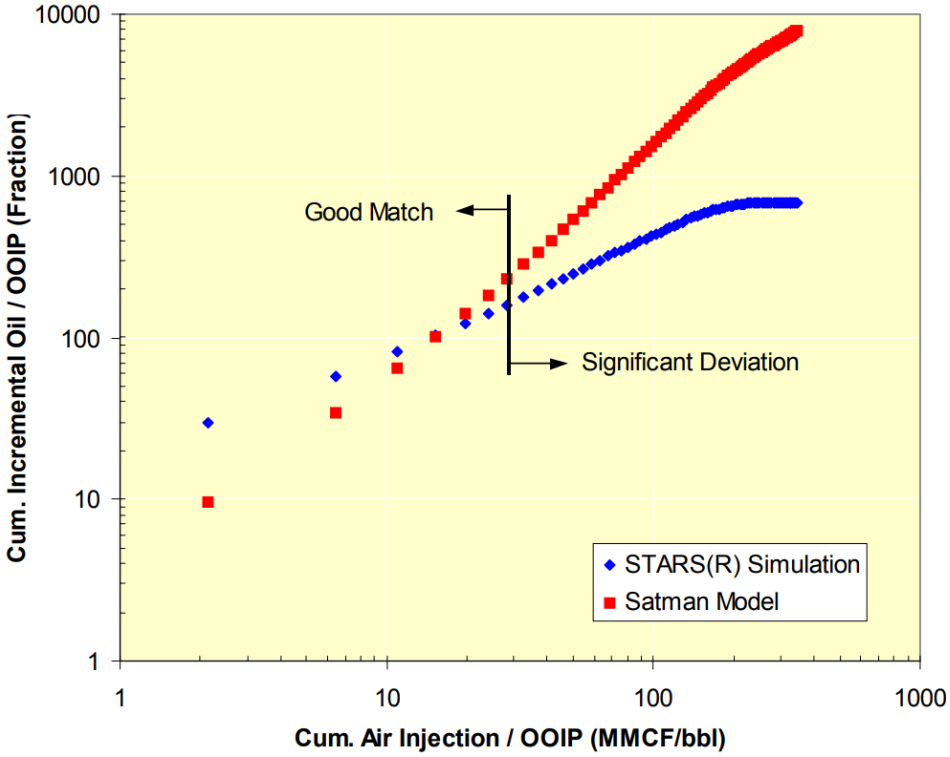


**Figure 2.12.** Analytical (Satman) model predicted vs. simulation oil recovery from Kulkarni and Rao (2004)

In the studies conducted by Greaves et al. (2011a) and Greaves et al. (2012b), the authors focus on the THAI process for heavy oil recovery. While Greaves et al. (2011a) emphasise the successful field piloting of THAI and the development of a numerical model to understand its behaviour, Greaves et al. (2012b) specifically investigate the operational production period of THAI through numerical simulation. Greaves et al. (2011a) discuss the field piloting of THAI by Petrobank in the Athabasca oil sands, highlighting the potential of this advanced in-situ combustion (ISC) technology. They present a novel numerical model that combines three-dimensional combustion cell data with Phillips thermal cracking kinetics. The simulation predictions show excellent agreement with measured parameters, providing insights into the process and the role of the mobile oil zone (MOZ) in producing partially upgraded oil. The study establishes the viability and promise of THAI, validating the field piloting efforts and the accuracy of the numerical model in predicting dynamic behaviour. In contrast, Greaves et al. (2012b) focus on the

operational production period of THAI through numerical simulation of a field-scale section of the Conklin THAI pilot. They investigate the time it takes for oxygen breakthrough into the production well and the factors influencing the termination of THAI operations. The simulation results suggest that oxygen breakthrough occurs after approximately 10.8 years of oil production, during the declining oil production period (Figure 2.13).

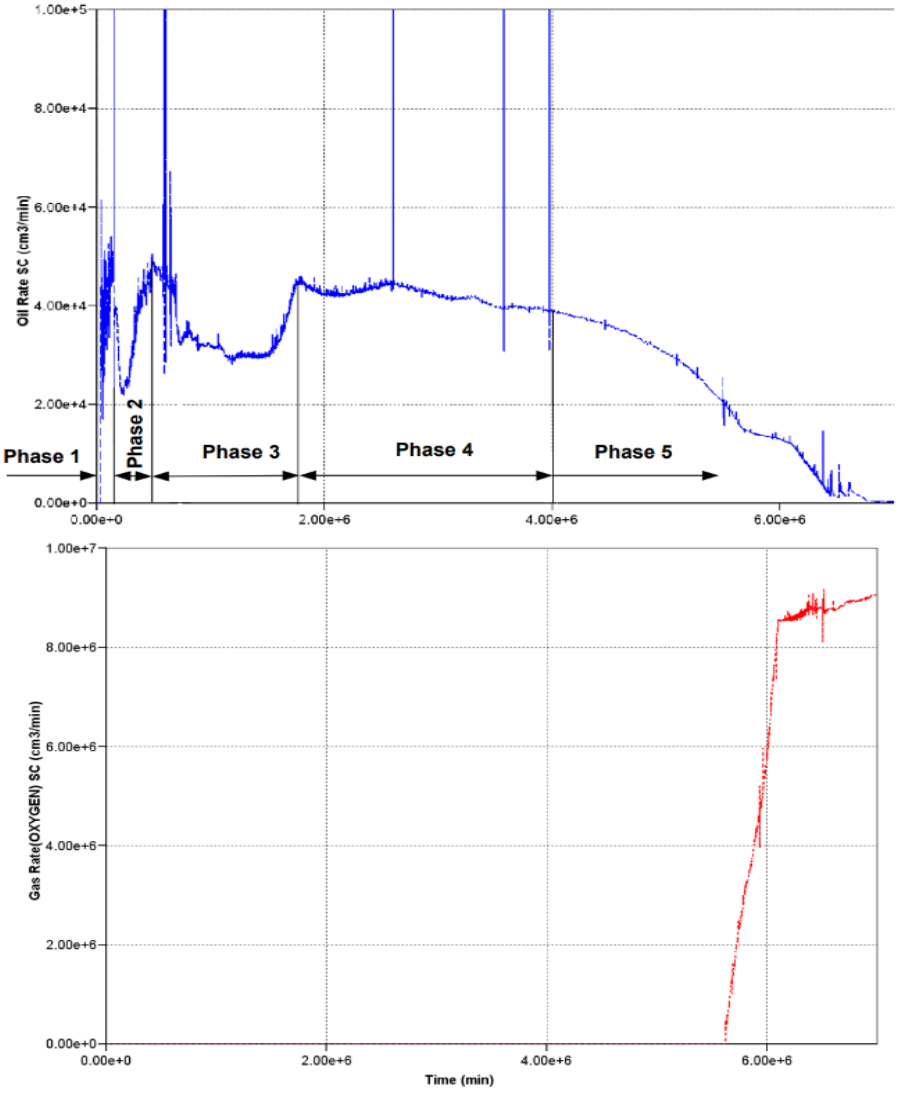


**Figure 2.13.** Oil rate and oxygen production graphs from (Greaves et al., 2012b) displaying oxygen breakthrough occurring after 10.8 years during the declining oil production period.

The study highlights the importance of economic and safety considerations in determining the optimal duration of THAI operations. Longer operation times result in

higher oil recovery but also raise safety concerns, particularly related to oxygen breakthrough. The authors emphasise the need to balance financial returns and total oil recovery, considering the prevailing oil price conditions and associated risks. Both studies contribute to the understanding of the THAI process and its application in heavy oil recovery. Greaves et al. (2011a) provide insights into the behaviour of THAI, the significance of the MOZ, and the accuracy of the numerical model in predicting dynamic parameters. Their findings support the viability and promise of THAI for in-situ upgrading. On the other hand, Greaves et al. (2012a) focus on the operational considerations of THAI, particularly the duration of production and the interplay between economic, safety, and technical factors. Their study highlights the complexities involved in decision-making regarding the termination of THAI operations. By examining both studies concurrently, it becomes apparent that Greaves et al. (2011a) lay the foundation for understanding the behaviour of THAI at Conklin through field piloting and numerical modelling. Greaves et al. (2012a) then build upon this foundation by investigating the operational period and the factors influencing the termination of THAI operations. The studies collectively provide valuable insights into THAI, encompassing its behaviour, potential for in-situ upgrading, and the economic and safety considerations involved in its implementation.

Ado et al. (2018) used STARS to simulate pre-ignition heating cycles (PIHC), air injection flux, and oil viscosity and their impacts on the THAI process stability and operational functionality. The model used a combustion cell from a previous laboratory investigation which was 2.000 cm × 2.105 cm × 1.467 cm (x, y and z) and 30 × 19 × 7 grid blocks, which when converted into a CMG STARS model because 38,000 grid blocks which translates to approximately 63 × 40 × 15 grid blocks. The model had the DYNAGRID option enabled, which allows the model to change grid parameters when certain

conditions are met during simulation in order to reduce simulation time. The petrophysical parameters were 0.85, 0.15 and 34% for oil saturation, water saturation and porosity respectively. The permeability in the i and j direction were both 3450 mD, and the $K_v/K_h$ was 0.3 (meaning permeability in the k direction was 1035 mD). The simulations showed that the use of steam for PIHC resulted in increased oil recovery independent of the arrangement of the wells. The simulations also showed that the THAI process operated more stably in reservoirs containing higher oil viscosities even at higher operating expenditures. This is down to an increase in the cumulative air-oil ratio when compared to reservoirs containing oil with lower a viscosity. Lastly, the study found that to safely and economically operate the THAI process an optimum air injection flux must be determined as the oil recovery increases with air flux in a non-linear manner. Optimum air flux should be determined through simulations in series and finding an appropriate scaling factor.

#### *2.6.1.3 Reaction scheme and kinetics in THAI simulations*

Some studies of the reaction kinetics used within the THAI simulations have been performed (Ado, 2020b; Ado, 2020c) using the Arrhenius equation and the rate equation (Table 2.7). Usually, kinetic studies involve regressing a proposed model to experimental or field data to determine the parameters, goodness of fit and identify the correct model. These are particularly useful as other controls on the method can be studied using laboratory setups such as combustion tubes and sand pack experiments.

**Table 2.7.** Arrhenius Kinetics Assumptions: Key factors for accurate reaction modelling, Arrhenius equation, and rate equation.

| Assumption | Description | Technical Detail |
|---|---|---|
| Arrhenius Equation | $\boldsymbol{k = Ae^{\frac{-Ea}{RT}}}$ | |
| Rate Equation | $\boldsymbol{Rate = k[S]^n}$ | |
| Reaction Types | Types of Reactions | Specify reaction types like combustion, pyrolysis, etc., impacting reaction pathways and model complexity. |
| Species Involved (e.g. [S] | Reactants and Products | List participating species with molecular formulae for balanced equations and stoichiometry. |
| Temperature Range (T) | Range of Temperatures | Define simulated temperature range considering system conditions and Arrhenius equation validity. |
| Activation Energy (Ea) | Activation Energy | Specify energy barrier for transition from reactants to activated complexes. Obtained from experiments or calculations. |
| Pre-exponential Factor (A) | Pre-exponential Factor | Determine collision frequency factor "A" accounting for reactant collisions. From experiments or theory. |
| Reaction Order (n) | Reaction Order | Indicate dependency of reaction rate on reactant concentrations. Determined experimentally. |

Mathematical modeling and simulation are essential for studying the impacts of reaction schemes and kinetics, allowing researchers to analyse the behavior of complex systems and investigate the influence of individual reactions and their rates. For example, adjusting values of the fitted parameters, introducing new reactions, or turning on and off particular reactions to examine their effects. Studies from Ado (Ado, 2020b; Ado, 2020c; Ado, 2022) highlight the importance of the oxidation reaction scheme and associated kinetics concluding that for THAI simulations a more extensive reaction scheme (i.e., a reaction scheme with more reactions) can produce more accurate results. However, the reaction scheme extended only to the oxidation and cracking reactions that occur during ISC. The presence of low-temperature oxidation (LTO) reactions was discovered to have minimal influence on the results of the THAI simulations. This is because the combustion front, which is primarily driven by high-temperature oxidation (HTO), is maintained at a temperature that is less conducive to low-temperature oxidation. Consequently, the only LTO to occur was a result of the minimal oxygen that bypassed the combustion front and reached lower temperature zones.

### 2.6.2 Simulation studies of THAI-CAPRI

Numerical simulation tools, such as reservoir simulators, assist in predicting and optimising the THAI-CAPRI process at various scales. These simulations consider factors such as temperature, pressure, catalyst characteristics, and reservoir properties to model the behaviour and performance of the process (Hasan and Rigby, 2019a). Simulation studies help evaluate the effects of different operating conditions on oil recovery, upgrading efficiency, and overall process economics. Field-scale studies and pilot projects are essential for validating the effectiveness of THAI-CAPRI under real-world conditions. These projects involve the construction and operation of well pairs, where one well serves as the air injection well and the other as the production well. The field data and performance metrics obtained from these projects provide valuable insights into the actual operating conditions, reservoir behaviour, and the economic viability of THAI-CAPRI (Turta et al., 2018).

THAI-CAPRI did not undergo numerical modelling until Hasan and Rigby (2019b) used CMG STARS, a thermal processes reservoir simulation software, to model laboratory scale THAI-CAPRI utilising the co-injection of air/oxygen and hydrogen. The injected hydrogen was used to represent the potential hydrogen produced through reactions such as water-gas shift and coke gasification. Their study investigated the oil recovery potential of THAI-CAPRI under different catalyst packing porosities and hydrogen to air ratios, concluding that increased air-to hydrogen ratios and increased catalyst packing porosity both positively influence the oil recovery of the THAI-CAPRI process. A follow up study (Ado et al., 2022a) again used CMG STARS to numerically model THAI-CAPRI, this time investigating the impact of operating pressure on the process' oil upgrading ability. It was concluded that a higher operating pressure (8000 kPa) produces higher API oils (up to

25 API) and in larger quantities than lower operating pressures (500 kPa) as seen in Figure 2.14.

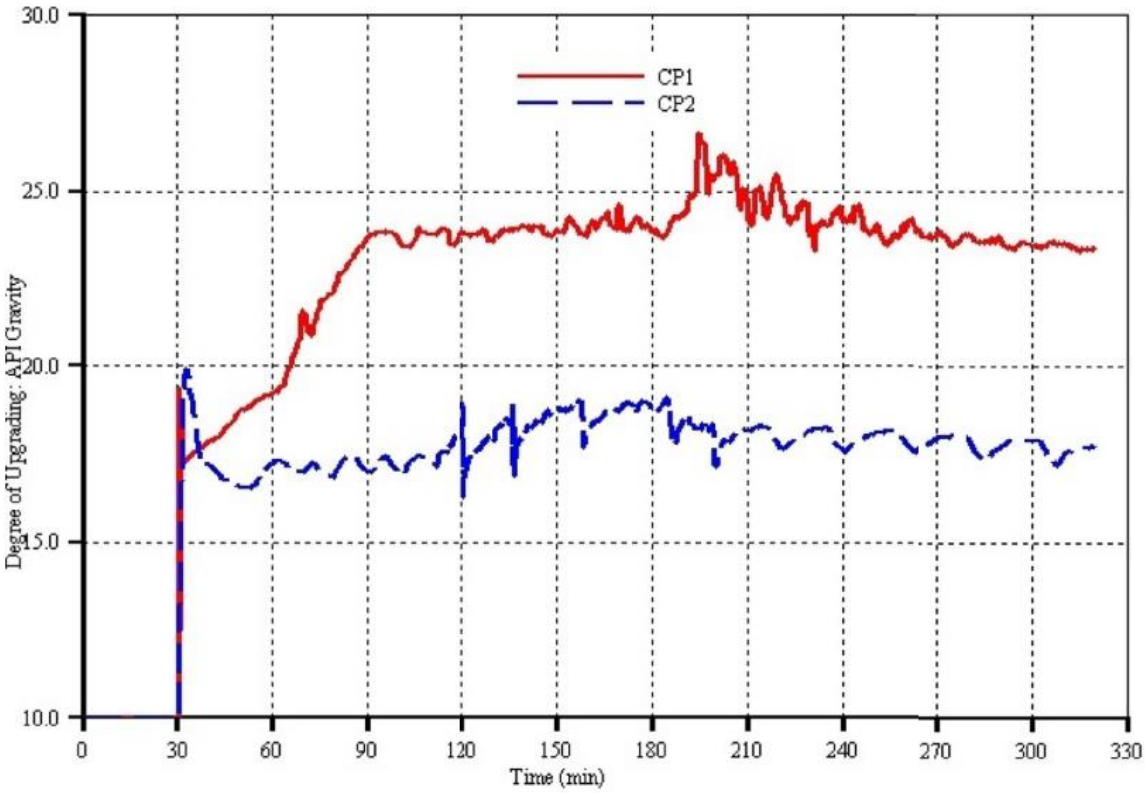


**Figure 2.14.** Effect of operating pressure on API upgrading during simulation study of THAI-CAPRI. CP1 = 8000 kPa. CP2 = 500 kPa. Taken from Ado et al. (2022a).

To fully utilise THAI-CAPRI as a method of heavy oil upgrading and production, it is first necessary to realise its predictive potential using accurate and reliable numerical modelling. Modelling to date has utilised injected hydrogen as a proxy for the hydrogen that would otherwise be created in-situ during the THAI-CAPRI process. However, due to the real-life risks associated with co-injecting oxygen and hydrogen, all hydrogen within the THAI-CAPRI process must originate from reactions occurring in-situ. Using in-situ hydrogen generation reactions for the modelling of the THAI-CAPRI process within a simulation software, such as CMG STARS, has not yet been investigated indicating a novel approach to modelling THAI-CAPRI is necessary.

#### *2.6.2.1 Summary of THAI-CAPRI simulations*

This study highlights the future need for THAI-CAPRI to undergo numerical modelling using hydrogen generation reactions, such as water-gas shift and coke gasification. Employing a novel method of modelling THAI-CAPRI within CMG STARS, which would include hydrogen generation reactions like those found within Kapadia et al. (2011), rather than injected hydrogen. Utilising in-situ generated hydrogen for the catalytic upgrading of heavy oil will result in more accurate upgrading results and a representation that is more aligned with how the process would operate in-situ. This future approach will bridge the gap in knowledge regarding the practical process design between the laboratory testing of CAPRI and the field-scale simulation and potential pilot trial implementation of CAPRI within existing or new THAI projects worldwide.

## 2.7 Hydrogen production during ISC

Existing crude oil reserves have the potential to be converted into hydrogen through in-situ combustion, whereby the combustion-produced carbon monoxide and carbon coke can react with steam to produce hydrogen through the water-gas shift and coke gasification reactions, respectively (Hajdo et al., 1985; Xia et al.; Kapadia et al., 2011). These reactions have been extensively studied in the laboratory, specifically for the optimisation of catalysing the reactions (Karimi et al., 2011; Pal et al., 2018; Reeve et al., 2022). However, this process is highly unknown, and despite being conceptualised over 30 years ago (Hajdo et al., 1985) the techniques for maximising hydrogen (rather than producing it as a byproduct) are largely unexplored and require further research and development. Typical syngas from THAI operations are observed to contain 1-14% hydrogen (Turta et al., 2018; Turta et al., 2023) requiring lots of ex-situ processing to separate it from the other gases to reach the required 99.98% purity for general use. This can typically be achieved through the use of separation technology, such as pressure

swing adsorption, at the surface (Luberti and Ahn, 2022), though some impurities like sulfur would prove difficult to remove (Sanchez et al., 2020).

### 2.7.1 Water-gas shift

The water gas shift reaction is a reversible chemical reaction that releases a moderate amount of heat. It can be expressed by the following equation:

$$CO + H_2O \rightleftharpoons CO_2 + H_2 \quad \Delta H^0_{298} = -41.09\ kJmol^{-1} \qquad (2.19)$$

#### *2.7.1.1 Industrial relevance*

It is an important reaction in various industrial processes, particularly in the production of hydrogen gas and purification of synthesis gas. The water-gas shift reaction is typically carried out at elevated temperatures and with the presence of a suitable catalyst. The insights garnered from laboratory experiments hold significant implications for industrial applications of the WGS reaction. Improved catalyst performance and mechanistic understanding contribute to cleaner hydrogen production, ammonia synthesis, and fuel cell operation. However, challenges related to catalyst deactivation and long-term stability remain areas of active research (Flaherty et al., 2011).

The reaction finds wide applications in industry. One of the primary uses is in the production of hydrogen gas (Chen and Chen, 2020). Hydrogen is a crucial feedstock for various industrial processes, such as ammonia synthesis, petroleum refining, and the production of methanol. The WGS reaction is an essential step in generating high-purity hydrogen gas for these applications. Moreover, the water-gas shift reaction is employed in the purification of synthesis gas, which is a mixture of carbon monoxide, hydrogen, and other gases (Chianese et al., 2015; Chen and Chen, 2020). By removing the excess carbon monoxide through the WGS reaction, the resulting synthesis gas can be used in the

production of various chemicals, such as methanol, dimethyl ether, and higher alcohols (Chianese et al., 2015).

#### *2.7.1.2 Catalyst selection and performance*

Numerous studies have been conducted to explore the catalytic activity of different materials in the WGS reaction. Metal oxides such as iron oxide ($Fe_2O_3$), copper-zinc oxide (Cu-ZnO), and cerium oxide ($CeO_2$) have emerged as prominent candidates due to their surface properties and reactivity (Pal et al., 2018). Researchers have investigated the influence of metal loading, crystalline structure, and redox properties on catalyst performance (Chianese et al., 2015; Pal et al., 2018). The choice of catalyst significantly affects reaction kinetics and product selectivity, motivating extensive experimentation in this area.

#### *2.7.1.3 Reaction Kinetics and Mechanisms*

Detailed kinetic studies have been undertaken to unravel the intricacies of the WGS reaction pathways. Isotopic labelling experiments and rate analyses have provided insights into the sequence of adsorption and surface reactions involved (Tibiletti et al., 2004; Smith et al., 2010). Surface species such as adsorbed CO and formate intermediates have been identified as key players in the reaction mechanism (Burch et al., 2011). These investigations contribute to a deeper comprehension of the elementary steps governing the WGS reaction.

#### *2.7.1.4 Optimisation of reaction conditions*

The ideal operating conditions for this reaction are usually between 200 and 250°C, and 310-450°C, during low-temperature shift and high temperature shift, respectively (Smith et al., 2010). At these temperatures, the reaction rate is significantly enhanced, and the equilibrium shift towards the desired products is achieved, depending on the catalyst

used. It is found that at higher temperatures (<500°C) that $H_2$ is the preferred product, with the concentration of $H_2$ in the production gas increasing at temperature increases throughout that range (Smith et al., 2010). The reaction is not very sensitive to the pressure of the system (Pal et al., 2018). The water-gas shift reaction is a reversible reaction. The reverse reaction, known as the reverse water-gas shift (RWGS) reaction, involves the conversion of carbon dioxide and hydrogen gas into carbon monoxide and water vapor. The reverse reaction can be useful in certain applications, such as carbon dioxide removal (Daza and Kuhn, 2016). The position of the reaction equilibrium is influenced by factors such as temperature, pressure, and concentration. Changes in these factors can lead to shifts in equilibrium, altering the relative concentrations of reactants and products and subsequently affecting the value of the equilibrium constant, shifting the reaction in a different direction.

#### *2.7.1.5 Water-gas shift during in-situ combustion*

During in-situ combustion, air or oxygen is injected into the reservoir, which initiates the combustion of the reservoir's heavy hydrocarbons. In the in-situ combustion process, water vapor and carbon monoxide are produced due to the thermal cracking, oxidation, and gasification of the reservoir fluids (Hajdo et al., 1985). The water-gas shift reaction occurs naturally in the reservoir, facilitated by the high temperatures present ahead of the combustion zone (Hajdo et al., 1985; Greaves and Xia, 2004; Turta et al., 2020; Ado et al., 2022a). As the combustion front advances, the WGS reaction helps in the conversion of carbon monoxide to carbon dioxide and hydrogen, releasing additional energy in the process. This energy release contributes to the heating of the reservoir and sustains the combustion process. Though the reaction is usually catalysed, it is hypothesised that the in-situ generated char can operate as a solid surface catalyst for the reaction (Hobbs et al., 1993).

### 2.7.2 Coke gasification

The coke gasification with steam reaction equation can be written as follows:

$$Coke + H_2O \rightleftharpoons CO + H_2 \quad \Delta H^0_{298} = +131.4\ kJmol^{-1} \qquad (2.20)$$

Coke gasification, with steam, is a chemical process that involves the conversion of coke, a solid carbonaceous material, into a mixture of carbon monoxide (CO) and hydrogen gas ($H_2$) through the reaction with steam.

#### *2.7.2.1 Industry relevance*

This gasification process is widely employed in various industries, including coal gasification and the production of syngas for energy generation and chemical synthesis. The gasification of coke with steam occurs at high temperatures and under controlled conditions. Coke gasification with steam finds extensive industrial application. Syngas produced through coke gasification with steam is primarily utilised for energy generation. It can be burned in power plants to produce electricity or used as a fuel in gas turbines. Additionally, syngas serves as a versatile feedstock for chemical synthesis processes. It can be further processed to produce valuable chemicals such as methanol, ammonia, and synthetic natural gas (SNG) (Roddy, 2013). Coke gasification with steam also plays a crucial role in the production of hydrogen gas (Trommer et al., 2005). Hydrogen gas is used in a wide range of applications, including petroleum refining, ammonia synthesis, and the production of methanol (Rostrup-Nielsen and Rostrup-Nielsen, 2002). The steam gasification of coke provides an efficient method to generate hydrogen gas with high purity.

#### *2.7.2.2 Effect of operating conditions*

The ideal operating conditions for this process typically involve temperatures of >675°C to optimise hydrogen yield (Hajdo et al., 1985; Hobbs et al., 1993). These elevated

temperatures facilitate the desired reactions and maximise the gas yield. Additionally, the process is carried out at lower pressures to enhance the gasification efficiency and hydrogen yield (Trommer et al., 2005; Fermoso et al., 2010), however, these studies used a maximum of 15 bar, well below the 30-50 bar that Xia et al. (2002b) recommend for ISC. The reaction is highly endothermic, requiring a substantial amount of heat energy to drive the process. Thus, a significant heat source is required to maintain the high temperatures necessary for coke gasification.

#### *2.7.2.3 Catalysts in Coke Gasification*

The role of catalysts in coke gasification has been extensively explored in laboratory settings. Catalysts, such as metal oxides and supported metals, influence gasification rates and product selectivity (Grigore et al., 2009; Chianese et al., 2015) . Studies have examined the interaction between coke and catalyst surfaces, shedding light on the promotion of gasification reactions and suppression of undesired side reactions (Karimi and Gray, 2011; Bai et al., 2018). These insights aid in designing catalysts for enhanced coke gasification performance.

#### *2.7.2.4 Coke gasification during in-situ combustion*

In the context of in-situ combustion for heavy oil and bitumen recovery, coke gasification with steam can occur as a secondary reaction. During the in-situ combustion process, when air or oxygen is injected into the reservoir, the high temperatures and oxygen content can lead to the partial combustion and transformation of heavy hydrocarbons into coke (Greaves and Xia, 2004; Hart et al., 2014). In the subsequent stages of the in-situ combustion process, steam injection is often introduced to enhance reservoir pressure and provide additional heat to mobilise the remaining heavy hydrocarbons. The steam reacts with the residual coke, leading to the gasification of coke and the release of

carbon monoxide and hydrogen gas. The generated carbon monoxide gas can participate in further reactions, such as the water-gas shift reaction, to generate additional hydrogen (Greaves and Xia, 2004; Turta et al., 2020).

### 2.7.3 Experimental work on hydrogen production during in-situ combustion

In this section, the focus is on experimental work related to hydrogen production during In-Situ Combustion (ISC) processes. It covers studies that have been conducted in laboratory settings to investigate the generation and behaviour of hydrogen during ISC. The findings from various experimental studies are summarised, providing insights into the potential for hydrogen production as a byproduct of ISC.

A laboratory investigation by Martin et al. (1958) was conducted to assess the viability ISC as an enhanced oil production method. However, during their investigation they found that hydrogen gas was produced as a result of the combustion process. They did not report any gas compositions or hydrogen fractions within the gas, but they did find that as the combustion temperature and air flux at the front are increased (>315℃), the quantity of hydrogen linked to the carbon burned through in situ combustion declines. More recently, Afanasev et al. (2021) conducted an autoclave experiment on Catalytic Methane Conversion (CMC), whereby the effects of methane in-situ combustion were replicated in the presence of steam and a Ni-based catalyst at 450°C. It was found that the maximum methane to hydrogen conversion at those conditions was 5.8%. The hydrogen fraction in the produced gas was found to be in the range of 18.5-33.9%, dependent on the rate of steam injection.

### 2.7.4 Field Trials of Hydrogen Production from THAI

Several ISC/THAI field trials have reported hydrogen gas within their produced gas stream, at varying fractions. After a full survey of the available literature, no field trial

using air injection for the purpose of generating in-situ hydrogen has ever occurred. The closest to a hydrogen generation field trial was reported by Hajdo et al. (1985) who wrote about the hydrogen generation potential at Marguerite Lake during their field trial of CSS followed by ISC. Resultantly, Kapadia et al. (2013) report this field trial to be both a trial of CSS/ISC and In-Situ Gasification (ISG). The hydrogen production at Marguerite Lake was reported to be as high as 25 mol%, averaging around 15%. Hajdo et al. (1985) report that the primary mechanism for hydrogen generation at the Marguerite Lake pilot is the coke gasification reaction (involving steam and coke), which leads to the creation of $H_2$ and CO. Subsequently, the water-gas shift reaction further contributes to the production of hydrogen. Other ISC/THAI field trials report much lower fractions of hydrogen in the produced gas, usually ranging from 1-14% (Turta et al., 2018; Turta et al., 2023), with most THAI wells experiencing >3% hydrogen. The noticeable difference between the average THAI setup and the Marguerite Lake process, is the use of intermittent steam injection. The steam enters a reservoir which is at an elevated temperature due to the previous air injection cycle, and reacts with the coke, producing hydrogen.

### 2.7.5 STARS Simulations

Kapadia et al. (2011) built a new kinetic model which was developed to examine the potential for hydrogen generation from Athabasca bitumen, the same bitumen that is found at Marguerite Lake. The kinetic model consisted of thermal cracking, oxidation/combustion, hydrogen generation, and hydrogen consumption reactions (Figures 2.16a, 2.16b and 2.17). A comparison of the simulation results and experimental data from the published literature revealed that the new model could accurately predict hydrogen generation from the gasification of methane, Athabasca bitumen, and coke. To further build on the hydrogen production at Marguerite Lake, Kapadia et al. (2013) used the field data to generate a reservoir simulation model within CMG STARS using the

previously produced reaction scheme (Kapadia et al., 2011). Using the novel reaction scheme, they performed several simulations on a reservoir model of Marguerite Lake and found that optimal hydrogen production is achieved in regions characterised by minimal oxygen content due to the utilisation of ISC to attain the required high gasification temperatures. To maximise hydrogen output, strategic positioning of the producer well relative to the injection well becomes imperative. It is crucial to devise a recovery process that effectively prevents hydrogen and oxygen mingling within the reservoir.

Intermittent oxygen injection, unlike continuous injection, can augment hydrogen production. This bears similarity to the cyclic steam and air injection techniques employed in in situ coal gasification procedures (Bhutto et al., 2013). Oxygen injection results in an escalation of the combustion zone temperature, followed by oxygen depletion upon injection cessation. Any hydrogen generated during this interval is also susceptible to consumption. As a result, in the aftermath of the combustion phase, as temperatures remain elevated, hydrogen-generating reactions persist, enabling substantial hydrogen generation. Over time, as the temperature subsides to the level of injected steam, the hydrogen generation capability deteriorates. Considering economic factors, the resumption of air injection can be considered to raise the temperature within the system.

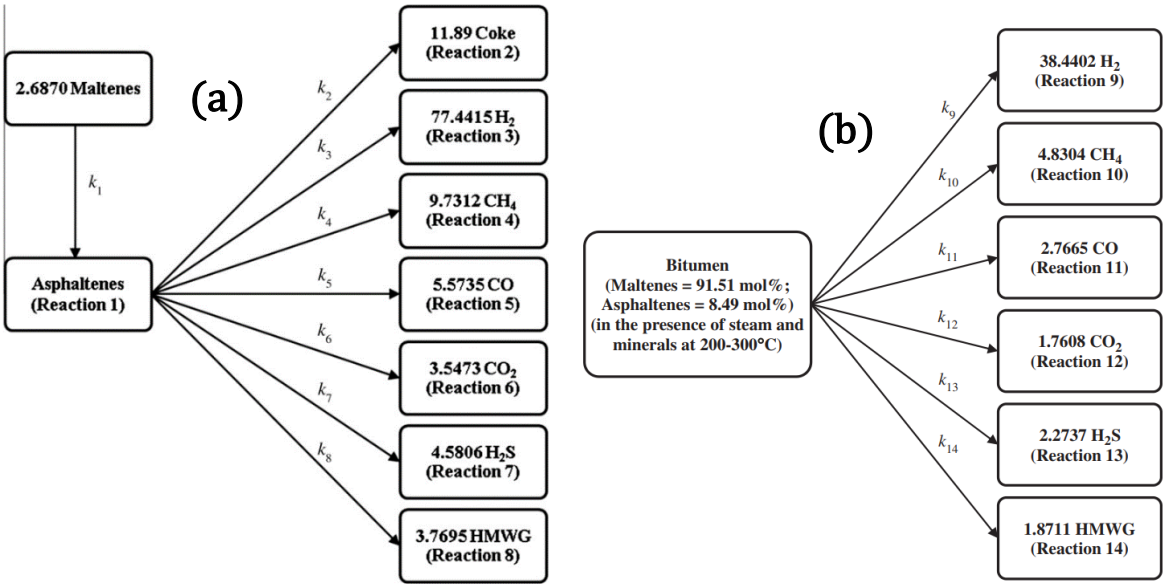


**Figure 2.15a.** (left) Flow chart depicting Bitumen pyrolysis reaction scheme, and **2.15b.** (right) Bitumen aquathermolysis reactions scheme. Bitumen consists of pseudo-components Maltenes and Asphaltenes. Taken from Kapadia et al. (2013).

Turta et al. (2020) also used this reaction scheme to calculate the quality of burning during the THAI process at Kerrobert, using coke gasification and WGS reactions as primary hydrogen production pathways, and calculating the non-oxidation generated $CO_2$, and therefore the apparent hydrogen-carbon (H/C) ratio of the generated gas. The hydrogen-to-carbon (H/C) ratio is commonly employed as an indicator of combustion quality, with high levels of carbon dioxide ($CO_2$) typically generated during the process. However, a conventional assumption that attributes all $CO_2$ production to combustion can lead to a misleadingly low H/C value.

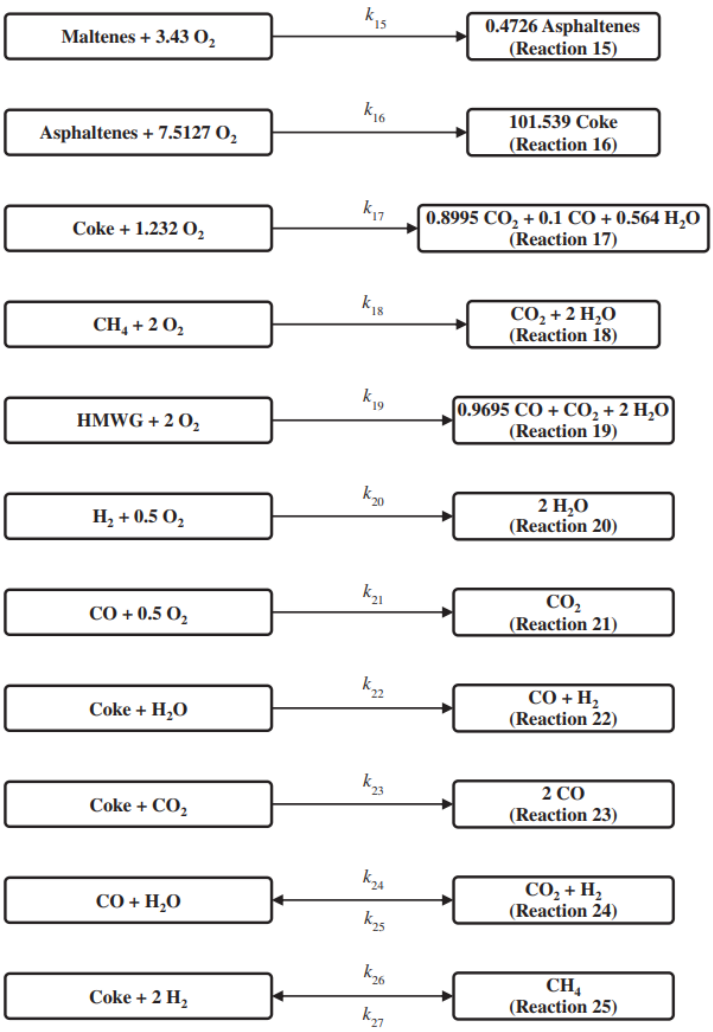


**Figure 2.16.** Bitumen low temperature oxidation (Reactions 15 and 16), high temperature oxidation (Reactions 17–21), coke gasification (Reactions 22 and 23), water gas shift (Reaction 24), and methanation (Reaction 25) reactions. Taken from Kapadia et al. (2013).

To address this limitation, Turta et al. (2020) investigated the $CO_2$ and $H_2$ fractions within the Kerrobert produced gas stream, enabling them to determine the proportion of $CO_2$ originating from combustion versus hydrogen generation reactions. Their findings revealed that disregarding the $CO_2$ generated through these reactions would inaccurately portray the burning quality as superior to what could realistically be expected. By incorporating these additional $CO_2$ sources, a more comprehensive assessment of burning quality can be obtained, avoiding misinterpretations based solely on H/C ratios.

### 2.7.6 Summary of THAI simulations for hydrogen

This section provides an overview of experimental work, field trials, and STARS simulations related to hydrogen production during In-Situ Combustion (ISC) processes. The experimental studies highlighted hydrogen gas production during combustion, with varying fractions observed based on temperature, air flux, and steam injection rate. However, detailed gas compositions and hydrogen fractions were lacking in some studies, suggesting a need for further investigation. Field trials revealed hydrogen gas presence in the produced gas stream. The Marguerite Lake trial reported higher hydrogen production through coke gasification and water-gas shift reactions (Hajdo et al., 1985). Other ISC/THAI field trials generally reported lower hydrogen fractions, emphasising the importance of intermittent steam injection for hydrogen generation (Turta et al., 2018). STARS simulations demonstrated the accuracy of a kinetic model in predicting hydrogen generation from Athabasca bitumen (Kapadia et al., 2011; Kapadia et al., 2013). This enabled the assessment of optimal hydrogen production regions and the strategic positioning of injection and production wells. Additionally, the incorporation of $CO_2$ sources in assessing burning quality highlighted the need to consider hydrogen generation reactions alongside combustion (Turta et al., 2020).

Future research opportunities involve conducting comprehensive simulation studies to investigate the impact of specific reactions on hydrogen production during ISC processes. One significant gap that can be addressed is the contribution of coke gasification and the WGS reaction to hydrogen generation during THAI. By conducting reservoir simulations with varying reaction schemes, the potential for these reactions to produce $H_2$ can be assessed and better understood. This research will optimise hydrogen production during ISC processes. Future studies should also emphasise the investigation on the influence of water-gas shift and coke gasification reactions and their kinetics on the overall behaviour

of the THAI process. By incorporating these reactions into simulation models, researchers can gain a more comprehensive understanding of complex interactions occurring during in-situ combustion. This, in turn, will contribute to the development of more precise predictive models and facilitate THAI optimisation for enhanced oil recovery.

# CHAPTER 3. MODEL DEVELOPMENT

In this chapter, the development of comprehensive simulation models for toe-to-heel air injection in CMG STARS is presented. The study begins with an exploration of the software framework, providing an overview of CMG STARS, its capabilities, and its relevance to modelling subsurface processes. Subsequently, this chapter delves into the fundamental governing equations that underpin the toe-to-heel air injection process, explaining the theoretical foundation upon which the simulation model is built. Furthermore, an in-depth discussion of the simulation model inputs, encompassing parameters and boundary conditions, is presented, outlining their pivotal roles in accurately representing the complex dynamics of this injection technique within the reservoir.

## 3.1 Computer Modelling Group (CMG) software suite

The CMG reservoir engineering suite (Figure 3.1) provides a range of software including IMEX (black oil and unconventional simulation), GEM (compositional and unconventional simulation) and STARS (thermal and advanced process simulation). It also hosts WinProp which allows the user to create customised fluid property descriptions from laboratory or experimental work to use within simulations.

The software suite also contains a pre-processor called ‘builder’ in which the reservoir and simulation model is created, allowing the user to input certain geological, petrophysical and geophysical variables along with production and injection parameters. Post-processing tools include ‘results’ and ‘CMOST’ allow further processing of the simulations to occur after running them through the simulators. ‘Results’ simply allows for the visualisation and analysis of the outcomes of the simulation runs. CMOST uses artificial intelligence to allow for fast machine learning of history matching, risk management and optimisation tools.

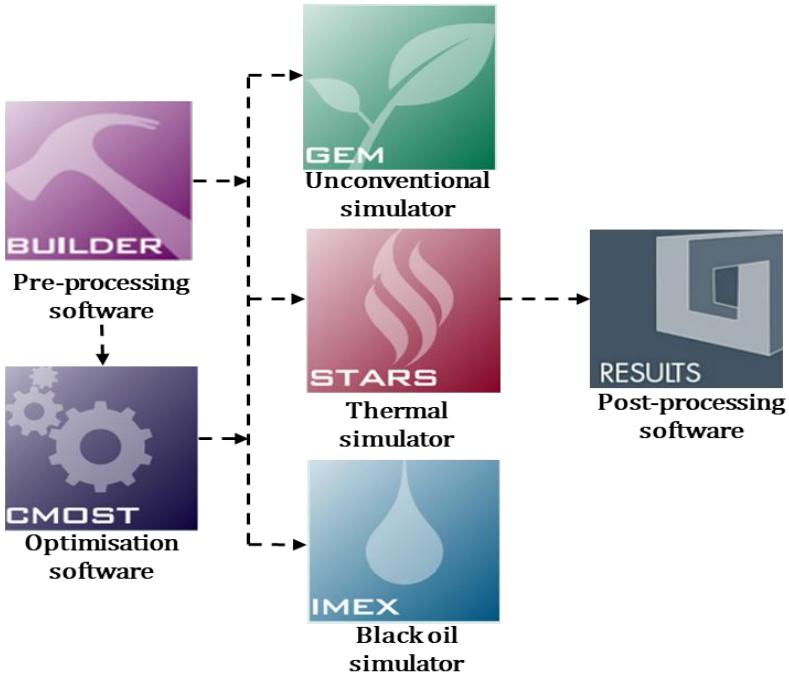


**Figure 3.1.** Flow diagram of CMG software suite

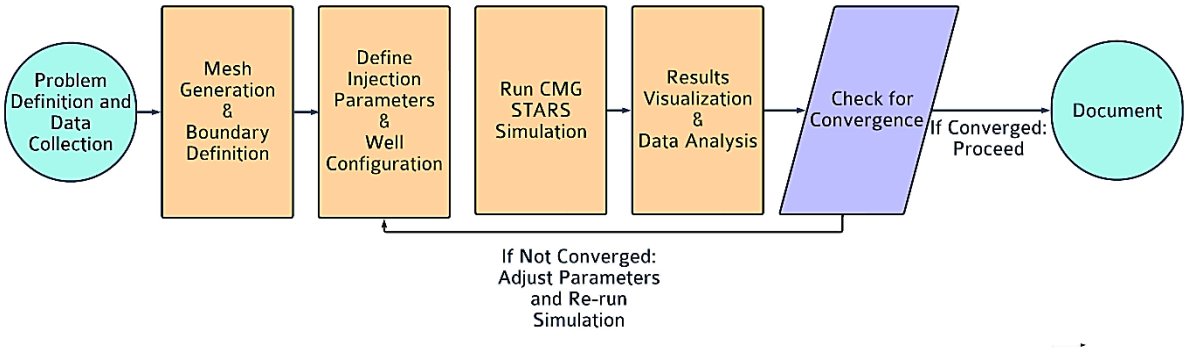


**Figure 3.2.** Flow diagram of CMG STARS modelling and simulation workflow

STARS is the simulator that will be the focus of this study, using its advanced modelling of enhanced recovery processes, especially those that use steam, solvents, air (combustion) and chemicals. It is the industry standard for modelling kinetic reactions in the context of hydrocarbon recovery, allowing users to model thermal recovery with complex wellbore designs. STARS was chosen as the primary simulation platform for modelling toe-to-heel air injection due to its tailored strength in handling complex thermal and compositional processes within the subsurface. Specifically designed for thermal recovery methods like steam-assisted gravity drainage (SAGD) and cyclic steam stimulation (CSS), STARS offers

an extensive suite of features that align with the intricacies of toe-to-heel air injection simulations. Notably, its advanced thermal compositional modelling capabilities allow for a detailed representation of multiphase fluid flow and thermal effects in heterogeneous reservoirs. While acknowledging the prominence of industry-standard simulators like tNavigator by Rock Flow Dynamics and Eclipse by Schlumberger, CMG STARS stands out due to its specialised focus on thermal processes and intricate compositional modelling. Furthermore, STARS distinguishes itself by offering the capability to integrate thermal reactions such as combustion into its models, enabling a more comprehensive representation of the complex thermal processes involved in toe-to-heel air injection—an aspect that sets it apart from other simulators like tNavigator by Rock Flow Dynamics and Eclipse by Schlumberger, which possess comparable built-in features for incorporating such intricate thermal reactions, but are not designed with these processes being prioritised.

STARS employs a grid-based approach to discretise the reservoir domain, enabling it to solve numerical flow and reaction equations governing fluid flow, heat transfer, and mass transport within the reservoir. It incorporates a physical property package that includes essential data like fluid properties, rock properties, and phase behaviour information. This enables accurate modelling of fluid behaviour under various pressure and temperature conditions. CMG STARS employs a comprehensive approach to address intricate reservoir characteristics, such as heterogeneity, anisotropy, and fractures, which significantly influence reservoir performance. The software integrates advanced modelling techniques to account for heterogeneous reservoir structures, capturing variations in properties across the reservoir. Moreover, it incorporates features to simulate anisotropic behaviour, acknowledging directional variations in properties such as permeability and porosity. Additionally, CMG STARS facilitates the modelling of

fractures, enabling a detailed representation of their impact on fluid flow, pressure distribution, and overall reservoir behaviour. These functionalities within CMG STARS allow for a more nuanced and accurate depiction of real-world reservoir complexities, contributing to a comprehensive evaluation of reservoir performance. Through its iterative simulation process, STARS provides insights into fluid movement, production rates, and overall reservoir behaviour, aiding reservoir engineers in making informed decisions for optimal hydrocarbon recovery strategies.

## 3.2 Model Development Objectives

The development of a robust and accurate reservoir simulation model for in-situ combustion within CMG STARS requires clear objectives to guide the research and ensure meaningful contributions to the field. This subsection outlines the specific objectives of the model development work and highlights the significance and potential impact of the research.

The primary objective of this study is to develop a comprehensive and reliable CMG STARS model for simulating THAI in-situ combustion processes in heavy oil reservoirs. The model will aim to capture the intricate interactions between fluid flow, heat transfer, and chemical reactions occurring during the combustion process. By incorporating the governing equations and appropriate numerical methods, the model will provide insights into the propagation and behaviour of the combustion front, the distribution of temperature and pressure, and the displacement of fluids within the reservoir.

Furthermore, this research aims to address key challenges and limitations associated with existing THAI modelling approaches. By focusing on model development within CMG STARS, this study seeks to overcome certain limitations such as the neglect of important physical phenomena or simplifications made in previous models. The objective is to

enhance the accuracy and reliability of in-situ combustion simulations, enabling better predictions and decision-making in practical reservoir engineering applications.

In addition to model development, this research also aims to contribute to the understanding of the fundamental processes governing THAI. By conducting sensitivity analyses and validation against experimental or field data, the developed CMG STARS model will provide insights into the sensitivity of key parameters, the reliability of predictions, and the uncertainties associated with in-situ combustion simulations. This knowledge will help improve the understanding of the underlying mechanisms and facilitate the optimisation of in-situ combustion strategies for enhanced oil recovery.

The significance of this model development work lies in its potential to advance the field of in-situ combustion reservoir simulation. By developing a reliable CMG STARS model, this research can contribute to the industry's ability to design and optimise in-situ combustion projects, reduce operational risks, and increase oil recovery efficiency. Moreover, the insights gained from this study can serve as a foundation for future research and development of advanced simulation tools and methodologies for in-situ combustion processes.

## 3.3 Governing Equations and Numerical Methods

The development of an accurate and reliable CMG STARS model for in-situ combustion requires the formulation of appropriate governing equations and the selection of suitable numerical methods to solve these equations. This subsection presents the governing equations that describe the fluid flow, heat transfer, and reactive transport processes in in-situ combustion. It also discusses the numerical methods employed within CMG STARS to solve these equations and simulate the in-situ combustion phenomena.

The CMG STARS model for in-situ combustion involves several governing equations that describe the fluid flow, heat transfer, and reactive transport processes within the reservoir. These equations are derived from fundamental principles and capture the essential physical phenomena occurring during in-situ combustion. This project aims to comprehensively model the intricate dynamics of THAI within a homogenous reservoir model utilising geological and petrophysical parameters from literature. The core equations governing this process involve multiphase flow and combustion phenomena. The fundamental equations include the mass conservation equations for each phase (oil, air, water), momentum conservation equations accounting for pressure gradients and interfacial forces, energy conservation equations to represent heat transfer due to combustion, and species transport equations for tracking chemical species involved in combustion reactions.

### 3.3.1 Governing Equations

These equations are critical as they track the transport of chemical species (e.g., oxygen, hydrocarbons) and their reaction rates, providing insights into the progress and dynamics of combustion reactions occurring during toe-to-heel air injection simulations. These equations collectively form the basis for understanding the movement, distribution, energy transfer, and chemical reactions crucial for accurate numerical simulations of toe-to-heel air injection processes in reservoirs. These equations form the backbone of our simulation, capturing the dynamic interactions between fluid flow, heat transfer, and chemical reactions during the THAI process.

#### *3.3.1.1 Mass Conservation*

The mass conservation equations for each phase (oil, air, water) in the reservoir are crucial in numerical simulations of toe-to-heel air injection. These equations are essential

as they describe the change in mass for each phase over time due to flow, providing insights into phase behaviour, movement, and distribution during toe-to-heel air injection simulations The following equation represents a comprehensive model describing the change in various components within different phases and the porous medium over time for flowing component i. It considers factors such as densities, porosities, saturations, diffusion, production rates, and changes in porosity associated with specific components in different fluid phases within a porous medium or reservoir.

$$V\frac{\partial}{\partial t}\left[\varphi_f\left(\rho_w S_w w_i + \rho_o S_o x_i + \rho_g S_g y_i\right) + \varphi_v A d_i\right]$$
$$= \sum_{k=1}^{n_f}\left[M_w \rho_w w_i \Delta\emptyset_w + M\rho_o x_i \Delta\emptyset_o + M_g \rho_g y_i \Delta\emptyset_g\right] + V\sum_{k=1}^{n_r}(s_{ki} - s_{ki})i_k$$
$$+\sum_{k=i}^{n_r}\left[\phi D_{wi}\rho_w \Delta w_i + \phi D_{oi}\rho_o \Delta x_i + \phi D_{gi}\rho_g \Delta y_i\right] + \delta_{iw}\sum_{k=1}^{n_f}\rho_w q a q_{wk}$$
$$+\rho_w q_{wk} w_i + \rho_o q_{ok} x_i + \rho_g q_{gk} y_{i\,[well\ layer\ k]} \qquad (3.1)$$

The following equation represents a comprehensive model describing the change in various components within different phases and the porous medium over time for solid component i:

$$\mathrm{V}\frac{\partial}{\partial t}[\varphi_v c_i] = +V\sum_{k=1}^{n_r}(s_{ki} - s_{ki})i_k \qquad (3.2)$$

### *3.3.1.2 Heat Conservation*

The following equation represents a conservation equation for heat within a porous medium or control volume. It accounts for changes in internal energies and enthalpies of different phases (water, oil, gas) and solid components over time, considering thermal conductivities, changes in porosity, temperature differences, heat production rates, enthalpy changes due to reactions, and heat loss or gain terms within the system:

$$V\frac{\partial}{\partial t}\left[\varphi_f\left(\rho_w S_w U_w + \rho_o S_o U_o + \rho_g S_g U_g\right) + \varphi_v c_s U_s + (1 - Q_v)U_r\right]$$

$$= \sum_{k=1}^{n_f}\left[T_w \rho_w H_w \Delta\emptyset_w + T_o \rho_o H_o \Delta\emptyset_o + T_g \rho_g H_o \Delta\emptyset_g\right] + V\sum_{k=1}^{n_f} K\Delta T$$

$$+\rho_w q_{wk} H_w + \rho_o q_{ok} H_o + \rho_g q_{gk} H_{g\,[well\ layer\ k]}$$

$$+\sum_{k=i}^{n_r}[H_{rk} r_k + HL_o + HL_v + HL_c] + \sum_{k=1}^{n_f}(HA_{CV+}HA_{CD})_k \qquad (3.3)$$

### *3.3.1.3 Darcy's Law for Flow in Porous Media*

Darcy's Law describes the flow of fluids through a porous medium, stating that the flow rate of a fluid is directly proportional to the pressure gradient within the medium. Mathematically, the equation in the flowing direction $x$can be represented as:

$$v_x = \frac{kk_r}{\mu}\frac{\partial \phi}{\partial x} \qquad (3.4)$$

### *3.3.1.4 Species Transport Equation*

The species transport equations are vital for modelling the movement and interaction of various chemical species involved in combustion reactions during toe-to-heel air injection simulations. A generalised form of the species transport equation can be expressed as:

$$\frac{\partial(\rho_i Y_i)}{\partial t} + \nabla \cdot (\rho_i v Y_i) = R_i \qquad (3.5)$$

**Table 3.1.** Breakdown and explanation of governing equation terms.

| Equation | Term | Description |
|---|---|---|
| 3.1 | $V\frac{\partial}{\partial t}\left[\varphi_f\left(\rho_w S_w w_i + \rho_o S_o x_i + \rho_g S_g y_i\right) + \varphi_v A d_i\right]$ | Time derivative of fluid-phase volume fraction, including densities and saturations of water, oil, gas, and vapor. |
| | $\sum_{k=1}^{n_f}\left[M_w\rho_w w_i\Delta\emptyset_w + M_o\rho_o x_i\Delta\emptyset_o + M_g\rho_g y_i\Delta\emptyset_g\right] + V\sum_{k=1}^{n_r}(s_{ki} - s_{ki})i_k$ | Summation over fluid phases, including terms related to transient flow and differences in phase saturations and properties + summation over rock types, considering differences in saturation and properties. |
| | $\sum_{k=i}^{n_r}\left[\phi D_{wi}\rho_w\Delta w_i + \phi D_{oi}\rho_o\Delta x_i + \phi D_{gi}\rho_g\Delta y_i\right] + \delta_{iw}\sum_{k=1}^{n_f}\rho_w q a q_{wk}$ | Summation over rock types, including terms related to dispersion/diffusion of fluid phases within the rock matrix. |
| | $\rho_w q_{wk} w_i + \rho_o q_{ok} x_i + \rho_g q_{gk} y_{i\,[well\ layer\ k]}$ | Injection of fluid into the reservoir through well |
| 3.2 | $\mathrm{V}\frac{\partial}{\partial t}[\varphi_v c_i]$ | Time derivative of the vapor-phase volume fraction multiplied by the vapor density and vapor concentration. |
| | $V\sum_{k=1}^{n_r}(s_{ki} - s_{ki})i_k$ | Summation over rock types, representing the change in vapor saturation within each rock layer due to injection. |
| 3.3 | $V\frac{\partial}{\partial t}\left[\varphi_f\left(\rho_w S_w U_w + \rho_o S_o U_o + \rho_g S_g U_g\right) + \varphi_v c_s U_s + (1 - Q_v)U_r\right]$ | Time derivative of total internal energy within the porous medium, including contributions from fluid phases and vapor. |
| | $\sum_{k=1}^{n_f}\left[T_w\rho_w H_w\Delta\emptyset_w + T_o\rho_o H_o\Delta\emptyset_o + T_g\rho_g H_o\Delta\emptyset_g\right] + V\sum_{k=1}^{n_f}K\Delta T$ | Summations over fluid phases, including terms related to heat transfer due to fluid flow and thermal gradients. |
| | $\rho_w q_{wk} H_w + \rho_o q_{ok} H_o + \rho_g q_{gk} H_{g\,[well\ layer\ k]}$ | Energy transferred by fluid production through wells, accounting for fluid densities, flow rates, and enthalpies. |
| | $\sum_{k=i}^{n_r}[H_{rk} r_k + HL_o + HL_v + HL_c] + \sum_{k=1}^{n_f}(HA_{CV+}HA_{CD})_k$ | Summations over rock types and fluid phases, including terms related to heat exchange and accumulation within the porous medium. |

### 3.3.2 Numerical Methods

CMG STARS employs numerical methods to discretise and solve the governing equations. Common numerical techniques include finite difference, finite volume, or finite element methods. These methods discretise the reservoir domain into a grid system, and the governing equations are solved on this grid. CMG STARS offers flexibility in choosing the numerical method and grid type based on the specific requirements of the in-situ combustion model. The software provides efficient algorithms for solving large-scale systems of equations and handles the dynamic coupling between the fluid flow, heat transfer, and reactive transport processes. The following equations illustrate how each numerical method can be applied to solve 3D heat transfer problems by discretising and solving the governing partial differential equations in different ways based on the principles of each method.

**Finite Difference Method for 3D Heat Transfer:**

The 3D heat equation in a solid medium can be expressed as:

$$\frac{\partial u}{\partial t} = \alpha\left(\frac{\partial^2 u}{\partial x^2} + \frac{\partial^2 u}{\partial y^2} + \frac{\partial^2 u}{\partial z^2}\right) \quad (3.6)$$

Where $\alpha = \frac{k}{\rho C_p}$

α: Thermal diffusivity ($m^2\ s^{-1}$)
k: Thermal conductivity ($W\ m^{-1}\ K^{-1}$)
ρ: Density ($kg\ m^{-3}$)
$C_p$: Specific heat capacity ($J\ kg^{-1}\ K^{-1}$)
Applying a central difference scheme for discretisation in all three spatial dimensions, the equation becomes:

$$\frac{u_{i,j,k}^{n+1} - u_{i,j,k}^{n}}{\Delta t} =$$

$$\alpha\left(\frac{u_{i+1,j,k}^{n-1}-2u_{i,j,k}^{n}+u_{i-1,j,k}^{n}}{(\Delta x)^2}+\frac{u_{i+1,j,k}^{n-1}-2u_{i,j,k}^{n}+u_{i-1,j,k}^{n}}{(\Delta y)^2}+\frac{u_{i+1,j,k}^{n-1}-2u_{i,j,k}^{n}+u_{i-1,j,k}^{n}}{(\Delta z)^2}\right) \quad (3.7)$$

Here, $u_{i,j,k}^{n}$ represents the temperature at the grid point ($i$,$j$,$k$) and time step $n$, while $\Delta t$, $\Delta x$, $\Delta y$, and $\Delta z$ represent the time, and spatial step sizes along the $x$, $y$, and $z$ directions, respectively.

**Finite Volume Method for 3D Heat Transfer:**

The 3D heat equation in integral form considering a control volume approach is:

$$\frac{\partial}{\partial t}\iiint_{CV} u dV = \oint_{\partial CV} \alpha \nabla u \cdot dS \quad (3.8)$$

Discretising this equation using finite volumes results in a system of equations similar to the finite difference method but solved in terms of control volumes and fluxes across their faces.

**Finite Element Method for 3D Heat Transfer:**

The 3D heat equation using the finite element method leads to a system of equations obtained by discretising the differential equation over a mesh of elements.

For instance, considering the steady-state form of the 3D heat equation:

$$-\nabla \cdot (\alpha \nabla u) = f(x, y, z) \quad (3.9)$$

Discretising this equation over a mesh of hexahedral elements and applying the variational formulation using finite element basis functions leads to a system of equations to solve for the nodal values of the temperature field $u$.

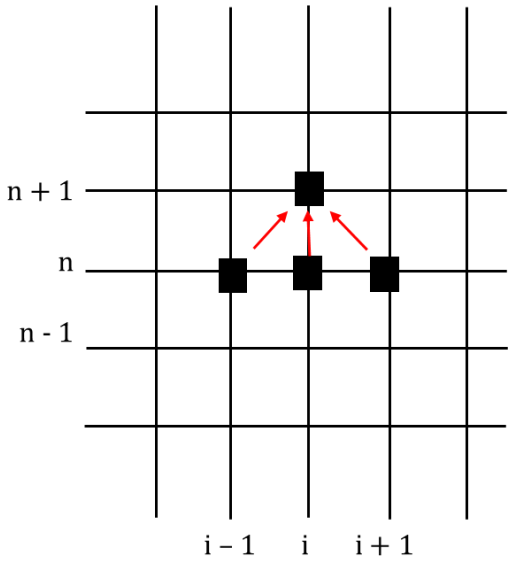


**Figure 3.3.** Diagram of finite difference: "n+1" is calculated through the current value of "n", as shown by the red arrows.

### 3.3.3 Solver Settings and Convergence Criteria

CMG STARS provides a range of solver settings that can be customised to achieve accurate and efficient simulations. These settings include convergence criteria, time step controls, iterative solvers, and preconditioning techniques. Adjusting these settings appropriately is crucial to ensure reliable and stable simulations. It is important to conduct sensitivity analyses and convergence tests to validate the chosen solver settings and to assess their impact on simulation results.

By formulating the appropriate governing equations and selecting suitable numerical methods within CMG STARS, the model can accurately capture the fluid flow, heat transfer, and reactive transport processes associated with in-situ combustion. In subsequent chapters, the model development work will focus on the calibration and validation of the

CMG STARS model, using available field or laboratory data to ensure its accuracy and reliability.

## 3.4 Laboratory Scale Model Setup and Assumptions

To develop a reliable and accurate CMG STARS model for in-situ combustion simulation, it is essential to define the model setup and the assumptions made during the modelling process. This subsection outlines the key components of the model setup for the laboratory scale THAI and THAI-CAPRI models, and discusses the assumptions made to represent the reservoir and its associated in-situ combustion processes. The original THAI model was built within CMG Builder with data from the University of Nottingham and information from the model within (Ado et al., 2019). The model created and used within this paper is based on the aforementioned model, comprised of 3990 evenly sized grid-blocks (30, 19 and 7 in the x, y and z respectively). The model contains eight components which participate in four reactions: one cracking reaction and three oxidation reactions. 3990 grid blocks were used to accommodate all complexities of model input, allowing for a trade-off between computing time and accuracy.

### 3.4.1 Reservoir Description

The model (Figure 3.3) requires a comprehensive description of the reservoir properties to accurately represent the in-situ combustion process at laboratory scale. This includes information about the reservoir geometry, rock properties, fluid properties, and initial conditions. The reservoir geometry can be based on field data or conceptual representations. The rock properties, such as permeability and porosity, can be assigned based on laboratory measurements or estimation techniques. The fluid properties, including viscosity and composition, can be obtained from laboratory experiments or

literature data. The initial conditions represent the reservoir conditions at the start of the simulation and can be based on historical data or estimated values.

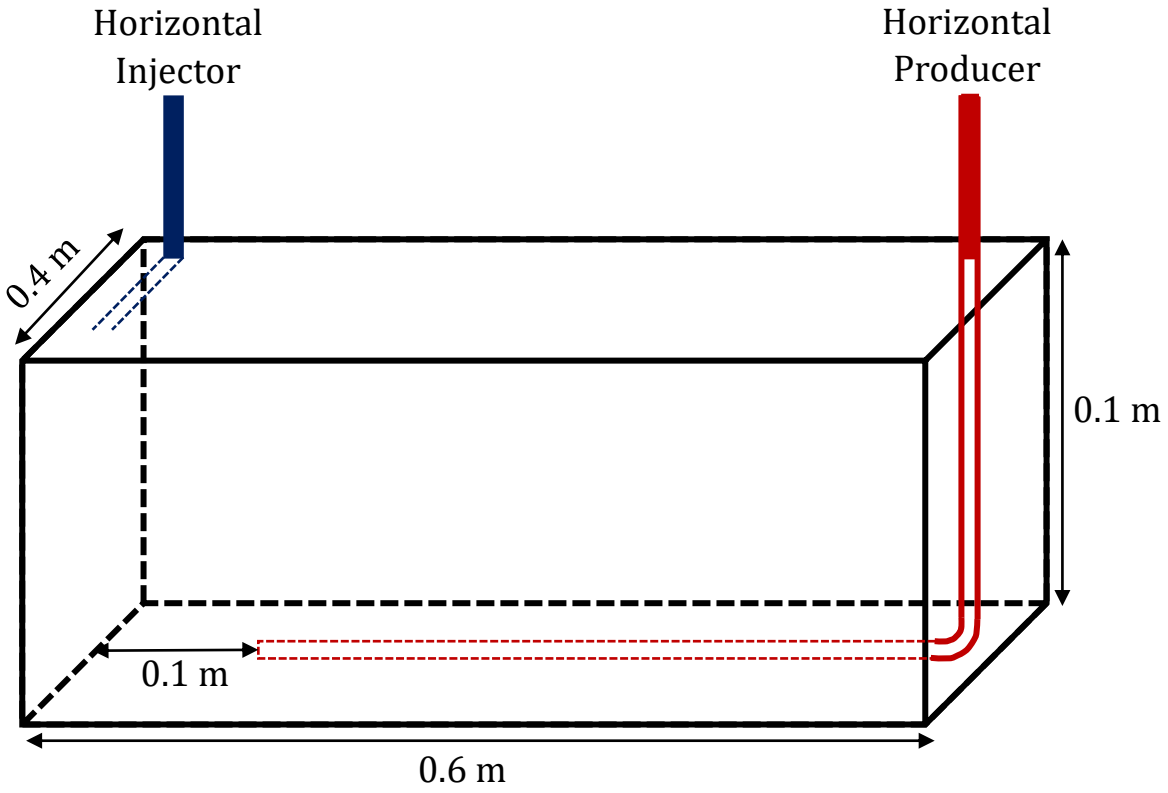


**Figure 3.4.** 3D schematic displaying geometry and dimensions of the laboratory scale model.

**Table 3.2.** Physical properties of the model grid.

| | |
|---|---|
| **Reservoir dimensions (i × j × k)** | 220 m × 97 m × 25 m |
| **Original number of grid blocks (i × j × k)** | 45 × 19 × 7 |
| **Total number of original grid blocks** | 5985 |
| **Refined number of grid blocks (i × j × k)** | 180 × 19 × 7 |
| **Total number of refined grid blocks** | 23,940 |
| **Well type and length** | Vertical Injector (1.5 m), Horizontal Producer (185 m) |
| **Reservoir porosity** | 0.32 |
| **Horizontal permeability, $k_h$ (mD)** | 4948 |
| **Vertical permeability, $K_v$ (mD)** | 3793 |

In transitioning from laboratory-scale models to field-scale simulations, it is crucial to recognise the fundamental distinctions and considerations inherent in this study's methodology. This initial phase of this study primarily focuses on simulating laboratory-scale models (10s cm scale), while the subsequent phase shifts its emphasis to field-scale

dimensions (100s m scale). Notably, this approach does not involve the direct scaling of physical parameters, such as permeability, from laboratory to field scale. Instead, the laboratory-scale models employ physical parameters identical to those utilised in the corresponding sand pack combustion experiments, ensuring a robust representation of the specific laboratory conditions. However, for the transition to field-scale modelling, we integrate distinct datasets obtained from an actual oilfield to reflect the diverse geological and reservoir properties characteristic of field-scale dimensions. Furthermore, while the laboratory-scale simulation incorporates downscaled reaction kinetics, a comprehensive discussion regarding the upscaling of reaction kinetics and additional considerations pertinent to field-scale modelling will be explained in subsequent sections dedicated specifically to field-scale simulations. This iterative approach allows for thorough exploration and comparison of the phenomena observed at both laboratory and field scales.

### 3.4.2 THAI-CAPRI Grid Resolution Dependence

The grid resolution plays a critical role in capturing the heterogeneity of the reservoir and accurately representing the in-situ combustion processes. The choice of grid resolution should be based on a balance between computational efficiency and the need to capture small-scale heterogeneities and flow behaviour associated with combustion fronts. It is important to conduct sensitivity analyses to evaluate the impact of grid resolution on simulation results. To investigate grid convergence effects, less coarse meshes were trialled to aid in the resolution of the results, with models of up to 35910 grid blocks (90×57×7) being used. However, due to the complexity of the proceeding CAPRI model (Model C) less coarse meshes failed to converge before resulting in any meaningful data, often only reaching 1% progress after 24 hours of run time, with large material balance errors. These issues have been attributed to the complexity and number of reactions

within the CAPRI model, with large kinetic values (e.g. frequency factor) being used within the same equations as very small physical values (e.g. volume). 3990 is the number of grid blocks that allowed both models to have comparable results whilst minimising grid-block size as much as possible, also factoring in reasonable computing time.

### 3.4.3 Component Properties and Reaction Scheme

Coke is primarily produced through thermal cracking of asphaltenes rather than a sequence of reactions, as expressed in the equation:

$$\text{asphaltene} \rightarrow \text{coke} + \text{volatile products} \tag{3.10}$$

Using two pseudo-components, heavy oil and light oil, Grabowski et al. (1979) describe the thermal cracking reaction of Cold Lake heavy oil as follows:

$$\text{heavy oil} + \text{light oil} \rightarrow \text{coke} + \text{gas} \tag{3.11}$$

Based on these insights, Phillips et al. (1985) conducted a series of extensive experiments, which led to the formulation of a more complex set of thermal cracking reactions. The Athabasca bitumen is divided into three pseudo-components: asphaltenes, heavy oil, and distillables. The chemical reactions governing thermal cracking are articulated in the following equations:

$$\begin{aligned} \text{Coke} &\leftrightarrow \text{asphaltene} \\ &\leftrightarrow \text{heavy oils} \\ &\leftrightarrow \text{distillables} \end{aligned} \tag{3.12}$$

Within the typical thermal cracking temperature range of 360 to 420 °C, the conversion of heavy oils to coke is observed to occur up to three times faster than that of distillables. Consequently, the heavy fraction is denoted as "heavy oil." However, distillables in

equation 3.12 are referred to as "light oil," which includes medium oil, light oil, and gases (Greaves et al., 2012a).

### *3.4.3.1 THAI Model (Model T)*

Subsequently, the laboratory THAI model uses the following reaction scheme adapted from (Greaves et al., 2011a; Greaves et al., 2012a) :

heavy oil → light oil + coke (3.13)

coke + $O_2$ → $CO_2$ + CO + $H_2O$ (3.14)

heavy oil + $O_2$ → $CO_2$ + $H_2O$ (3.15)

light oil + $O_2$ → $CO_2$ + $H_2O$ (3.16)

Consequently, the THAI simulation model within this study utilises the components outlined within Table 3.3, where HO and LO represent “heavy oil” and “light oil” from Greaves et al. (2012a), respectively.

**Table 3.3**. List of components within the lab-scale THAI model (model T) (Hasan and Rigby, 2019a).

| Component | Critical Pressure (kPa) | Critical Temperature (K) | Molecular Weight (kg $mol^{-1}$) | Density ($10^{-3}$ kg $cm^{-3}$) |
|---|---|---|---|---|
| Water ($H_2O$) | 22048 | 647.4 | 0.018 | 0.999 |
| Heavy Oil (HO) | 1031.29 | 1053.2 | 0.878 | 1.1075 |
| Light Oil (LO) | 2306 | 698.3 | 0.172 | 0.9038 |
| $CO_2$ | 7376 | 304.2 | 0.044 | N/A |
| CO | 3496 | 132.9 | 0.028 | N/A |
| $N_2$ | 3394 | 126.2 | 0.028 | N/A |
| $O_2$ | 5033 | 154.82 | 0.032 | N/A |
| Coke | N/A | N/A | 0.013 | N/A |

### *3.4.3.2 THAI-CAPRI Model (Model C)*

The THAI model (Model T) was supplemented with the addition of three new components as a novel aspect of this work; hydrogen, hydro-treating catalyst and upgraded heavy oil components (Table 3.4). Furthermore, a catalyst pseudo-component

was added to represent the catalyst in the THAI-CAPRI process. STARS does not have the capacity to directly model a catalyst, so a solid component (CAT) is used to represent the catalyst within the model. The CAT is included within the same horizontal blocks that the producer is found at a concentration of 0.1 mol $cm^{-3}$ (Figure 3.5). Reaction 8 (Table 3.6) is only able to take place where the CAT component is found representing the simplified behaviour of a catalyst. Details of the catalyst component details can be found in Hasan and Rigby (2019a) where the 44% packing porosity is employed. To mitigate any 'clogging' effects that the catalyst may have due to the size of the grids, the porosity in the CAT containing blocks was set to 0.99 (Hasan and Rigby, 2019a).

To represent the catalytic upgrading of the heavy oil, a new hydrogenation reaction was introduced into the model (Reaction 5; Table 3.6). This reaction produced the new component Upgraded Heavy Component (UHC) (Table 3.4), which represents an upgraded version of the heavy oil component through a decrease in density and molecular weight (Escobar et al., 2017). UHC is an adapted version of the upgraded component from Hasan and Rigby (2019a) and is defined as a generalised heavy oil component that has undergone hydrogen addition to decrease the density of the component. This reaction only took place where the catalyst pseudo-component occupied the cell, as the actual reaction would require the presence of a hydrotreating (HDT) catalyst to occur. This was represented within STARS by having the CAT component on both sides of the reaction, as both a reactant and product, with a ratio of 1:1 (Table 3.6).

**Table 3.4** List of components within the lab-scale CAPRI model (Model C) (Rabiu Ado, 2017).

| Component | Critical Pressure (kPa) | Critical Temperature (K) | Molecular Weight (kg mol$^{-1}$) | Density ($10^{-3}$ kg cm$^{-3}$) |
|---|---|---|---|---|
| Upgraded Heavy Component (UHC) | 1523.5 | 775.3 | 0.253 | 0.8505 |
| Hydrogen ($H_2$) | 1315.5 | 33.4 | 0.002 | N/A |
| Catalyst (CAT) | N/A | N/A | 0.013 | 1.0531 |

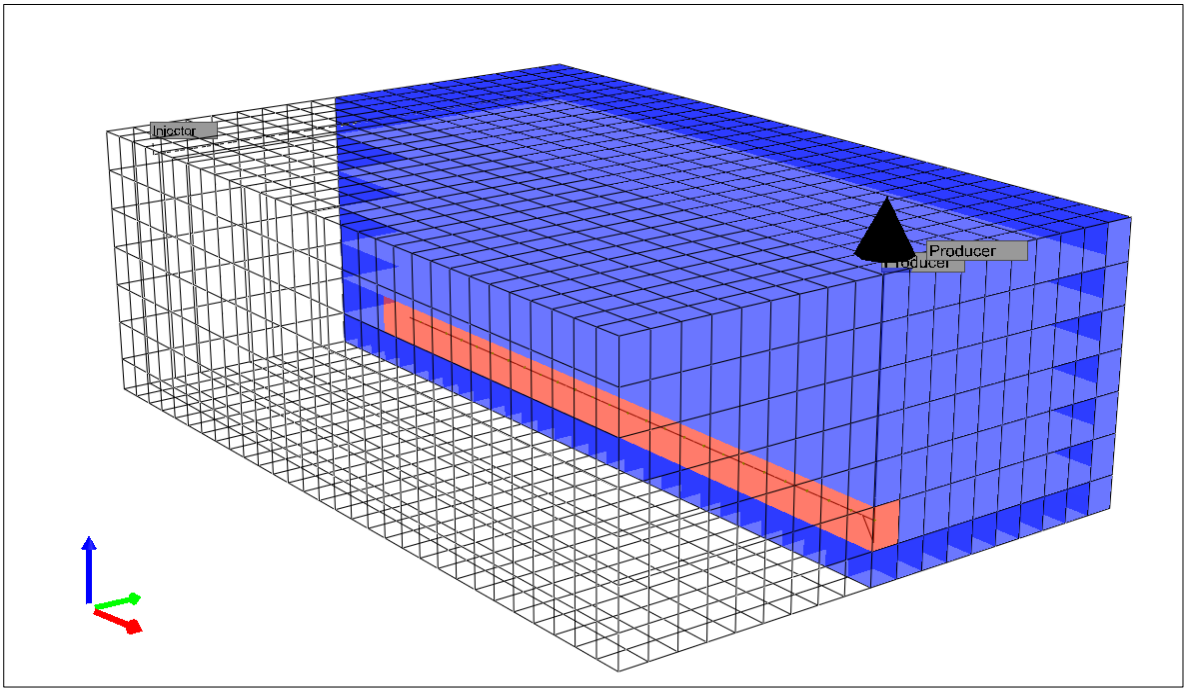


**Figure 3.5.** 3D model showing catalyst (red) running along horizontal producer.

### *3.4.3.3 Development of CAPRI reactions*

As previously stated, injecting hydrogen into an oil reservoir can lead to several risks, alongside economic disadvantages. Therefore, a paramount novel objective of this study is to model, using STARS, THAI-CAPRI without injecting hydrogen. Several mechanisms for hydrogen production are possible (e.g., methane reforming), but many encounter problems when under the conditions that are feasible within an oil reservoir, especially shallow heavy oil/bitumen deposits due to low pressure gradients and temperature

limitations. In this study water-gas shift and coke gasification with water (coke steam reforming) have been selected (reactions 5a and 6 from Table 3.6) as they are known to occur in the well (Xia et al., 2002e). Oil upgrading is then achieved through the hydrodesulfurization, hydrodenitrogenation and hydrocracking of the heavy end components within the in-situ crude oil (Greaves and Xia, 2004; Ferdous et al., 2006) represented in this study by the simplified hydroprocessing in reaction 8 (Table 3.6).

#### *3.4.3.4 CAPRI reaction scheme*

The reaction equations and kinetics for the CAPRI reactions are shown in Table 3.6. The kinetics for reactions 5, 6 and 7 were taken from Kapadia et al. (2013) and are all modelled as first-order reactions. Reaction 7 is split into two separate reactions (a and b) which both represent each direction of the reversible reaction. Reaction 8 is adapted from Hasan and Rigby (2019a) through the removal of $H_2S$ and $NH_3$ from the reaction for a simplified, all-encompassing version. Hydroprocessing of only the heavy end component, and not the lighter components, as reported by Greaves and Xia (2004).

#### *3.4.3.5 Kinetics Scheme for both models*

Reaction kinetics in reservoir simulations of thermal processes involve modelling the speed of chemical reactions at high temperatures. By incorporating these kinetics, optimising recovery methods, predicting reservoir behaviour, and mitigating undesired reactions for more efficient and sustainable hydrocarbon extraction can be accomplished. All reactions are assumed to be pseudo-first order, and some frequency factors may be higher than the diffusion rate. When simulating in-situ combustion in a reservoir model, certain factors can help reduce the expected consequences of a reaction with a higher frequency factor than the diffusion rate. These factors include continuous supply of

reactants through injection wells, improved mixing driven by the flow of reservoir fluid, and the dominance of large-scale reservoir dynamics.

**Table 3.5** List of reactions found within the lab-scale THAI model (Model T) (Greaves et al., 2011c).

| Reaction | Frequency Factor ($s^{-1}$) | Activation energy (J $mol^{-1}$) |
|---|---|---|
| 1. HO → LO + Coke | $1.5 \times 10^{9}$ | $0.99 \times 10^{5}$ |
| 2. LO + $O_2$ → $H_2O$ + $CO_2$ + CO | $1.812 \times 10^{12}$ | $1.38 \times 10^{5}$ |
| 3. HO + $O_2$ → $H_2O$ + $CO_2$ +CO | $1.1812 \times 10^{11}$ | $1.38 \times 10^{5}$ |
| 4. Coke + $O_2$ → $H_2O$ + $CO_2$ +CO | $8.6 \times 10^{7}$ | $1.23 \times 10^{4}$ |

**Table 3.6** List of reactions found within the lab-scale CAPRI model (Model C) (Kapadia et al., 2013; Hasan and Rigby, 2019a).

| Reaction | Frequency Factor ($s^{-1}$) | Activation energy (J $mol^{-1}$) |
|---|---|---|
| 5a. $H_2O$ + CO → $H_2$ + $CO_2$ | $5 \times 10^{9}$ | $1.49 \times 10^{5}$ |
| 5b. $H_2$ + $CO_2$ → $H_2O$ + CO | $5 \times 10^{7}$ | $1.9 \times 10^{5}$ |
| 6. Coke + $H_2O$ → CO + $H_2$ | $2.12 \times 10^{12}$ | $9.2 \times 10^{4}$ |
| 7. Coke + $CO_2$ → CO | $2.59 \times 10^{8}$ | $5.4 \times 10^{4}$ |
| 8. HO + $H_2$ + CAT → UHC + CAT | $8.5 \times 10^{18}$ | $8.7 \times 10^{4}$ |

### 3.4.4 Well Configuration and Injection Strategy

THAI involves an injection well, either vertical or horizontal across the top of the producible fraction of the reservoir, and a horizontal producer. This model utilises the horizontal injector due to gas override issues involving the vertical injector observed at this scale and mesh size. The injection well runs horizontally across the top layer (layer 1) on the left side (i = 1) of the model, whilst the production well runs vertically down the opposite side (i = 30) and horizontally across one of the bottom layers of the model until it terminates approximately 75% of the way across.

The injection well is heated for 30 minutes through an electrical heater within the wellbore before any injection occurs in a pre-injection heating cycle (PIHC). At 30 minutes air is injected into the model, at 21% oxygen, and initial combustion occurs. The reactions then proceed for another 290 minutes to generate comparable data with Greaves et al. (2011c) at which point the composition of the products and plots of the ending

parameters can be investigated. A diagrammatic representation has previously been presented (Ado et al., 2019).

#### *3.4.4.1 Hydrogen Injection Model (Model Ci)*

The THAI model was supplemented with the addition of four new components as a novel aspect of this work; hydrogen, hydro-treating catalyst and upgraded oil components (Table 3.4). Hydrogen was included in the injection gas at 1:1 volume with oxygen and both gases are injected at the same individual rate (1600 $cm^3\ min^{-1}$) throughout the whole run. Furthermore, a catalyst pseudo-component was added to represent the catalyst in the THAI-CAPRI process. STARS does not have the capacity to directly model a catalyst, so an unreactive solid component (CAT) is used to represent the catalyst within the model. The CAT is included only within the horizontal blocks that the producer is found at a concentration of 0.1 mol $cm^{-3}$ (Figure 3.6).

#### *3.4.4.2 Steam variations for model investigations*

Three different steaming variations are used for both THAI and THAI-CAPRI models to investigate the impacts of steam on the upgrading process (Table 3.7). All models have a 30-minute pre-heating time before air injection occurs, with dry models (T1 and C1) utilising electrical heaters on around the injection wells to aid in oil ignition at a rate of 2115 J $min^{-1}$ (Rabiu Ado, 2017). Steamed models employ a combination of electrical heaters and steam for pre-heating.

**Table 3.7** Steaming variations for models

| Model | Steam protocol |
|---|---|
| T1 | THAI + no steam |
| T2 | THAI + 30-minute pre-steam |
| T3 | THAI + 780-minute constant steam |
| C1 | CAPRI + no steam |
| C2 | CAPRI + 30-minute pre-steam |
| C3 | CAPRI + 780-minute constant steam |

### 3.4.5 CMOST

CMOST is a machine learning tool within the CMG software suite. Selected model initialisation input parameters are used as variables. CMOST then runs several models using these variables, varying the input values within a set range until a user-selected output result is reached. This study employs CMOST optimisation as an automated validation tool. The selected parameters to carry out the optimisation were the pre-exponential factors within Table 3.5 and 3.6. The reasons for this decision are two-fold: the exact kinetics experienced in-situ are mostly unknown; and reaction kinetics are varied by the user to overcome the issues associated the grid volume(s) used within a simulation model. The range of values used for each variable was left as the suggested CMOST default range for consistency. Equations 3.18 and 3.19 were used to calculate the API at each time step for the produced oil:

$$\rho_R = \frac{\sum rate\ of\ produced\ oil\ mass}{\sum rate\ of\ produced\ oil\ volume} \quad (3.17)$$

$$API = \left(\frac{141.5}{\rho_R \cdot 1000}\right) - 131.5. \quad (3.18)$$

A constant of 1000 is used within Equation 3.19 because oil density units were used in g $cm^{-3}$. To find the average API, and therefore the average overall upgrading, the sum of the API for each time step was divided by the number of time steps.

#### *3.4.5.1 Model T*

Initial CMOST inputs were obtained through published reaction kinetics within Greaves et al. (2011c) (stoichiometry, frequency factor, and activation energy for reactions 1-4). The optimisation routine CMOST was set to run Model C until a convergence criterion of an overall average API upgrading of ~5° above the initial API was observed (Xia et al.), which took 27 iterations.

#### *3.4.5.2 Model C*

Initial CMOST inputs were obtained through published reaction kinetics within Greaves et al. (2011c) (reactions 1-4), (Kapadia et al., 2013) (reactions 5a–7) and Hasan and Rigby (2019a) (reaction 8). The optimisation routine CMOST was set to run Model C until a convergence criterion of an overall average API upgrading of ~12° above the initial API was observed (Xia et al., 2002e), which took 32 iterations.

#### *3.4.5.3 Model C(i)*

Model C(i) validation was achieved through altering the frequency factor of the hydroprocessing reaction (Hasan and Rigby, 2019a). This validation was done through CMG CMOST. The CMOST machine learning process will fine tune selected parameters and run the Ca model repeatedly while varying these selected parameters until the output of the model matches the historic data as best as possible. It ran until the desired API for history matching Hart and Wood (2018) was observed, which took 44 iterations.

### 3.5 Field Scale Model Setup and Assumptions

Laboratory-scale THAI simulations typically involve controlled conditions with simplified inputs, such as uniform rock properties and well-defined fluid compositions. In contrast, field-scale simulations for THAI in reservoirs require more complex inputs, considering heterogeneous rock properties, diverse fluid compositions, and the influence of reservoir geometry and connectivity for accurate representation of real-world conditions. The transition from laboratory to field scale necessitates a more comprehensive understanding and integration of diverse parameters to ensure realistic and predictive reservoir behaviour in the simulation.

### 3.5.1 Reservoir Description

The model was developed within Builder from the lab-scale model found within Lopeman et al. (Lopeman et al., 2022) and upscaled by 244 times in the i direction, and adding 15 extra grids in the i direction, to match the size and production potential of the K2 pilot test of the Kerrobert THAI project (Figure 3.5), previously displayed in Anbari et al. (Anbari et al., 2023). It deploys a Cartesian grid system, totaling 5985 to 23,940 grid blocks, depending on the refinement level. A vertical injector penetrates 1.5 m into the top of the reservoir model in the middle j plane. A horizontal producer, sharing the j plane, penetrates vertically down 19.6 m and horizontally across the $6^{th}$ k layer 185 m. The initial conditions and reservoir properties of the model were taken from Anbari et al. (2023) and adapted into the aforementioned upscaled grid model from Lopeman et al. (2022). The model is then refined down by 4 times in the i direction, whereby a block of X m in the i direction would be split into 4 block of X/4 m in the i direction. The petrophysical properties used within this study are those of the eastern Kerrobert reservoir (Anbari et al., 2023) and can be found in Table 3.7.

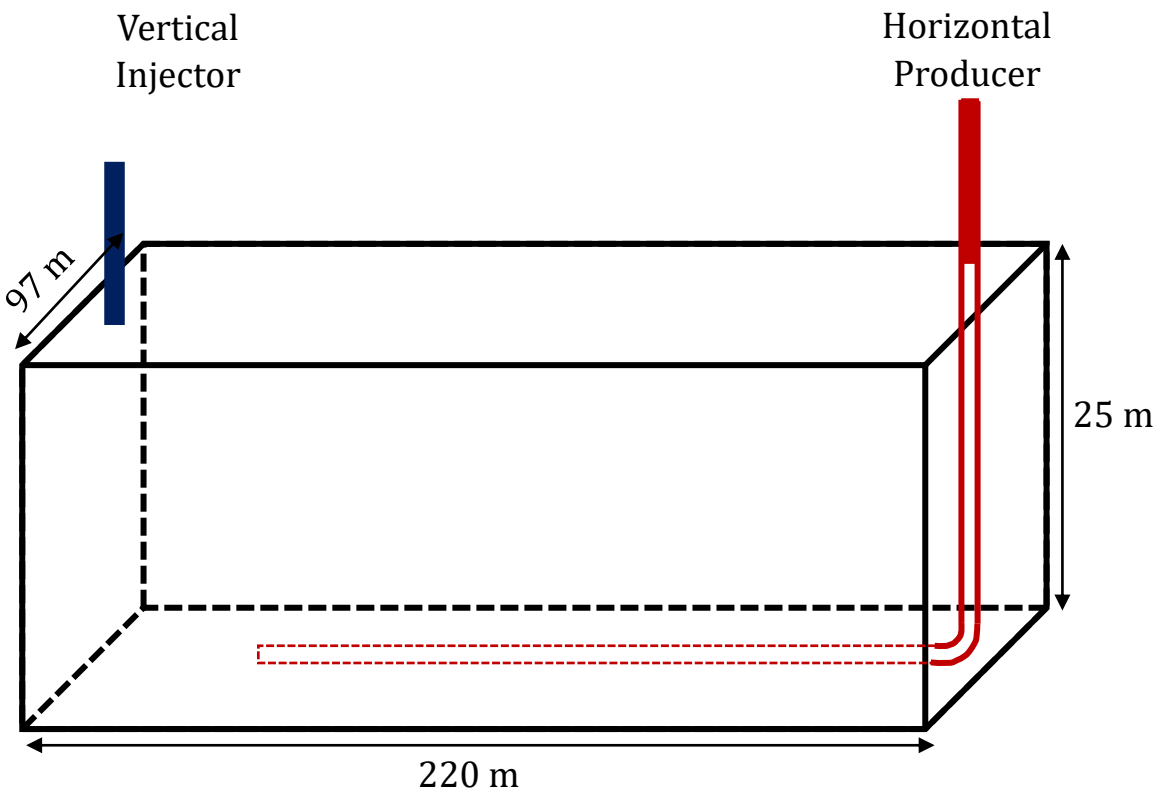


**Figure 3.6.** 3D schematic displaying geometry and dimensions of the field scale model.

**Table 3.8.** Physical properties of the model grid.

| | |
|---|---|
| **Reservoir dimensions (i × j × k)** | 220 m × 97 m × 25 m |
| **Original number of grid blocks (i × j × k)** | 45 × 19 × 7 |
| **Total number of original grid blocks** | 5985 |
| **Refined number of grid blocks (i × j × k)** | 180 × 19 × 7 |
| **Total number of refined grid blocks** | 23,940 |
| **Well type and length** | Vertical Injector (1.5 m), Horizontal Producer (185 m) |
| **Reservoir porosity** | 0.32 |
| **Horizontal permeability, $k_h$ (mD)** | 4948 |
| **Vertical permeability, $K_v$ (mD)** | 3793 |

**Table 3.9** Dynamic and petrophysical properties of the model.

| | | | |
|---|---|---|---|
| **Initial reservoir temperature (°C)** | 25 | | |
| **Initial reservoir pressure (kPa)** | 3000 | | |
| **Initial oil saturation** | 74% | | |
| **Initial water saturation** | 24% | | |
| **Initial oil API** | 10 | | |
| **Average air injection rate ($m^3$/day)** | 21,600 | | |
| **Pre-steam protocol** | Length (days) | Temperature (°C) | Injection rate ($m^3$/day) |
| | 31 | 250 | 260 |

### 3.5.2 Grid Independence Analysis

To best understand the impacts of variables upon the performance of the THAI process as modelled in this study, the results of the model must first be checked as independent of the grid block size. Though, previous studies have employed localised grid refinement (LGR), often mixed with dynamic gridding whereby grid blocks are refined or coarsened dependent upon a variable limit (e.g., no refinement in grids of <300 °C). However, due to the results of Tijink and Cottier (2019), this study sought to eliminate any irregularities occurring as a result of localised grid refinement. Tijink and Cottier (2019) claim that LGR in the ij direction results in minor erroneous results, and LGR in the k direction results in major erroneous results. For this reason, the whole model was refined in the i direction at each refinement step. Refinement was not realised in the jk direction due to computational power and lack of necessity due to the direction of combustion propagation being the i direction.

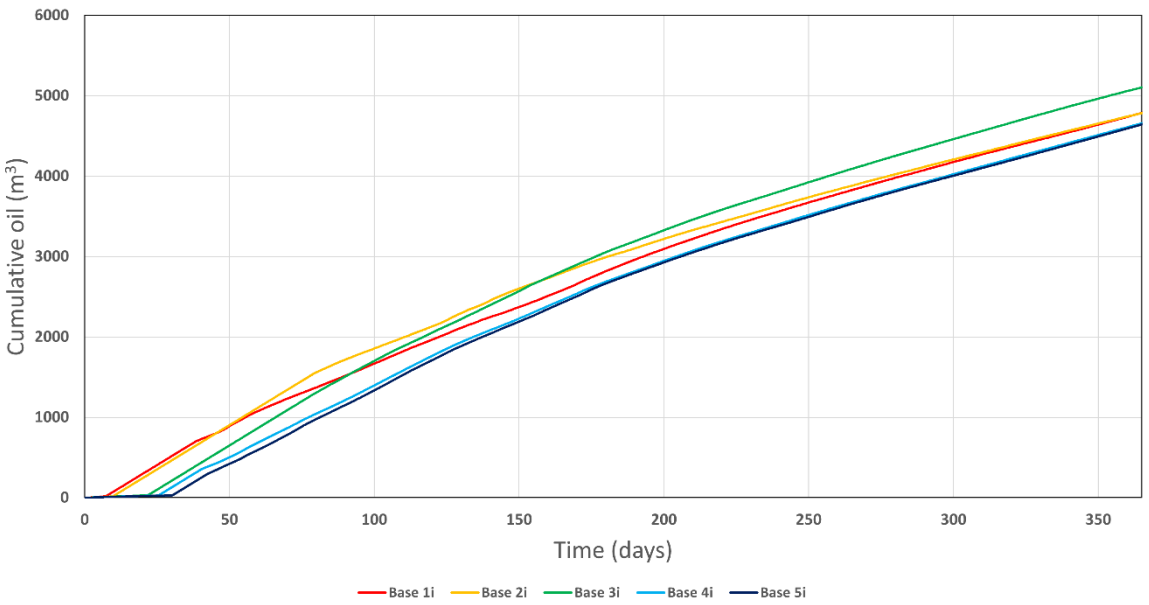


**Figure 3.7.** Cumulative oil production ($m^3$) of the 5 grid variations of Model T1. Base 1i refers to the 5985-grid model, with each step up being a refinement of each grid in the i direction by a multiple of that number (e.g., 4i is 4 times the number of grids in the i direction than 1i, but at 1i/4 width).

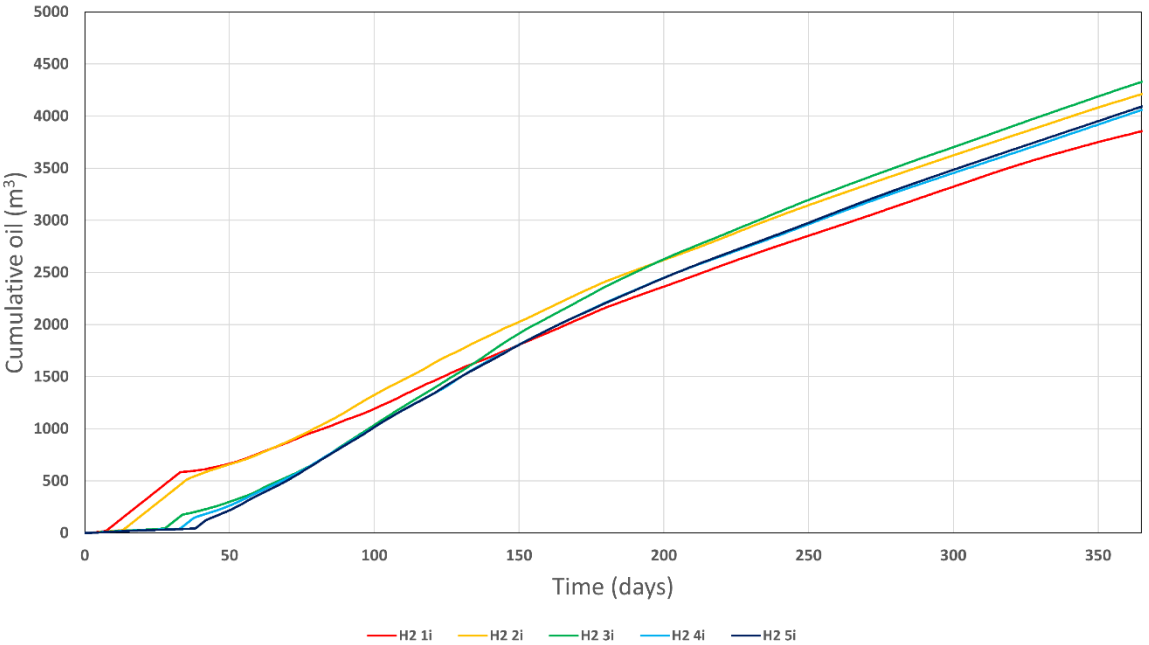


**Figure 3.8.** Cumulative oil production ($m^3$) of the 5 grid variations of Model T5. H2 1i refers to the 5985-grid model, with each step up being a refinement of each grid in the i direction by a multiple of that number (e.g., 4i is 4 times the number of grids in the i direction than 1i, but at 1i/4 width).

Figure 3.7 and Figure 3.8 display the cumulative oil production of Model T1and Model T5, respectively, at 5 varying refinements of the grid blocks in the i direction: the direction of the combustion front propagation. Each refinement step divides the i direction of the original grid block (1i) by the refinement number (i.e., 5i is 1i divided by 5 in the i direction). Despite no discernible pattern in the cumulative oil production as grid block size decreases, there is a clear convergence point at 4i, where any further refinement has no apparent impact on the results calculated by the model, for both Model T1 and T5. The results in oil production change due to variations in temperature and fluid composition as the grids become smaller. A smaller grid is likely to have a higher temperature and more accurate fluid concentrations as less averaging occurs across the volume of the grid block at each time step. For this reason, the history matching, and all further investigations were carried out using the 4i model.

### 3.5.3 Component Properties

The components within the field scale models are the same as those found in the laboratory model in Table 3.4.

### 3.5.4 Reaction and Kinetics Scheme

Table 3.10 outlines the four main oxidation and cracking reactions used within the base model of this study (Model T1). It comprises of one cracking reaction (reaction 1) and three oxidation reactions of the three main hydrocarbon pseudo-components (reactions 1, 2, and 3). Although Ado (2020b) postulates that a more extensive reaction scheme, comprising of nine reactions can provide more accuracy to the calculated results of the simulation, the additional computing power required when adding the reactions within Table 3.11 on top of those could cause convergence issues. The frequency factor and activation energy of each reaction was ascertained through the machine learning tool,

CMG CMOST. The frequency factor and activation energy for each reaction at the laboratory scale were sourced from Table 3.5 which are based on the history matching of laboratory data and formed the initial estimate for the history matching procedure. These kinetic parameters were then employed as variables that influenced the model results and converged to produce the best match of the model with historical field data. Through 39 iterations of the model with different kinetic values for the reactions within Table 3.10 each time, CMOST was able to achieve a qualitative history match of the field data using the kinetic values displayed in Table 3.10. The history match will be discussed in chapter 5. Due to the irregular and fluctuating nature of the field data used for comparison, it is challenging to make a meaningful quantitative comparison of history matched data in this case. The undulating and inconsistent nature of the field data hinders the possibility of conducting a reliable mathematical comparison. A "decent" visual match between two data sets can be described as having a reasonable level of agreement or similarity (Ado, 2020a; Anbari et al., 2023). It indicates that there are observable similarities and trends between the datasets, suggesting a meaningful correspondence. Although precise mathematical comparisons may not have been conducted, the data sets exhibit consistent patterns or alignment, implying a reasonable level of concordance. The reactions and associated kinetic values within Table 3.11 were adapted from Kapadia et al. (2011). Table 3.12 provides an overview of the reactions present in each intermediate model, highlighting the unique set of reactions in each model. This approach allows for the examination of individual effects of these reactions on the THAI process, enabling a more detailed exploration of their specific impacts.

**Table 3.10** List of reactions used within the base THAI model.(Greaves et al., 2011a)

| Reaction | Frequency Factor ($min^{-1}$) | Enthalpy ($J\ mol^{-1}$) | Activation energy ($J\ mol^{-1}$) |
|---|---|---|---|
| 1. $HO_{(l)} \rightarrow LO_{(l)} + Coke_{(s)}$ | $2 \times 10^9$ | N/A | $1.15 \times 10^5$ |
| 2. $LO_{(l)} + O_{2(g)} \rightarrow H_2O_{(g)} + CO_{2(g)} + CO_{(g)}$ | $3.069 \times 10^6$ | $-4 \times 10^7$ | $1.38 \times 10^5$ |
| 3. $HO_{(l)} + O_{2(g)} \rightarrow H_2O_{(g)} + CO_{2(g)} + CO_{(g)}$ | $3.069 \times 10^7$ | $-1.6 \times 10^7$ | $1.38 \times 10^5$ |
| 4. $Coke_{(s)} + O_{2(g)} \rightarrow H_2O_{(g)} + CO_{2(g)} + CO_{(g)}$ | $5 \times 10^3$ | $-3.9 \times 10^5$ | $1.23 \times 10^5$ |

**Table 3.11** Reactions used within the augmented THAI models (Kapadia et al., 2011).

| Reaction | Frequency Factor ($min^{-1}$) | Enthalpy ($J\ mol^{-1}$) | Activation energy ($J\ mol^{-1}$) |
|---|---|---|---|
| 5. $Coke_{(s)} + H_2O_{(g)} \rightarrow CO_{(g)} + H_{2(g)}$ | $7.5 \times 10^5$ | $+1.314 \times 10^5$ | $9.2 \times 10^4$ |
| 6. $H_2O_{(g)} + CO_{(g)} \rightarrow H_{2(g)} + CO_{2(g)}$ | $8 \times 10^{10}$ | $-4.13 \times 10^4$ | $1.49 \times 10^5$ |
| 7. $H_{2(g)} + CO_{2(g)} \rightarrow H_2O_{(g)} + CO_{(g)}$ | $6.06672 \times 10^{12}$ | $+4.13 \times 10^4$ | $1.9 \times 10^5$ |

**Table 3.12** Reactions included in each model variation

| Model name | Reaction included |
|---|---|
| T1 | 1-4 |
| T2 | 1-4, 5 |
| T3 | 1-4, 6 |
| T4 | 1-6 |
| T5 | 1-7 |

### 3.5.5 Well Configuration and Injection Strategy

Table 3.13 presents the details of the injected air composition, along with its injection pressure and temperature, into the reservoir. Additionally, specific constraints, such as a minimum bottom-hole pressure and a maximum surface liquid rate, were established for the horizontal producer. These values are reported in Anbari et al. (2023).

**Table 3.13** The injection protocol of the model.

| Injected fluid composition (%) | Injection Pressure (kPa) | Injection Temperature (°C) | Production well minimum bottom-hole pressure (kPa) | Production maximum surface liquid rate ($m^3$/day) |
|---|---|---|---|---|
| $N_2$ (79), $O_2$ (21) | 3500 | 25 | 2800 | 300 |

# CHAPTER 4. LABORATORY SCALE MODELLING OF THAI AND THAI-CAPRI

## 4.1 Introduction

This chapter both compares the oil upgrading potential of THAI and THAI-CAPRI as predicted by laboratory simulations and examines a critical aspect of the THAI-CAPRI process that has been underexplored in prior THAI-CAPRI simulation studies: the reliance on injected hydrogen versus the in-situ hydrogen generated during the process. The inherent risks associated with co-injecting oxygen and hydrogen in real-life scenarios necessitate a crucial shift to the study of the origin of hydrogen within the THAI-CAPRI process to be exclusively from in-situ reactions (Schröder and Holtappels, 2005). In this context, investigating the integration of in-situ hydrogen generation reactions within simulation software, such as CMG STARS, emerges as both a novel and imperative approach to accurately model THAI-CAPRI.

This chapter underscores the pivotal role of incorporating hydrogen generation reactions, particularly water-gas shift, and coke gasification, into the numerical modelling framework for THAI-CAPRI. The proposed methodology introduces a adaptation in modelling THAI-CAPRI within CMG STARS by leveraging hydrogen generation reactions akin to those uncovered in the work of (Greaves and Xia, 2001a; Xia et al., 2002d; Kapadia et al., 2011), instead of relying on externally injected hydrogen. By harnessing in-situ generated hydrogen for catalytic upgrading of heavy oil, this approach has the capability to yield more precise and accurate upgrading outcomes, aligning more closely with the actual in-situ dynamics of the process.

This methodology aims to bridge the knowledge gap between laboratory-based testing of THAI-CAPRI and the intricate dynamics at play in field-scale simulations. By incorporating in-situ generated hydrogen, this approach holds the potential to facilitate

more accurate representations of the THAI-CAPRI process, paving the way for potential pilot trials of THAI-CAPRI within existing or future THAI projects on a global scale (Turta et al., 2018). This shift not only enhances the reliability of simulations but also offers a tangible pathway for better aligning laboratory insights with field-scale realities, thereby advancing the efficacy and applicability of THAI-CAPRI within real-world operational scenarios (Singh et al., 2019b; Ado et al., 2022b).

## 4.2 Model validation

Both models have been successfully validated against published experimental data using CMOST. Model T was validated against two sets of published experimental data. Two variables are each compared against two separate published datasets, being API upgrading over time (Greaves et al., 2000b) and peak temperature (Greaves et al., 2011a). Overall, the subsequent matches in the following sections are visually agreeable and show good similarity. Model C was validated against data from (Xia et al., 2002c) where an experiment was conducted using 10.5° API oil for THAI-CAPRI and noted an upgrade of ~11° to 22° API. Addition of the catalyst in CAPRI causes an increase in upgrading of about 5-7° API compared with only THAI, which is similar to the experimental observations of THAI-CAPRI versus THAI only as reported by Xia et al. (2002c) and Greaves et al. (2004b). Since the model reported here contained new features, before investigating the effects of different variables, a base-case was validated by history matching to a set of experimental data gathered under similar conditions. Other studies of THAI-CAPRI oil upgrading in the lab produced similar overall upgrading of API to Greaves et al. (2004b) but varied in API vs. time profile due to variations in experimental conditions. For this reason, the model could only be validated graphically against one study (Xia et al., 2002c), however, the results are representative of experimental THAI-CAPRI results on the whole.

### 4.2.1 Model T peak temperature

Both data sets display an initial rise to the peak temperature at 30 minutes, followed by a settling down to a stable, lower value ~200°C to 250°C less than peak. Peak temperature is reached at the same time for both Model T and experimental work within Greaves et al. (2011a) reaching the same temperature of just under 900°C. However, there are some deviations within the profile throughout the 320 minutes, especially around 100 minutes and 250 minutes. General deviations and undulations throughout could be explained by the low sampling rate, and subsequent interpolation of the experimental temperature, in addition to the coarseness of the grid used in Model T. However, the peak at 250 minutes is unexpected, and as a result of the combustion of a large built-up area of coke within the coarse blocks of Model T. Figure 4.1 shows the good agreement between the experimental results obtained from Greaves et al. (2011a) and compares well to the simulated results from the same study.

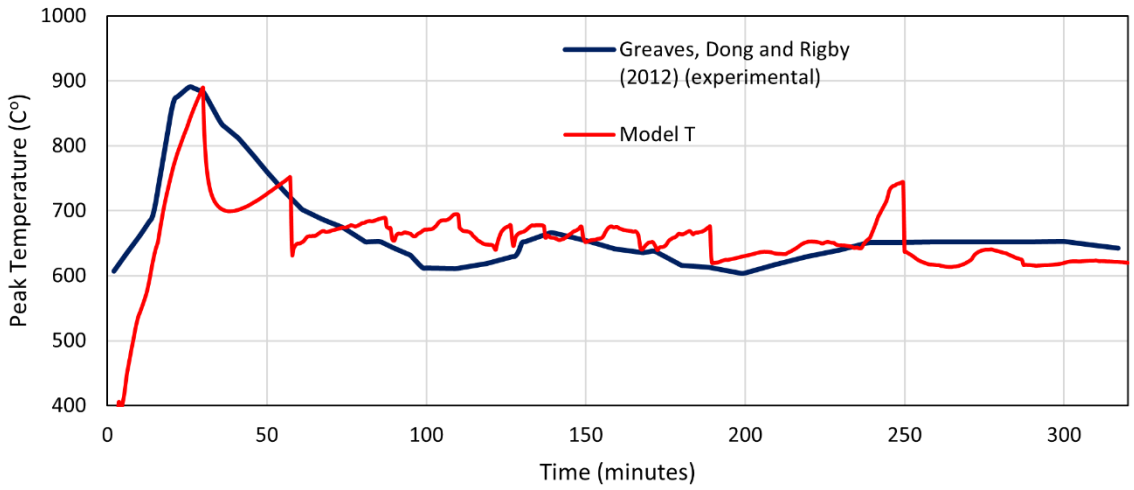


**Figure 4.1.** Peak temperature profile of Model T against experimental data from Greaves et al. (2011a)

### 4.2.2 Model T API matching

Model T was run with a starting API of 10.5° to represent the measure API of the Wolf Creek oil, which was used to validate against experimental work from Greaves et al.

(2000b). Figure 4.2 shows the API of the produced oil against time for both data sets. The first 50 minutes display a large difference, due to the low sampling rate of the experimental data combined with the start-up process of the simulation being impacted by more coarse grids. Visually, a good match is seen after 50 minutes for the API degrees of the produced oil over time with the general trend and average values being extremely similar. Model T has a much higher variability, which again comes from a combination of the low sampling rates of the experimental data from (Greaves et al., 2000b) and the coarse grid used in Model T.

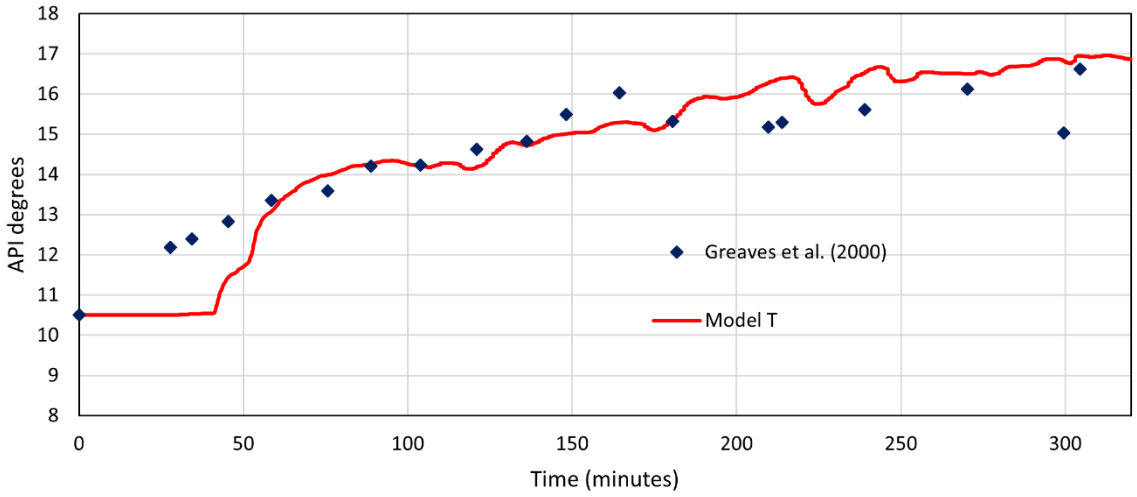


**Figure 4.2.** API degrees profile for Model T against experimental data from Greaves et al. (2000b).

### 4.2.3 Model Ci (hydrogen injection) matching

The hydrogen injection THAI-CAPRI model was validated against Hart and Wood (2018), where an experiment was conducted using the same API upgrading experiment for CAPRI and noted an upgrade of 13° (original THAI oil) to 18° API (average upgrading of 5°). This is an upgrade of 5° API from THAI to THAI-CAPRI, the same upgrading amount from THAI to THAI-CAPRI as seen in Greaves et al. (2004b). The results can be seen in Figure 4.3.

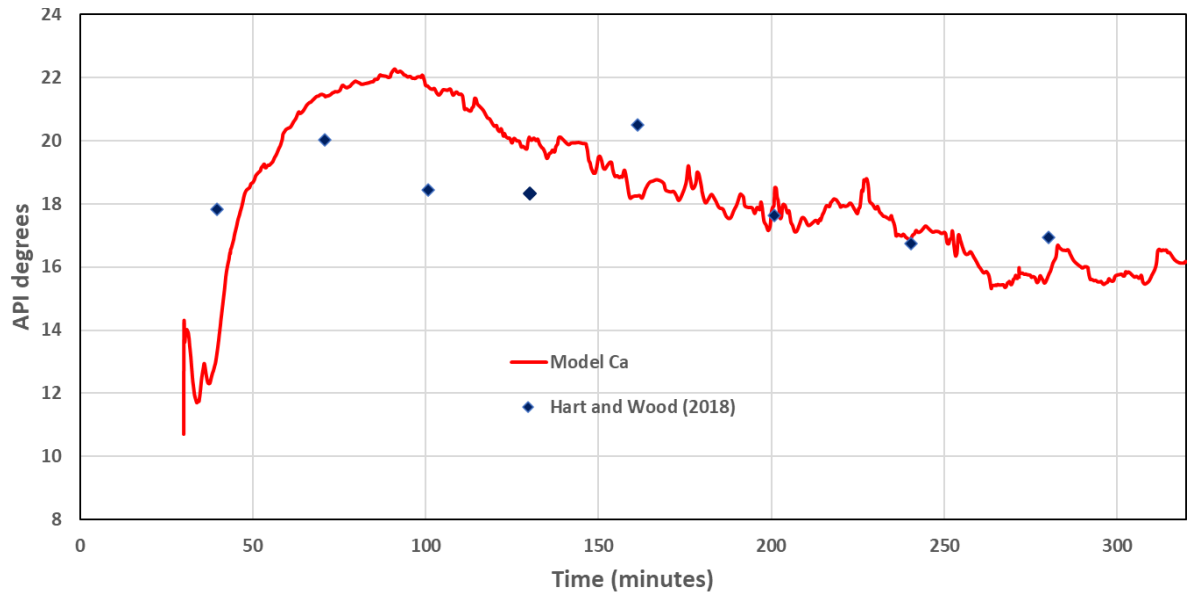


**Figure 4.3.** Oil upgrading profile of Model Ci against Hart and Wood (2018).

### 4.2.4 Statistical modelling

API gravity similarities have been compared statistically for pseudo-$R^2$ using python computer coding. $R^2$ values fall between 0 and 1, with 1 being 100% matched and 0 being no match, respective to their linear trend. Moore (1996) state that an $R^2$ value of 0.7 or higher indicates a strong correlation, and so 0.7 was used as the baseline for a good match within this study. However, fluctuations in the trends of the data are not represented, only the overall, overriding trend of the data. For this reason, data that visually matches more closely could produce a lower score if the trend of the datasets fluctuates up and down over time. Different variables are compared to data from various sources due to lack of full datasets within publications (e.g. no oil production rate data within Greaves et al. (2011a)).

#### *4.2.4.1 Model T*

Using the experimental data from (Greaves et al., 2000b) as the model data, Model T is then compared against it for an R2 value to assess similarity. Figure 4.3 has an R2 value of 0.89 and an API mean difference of 0.72. This value confirms that Model T, when using consistent operational and model-development inputs as the experimental laboratory

tests, is a very good match. Modelling laboratory-scale THAI processes in this approach produced accurate and valid results.

#### *4.2.4.2 Model C*

Using the experimental data from Xia et al. (2002c) as the validation data, Model C is then compared against it for an R2 value to assess similarity. Figure 4.4 has an R2 value of 0.716 and an average API mean difference of 0.48. This value is lower than that seen for Model T. However, due to the increased complexity of both the model, as well as the data used for validation from Xia et al. (2002c) this decreased match is somewhat expected.

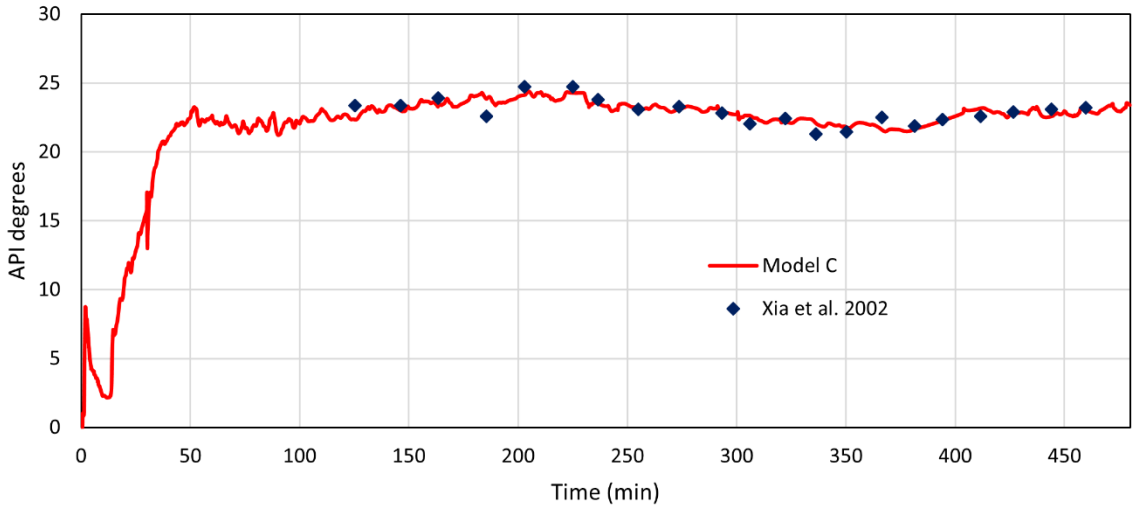


**Figure 4.4.** API of produced oil vs time showing oil upgrading of Model C against (Xia et al., 2002c).

### 4.3 Comparisons of THAI and THAI-CAPRI

#### 4.3.1 Peak temperature

The temperature calculated by Model T can be observed to reach a peak of ~900°C after the injection of oxygen initiates, with initial temperatures being raised through the use of an electrical heater in the injector well, heating up the inlet area prior to oxygen injection. However, the temperature calculated by Model C is observed reaching slightly higher, up to 1000°C (Figure 4.5).

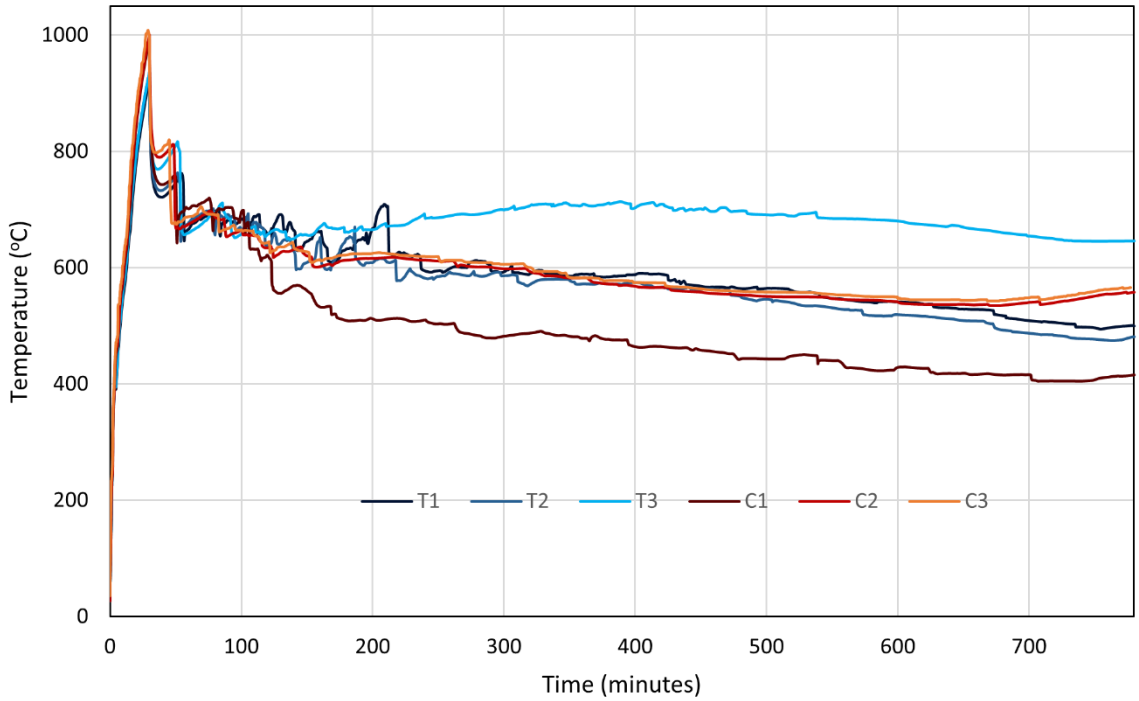


**Figure 4.5.** Temperature against time for both THAI dry (T1), pre-steam (T2), and constant steam (T3) and THAI-CAPRI dry (C1) pre-steam (C2), and constant steam (C3)

The difference is explained through the additional electrical heating of Model C to account for the endothermic coke gasification reactions. As the electrical heater raises the temperature of the inlet area, the heavy oil will begin the thermally upgrade and crack into light oil and coke. Due to the lack of oxygen injection at this time, the coke produced through this mechanism has no effect on the peak temperature of THAI, but in the CAPRI models the coke is able to react with water (either native or injected) and bring the temperature down. As this occurs, additional electrical heating must be applied to the inlet area to maintain peak temperature. The temperatures calculated by Model T and Model C both then show an undulating decrease in temperature down to ~680°C at 100 minutes. At 100 minutes, variations in temperature start to become evident across the different models. The temperatures of Models T3 and C3 tend to level off or decrease gradually at ~100°C higher than those of models incorporating steaming between 100 minutes until 780 minutes. All model variations show a gradual decrease in peak temperature from 150 minutes onwards, except for Model T3 which displays a slight

increase until 400 minutes, at which point the same decrease is then observed until 780 minutes.

### 4.3.2 Temperature distribution

Figure 4.6 displays the temperature distribution of all 6 models at 320 minutes, which is a point at which combustion has been initiated and the system should be in a stable process (Rabiu Ado, 2017). Model T displays a forward leaning combustion front shown by the orange grids, with mostly vertical or forward leaning contacts between all temperature regions, indicating that a stable combustion front has formed, and the sweep efficiency is high. Vertical or slightly forward leaning combustion zone indicates a smoothly moving area of combustion that consumes the oil from the sand-pack without causing effects such as channeling or gas overriding. Oil will also flow directly downwards from the heated zone towards the producer well. Model C, however, displays a very prominently forward leaning combustion front, with vertical or backwards leaning contacts between all other temperature regions (as indicated by the red arrow). This indicates that the combustion front is somewhat unstable and may show poor performance in its ability to sweep the reservoir. These differences are caused by an increase in temperature along the producer well of Model C, shown by an elongation of the temperature regions towards the heel of the producer (also see Figure 4.3). This temperature increase will be as a direct result of exothermic catalysis in that area, with the higher temperatures caused by catalytic upgrading reactions of the heavy oil causing a backwards leaning temperature gradient. This is most evident in the regions of lower temperature (200℃ +) and is concurrent with temperature profiles seen within experimental work from (Xia et al., 2002c). The decrease in temperature calculated by Model C when compared to Model T is due to lowered fuel availability (Ado et al., 2022a). The inclusion of coke gasification and heavy oil hydrogenation within Model C, there is

competition of those components to be oxygenated, resulting in lower levels of combustion occurring and thus lower temperatures.

Figure 4.7 displays the temperature distribution of the models at 320 minutes for the plane in the downward (k) direction that contains the producer well at a cross-section containing the injection and production wells. Little variation between the dry and pre-steamed variation of each model is observed, with differences between each dry and pre-steamed variation also minimal when compared the constant steam injection variations. Model T1 and T2 display more grid blocks at 400°C or higher than Model C1 and C2, which again is due to lower fuel availability in that area as heavy oil concentrations diminish more quickly in CAPRI as a result of additional reactions containing heavy oil as a reactant. Pre-steaming the models appears to have negligible impact on the temperature distribution seen throughout the models during stable combustion. This is expected as the additional steam from the start will have, by this point, joined the steam bank that has arisen ahead of the combustion front and will provide little to no additional help in heating the model. Constant steam injection, as occurs in models T3 and C3, ensures that the producer well is maintained at a higher overall temperature for maximum thermal cracking and viscosity reduction of the heavy oil in that area. These attributes are thought to increase the quality and quantity of the producer oil and demonstrated in the API upgrading observed in this study.

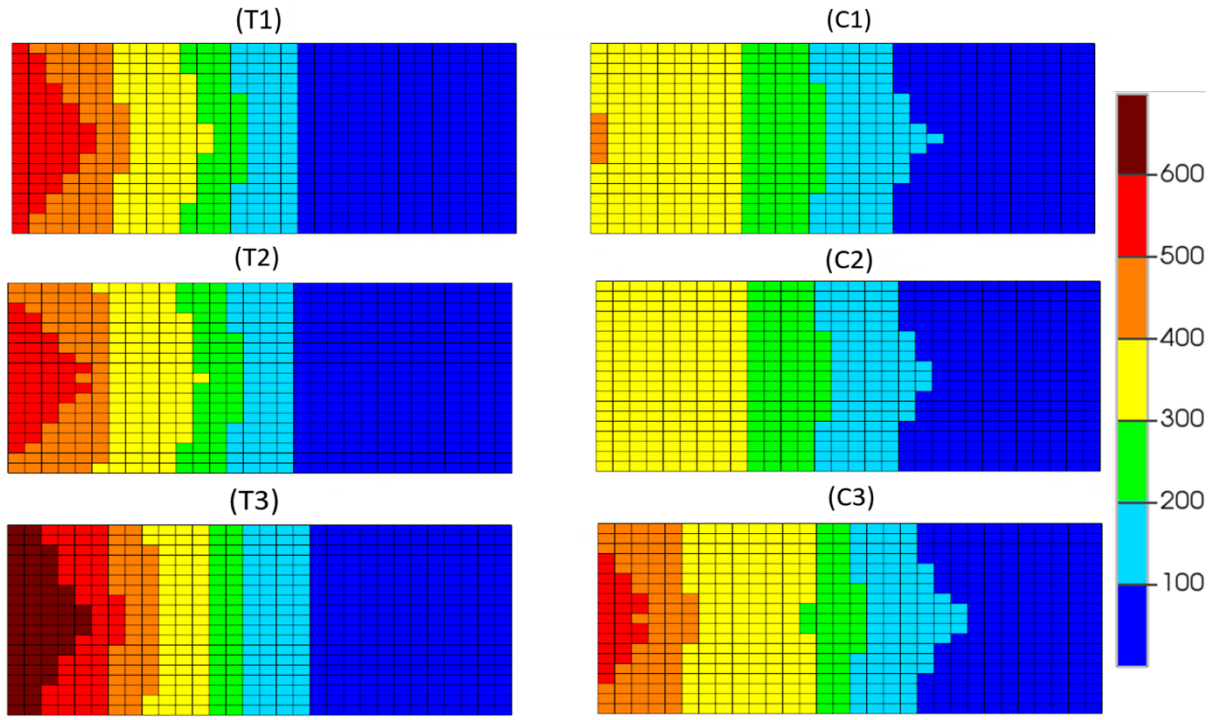


**Figure 4.6.** Temperature distribution (°C) for THAI dry (T1), pre-steam (T2), and constant steam (T3) and THAI-CAPRI dry (C1) pre-steam (C2), and constant steam (C3) at 320 minutes in the 10$^{th}$ j plane (scaled by a factor of 2 in the z direction).

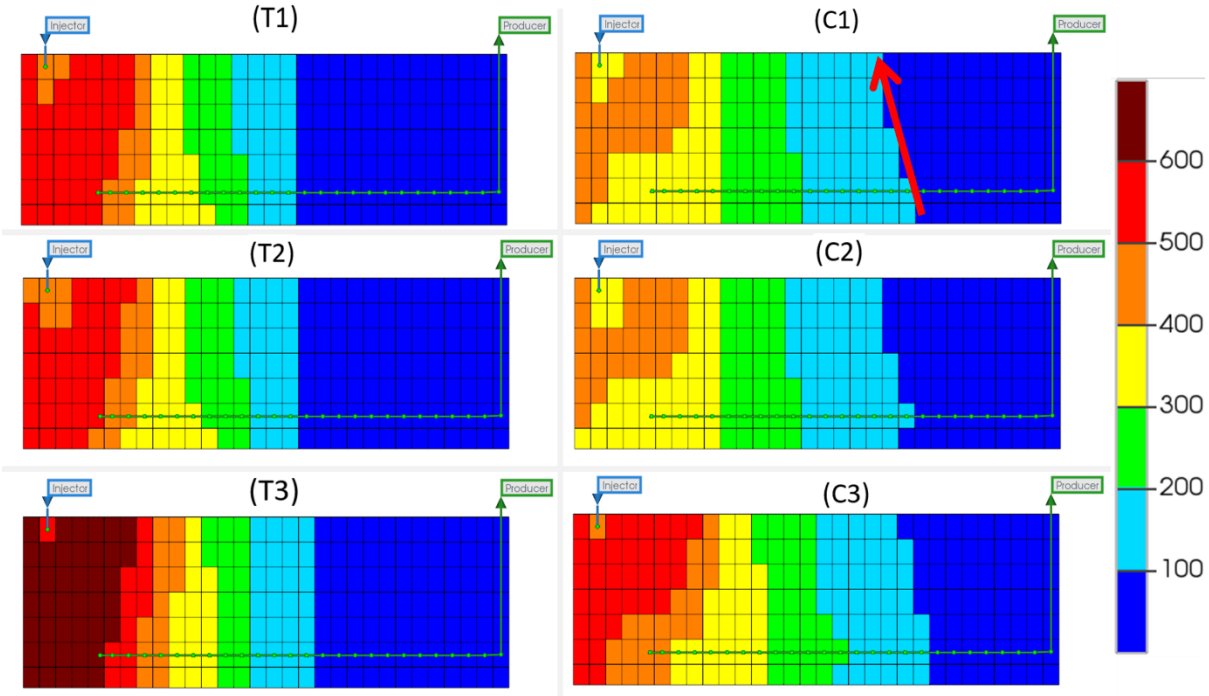


**Figure 4.7.** Temperature distribution (°C) for THAI dry (T1), pre-steam (T2), and constant steam (T3) and THAI-CAPRI dry (C1) pre-steam (C2), and constant steam (C3) at 320 minutes in the 6$^{th}$ k plane (scaled by a factor of 3 in the i direction).

### 4.3.3 Impact of steam

The temperature of Model C3 is seen to fall along the same time-series profile as Model T1 and T2 (Figure 4.5) due to the increased heat provided by the constant steam injection. Model T3 reacts in the same way, producing a higher peak temperature and higher temperatures around the injector well than all other models due to the heat provided by constant steam injection. It is believed that the temperature increase from the constant steam injection occurs dominantly as a result of physical heating of the process, rather than being related to exothermicity induced by steam reacting. This is because none of the THAI models contain reaction with steam/water as a reactant, yet still observes an increase in peak temperature over those models with less or no steam.

### 4.3.4 Impacts of MOZ on catalysis

Rabiu Ado (2017) states that simulations of the THAI process have shown that the mobile oil zone (MOZ) temperatures are not high enough for catalysis of the heavy oil hydrogenation to occur (300°C), however, it can be seen that large areas of the Model T and Model C are observed to be at least 300°C, with most blocks surrounding the producer well in Model C1, C2 and C3 being calculated to be 380°C or higher which is close to the optimum temperature of 425°C observed in Hart and Wood (2018). This suggests that catalysis is a feasible process that could occur within the THAI-CAPRI process within STARS through the addition of the catalyst component, though for optimum results in oil API upgrading, optimisation of operational processes that increase temperature (e.g., increased air flux or oxygen enrichment) would benefit.

### 4.3.5 Combustion front

During ISC the region of the reservoir behind the combustion front is generally 100% saturated by gas, largely composed of unreacted oxygen (Rabiu Ado, 2017). The shape of

this oxygenated region should define the inner boundary of the combustion front as this is where oxygen begins to react with hydrocarbon fuels, bringing its saturation to zero, this region has been depicted in Figure 4.8 for the THAI and CAPRI models. Figure 4.8 displays the models in 3-D at 320 minutes, presenting only those grids that contain oxygen alongside the producer well. It is therefore an excellent indicator of the shape of the combustion front itself. By 320 minutes the combustion front in all models has expanded to the full width of the model, gradually tapering down towards the toe of the producer (Figure 4.8). The distance between the toe of the producer and the bottom of the combustion front (i.e., the closest coloured block to the producer well toe) varies from model to model, with Model T3 displaying the largest value. All other models appear to display the combustion front contacting the producer well, due the higher peak temperature of Model T3 allowing for better oxygen consumption rates, allowing less oxygen to bypass the combustion zone unreacted. Unreacted oxygen reaching the production well is a key indication of early oxygen breakthrough (Ado et al., 2022a) the lateral advancement of the combustion front is similar for all models, being 10 cm expansion at 320 minutes. This indicates an approximate combustion front velocity of 2 cm $h^{-1}$ which is in-line with results observed in Xia et al. (2002a) for experiments operated under similar air injection flux.

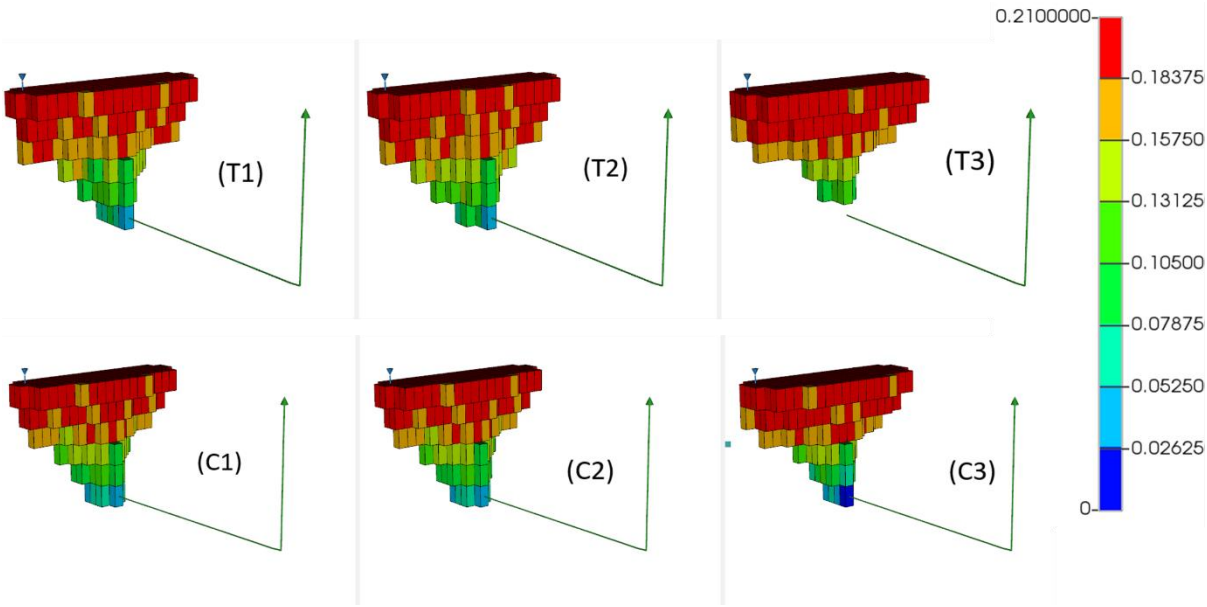


**Figure 4.8.** Oxygen gas mole fraction distribution for THAI dry (T1), pre-steam (T2), and constant steam (T3) and THAI-CAPRI dry (C1), pre-steam (C2), and constant steam (C3) at 320 minutes showing only those grids that contain oxygen (scaled by a factor of 3 in the i direction).

### 4.3.6 Oil upgrading

#### *4.3.6.1 API*

The main use for both the THAI and THAI-CAPRI processes is the in-situ upgrading of heavy oils and bitumen for the purpose of a lower energy input route to fuel production. Figure 4.9 displays the API of the produced oil for dry, pre-steamed and constant-steamed variations of both Model T and Model C as a function of production time. All three THAI models display similar trends in API over time, showing a gradual increase and decrease over the first ~600 minutes until sharp increases are observed in all three THAI models, to varying degrees. This is due to variations in the amount of lighter oil that build up around the producer wellbore as a combined result of thermal cracking and gravity drainage due to lowered density and viscosity. These lighter oils are therefore produced in these larger quantities at different times, with the higher temperatures of Model C3 and T3 inducing higher rates of thermal cracking than Models C1 and C2 and Models T1 and T2, respectively, earlier within the 780-minute run. Model T3 displays a lower API

output than Models T1 and T2 until 650 minutes when Model T1 observes a sharp increase to ~24.5° API causing it to become higher than Model T2 and T3, which also observe a lessened increase to ~22° and ~20° API respectively. This eventual increase in API towards the end of the run is possibly explained through the comparable increase in LO production at that time (Figure 4.9 and Figure 4.10). Model C3 displays a higher API output than Models C1 and C2 at almost all times, indicating that increased steaming of Model C causes higher amounts of heavy oil to be upgraded. Model C is observed producing oil with an API of 2-5° higher than Model T for most of the 780-minute simulation run, implying that the presence of a catalyst does indeed aid in the in-situ upgrading of heavy oil through heavy oil hydrogenation. These upgrading values for CAPRI over THAI are similar to reported values under experimental conditions, averaging at 3.4°, 5.8°, and 6.3° API over THAI for no-steam, pre-steam, and constant-steam respectively. However, this improvement varies over time, with API values for Models T, C1 and C2 seemingly meeting by the end of the 780-minute simulation run. This time-period is synchronous with a decrease in temperature and could therefore indicate that higher degrees of API upgrading could occur through thermal cracking at lower temperatures due to the lower extent of HTO occurring. This is consistent with reported results of Xia et al. (2002c) where it was found that API decreases during time of temperature increase. The sharp decrease followed by the gradual increase in API at around 35 minutes in all six runs is attributed to the start-up effect. This consists of the light oil present in the grids around the producer being produced before the oxidation process begins to occur during combustion.

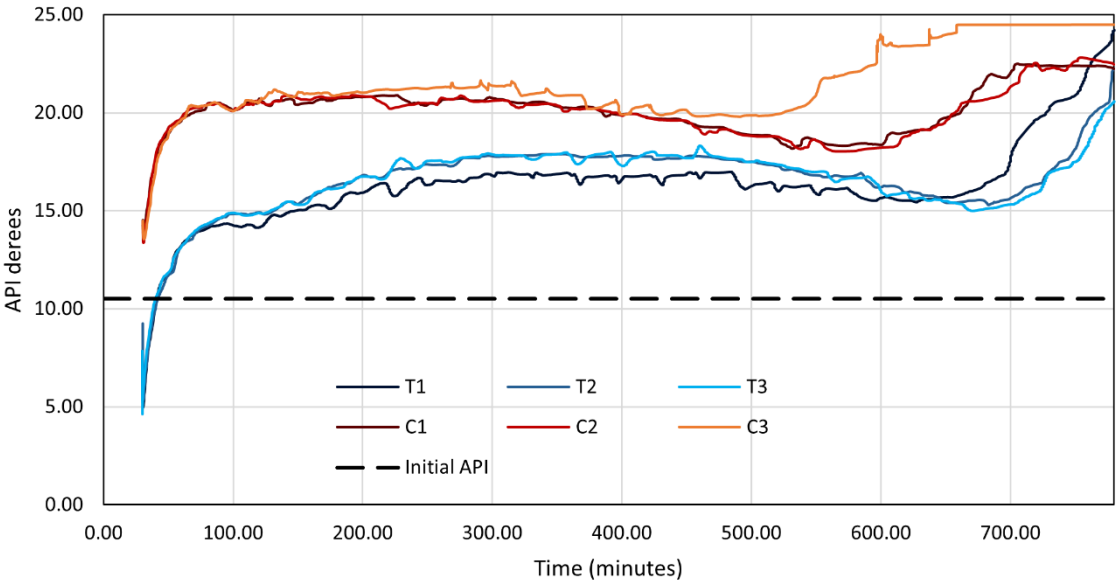


**Figure 4.9.** API against time for both THAI and THAI-CAPRI for the three investigated steam operating conditions. A black dashed line is used to represent the initial API of the oil before combustion.

#### *4.3.6.2 Produced oil composition*

The ratio of oil components/fractions produced through both the THAI and THAI-CAPRI processes can be indicative of the extent and mechanism of upgrading (catalytic vs. thermal cracking). To the author's best knowledge, the produced fractions of oil have not yet been investigated within STARS simulations of THAI and THAI-CAPRI. This novel analysis will shed light on the catalytic extent of CAPRI in lab-scale simulations. Figure 4.10 displays the volume fractions of produced light oil for all six models. Light oil component (LO) production from Models T1, T2 and T3 display significant undulation, which appears to be absent in the CAPRI models and API upgrading profiles for Models T1, T2 and T3. This undulation could be indicative of unstable upgrading, despite a stable combustion front being present, possibly caused by the use of a coarse gridding system within the model incrementally producing oil in larger quantities rather than consistently producing at a constant rate. This trend is absent in Models C1, C2 and C3 due to the lower rate of thermal cracking occurring and lower temperatures leading to a lower decrease in viscosity of the LO fractions allowing for a slower, but more stable production.

At ~650 minutes Model C3 displays a plateau of LO production, reaching 100% volume fraction, indicating that all heavy oil, at least near the producer well, has been thermally cracked. This is concurrent with volume fractions of produced UHC shown in Figure 4.10, where at the same time in Model C3 UHC reaches zero, due to no HO being available for catalytic upgrading as it has already all been thermally cracked. The same trends in increased LO and decreased UHC production in Models C1 and C2 also occur concurrently, for the same reasons of HO becomes less available for catalytic upgrading due to increased thermal cracking. Despite this, between ~100 minutes and ~600 minutes UHC production appears to be very stable in Models C1, C2 and C3. These results are comparable to the interpretation of hydrogen to carbon (H/C) ratios and produced API within literature of THAI and THAI-CAPRI laboratory exepriments (Xia et al., 2002c). However, laboratory experiments of THAI-CAPRI often show API upgrading and H/C declines towards the end of the experiment after peaking (Xia et al., 2002c; Greaves and Xia, 2004; Hart and Wood, 2018). These declines aren't observed in Models C1, C2 and C3 in this investigation, being explained through the lack of catalyst deactivation within the STARS models.

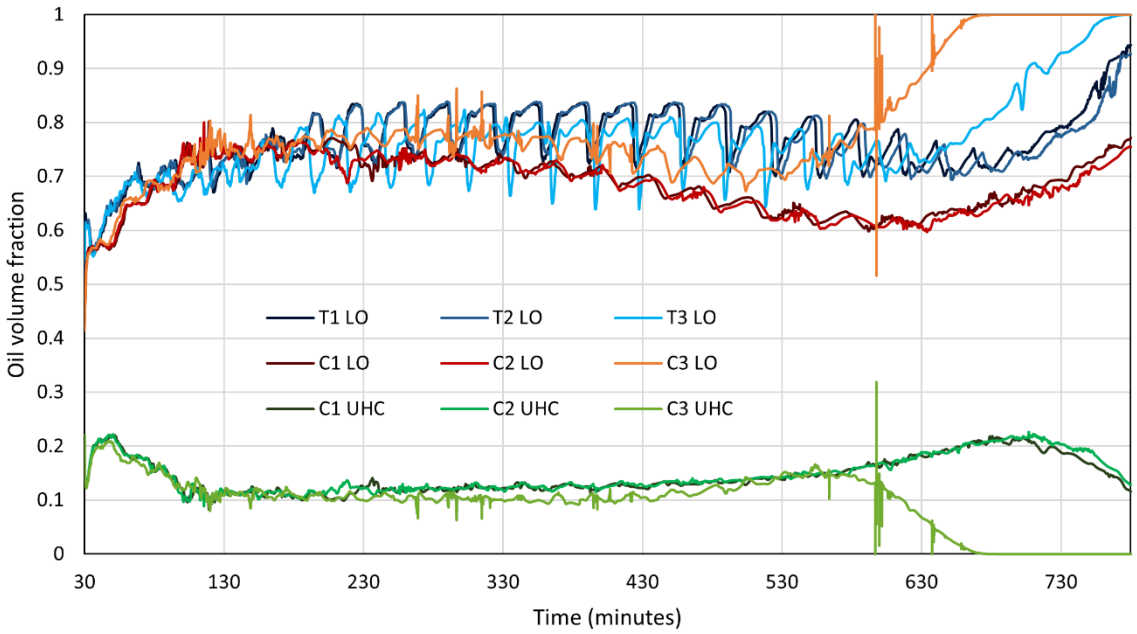


**Figure 4.10.** LO component oil volume fraction against time for both THAI and THAI-CAPRI for the three investigated steam operating conditions and the UHC component oil volume fraction for THAI-CAPRI for the three investigated steam operating conditions

#### *4.3.6.3 Oil density distribution*

Figure 4.11 shows oil density distribution, indicating that at 780 minutes the average oil density for Model C is lower than Model T, with the black-coloured grid squares representing oil that has experienced no change in density and coloured squares representing oil of varying densities. It is also observed that although Model T displays less grids containing oil of 0.0006 kg $cm^{-3}$ or higher than Model C, the average oil density visually remaining (determined by a higher proportion of grids containing oil of a lower density) within the Model T is higher than that of the oil remaining as calculated by Model C at the same time. This is due to oil around the producer well in all Model C variations displaying much lower average densities than the same blocks in all Model T variations (represented by light-green and light-blue blocks), exhibiting the increased upgrading due to the catalyst. It should also be noted that the black grids displayed in Models T1, T2 and T3 represent oil that has undergone no upgrading, indicating that certain regions of the model appear to be bypassed during the air injection process, as a result of oxygen

breakthrough creating override channels within the reservoir, suggesting that since the 320-minute mark stability has decreased within the process.

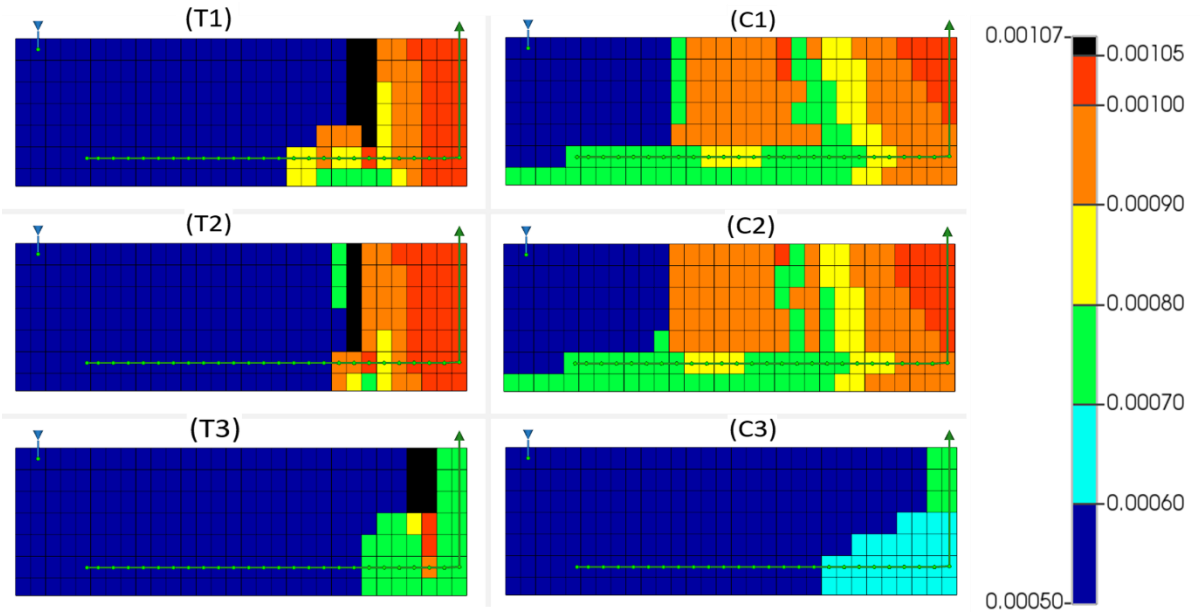


**Figure 4.11.** Oil density distribution (kg $cm^{-3}$) for THAI dry (T1), pre-steam (T2), and constant steam (T3) and THAI-CAPRI dry (C1) pre-steam (C2), and constant steam (C3) at 780 minutes in the $10^{th}$ j plane (scaled by a factor of 2 in the z direction).

Models T1 and T2 display oil density to generally decrease linearly from left to right, with the regions further away from the combustion front being higher in density. However, the same cannot be said for Model C1 and C2, regions of the model undergo varying degrees of upgrading, consistent with decreasing temperature zones of the combustion front combined with disproportionate gravity segregation due to the augmented density decrease of oil around the production well, leading to heavier oils displacing less dense oil behind the combustion front, prompting an oil density distribution not observed in the catalyst absent THAI models. Similar occurrences are observed within Ado et al. (2022a). Constantly steaming the process appears to have the biggest impact on decreasing the density of the in-situ oil, with Model C3 displaying all residual oil to be less than 0.0008 $gcm^{-3}$, or 45° API. The results of Model T3 show some similarity to Model C3 in increased density decrease through constant steam injection. However, it appears to

still have regions of unreacted or less significant decreases in density, due to the absence of catalytic upgrading within the model.

### 4.3.7 Coke production

Coke is deposited during thermal cracking of HO and occurs in the region just ahead of the combustion front, and primarily used as fuel for the advancing combustion front (Xia et al., 2003c; Rabiu Ado, 2017). Coke that is observed to be behind the combustion front is HTO fuel that has been bypassed by the advancing combustion front, indicating that perhaps higher air injection rates are required for complete combustion of coke fuel. This bypassing is observed in all six models (Figure 4.12). Also observed are the regions of higher coke concentration as indicated by regions of darker orange/red shaded grid squares. These areas are the symptomatic of the coking front found just ahead of the combustion front where thermal cracking occurs, displaying a relationship between coke concentration and combustion front shape. In Models T1, T2 and T3 more coke is observed in the grids where the horizontal producer well is located, suggesting that coke that is laid down on the well is more likely to be bypassed by the advancing combustion front. Conversely, Models C1, C2 and C3 display the same grids containing negligible coke within them. However, this is thought to be an artefact of the simulator not depositing solid coke component in the grids where the solid catalyst component is located. There can also be seen a relationship between coke concentration and peak temperature when Figure 4.12 and Figure 4.7 are compared. This is particularly evident through the decrease in coke concentration in Models T3 and C3 when compared to their lesser steamed counterparts, due to increased coke consumption leading to higher temperatures, which in turn also accelerates the coke consumption. Interestingly, Models C1, C2, and C3 display significantly higher concentrations of coke than their non-catalysed counterparts in THAI, despite having additional coke consumption reactions via coke

gasification. This is possibly explained through lower temperatures leading to much lower HTO rates of coke, (Xia et al., 2002c; Ado et al., 2022b) allowing more coke to be bypassed by the combustion front than in Models T1, T2 and T3, whilst already having been bypassed by the steambank reducing the coke gasification of the combustion bypassed coke.

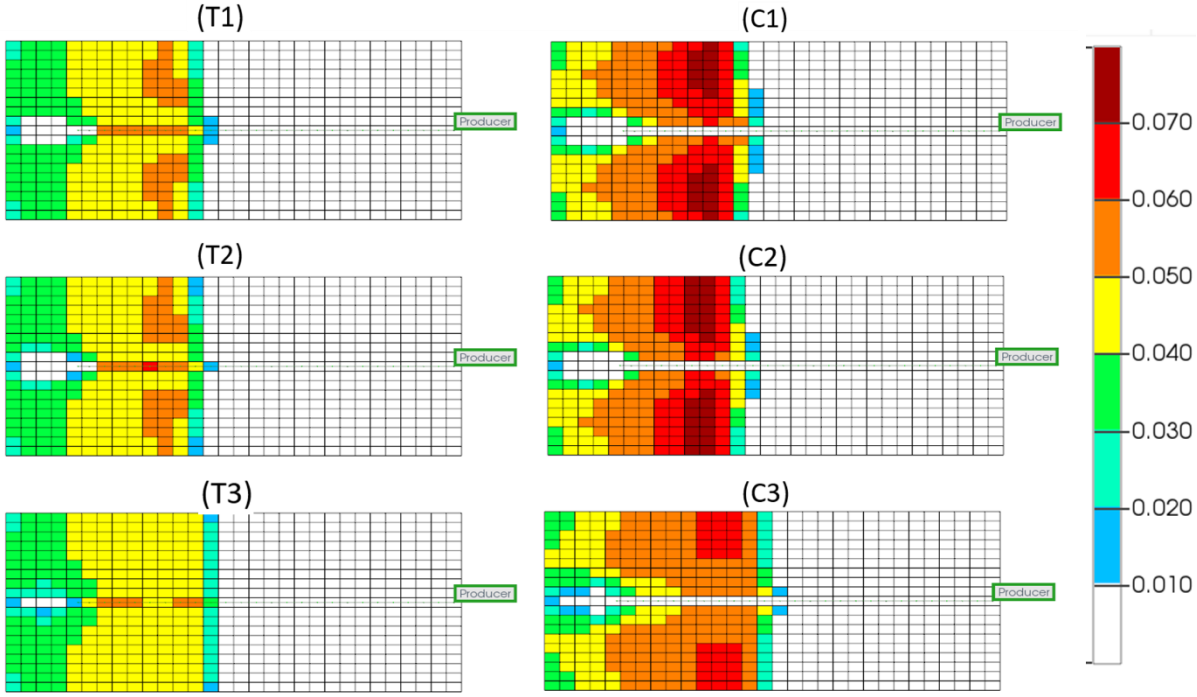


**Figure 4.12.** Coke concentration (mol $cm^{-3}$) for THAI dry (T1), pre-steam (T2), and constant steam (T3) and THAI-CAPRI dry (C1), pre-steam (C2), and constant steam (C3) at 320 minutes in the 6$^{th}$ k plane (scaled by a factor of 3 in the i direction).

### 4.3.8 Oil production

Figure 4.13 shows cumulative oil production from all THAI and CAPRI models. Negligible difference is observed between any of the no-steam and pre-steamed models, with Model C1 displaying the highest cumulative production of the four (Figure 4.13). However, constant steaming of the models, as incorporated into Models T3 and C3 results in significantly higher cumulative production, with Model T3 and Model C3 experiencing an increase of ~200 $cm^3$ and 400 $cm^3$ respectively above the ~3150 $cm^3$ of the other four models. This is concurrent with thermal cracking which occurs in Models T3 and C3,

converting most, if not all HO into LO, which has a much lower viscosity allowing for easier flow and production. A larger increase in cumulative production is displayed in Model C3 due to the increased proportion of HO that is converted into UHC, which again has a much lower viscosity than HO allowing for more efficient production of the oil. The above factors and higher temperature associated with constant steaming leads to much lower viscosities of all oil components and increased cumulative production. Very little variation between Models T1 and T2 is seen, similarly negligible variation occurs between Models C1 and C2, suggesting that pre-steaming of these processes does little to increase the production potential. It should also be noted that Model C1 and C2 display very little increase in production over Models T1 and T2, implying that the addition of a catalyst to the THAI process does little to increase the cumulative production unless constant steaming of the process is applied, consistent with (Xia et al., 2002c). This does not, however, account for the quality of the produced oil, which will still be higher and more favourable in the THAI-CAPRI process.

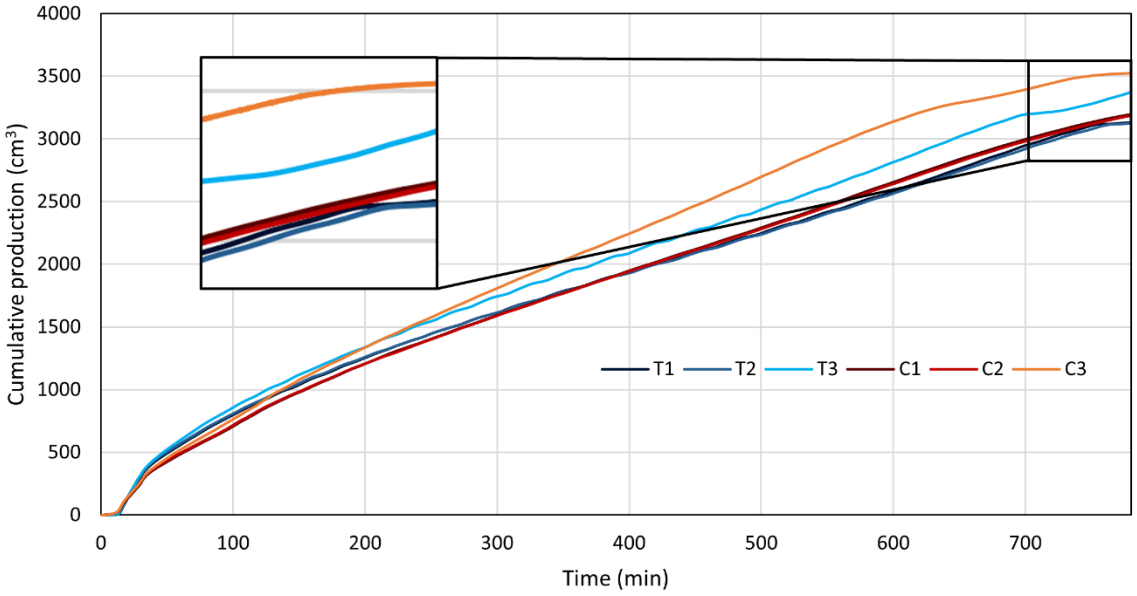


**Figure 4.13.** Cumulative oil production against time for both THAI and THAI-CAPRI for the three investigated steam operating conditions

### 4.3.9 Comparison of models

Overall, all six models experienced an increase in API over the original oil of at least 58.76%. Constant steaming of the THAI and THAI-CAPRI process increases oil production by at least 7.7% and 10.6% over the dry variations, respectively (Table 4.1). Model C3 showed the greatest API upgrading and cumulative oil production when compared to all other models, with Model T3 showing the second largest increase in cumulative oil and Model C2 the second largest increase in API upgrading. The utilisation of either or both constant steaming and a producer well loaded catalyst would be dependent on the needs of the process. It is evident, that even without the use of any steaming that CAPRI can significantly upgrade in-situ heavy oil. However, CAPRI has been shown not to increase oil production over THAI until constant steaming is exploited, with constant steaming of THAI performing well in increasing oil production also, at the cost of no increased API upgrading over dry THAI. Overall, pre-steaming has been shown, for both THAI and THAI-CAPRI that pre-steaming has negligible impacts, due to the timing of the steam bank formation.

**Table 4.1**. Comparison of end-of-run results ($^+$ being a change over T1 and $^*$ being a change over C1).

| Model number | Average produced API° | % Increase over initial API | Cumulative produced oil ($cm^3$) | % Increase in cumulative oil over $T1^+/C1^*$ |
|---|---|---|---|---|
| T1 | 16.74 | 59.43 | 3124.38 | N/A |
| T2 | 16.67 | 58.76 | 3117.92 | $-0.21^+$ |
| T3 | 16.77 | 59.71 | 3365.89 | $7.73^+$ |
| C1 | 20.14 | 91.81 | 3184.71 | N/A |
| C2 | 22.49 | 114.19 | 3173.35 | -0.36* |
| C3 | 23.08 | 119.81 | 3524.37 | 10.67* |

## 4.4 Comparison to hydrogen injection using WhiteSands oil

Modelling THAI-CAPRI using the co-injection of oxygen and hydrogen can provide a good idea of the potential upgrading of the process. It can suggest an optimal oxygen to hydrogen ratio for the operation of THAI-CAPRI, offering optimum hydrogen

concentrations for oil upgrading under THAI conditions. Several papers have published results of such investigations (Ado et al., 2022b) citing similar upgrading potential to the models within this study. However, the inclusion of hydrogen generation reactions leads to differing results for fuel availability, temperature, and oil production. The inclusion of coke gasification in Model C leads to less fuel availability and therefore less HTO of coke. This results in a lower calculated temperature, which is exacerbated by the endothermicity of the coke gasification reaction. These lower temperatures are realised in the oil production where the cumulative oil production for Model C1 in Figure 4.9 at 320 minutes sits approximately 450 $cm^3$ less than the cumulative oil production from Ado, Greaves and Rigby (Ado et al., 2022b) at the same time. The lower temperatures lead to decreased viscosity reduction and thermal cracking, causing a reduced flow potential of the oil. Hydrogen injection within THAI-CAPRI results in an overestimation of the absolute cumulative oil production.

Ado, Greaves and Rigby (Ado et al., 2022b) also used a minimum activation temperature ($T_a$) of 400°C for the catalytic hydrogen addition reaction, meaning that if a grid block containing all the necessary reactants was below $T_a$ then 400°C would be used within the Arrhenius equation to calculate the reaction rate. However, Ado, Greaves and Rigby (Ado et al., 2022b) used the same activation energy as this study, with both investigations reporting similar oil upgrading when compared to THAI, yet this study did not use a $T_a$. Not using a $T_a$ would lead to more accurate density distributions as only those areas that are at the correct conditions will demonstrate catalytic oil upgrading. This study also demonstrates that using the activation energy from Ado, Greaves and Rigby (Ado et al., 2022b) then catalytic upgrading is possible at the temperatures within the THAI process without the need of using a $T_a$.

### 4.4.1 Oil upgrading

Figure 4.14 depicts the contrasting upgrading patterns between Model Ci and Model C, and Model Cz, using the same initial conditions. Model C is the same model from section 4.2.7.2, Model Ci is the hydrogen injection augmented THAI model from Section 4.2.7.3, and Model Cz is Model C with the same injection parameters as Model Ci (oxygen and hydrogen 50/50 volume). Therefore, Model Cz is a combination of Model C and Ci, utilising both in-situ hydrogen generation and injected hydrogen. The analysis of the three models' upgrading trends reveals distinct patterns over the course of the simulation. Initially, within the first 80 minutes, Model Ci demonstrates a rapid surge in API upgrading, escalating from 10.5 to 22 degrees. In contrast, Model C maintains relative stability within the range of 16 to 18 degrees, following an initial quick increase from 10.5. Model Cz, the combination model, exhibits an extraordinarily swift API rise from 10.5 to 30 degrees. However, after remaining stable around 29.5 to 30 degrees for approximately 55 minutes, it undergoes a sharp decline, reaching 22 degrees by the 80th minute. Subsequently, during the following 100 minutes, Model C and Cz display a relatively steady API output, ranging from 16 to 18 degrees. Model Cz tends towards the higher end, while Model C leans towards the lower side of the range. In contrast, Model Ci experiences a decrease from 22 degrees to approximately 18 degrees API. Continuing into the subsequent 140 minutes, Model Ci maintains a downward trend, gradually declining from 18 degrees to a final API value of 17 degrees. On the other hand, both Model C and Model Cz demonstrate strikingly similar patterns, showing a consistent increase from an initial API value of 17 degrees to 22 degrees. These two models exhibit no indications of decreasing beyond the end time of the simulation.

The resemblance between the trends of Model C and Model Cz, particularly after the 80$^{th}$ minute and notably from the 180$^{th}$ minute onwards, suggests that the injected hydrogen's

importance diminishes within the upgrading process. This observation is supported by a decline in upgrading from 80 minutes to 320 minutes in Model Ci. Moreover, the analysis suggests that the oil in close proximity to the catalyst is produced in the producer well before the injected hydrogen has an opportunity to contact it. In contrast, the in-situ generated hydrogen has a significantly shorter distance to travel from its generation site to reach the hot oil at the catalyst, making it more susceptible to involvement in the upgrading process.

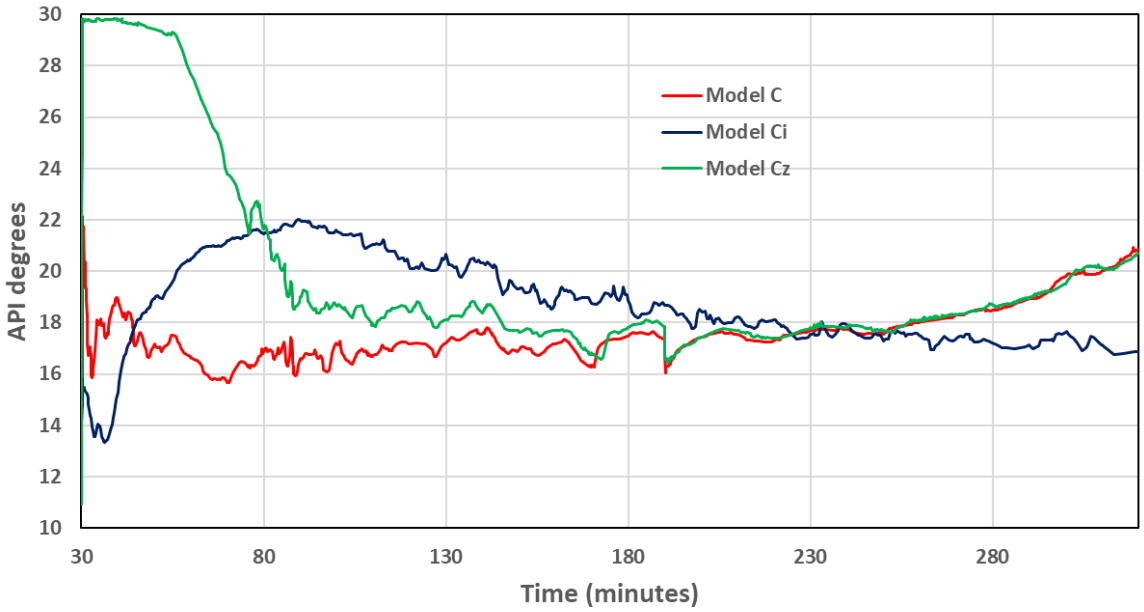


**Figure 4.14.** Comparison of API upgrading between Model C, Model Ci and Model Cz

### 4.4.2 Production of upgraded oil

Figure 4.15 visually presents the impact of hydrogen injection on the volume of upgraded oil generated through its reaction. The graph clearly demonstrates a significant reduction in the volume of upgraded oil when hydrogen is injected. A crucial observation can be made at the 170-minute mark in Model Ci, where the production of upgraded oil reaches a plateau. At this point, the production rate becomes negligible, indicating a saturation point (Figure 4.16). In contrast, Model C exhibits a distinct pattern of continuously accelerating upgraded oil production throughout most of the simulation.

Figure 4.16 illustrates a notable surge in the production of upgraded oil in Model C shortly after the 30-minute mark. This sudden increase can be attributed to the initiation of combustion, which leads to the generation of water utilized in the water-gas shift reaction. This reaction plays a vital role in producing the required hydrogen for the upgrading process. Subsequently, after the initial surge, the production rate experiences a sharp decline, reaching approximately 1 $cm^3$ $min^{-1}$. However, the decline is followed by a gradual increase that persists until the end of the simulation. This pattern indicates that the hydrogen injection and associated reactions in Model C result in a sustained and continuous acceleration in the production of upgraded oil.

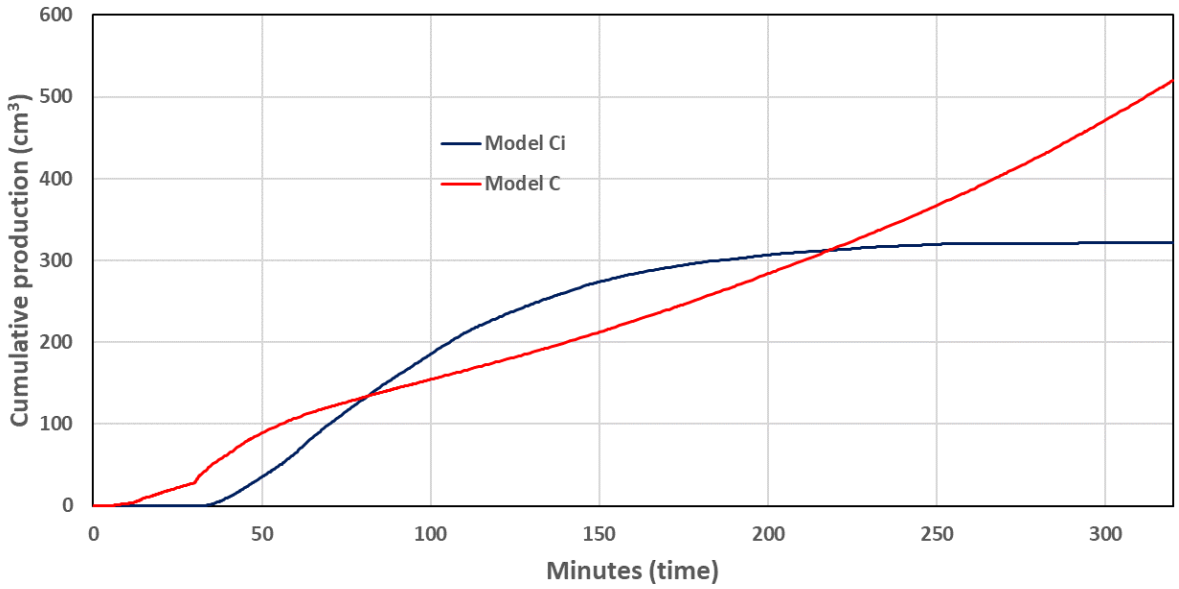


**Figure 4.15.** Comparison of cumulative production of catalytically upgraded oil between Model C and Model Ci

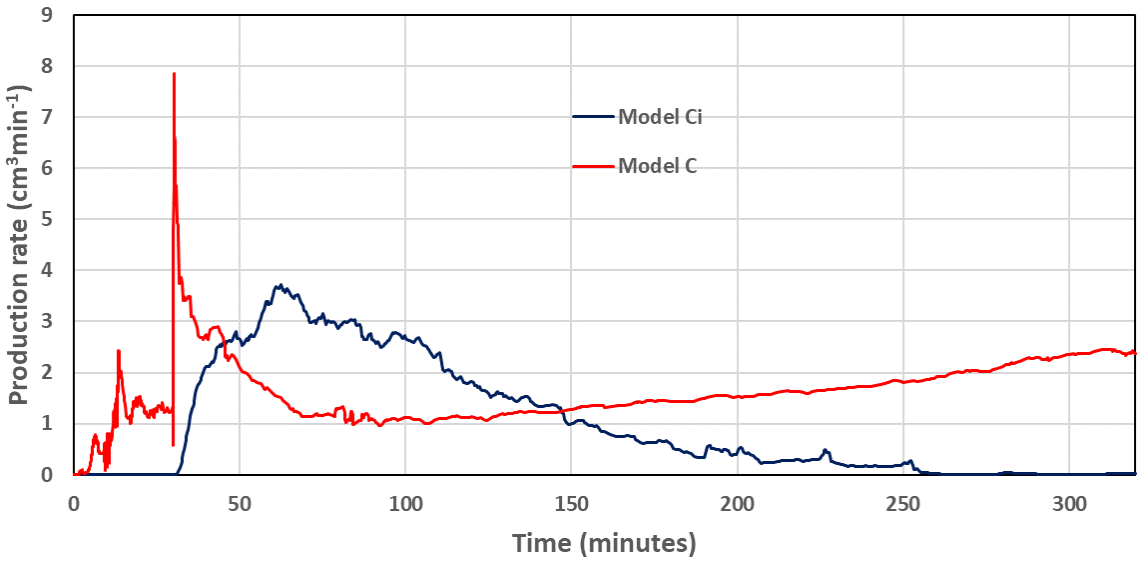


**Figure 4.16.** Comparison of oil production rates of catalytically upgraded oil between Model C and Model Ci

## 4.5 Conclusions

### 4.5.1 THAI vs THAI-CAPRI

Simulation of experimental THAI and THAI-CAPRI processes is possible within CMG STARS and can readily lead to the ability to investigate phenomena related to reaction kinetics and operation conditions. The THAI-CAPRI process has also been modelled using in-situ produced hydrogen and has been shown to offer potentially more accurate oil upgrading behavior of in-situ heavy oil. Validated models of both processes display both good matches through visual comparison and statistical $R^2$ analysis (0.89 and 0.71 for THAI and CAPRI for API upgrading respectively). Both models in this study were validated and matched against experimental data taken from extant literature, with CMG CMOST machine learning being a valuable tool in the validation through comparing and matching of simulated and experimental data respectively. This study investigated the effects of various steaming protocols on the THAI and THAI-CAPRI processes through numerical modelling and simulation. Three protocols were used: no steam injection, 30-minute pre-steam and 780-minute constant steam. Overall, constant steaming of the

processes displayed the highest quality of oil produced, alongside the higher cumulative production of oil. THAI-CAPRI was found to be favourable for API upgrading irrelevant of the steaming protocol used. However, constantly steaming the THAI-CAPRI process resulted in the highest amount of API upgrading of both the in-situ and produced oil. Overall, THAI-CAPRI experienced an increase in average API upgrading of 3.4, 5.8 and 6.3 over THAI for no-steam, pre-steam, and constant-steam respectively. Cumulative production rates varied from ~3150 $cm^3$ to ~3500 $cm^3$, with constant steaming of the process increasing production the most through improved oil viscosity reduction.

### 4.5.2 Hydrogen injection and In-situ hydrogen generation

In conclusion, the research study explored the potential upgrading capabilities of the THAI-CAPRI process through the co-injection of oxygen and hydrogen. By optimising the oxygen to hydrogen ratio, the study aimed to determine the optimal conditions for oil upgrading under THAI conditions. Several papers in the field have reported similar findings, indicating the viability of this approach. However, the inclusion of hydrogen generation reactions introduced variations in fuel availability, temperature, and oil production. One model, which incorporated coke gasification, showed lower fuel availability, and resulted in lower calculated temperatures. Consequently, this led to reduced oil production compared to previous studies. It was observed that hydrogen injection within the THAI-CAPRI models tended to overestimate the cumulative oil production. Furthermore, the research examined the impact of using a minimum activation temperature ($T_a$) for catalytic hydrogen addition. Comparing the results to a study that used $T_a$, it was found that not utilising $T_a$ resulted in more accurate density distributions. Additionally, the activation energy used in the study allowed for catalytic upgrading at the temperatures within the THAI process without the need for $T_a$. Regarding oil upgrading, the study analysed the behaviour of different models. One model

exhibited a rapid surge in API upgrading followed by a decline, while another model maintained relative stability. A combined model incorporating both in-situ hydrogen generation and injected hydrogen demonstrated an initial significant increase in API followed by a sharp decline. It was observed that the importance of injected hydrogen diminished over time in the upgrading process. Moreover, the production of upgraded oil was influenced by hydrogen injection. While one model showed a continuous acceleration in upgraded oil production, another model reached a plateau, indicating a saturation point.

# CHAPTER 5. FIELD SCALE MODELLING OF THAI

## 5.1 Introduction

This chapter reports an investigation of the reaction scheme used within THAI simulations, comprising the inclusion of several hydrogen generation/destruction reactions (e.g., water-gas shift reaction). The chapter also reports on the method of upscaling from laboratory to field scale simulations, and impact on the reaction scheme's kinetic Arrhenius values. The implication of the reaction scheme is evaluated for its potential to predict hydrogen generation from THAI, and the impact the reactions included within the simulation model have on the history match process against field data. The need for this evaluation arises from the uncertainty surrounding the composition of oil fractions in compositional oil models, resulting in unknown reaction kinetics (Ado, 2020a). Crude oil comprises a multitude of hydrocarbon species and chains that react at varying temperatures, undergoing distinct changes in energy, and exhibiting different rates. Given computational limitations, it is impractical to simulate every individual reaction, necessitating the use of a lumped oil model. This simplification entails grouping hydrocarbon species into a small number of oil pseudo-components (e.g., light oil and heavy oil). However, the kinetics have to be updated for a new grouping since those reported in the literature pertain to specifically tailored oil pseudo-components derived from historical matching of field or laboratory data (Greaves et al., 2011a). Consequently, the reaction kinetics of a hydrocarbon reaction are presumed as a variable for historical matching.

There are two scales of approach to determine the reaction kinetics of a THAI (Toe-to-Heel Air Injection) field-scale model. The first involves matching a laboratory-scale model with laboratory data and subsequently scaling up the reactions and physical model

to the desired field-scale. The second entails matching a field-scale model with dynamic field data at the same scale that the field-data is associated. Although the former is more commonly employed, likely due to the greater accessibility of laboratory-derived data, it carries the risk of potential inaccuracies during upscaling. This is because upscaling relies on mathematical theory and a number of assumptions, as highlighted in Ado (Ado, 2020a). The second approach generates THAI models that exhibit improved accuracy when predicting physical processes as they are based upon real-world data collected at a corresponding level (Anbari et al., 2023), though it comes at the cost of non-variable scaling. Nonetheless, achieving a satisfactory fit between the historical data from this domain can be challenging, with numerous factors capable of influencing the final result. The significance of incorporating reactions beyond oxidation and cracking in the reaction scheme during in-situ combustion (ISC) simulations has been emphasised in this research. These additional reactions, that have been observed to occur in laboratory experiments such as water-gas shift and coke gasification (Xia et al., 2002c; Shah et al., 2010), have a notable influence on the model's performance and its capability to accurately match historical data.

Despite an extensive review of the literature, no prior studies have been found that simulate THAI incorporating any of these reactions or explore the potential for hydrogen generation during the process. This study addresses the gap by incorporating water-gas shift reactions (both forward and reverse) and coke gasification with steam into a history matched model to compare the outcome with other THAI models that do not incorporate these reactions. Previous laboratory investigations have hypothesised the sequential nature of the water-gas shift reactions with coke gasification. However, this chapter emphasises the mathematical interplay between these reactions under in-situ combustion conditions by employing an innovative modeling approach that captures

both the individual and concurrent occurrences of the reactions. Furthermore, this study assesses the influence of each reaction on the model, examines the origin of hydrogen, and considers the practical implications of adopting THAI for hydrogen generation.

This chapter presents a novel investigation that employs an innovative modelling approach to intricately capture the mathematical interplay of reactions in in-situ combustion conditions. Notably, the methodology surpasses conventional models by simultaneously considering individual kinetics and concurrent reactions, offering a comprehensive understanding of this complex system. Significantly, the study thoroughly assesses the influence of each reaction, revealing previously unexplored insights into their contributions within the model. Moreover, the research unveils the mechanisms driving hydrogen generation during in-situ combustion, marking a notable breakthrough in understanding hydrogen origin within this thermal environment. Additionally, the findings highlight the practical implications of adopting Toe-to-Heel Air Injection (THAI) for efficient hydrogen production, underscoring its potential applications within in-situ combustion systems. Collectively, this work advances the field by introducing an innovative modelling approach, evaluating reaction influences, uncovering hydrogen origin, and showcasing THAI's practical prospects for hydrogen generation in in-situ combustion. The effects of upscaling have not been considered to isolate the impact of the reaction schemes only. Reports of the upscaling effect on the results of the simulation models within THAI have previously been considered (Ado, 2020a; Ado, 2021b).

## 5.2 K2 pilot history matching

The methodology employed in this study for history matching and dataset selection is underpinned by the challenges posed by the scarcity of published data from THAI field

trials. Recognising the limitations inherent in certain datasets that lack comprehensive variables of interest, a strategic approach has been adopted. This strategy involves the definite matching of oil production, both rate and cumulative, for the field that the simulation model is based upon (Kerrobert THAI pilot), whilst comparing the product gas production against a similar but different THAI pilot altogether (Whitesands THAI pilot). The selection of different datasets serves as a deliberate tactic aimed at accommodating the variability in available data sources and maximising the breadth of information used in this study. The subsequent sections will elaborate on the specifics of this methodology, shedding light on the steps taken to negotiate these challenges and derive important insights.

### 5.2.1 Kerrobert THAI pilot

The Kerrobert THAI project, located in Southeast Saskatchewan, Canada, focuses on heavy oil recovery within the Waseca sandstone formation (Hill, 2017; Wei et al., 2020). This specific formation, identified as a fine-grained sandstone reservoir, presents a depth to the top ranging from 758 m to 774 m, with the oil-water contact at 789 m (Turta et al., 2018). The oil zone thickness varies between 12-20 m in the Western region and expands to 25-30 meters in the Eastern part, accompanied by a bottom water depth of approximately 20 m in the Western area and around 10 m in the Eastern section. The project faces challenges due to the high viscosity of the oil and the presence of bottom water, resulting in a modest primary oil recovery of merely 1.5%. Operators in Western Canada often resort to thermal methods for recovering residual heavy oil when primary extraction becomes economically unviable (Wikel and Kendall, 2012; Wei et al., 2020). The observed limitations in primary recovery leave ample scope for secondary recovery or enhanced oil recovery (EOR) techniques to exploit the remaining resources effectively. These geological conditions, coupled with the challenges posed by oil viscosity and

bottom water, provide an ideal landscape for the implementation of thermal methods aimed at extracting the remaining heavy oil within the Waseca sandstone formation (Wei et al., 2020).

### 5.2.2 Analysis of field data

Figure 5.1 displays the Kerrobert THAI pilot oil rate data from 1st June 2014 to the 1st June 2015 (Turta et al., 2018). Air injection and ignition of the in-situ crude occurs at day 0. From Days 7 to 40, following the activation of controlled combustion and air injection initiating the Toe-to-Heel Air Injection (THAI) method, there is a consistent and steady increase in oil extraction rates. This phase indicates successful stimulation of the THAI method, signifying the effective initiation of controlled hydrocarbon oxidation within the reservoir. Between Days 41 and 140, fluctuations in oil production rates occur, lacking a distinct stabilisation pattern. This period does not reflect consistent plateauing but rather presents variations in extraction rates. Factors contributing to these fluctuations might include geological heterogeneity, varying rock properties impacting oil flow, potential inconsistencies in data measurements, and operational changes within the THAI method. Some of the variable effects surpass the predictive capacity of the mathematical model, consequently resulting in a smoothing effect on the trends observed as calculated by the model. Continuing from Days 141 to 180, a decline in oil rates becomes noticeable. This decline might stem from factors such as reservoir depletion, alterations in reservoir pressure, or dilution of the oxygen within the reservoir as the oxygen front expands (i.e., inverse square law), influencing the THAI method's effectiveness in oil extraction (Akkutlu and Yortsos, 2003; Ado et al., 2019; Ado et al., 2022a). The subsequent phase, between Days 181 and 230, reveals signs of stabilisation or slight recovery in oil rates. Operational adjustments might have contributed to this phase, aiming to optimise extraction methods and stabilise production. From Days 231 onwards, despite sporadic

peaks and troughs, an overall continual decline in oil rates is evident. This prolonged decline could indicate natural reservoir depletion or a decreasing efficiency of the THAI method over time due to evolving reservoir characteristics.

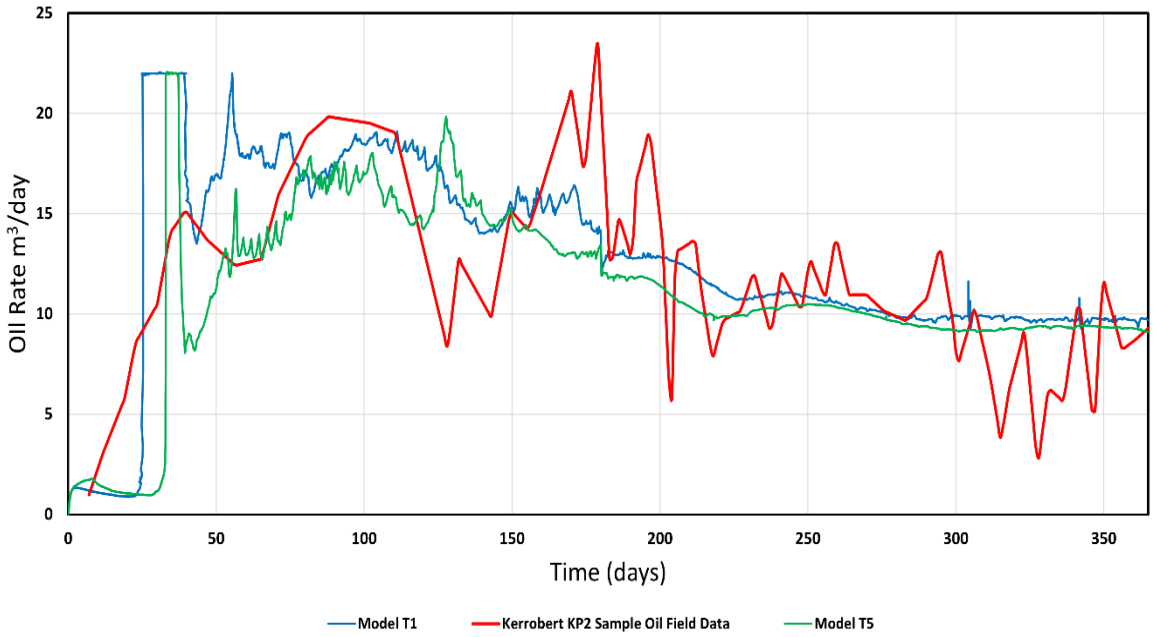


**Figure 5.1.** Oil production rate ($m^3day^{-1}$) calculated by Model T1 and Model T5 and field data from Kerrobert KP2 well.

Each distinct period demonstrates different trends in oil extraction rates, influenced by various factors such as geological heterogeneity, inconsistencies in data measurements, fluctuations in operational parameters, and the evolving state of the reservoir. Understanding these diverse influences is crucial for refining and optimising the THAI method for more consistent and efficient oil production in similar projects.

### 5.2.3 History match quality

Figure 5.1 displays the oil rate of the KP2 producer well from the Kerrobert THAI pilot test plotted against the history matched oil rate as calculated by Model T1 from this study. In general, the match is visually satisfactory, although there are some irregularities mainly stemming from inconsistencies in the KP2 production information. It is important to note that real field data is influenced by factors beyond the in-situ processes, which can

contribute to variations and discrepancies in the data. During the periods of undulation from the KP2 field data, the simulation does a good job of predicting an oil rate which appears to be a qualitative average. Only the data from the time that combustion has initiated (~35 days) has been compared due to a lack of data from the KP2 well covering air injection. To aid in the history match, an air injection rate of 28,880 $m^3day^{-1}$ was used for the first 180 days, decreasing down to 14,440 $m^3day^{-1}$ for the remaining 185 days. Figure 5.2 displays the cumulative oil of the KP2 producer well from the Kerrobert THAI pilot test plotted against the history matched cumulative oil as calculated by Model T1. Overall, the match is decent, with the model predicting a similar overall oil production with both sets of data converging at ~4700 $m^3$ after 365 days of air injection, with Model T1 predicting 4656 $m^3$, <1% less than the Kerrobert field data at 4700 $m^3$. The history matched model could not capture the breakthrough time for the oil, likely due to variations in start-up and ignition method between the field process and the simulation model. The ignition process of the Kerrobert THAI pilot is vaguely described as steam injection for time, and so matching the operation precisely is a difficult endeavor. Discrepancies between the two datasets during production will come from the stable production of the KP2 well data, and the effects of the kick-off air injection initiation with the Model T1 simulation run. In addition, the simulation model does not capture the heterogeneity of the reservoir at the Kerrobert pilot, due to a lack of fundamental data available. A homogenous “sugar-cube” style model has been employed to best capture the in-situ processes without adding to potential matching discrepancies by using inaccurate heterogeneity. An underprediction within the 120 days during combustion initiation is offset by an overprediction for the remaining 245 days of stable production.

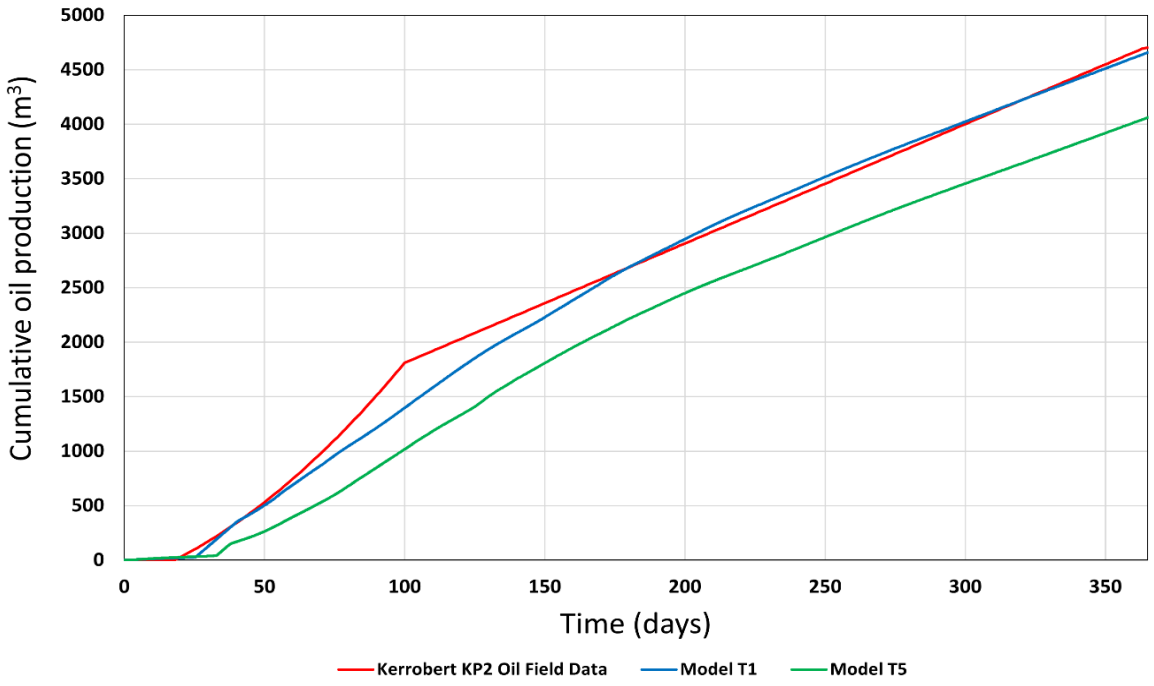


**Figure 5.2** Cumulative oil production ($m^3$) calculated by Model T1 and Model T5 and field data from Kerrobert KP2 well.

## 5.3 Impacts of hydrogen generation on the history match

The inclusion of reactions additional to the usual in-situ combustion reactions that are often used in THAI simulations (cracking and oxidation) will impact the performance and the results of the model. For this reason, it is of great interest to investigate the effects of these reactions upon the history matching process because this will likely impact the predictions of field performance. Knowing that these reactions occur in-situ (Greaves and Xia) reactions 5, 6 and 7 were added to Model T1 one reaction at a time to observe the individual and combined effects of each reaction upon the THAI process. This was done because the majority of THAI model simulations within literature incorporate only oxidation and cracking reactions, however, these additional reactions will impact several model outputs (e.g., temperature, oil saturation, fuel availability, oil production etc.). Therefore, models that only utilise oxidation and cracking reactions within their THAI model validations are possibly less accurate.

Figure 5.2 displays the oil rate of Model T5 against the history matched Model T1 and the KP2 field data. Model T5 predicts a lower oil production rate at almost all times than Model T1. This is due to a decrease in temperature calculated at the combustion front which will affect the temperature, and therefore performance of the mobile oil zone (MOZ) ahead of the combustion front. A lower temperature in the MOZ will result in a lower calculated viscosity and decreased cracking of the oil, both of which will impact the flow performance of the oil towards the producer well. However, despite this decrease in oil production rate from Model T1 to Model T5, the match between Model T5 and KP2 field data is still visually acceptable but is visibly less accurate than the match with Model T1. When the oil production is viewed from a cumulative perspective (Figure 5.3) a major reduction in oil production is highlighted, inferring that a visual inspection of only the oil rate is not an acceptable method of history matching the THAI process. Also, the additional reactions within Model T5, when combined with the base THAI reactions result in an increased gas generation as calculated by the simulation. Consequently, a higher gas saturation occurs within the grid blocks containing the reaction front within Model T5 when compared to Model T1. This results in a higher gas relative permeability within those grid blocks resulting in a decreased oil relative permeability, and thus decreased oil production.

The hydrogen reactions added within Model T5 substantially increase the run-time of the simulation. The run-time for Model T1 was roughly 50 minutes. Model T5 saw an increase of over 2 hours in run-time. It can be assumed that each additional reaction will increase the number of calculations required from the simulation during the run, and thus increases the time taken to reach convergence. It should be noted that the convergence, and the mass balance of model T5 was not noticeably worse than Model T1, with both

models performing very well with mass balance errors during the simulation of $\leq X^{-5}$ throughout the whole run.

## 5.4 Reaction scheme results and discussion

Examining reaction schemes employed in reservoir simulations of THAI (Table 5.1), particularly the incorporation of coke gasification and water-gas shift reactions, is fundamental for enhancing the technology's performance and ensuring its practical applicability. This section directs attention towards the pragmatic aspects of these reaction schemes. The reaction schemes used hold a central role in refining THAI efficiency (Rabiu Ado, 2017; Ado, 2022), enhancing calculated oil recovery rates (Ado, 2020b), and possibly advancing sustainable hydrogen production within this innovative technology. Appreciating their impact on the THAI process is imperative for fully unlocking its potential in the domains of energy production and oil refinement. Through a thorough analysis of the findings, practical considerations come forward, ultimately guiding the future deployment of THAI for sustainable energy solutions and efficient oil recovery practices.

**Table 5.1** Breakdown of the reactions within each model. Reaction numbers can be found in Table 3.10 in Chapter 3.

| Model name | Reaction included |
|---|---|
| T1 | 1-4 |
| T2 | 1-4, 5 |
| T3 | 1-4, 6 |
| T4 | 1-6 |
| T5 | 1-7 |

### 5.4.1 Impacts of coke gasification on the THAI process

The process of coke gasification involves reacting steam with hydrocarbon coke, resulting in the production of hydrogen and carbon monoxide. In the THAI process, coke is generated by subjecting heavy oil to high-temperature cracking, leaving behind a carbonaceous deposit.

The mole percentage of hydrogen present in the produced syngas calculated by Model 2 is illustrated in Figure 5.3 from 50 days onwards. 50 days is the period after which the effects of the pre-steaming and combustion initialisation have subsided, and hydrogen breakthrough has occurred. The hydrogen production in the initial 50 days is observed to be disproportionately high, exceeding 40%. Nevertheless, this data is misleading due to the minimal overall volume of gas produced. During the stabilisation of combustion (initial 120 days), the fraction of hydrogen remains relatively low, <1%. This pattern persists up to 180 days, after which a sharp surge in the mole percentage of hydrogen occurs, quickly increasing to 1.2%. The increase is observed between the 180-day mark and 720 days, with the hydrogen mole percentage rising from 1.2% to 6%, respectively. This sharp increase at 180 days is consistent with the decrease in air injection rate from 28,880 $m^3day^{-1}$ to 14,440 $m^3day^{-1}$. This implies that a higher percentage of hydrogen is produced through coke gasification within the syngas when lower air injection rates are used.

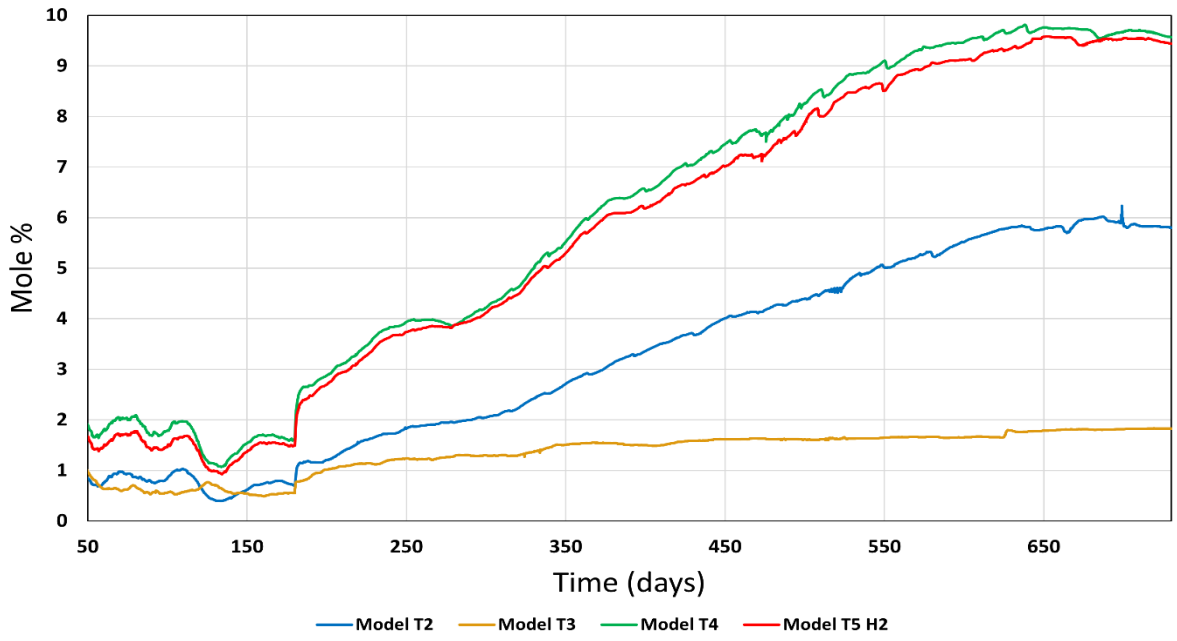


**Figure 5.3.** Molar fractions (mol%) of hydrogen within the produced syngas calculated by Model T2 – T5

The cumulative volume of hydrogen produced, as calculated by Model 2, is displayed in Figure 5.4. A rapid surge in hydrogen production is evident between 4 and 35 days, which can be attributed to a stepwise mechanism during the pre-steaming process. In this process, hot steam cracks the heavy oil, resulting in the production of small quantities of coke, which then rapidly undergoes gasification, producing large amounts of hydrogen. As the steaming stops and oxygen injection commences, a sharp reduction in hydrogen production is noticeable, with cumulative hydrogen volume rising from 100,000 $m^3$ at 35 days to 450,000 $m^3$ at 720 days. The hydrogen gas is produced through the interaction of coke and steam at toe of the producer, where the back end of the steam bank and front of the coke laydown zone meet. Any hydrogen that is not produced at the first perforation of the producer well quickly rises to the top of the reservoir through gravity (density) before being reaching the next perforation. This suggests that the hydrogen is mainly produced at the bottom of the reservoir between the injector and the toe of the producer. It should also be noted that the use of a catalyst (such as in THAI-CAPRI) could increase the rate of the gasification reaction and therefore aid in the increased production of hydrogen (Zhu et al., 2023).

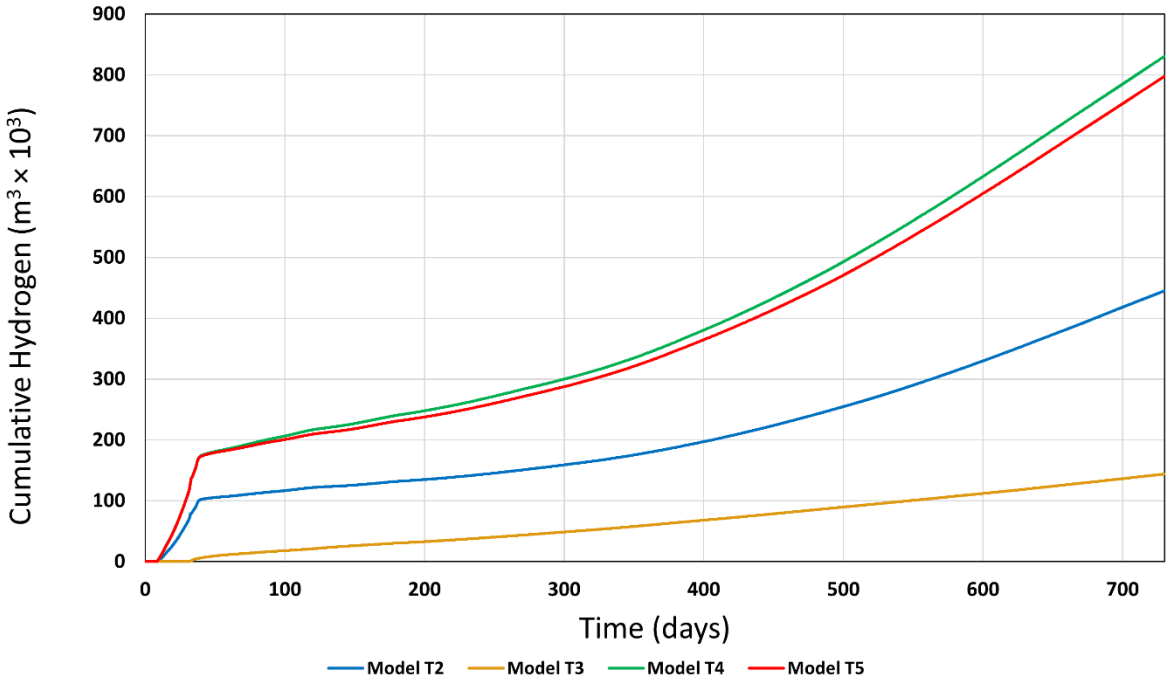


**Figure 5.4.** Volume of produced hydrogen ($m^3$ x $10^3$) within the produced syngas calculated by Model T2 – T5

Figure 5.5 illustrates the calculated oil rate by Model T1 and Model T2, with the latter indicating a reduction of up to 5 $m^3$ $day^{-1}$ at approximately 35 days. Nonetheless, beyond the initial 75-day mark, the variation between the two sets of data is reduced, with the greatest difference being only 2 $m^3$ $day^{-1}$ after 170 days. By the 365$^{th}$ day, Model T2 is expected to meet Model T1 in the calculated oil rate. The initial decrease in oil production is due to reduced heat resulting from a combination of endothermicity and reduced fuel availability. The reduced fuel availability is caused by coke gasification using up coke that is necessary for the HTO reaction that provides most of the heat within the THAI process. This reduced heat, as calculated by the model, results in lowered oil cracking and viscosity reduction. Oil production rate is therefore reduced.

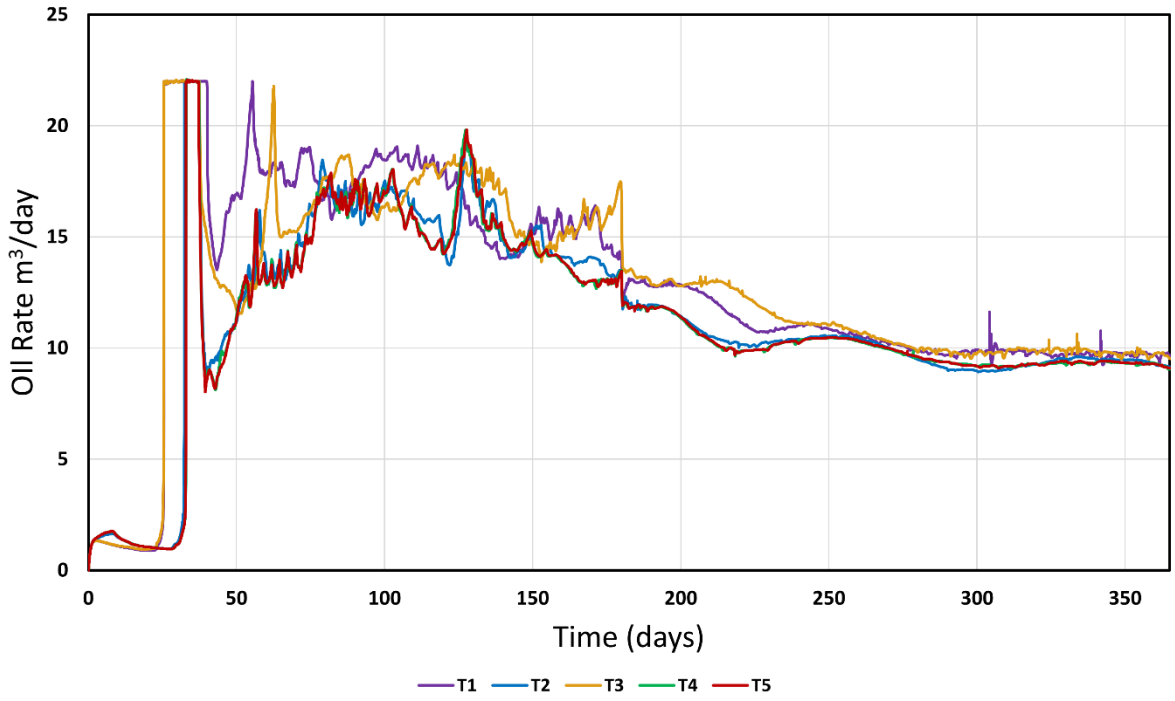


**Figure 5.5.** Oil production rate ($m^3$) calculated by Model T1 – T5

### 5.4.2 Impacts of forward water-gas shift (FWGS) on the THAI process

The process of water-gas shift involves reacting steam with carbon monoxide, resulting in the production of hydrogen and carbon dioxide (reaction 6 in Table 3.10 in Chapter 3). In the THAI process, carbon monoxide is generated in small quantities through the high-temperature oxidation of hydrocarbon species.

Figure 5.3 displays the mole percentage of hydrogen present in the produced syngas calculated by Model 3, showing only data from 50 days onwards. The mole percentage of hydrogen within the syngas of Model 3 follows a very similar trend to that calculated by Model T2. The mole percentage remains steady at <1% until 180 days, where a sharp increase is seen, followed by a gradual increase until the 720-day mark. However, unlike Model T2, Model T3 only predicts a peak mole percentage of 1.9% at 720 days. The sharp increase at 180 days indicates that FWGS is also negatively related to air injection rate.

Figure 5.4 illustrates the cumulative hydrogen volume produced, as calculated by Model T3. No hydrogen is produced until 35 days into the simulation run, indicative of the initial lack of carbon monoxide within Model T3. The WGS reaction initiates only when combustion takes place, releasing carbon monoxide, which reacts with steam produced during combustion, yielding hydrogen (Turta et al., 2020). Model T3 predicts a lower hydrogen production than Model T2, with cumulative hydrogen volume rising from 0 $m^3$ at 35 days to 143,000 $m^3$ at 720 days. This is concurrent with the mole percentage of hydrogen being lower in Model T3 than Model T2. The hydrogen gas within Model T3 is generated as a result of the interaction of combustion-generated carbon monoxide and steam, ahead of the combustion front (Greaves et al., 2004a). The hydrogen is generally produced at the toe of the producer well and quickly rises to the top of the reservoir through density. Any hydrogen that is not produced at the first perforation is produced at the second perforation of the producer. This suggests that the hydrogen generated through FWGS is generated further along the producer well (away from the injector) than the hydrogen generated through coke gasification in Model T2. This is a novel finding of this investigation, and could have further implications into the optimisation of the in-situ process for the commercial production of hydrogen from THAI.

The calculated oil rate by Model T1 and Model T3 is displayed in Figure 5.5, demonstrating less difference than that observed between Model T1 and Model T2. This is because reaction 6 (Table 3.10, Chapter 3) which is the forward water-gas shift reaction, does not necessitate any hydrocarbon-based reactants. As a result, the availability of fuel and the oil saturation within the process are not significantly affected, leading to no noticeable influence on the produced oil rate as a result of those variables. The reduction in oil production likely occurs as a result in decreased temperature within the model through decreased exothermicity. FWGS is less exothermic than oxidation

(Table 6) and so for each unit of heat consumed by the reactions in Model T3, a lower heat generated will be calculated than in Model T1 after all the reactions have occurred. This decreased calculated heat will result in reduced oil cracking and lessened oil viscosity reduction, resulting in reduced oil production. Thus, even though Model T2 and Model T3 show a decrease in oil production compared to Model T1 due to the same cause, the underlying mechanisms influencing this decreased difference.

### 5.4.3 The combined effect of FWGS and coke gasification

Though it is important to understand the impacts of both coke gasification and FWGS, they are unlikely to occur independently in-situ during stable combustion. Investigating the combined effect of both reactions during combustion is vital to the understanding of how the process is impacted by the inclusion of hydrogen generation.

The results in Figure 5.3 showed that Model T4 exhibited the highest peak at 9.8% mole percentage of hydrogen gas within the produced syngas, which was more than Model T2 and T3 combined. Moreover, the trend observed in Model T4 was similar to that of Model T2, but with an increase in the ratio of T4 to T2 and T3 over time until 720 days. At this point, the ratio was approximately 25% higher in Model T4 than in Model T2 and T3 combined, decreasing from 33% higher at 150 days. The cumulative hydrogen produced by Model T4 at 720 days was 820,000 $m^3$ (Figure 5.4), which was 227,000 $m^3$ more than that produced by Model T2 and T3 combined, and 38% higher than the cumulative hydrogen produced by Model T2 and T4 combined. These findings suggest that there may be a synergistic effect of the two reactions, whereby one reaction will subsequently impact the other, with the most likely scenario being coke gasification increasing the effects of FWGS (Greaves and Xia). The carbon monoxide generated through coke

gasification will increase the concentration of carbon monoxide within the syngas calculated by the model.

Model T4 also exhibits a lower oil production rate compared to Model T1 and Model T3 (Figure 5.5). However, it demonstrates similar outcomes to Model T2 with minor fluctuations after 120 and 170 days. These findings suggest that the use of FWGS in combination with coke gasification can minimise its impact on oil production within THAI. This is contrary to the expected outcome, as the inclusion of FWGS generally reduces oil production by decreasing the temperature. Since coke gasification boosts the rate of FWGS by providing a higher concentration of carbon monoxide, a further reduction in oil production rate in Model T4 compared to Model T2 would be anticipated. These results imply that there could be a limit to how much including the additional hydrogen reactions can reduce the oil production rate through temperature reduction under the conditions studied.

### 5.4.4 Impact of reverse WGS

The reverse water-gas shift (RWGS) reaction (Table 3.10 in Chapter 3, reaction 7) is a process that involves the conversion of carbon dioxide and hydrogen into carbon monoxide and water. The reaction is known to occur under specific temperature and pressure conditions, and it is commonly used in industrial applications. Figure 5.3 shows that the RWGS reaction has a small effect on the hydrogen fraction within the produced syngas, decreasing the peak mole percentage of hydrogen by only 0.2%. Figure 5.4 shows that the produced cumulative hydrogen is reduced by only 33,000 $m^3$ in Model T5 from Model T4, which represents a reduction of only 3%. One explanation for the lack of significant reduction in the produced hydrogen could be that the temperature and pressure conditions calculated by the Model T5 are not optimal for the RWGS reaction.

The reaction requires higher energy to begin than the FWGS, meaning that if temperatures are not high enough the reaction rate may be slower than expected (Chen and Chen, 2020). Another possibility is that the RWGS reaction is not occurring in significant quantities due to the limited interaction between carbon dioxide and hydrogen. Despite favourable pressure and temperature conditions, it is possible that the amount of interacting carbon dioxide and hydrogen available for the reaction is not sufficient to produce fast reaction rates. Typically, higher temperatures and specific catalysts are required for vigorous reaction between $CO_2$ and $H_2$ (Pal et al., 2018), which would explain negligible impacts in the non-catalysed low-temperature interaction zones within the THAI simulation.

### 5.4.5 Comparison of hydrogen production against field and experimental data

Due to the lack of graphical or temporal data on $H_2$, $CO_2$ and CO from the Kerrobert THAI pilot, the results of the simulations from this investigation are being compared against a very similar THAI pilot project at Whitesands. It was observed at Whitesands that initial and produced oil API and the oil chemistry can be assumed to be similar. Although the operational processes may vary between the two pilot projects, it can be assumed that this had very little impact on the composition of the produced gas, but rather impacted the oil recovery from the reservoir. Comparing Model T5 to field data from the Whitesands THAI pilot (Turta et al., 2018) (Figure 5.6) there is a good match for the carbon monoxide and carbon dioxide within the produced syngas. Model T5 predicts a more stable outcome than the field trial, likely due to the lack of geological and petrophysical imperfections that would be found within the Whitesands reservoir. Also, the field data available is jagged due to a lack of consistent time-steps in the field measurements available. Despite this, Model T5 quite accurately predicts a smooth average for both the carbon dioxide and carbon monoxide syngas fractions. However, the

calculated hydrogen fraction within Model T5 is higher than that seen in the Whitesands pilot. This could be due to the necessity of tuning the kinetic variables for reactions 5, 6, and 7 against hydrogen production in real-life field trials. It could also be a function of history matching against the Kerrobert pilot rather than the Whitesands pilot, however, no graphical hydrogen production data could be found for the Kerrobert pilot. However, Turta et al. (2018) report the Kerrobert KP2 producer well produced 2% $H_2$ within the first 6 months, rising up to 8-14% after this. This is also very consistent with the findings within this study. Despite the over prediction of hydrogen between 350 days and 500 days, the match is overall satisfactory in the general trends, showing an increase from <2% to >9% over the course of the 720-day runtime. The large variation in data between 350 and 500 days could also be explained by a rapid drop in total gas production of the producer well in Whitesands during that time. The investigation would have benefited from matching hydrogen volume produced rather than molar fraction as this can be heavily influenced by the volumes produced and operational conditions. However, the lack of available field data prevented further exploration in this regard. Kapadia et al. (2013) investigated hydrogen generation by alternating between 100 days of steaming and 100 days of oxygen injection. The reported range of hydrogen content varied between 5 mol% and 40 mol%. Notably, the hydrogen content in the range of 30-40% was primarily observed during the cyclical periods of steam injection, while during oxygen cycles remained closer to 5%. These observations indicate a distinct variation in hydrogen production depending on the phase of the cycle. Although this study does not observe hydrogen content as high as 40 mol% the model also does not include the cyclical periods of steam injection (apart from the initial steam injection during the PIHC). The 5% observed during periods of oxygen injection is congruent with the results of this study, with variations between the two values likely to be a result of continued oxygen

injection rather than 100-day periods within the study of Kapadia et al. (2013) not allowing temperature to build. Kapadia et al. (2013) employed coke gasification and water-gas shift as the primary sources for hydrogen production, consistent with the approach adopted in this study. The findings of this study align with the theory proposed in Kapadia et al. (2013) and Greaves et al. (2004b), suggesting that hydrogen is predominantly produced through coke gasification followed by water-gas shift, as shown by the match to field data. These consistent findings reinforce that coke gasification and water-gas shift are key pathways for hydrogen generation.

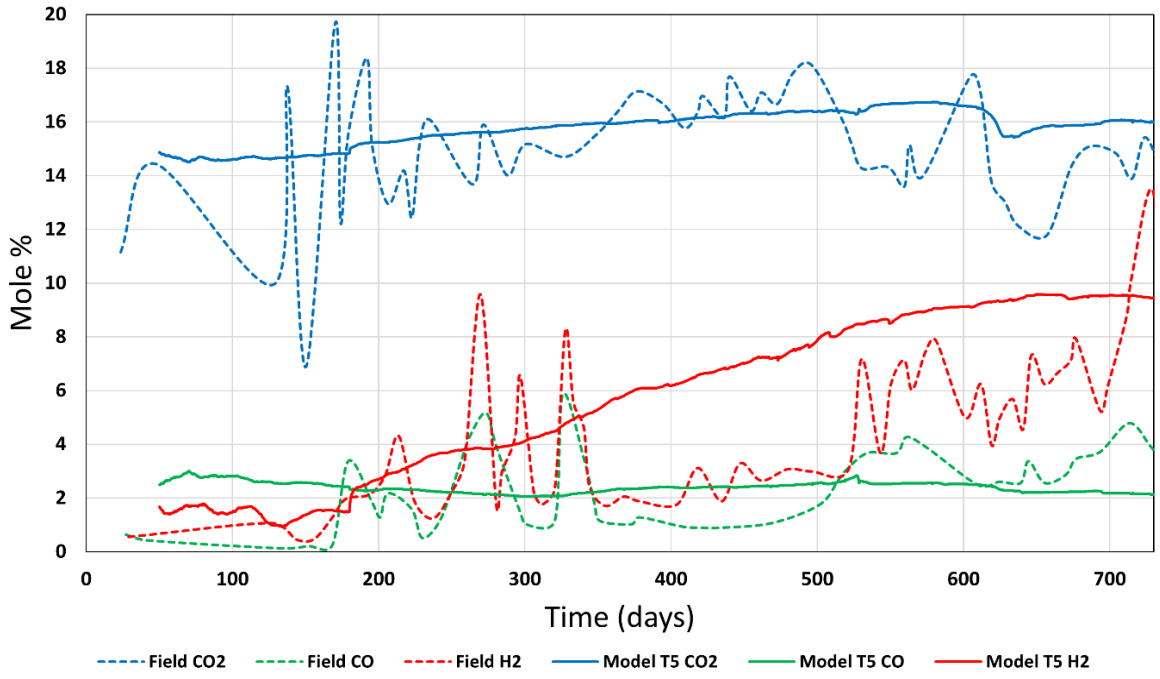


**Figure 5.6.** Comparison of syngas fractions of $CO_2$, CO and $H_2$ for the Whitesands THAI field pilot and as calculated by Model T5

In contrast to this study and the findings of (Kapadia et al., 2013) and (Greaves et al., 2004b), Yang et al. (2022) reported that hydrogen generation occurs at higher temperatures, largely above 528 °C, with small amounts being generated between 351 °C and 528 °C. They proposed that the sources of hydrogen in their study were primarily coke dehydrogenation and pyrolysis reactions. Furthermore, this study incorporated the water-gas shift (WGS) reaction as a significant aspect of the hydrogen generation process,

which was not considered in Yang et al. (2022). This additional reaction pathway contributes to the overall hydrogen generation process in this study. Despite the differences in reaction types and temperature requirements between Yang et al. (2022) and this study, both studies reported a substantial portion of hydrogen generation from coke-based reactions. This study indicated that 70% of the generated hydrogen resulted from coke reactions, whereas Yang et al. (2022) reported 80%. However, it is important to consider that the variations in reaction types and temperature requirements likely contribute to the differences in the specific percentages reported. The reaction pathways employed in each study might have different efficiency levels in terms of hydrogen production, leading to the observed disparities. These differences highlight the complexity of the hydrogen generation process and the diverse factors that influence hydrogen provenance. Reaction types, temperature conditions, and the specific mechanisms employed all play critical roles in determining the efficiency, the extent of hydrogen generation, and purity of the hydrogen produced.

## 5.5 Practical operations of THAI for hydrogen

Investigating practical reservoir engineering is essential for optimising resource recovery and ensuring economic viability. This section will turn the focus to the practical implications surrounding injection fluid composition, reservoir depth, and production well orientation. These thematic elements play pivotal roles in optimising THAI performance, enhancing oil recovery rates, and developing sustainable hydrogen production. Understanding their influence on the THAI process is essential for realising the full potential of this transformative technology in the fields of energy production and oil refinement. Through a comprehensive examination of the findings, practical considerations emerge, ultimately shaping the future deployment of THAI for sustainable energy solutions and efficient oil recovery practices.

### 5.5.1 Impact of injection fluid

Researching the differentiation between air and oxygen injection in ISC reservoir simulations holds paramount importance due to its direct implications for enhanced oil recovery (EOR) strategies and reservoir management. The choice between these injection fluids profoundly influences combustion dynamics, temperature distribution, and overall reservoir performance. Three models are utilised for analysis: Model B, serving as a benchmark and representing history-matched air injection (Model T5); Model O1, introducing pure oxygen injection while maintaining the same oxygen injection rate as Model B (21% of Model B injection rate); and Model O2, exploring the effects of pure oxygen injection while maintaining the same air injection rate as Model B (100% of Model B injection rate). These models enable a comprehensive exploration of the intricate relationship between air and oxygen in THAI reservoir simulations, offering insights into their respective advantages and challenges for optimising EOR strategies and reservoir management practices.

When employing pure oxygen in Model O1 as opposed to the traditional practice of injecting air in Model B, the outcome is a substantial increase of approximately $180 \times 10^3$ $m^3$ in hydrogen production over the course of a year, as indicated by the data depicted in Figure 5.7. Nonetheless, this increase in yield is achieved while maintaining a consistent trend. The rationale behind this augmentation likely stems from the resulting elevation in oxygen partial pressure within the reservoir, as corroborated by the findings in Ren et al. (2005).

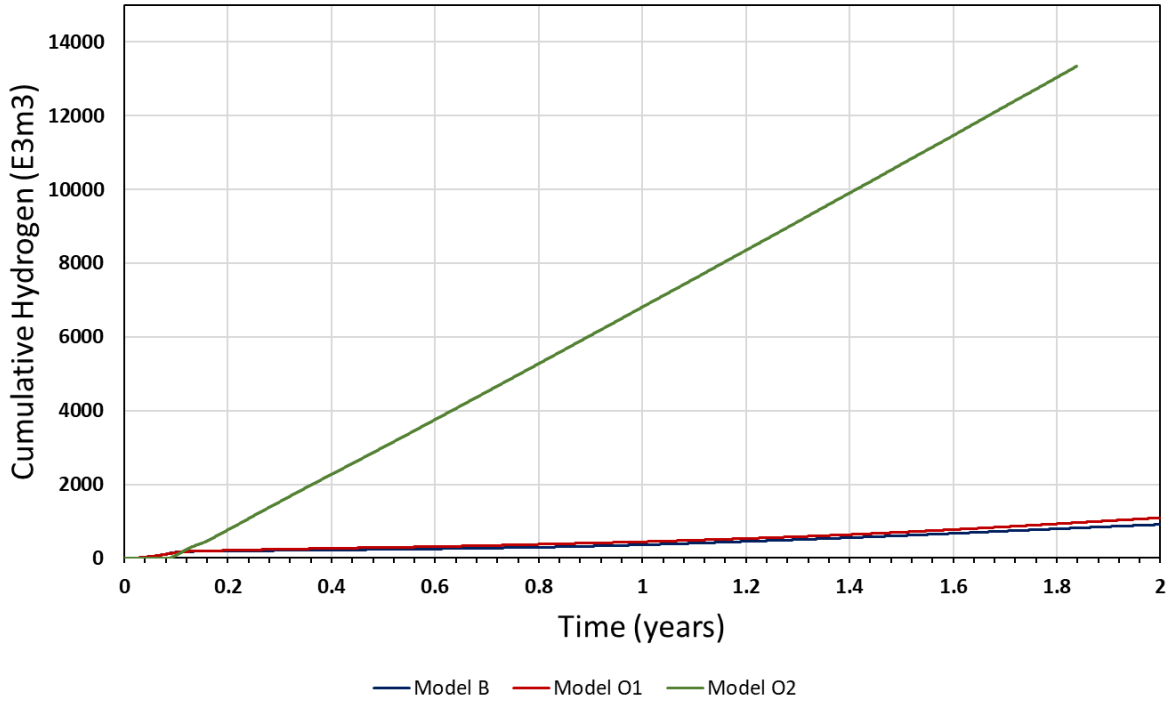


**Figure 5.7.** Comparison of hydrogen cumulative volume for Models B, O1 and O2

Using pure oxygen instead of air for injection translates into a more efficient process due to the absence of inert nitrogen, thereby minimising heat loss (Ado, 2021a). This enhanced efficiency is visually represented in Figure 5.8, where the temperature profile in the layer containing the horizontal producer extends slightly beyond that of the air injection scenario. The pivotal role of oxygen partial pressure becomes evident in governing the availability of oxygen for combustion reactions. An inadequate oxygen partial pressure invariably leads to diminished combustion, resulting in reduced reaction rates and a consequential decline in both the longevity and efficacy of endothermic reactions. One such endothermic reaction is the coke gasification process used to generate hydrogen (Murthy et al., 2014). There are noticeable differences across all three parameters, especially Model O2 with the other two. The difference between Model B and Model O1 is minimal.

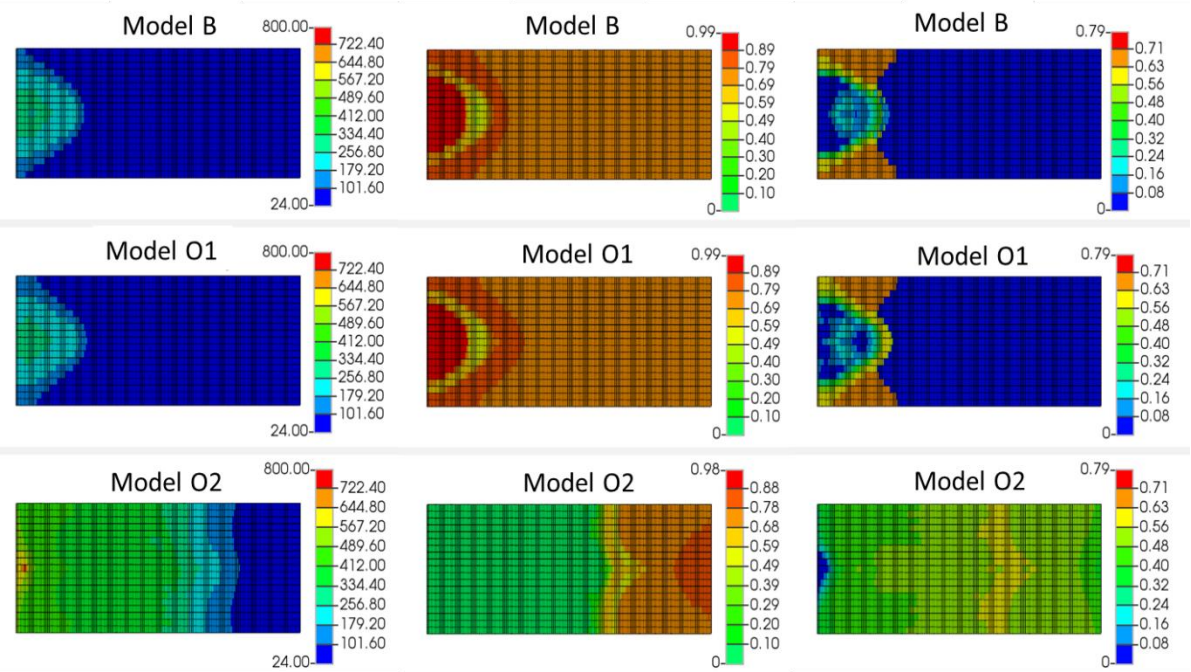


**Figure 5.8.** A visual representation of the effect of reduced nitrogen within the injection stream. Is displays a comparison of temperature (left column), oil saturation (middle column), and hydrogen gas fraction (right column) within layer 6 (the layer containing the horizontal producer) for Models B, O1 and O2.

The primary distinction between the models as displayed by Figure 5.8 lies in the spatial distance from the injector at which each parameter is measured. A notable divergence appears in the increased concentration of hydrogen gas within the central area of the model, particularly around the location of the producer in Model O1 when compared with Model B. This observation reinforces favoring the adoption of pure oxygen as it results in a more optimised THAI process, especially for the production of in-situ hydrogen. By diminishing the presence of nitrogen in the gas stream used for production, it allows for the more efficient flow of other gases, notably hydrogen, through the producer.

The contrast between Model O2 and the remaining two models is significantly more pronounced. Implementing 100% O2 at an equivalent injection rate as the air in Model B ($X$ air vs. $X$ oxygen) triggers an exceptionally quick advancement of the combustion front across the reservoir. Grid blocks situated more than 100m away from the injector exhibit temperatures surpassing 400°C, while their counterparts in Model B and Model

O1 register temperatures below 100°C. This rapid temperature surge leads to a drastic reduction in oil saturation due to a substantial decrease in viscosity and density due to thermal upgrading. Consequently, there is an immediate surge in production from the producer well. Moreover, this accelerated oxidation and thermal upgrading of the oil notably contribute to the heightened production of coke and carbon monoxide, likely resulting in rapid hydrogen generation through elevated water-gas shift and coke gasification kinetic pathways. This phenomenon becomes apparent from the hydrogen gas fraction, ranging between 32% and 63%, observed across a majority of grid blocks within layer 6 of the model.

This cascade of effects, triggered by the implementation of pure oxygen, underscores the complex interplay of various parameters in the oil reservoir and emphasises the significance of considering not just hydrogen concentration but also temperature variations and gas composition in optimising oil recovery processes (Ado, 2021a).

The pronounced disparity in yield between Model O2 and Model O1 constitutes a notable finding within this study. Model O2 demonstrates a yield of $13.34 \times 10^6$ $m^3$ of hydrogen. This outcome contrasts with the comparatively modest yield achieved by Model O1, which amounts to a fraction of Model O2's output. The graphical representation of these findings in Figure 5.9 clearly highlights this substantial difference. The critical factor underpinning this divergence in performance is the improved oxygen utilisation within Model O2. Notably, the introduction of elevated oxygen flow rates results in a profound acceleration of combustion reactions. The combustion front, as exemplified in Figure 5.8 exhibits a rapid and efficient progression towards the producer's heel. This exceptional efficiency in combustion reaction advancement is a distinctive hallmark of Model O2. Furthermore, the advantageous attributes arising from the minimisation of heat loss, a

consequence primarily associated with the exclusion of nitrogen, assume amplified significance within the context of Model O2. In the absence of nitrogen, the potential for heat loss is significantly reduced. However, any heat dissipation to the oxygen medium holds the potential to initiate additional reactions. This occurrence entails a self-perpetuating cycle of combustion reactions, effectively augmenting the already accelerated combustion processes transpiring within the reservoir of Model O2.

In both scenarios, the syngas produced exhibits significantly higher hydrogen purity when compared to using air as the injection fluid. Within Model O1, the hydrogen content ranges between 10% and 28% during oxygen injection. In contrast, Model O2 demonstrates a remarkable surge, starting at 5% and reaching a stable plateau at 58% for an extended period of nearly one year (Figure 5.9). The absence of nitrogen in the feedstock plays a fundamental role in interpreting the disparity between Models O1 and O2 and Model B, concerning hydrogen fraction. In the case of Model O1, the absence of nitrogen results in a substantial increase in the volume fraction of all other gases within the produced gas stream. This accounts for the notably higher hydrogen content observed in Model O1 when compared to Model B.

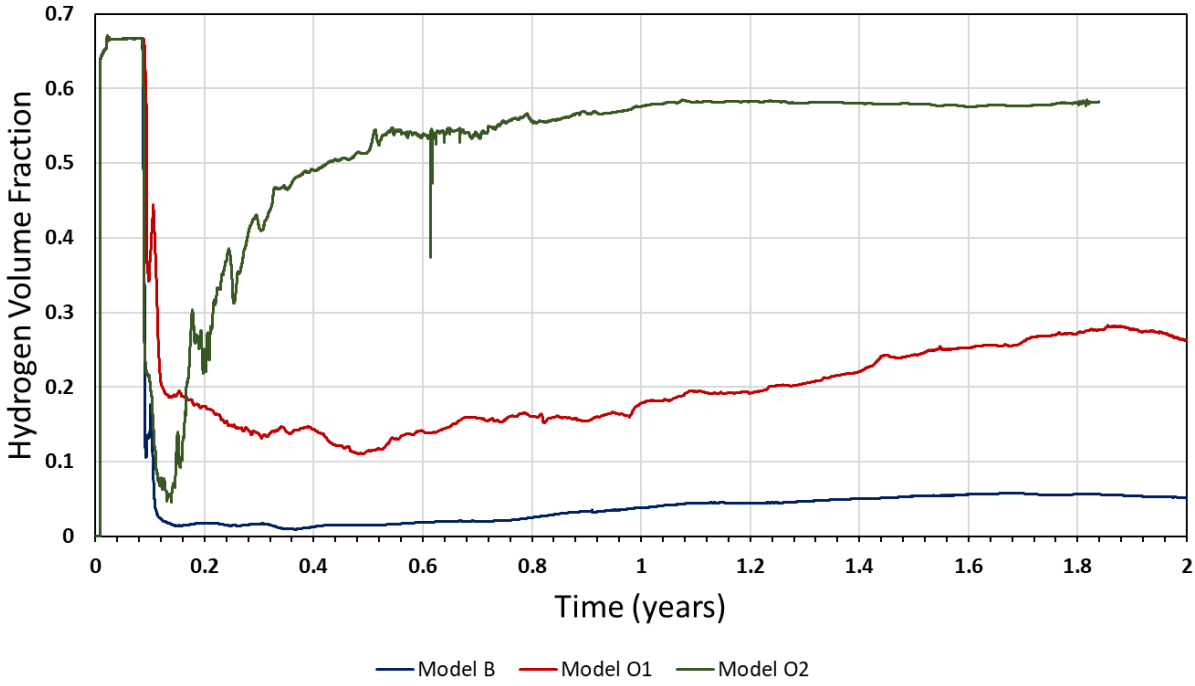


**Figure 5.9.** Comparison of syngas fractions calculated by Models B, O1 and O2

Conversely, the expanded temperature zone characteristic of Model O2, relative to Model O1, likely promotes more rapid water-gas shift and coke gasification. This is underscored by the exceedingly low production of carbon monoxide. Consequently, the augmented volume fraction of hydrogen in Model O2 becomes more apparent. Additionally, the absence of oxygen breakthrough in Model O2 is a noteworthy observation, likely attributable to the elevated temperature driving accelerated combustion rates. This accelerated combustion effectively consumes a larger portion of the injected oxygen, in contrast to Model O1, which exhibits oxygen breakthrough after a year of operation.

Heat generation plays a crucial role in in-situ combustion, serving several key functions such as reducing the viscosity of heavy oil, improving the flow of reservoir fluids, and pushing oil towards production wells. Additionally, elevated temperatures promote the thermal upgrading of oil. The oxygen partial pressure directly influences combustion temperature, which in turn impacts heat production. This relationship is clearly

illustrated in Figure 5.10, where it becomes evident that the use of pure oxygen results in a higher recovery of light oil compared to air injection. This outcome is a direct consequence of the enhanced thermal upgrading of heavy oil. Model O1 yields 525 $m^3$ more light oil over the two-year production period than Model B, and Model O2 surpasses Model B by at least 1150 $m^3$. However, it's worth noting that light oil production from Model O2 experiences a delay compared to the other two models. Significant production acceleration is observed only after 7 months, surpassing the production potential of both Model B and Model O1 around the 1.5-year mark. The production trend indicates that if the model were extended further, there is a high likelihood of significantly increasing light oil production. This pattern is also evident in Figure 5.7, where in Model O2, oil saturation remains below 10% for over half of the reservoir. This is in contrast to Model B and Model O1, where oil saturation remains much higher in the mobile oil zone. Precise control of the oxygen partial pressure offers operators the ability to manage combustion temperature effectively, aligning it with reservoir conditions to optimize heat transfer and enhance oil recovery.

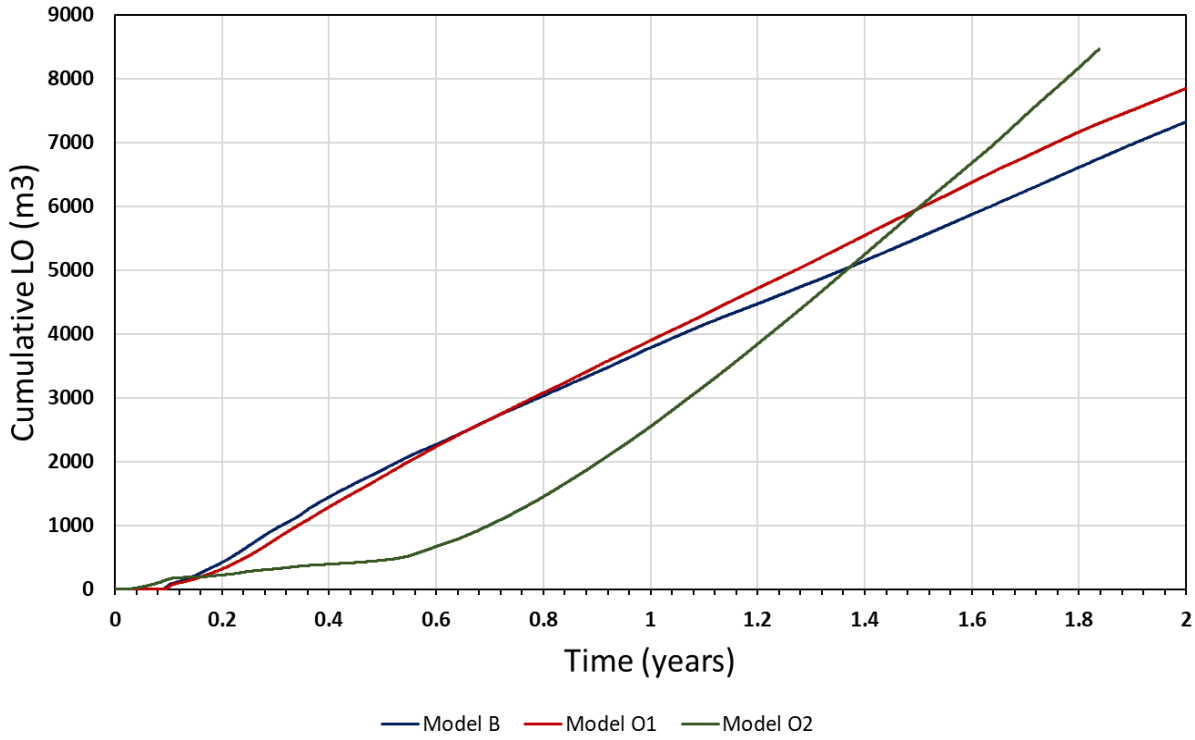


**Figure 5.10.** Comparison of light oil cumulative volume calculated by Models B, O1 and O2

### 5.5.2 Impact of reservoir depth

Exploring the differential dynamics between shallow and deep reservoirs is essential within the context of THAI reservoir simulations, both critical components of reservoir engineering and hydrocarbon recovery strategies. In Model B, which replicates the previously history matched THAI air injection scenario (Model T5), the focus shifts to a shallow reservoir positioned at approximately 760 m true vertical depth (TVD) within the Kerrobert pilot well. This reservoir's conditions are characterised by a temperature of 20°C and a pressure of 2700 kPa. In contrast, Model D simulates a deep reservoir located at approximately 3000 m TVD, as determined by the geothermal gradient from Nurmi and Oy (2021). Here, THAI simulations are conducted under conditions characterised by an elevated temperature of 60°C and a pressure of 30,000 kPa (Dutta et al., 2021). These comprehensive models serve to illuminate the unique challenges and opportunities presented by shallow and deep reservoirs, offering valuable insights into their specific impacts on THAI processes, as well as their implications for optimising

reservoir management strategies and enhancing hydrocarbon recovery operations. Model D demonstrates a hydrogen production rate over ten times greater than that of Model B, whilst not impacting the purity (Figure 5.11). This outcome deviates from conventional industry gasification practices, typically conducted at lower pressures, usually below 15,000 kPa (Fermoso et al., 2010). However, a previous study by Fermoso et al. (2009) reveals a notable increase in hydrogen production during high-pressure gasification, reaching up to 30,000 kPa. Nevertheless, it is crucial to note that the disparity between Model B and Model D is not as pronounced in Fermoso et al. (2009), which underscores the complexity of the underlying in-situ mechanisms.

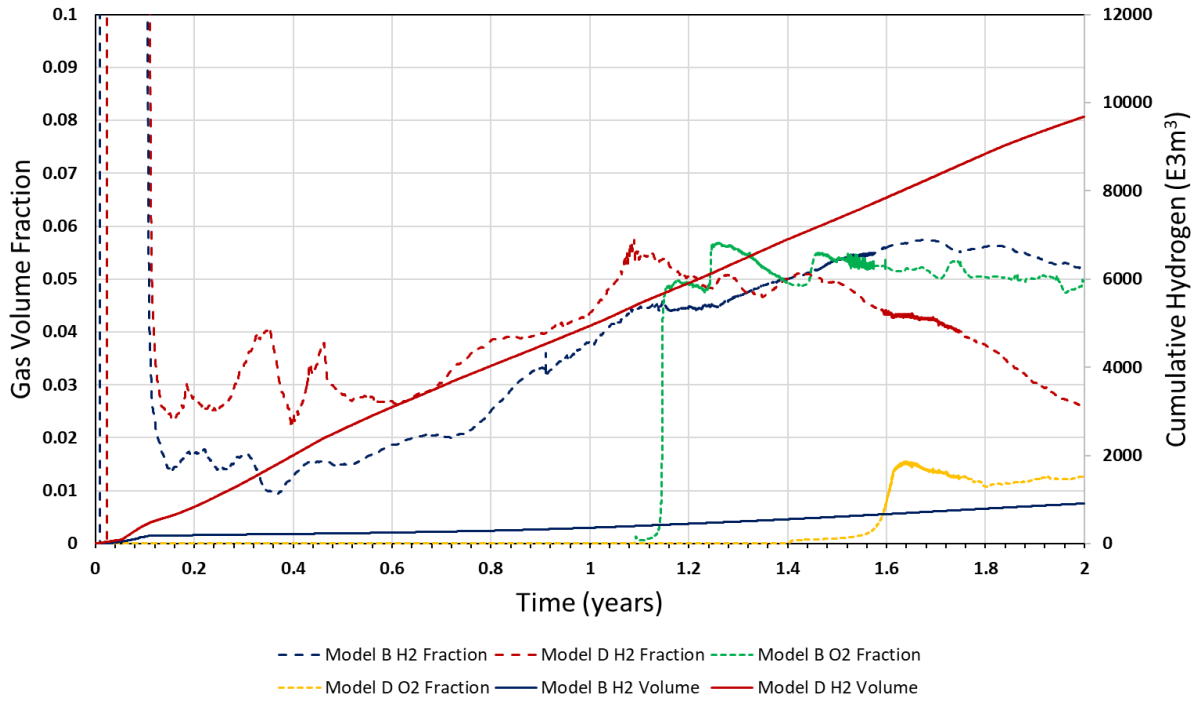


**Figure 5.11.** Comparison of hydrogen cumulative volume, hydrogen gas fraction, and oxygen gas fraction calculated by Model B and Model D

This observation hints at the influence of pressure as an indirect consequence ISC process rather than a direct effect on hydrogen reactions themselves. Elevated pressure levels may enhance oxygen dispersion throughout the oil, leading to heightened combustion rates. As corroborated by the Figure 5.11 depicting the oxygen volume fraction in the produced gas stream, Model D exhibits significantly superior oxygen utilisation within the

reactions. This is evident from the substantially reduced oxygen production back at the producer well in comparison to Model B. These findings align with the conclusions drawn from (Ado et al., 2022a), where researchers noted that higher operating pressures, 8000 kPa, led to improved oxygen uptake and a concurrent decrease in oxygen production than operating pressures of 500 kPa in laboratory-scale THAI-CAPRI simulations.

This consistency across multiple studies strengthens the argument that pressure plays a pivotal role in shaping the combustion dynamics within the reservoir. Furthermore, Model D operates at higher temperatures (Figure 5.12). The combustion front in Model D is observed to be twice as thick and extends deeper into the reservoir compared to Model B. Moreover, the peak temperatures achieved by Model D exceed those in Model B by 200°C. These temperature differentials underscore the impact of pressure on the combustion process, highlighting the potential for enhanced hydrocarbon conversion and hydrogen production in high-pressure ISC systems like Model D.

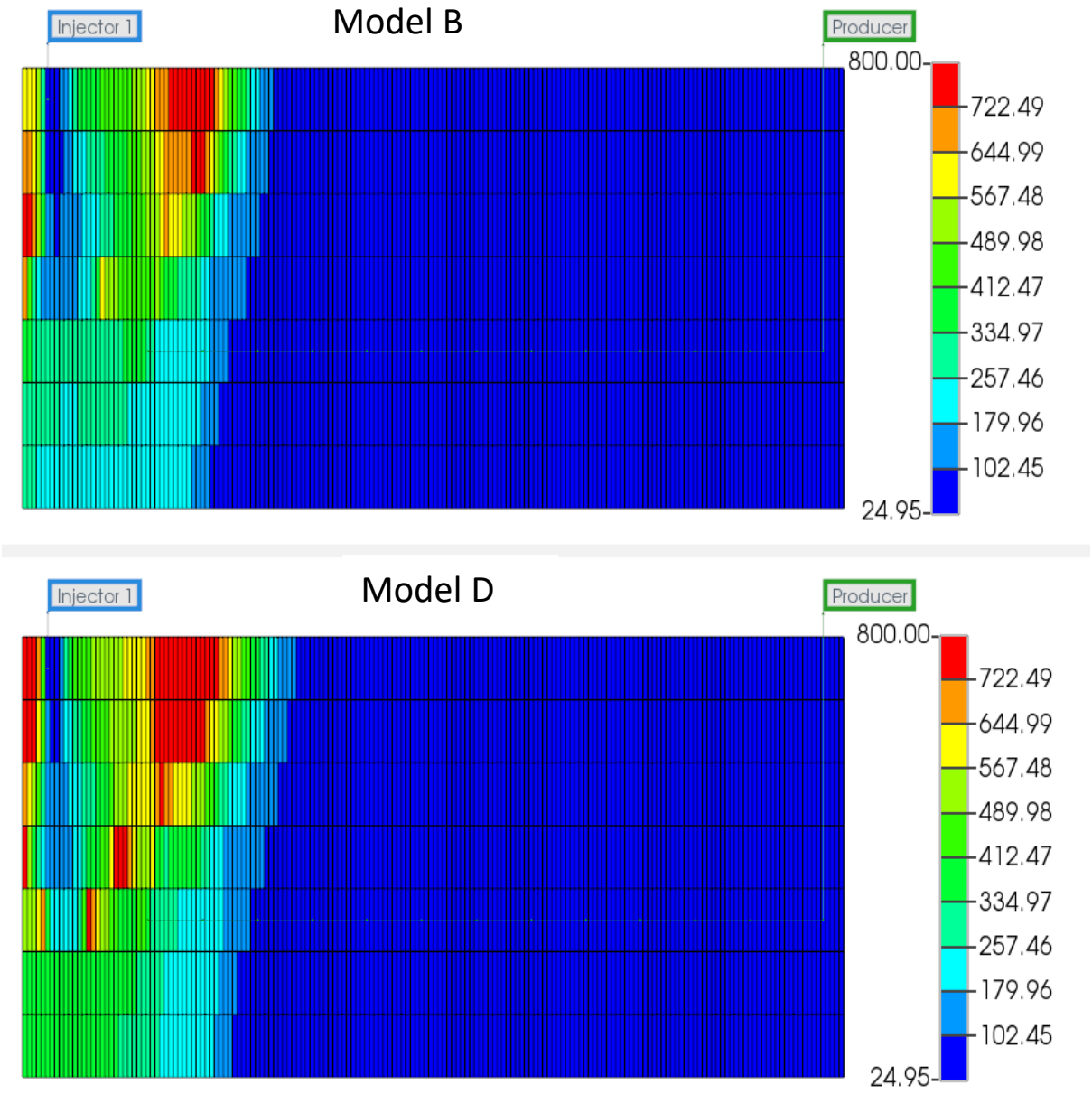


**Figure 5.12.** Comparison of temperature (°C) profiles along the horizontal producer in Model B and Model D

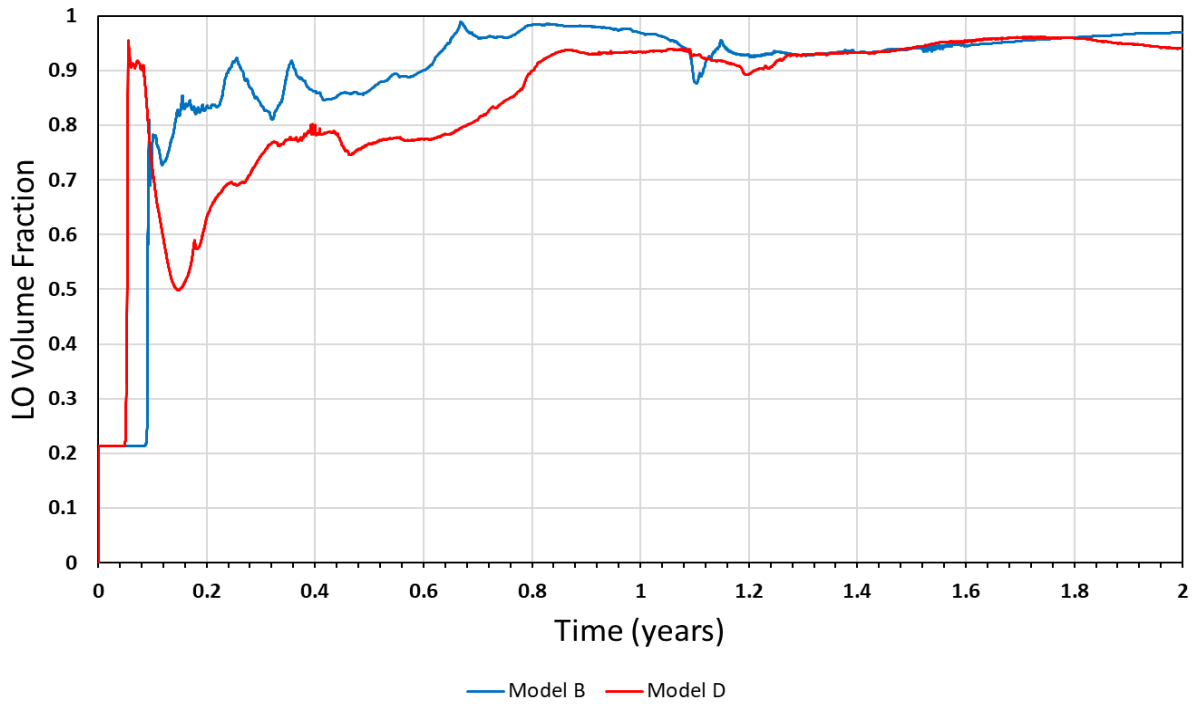


**Figure 5.13.** Comparison of light oil fraction calculated by Model B and Model D

### 5.5.3 Impact of producer orientation

For optimal hydrocarbon extraction from complex reservoirs while focusing on hydrogen production, alternative recovery methods are crucial. The implications of a traditional THAI technique with a horizontally configured producer well are analysed for hydrocarbon recovery and hydrogen production in Model B. This study revisits a previously history-matched scenario (Model T5). Conversely, Model V employs a more traditional vertical well configuration, shedding light on potential differences in hydrogen production and recovery efficiency. As well as providing insights into varying hydrogen production dynamics between THAI and traditional ISC processes, these models serve as a platform for evaluating the adaptability of recovery methods to reservoir conditions.

In a comparative analysis of two distinct models, Model V and Model B, significant variations in their performance and outcomes were observed. Model V demonstrated remarkable efficiency in hydrogen production, generating an impressive $2.65 \times {}^{106}$ m3 of hydrogen, which is nearly three times greater than Model B's comparatively modest

output of 900 $Em^3$ hydrogen (Figure 5.14). The difference in hydrogen purity between the two models further accentuates their disparities, with Model V yielding hydrogen gas of exceptional quality, achieving an impressive purity level of almost 18% after a span of two years (Figure 5.14). Conversely, Model B only managed to maintain a relatively lower purity level, stagnating at around 5% over the same duration.

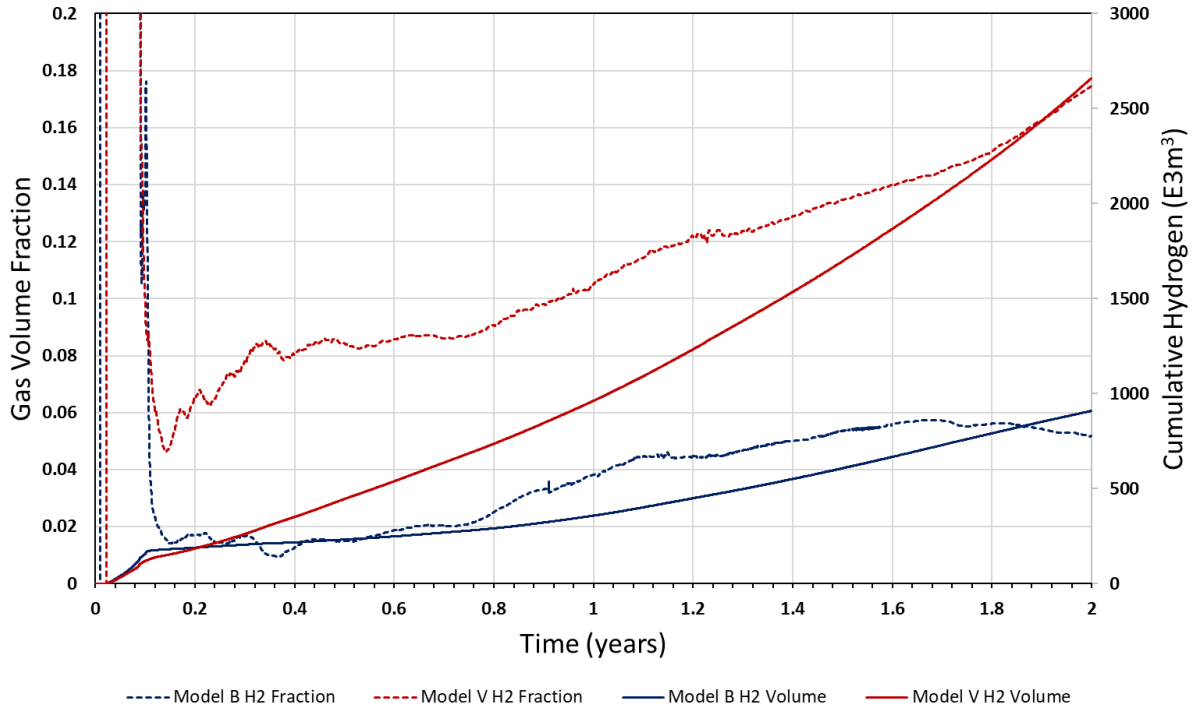


**Figure 5.14.** Comparison of hydrogen cumulative volume and hydrogen gas fraction calculated by Model B and Model V

The significant disparity in hydrogen production potential between Model V and Model B can be attributed to fundamental differences in their operational principles. A key factor contributing to this difference is the behavior of hydrogen within the production well. In the case of the THAI horizontal well (Model B), the buoyancy of hydrogen often leads to it bypassing the well as it ascends and travels over the wellbore, effectively avoiding capture and production. Conversely, Model V employs a vertical well configuration, which enables it to effectively capture hydrogen at various depths within the reservoir, particularly at the uppermost levels.

This contrasting behavior of hydrogen also provides insight into the observed increase in hydrogen purity in Model V. In this vertical well setup, the lighter hydrogen molecules tend to rise more readily, while the other, heavier gases present in the reservoir are pushed down to deeper layers and become incorporated into the remaining oil. This selective displacement allows a higher proportion of the hydrogen to reach the production well first, resulting in the production of purer hydrogen gas. Conversely, in the THAI horizontal well, the heavier gases, such as carbon dioxide ($CO_2$), are favoured in terms of production preference. These heavier gases tend to sink and accumulate in proximity to the producer well, further limiting the capture and production of hydrogen. Therefore, the choice of well configuration plays a crucial role in determining the composition and yield of gases extracted from the reservoir, highlighting the advantages of Model V's vertical well approach in optimising hydrogen production.

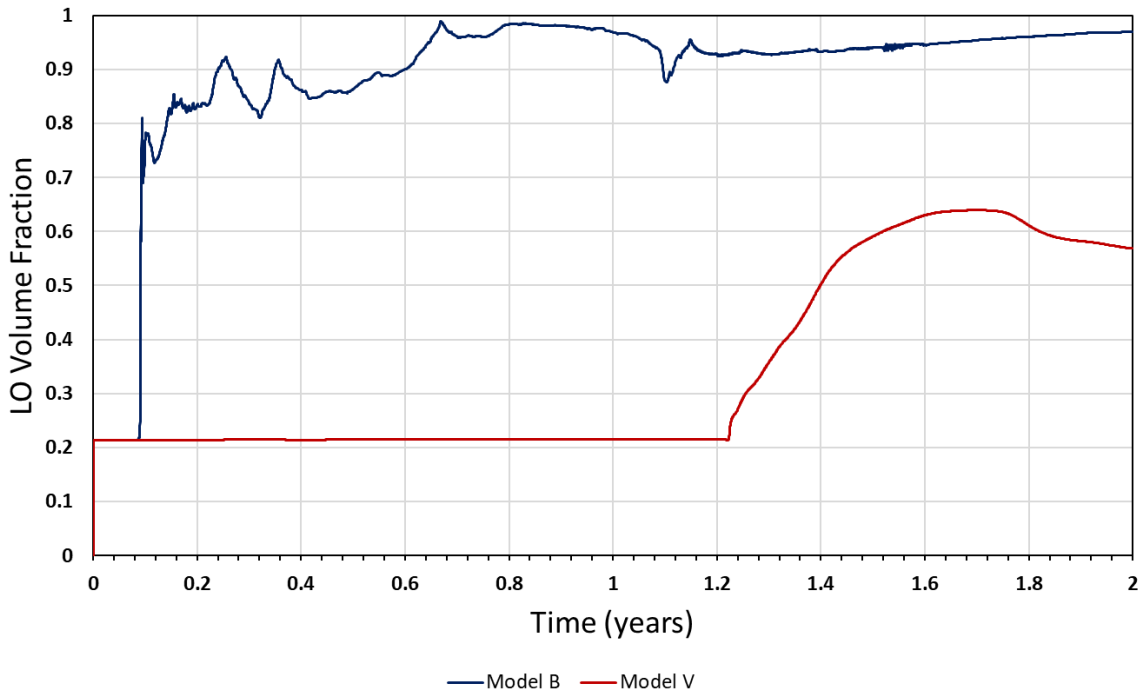


**Figure 5.15.** Comparison of light oil fraction calculated by Model B and Model V

However, Model V's capability in hydrogen production is countered by its underwhelming performance in light oil production, where it lags significantly behind Model B, producing one-twelfth of the light oil output. The disparity extends to the composition of the produced oil, with Model V's output containing a substantially lower fraction of light oil. In the initial 1.2 years, it hardly surpasses 20%, and then experiences a rapid spike to 60%. In stark contrast, Model B consistently maintains a high light oil fraction, ranging from 80% to 95% throughout the entire two-year operation (Figure 5.15).

Ultimately, the primary motivation behind the development of the THAI (Toe-to-Heel Air Injection) process was to facilitate the temporary displacement of thermally upgraded oil. This aimed to enhance the potential for thermal Enhanced Oil Recovery (EOR) within heavy oil reservoirs. This explains the discrepancy in performance between the vertical producer and the horizontal THAI producer. The extended displacement distance in the vertical setup necessitates thermally upgraded oil to traverse a longer pathway, passing through colder sections of the reservoir before reaching the producer. As a consequence, this longer journey leads to a re-elevation of viscosity, thereby diminishing efficiency and impeding breakthrough speed. This explains why the horizontal THAI producer outperforms its vertical counterpart (Xia et al., 2003a).

These findings underscore the divergent capabilities and limitations of these two models in the domains of hydrogen and light oil production, suggesting that they may be better suited for specific industrial applications and operational scenarios. This difference is due to the difference in thermal performance of the two models. The gravitational drainage of Model B due to the horizontal THAI well results in a much more stable combustion front, sweeping evenly across the reservoir. Conversely, the vertical producer in Model V produces a much less stable combustion front, with a very “top-

heavy" system, resulting in uneven oil upgrading and viscosity changes (Figure 5.16). Figure 5.16 shows that the oil saturation within Model V only impacts the top layer, with lots of the less viscous draining down into the lower layers where it accumulates (red zones of >89% oil saturation). However, the oil saturation changes in Model B are much more evenly distributed down the reservoir, with small accumulations of oil in the bottom layers beneath the injector, and within the mobile oil zone (red zone extending upwards form the second perforation of the producer well). Figure 5.17 shows that these effects are exaggerated with time.

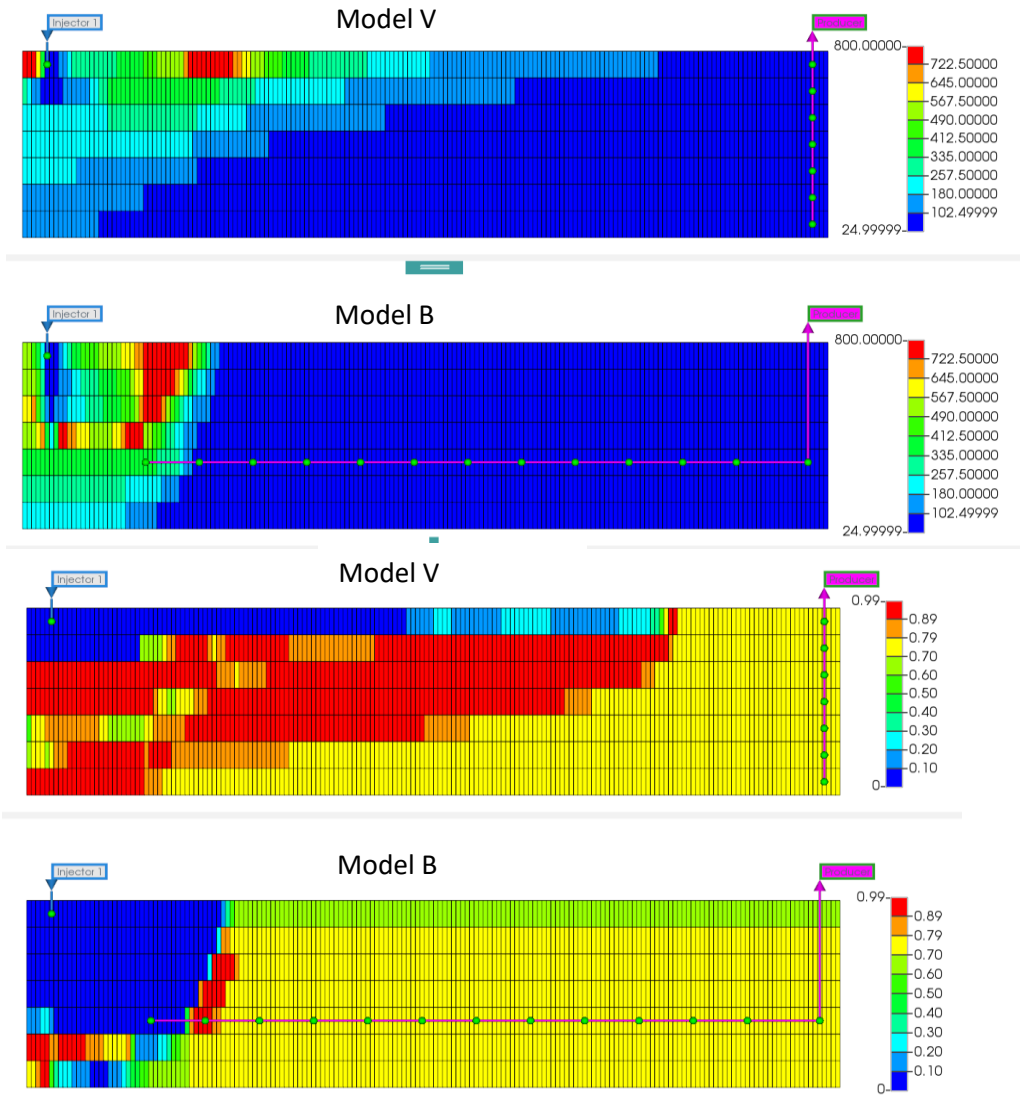


**Figure 5.16.** Comparison of temperature profiles (top) and oil saturation profiles (bottom) in Model B and Model V after 1 year of air injection

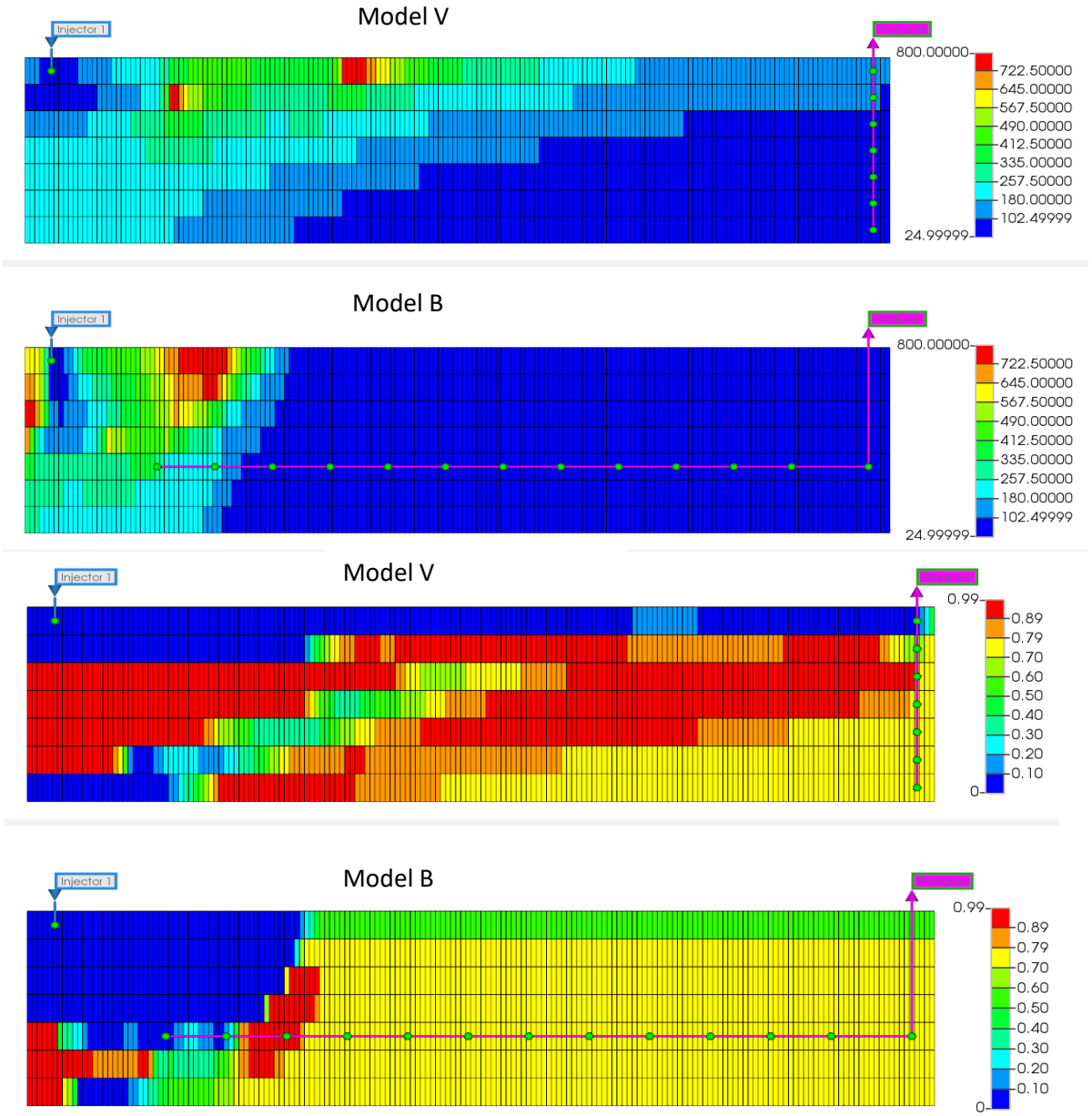


**Figure 5.17.** Comparison of temperature profiles (top) and oil saturation profiles (bottom) in Model B and Model V after 2 years of air injection

## 5.5 Hydrogen Potential from THAI

The evaluation of THAI for hydrogen production reveals a complex interplay between its potential as a source of hydrogen and the challenges associated with the in-situ process optimisation, and the surface purification process. Undoubtedly, THAI exhibits promise in generating hydrogen, leveraging its in-situ conversion of hydrocarbons. However, it is essential to acknowledge that the hydrogen produced through THAI may necessitate substantial purification efforts. The produced gas typically contains impurities, including

but not limited to methane, carbon dioxide, carbon monoxide and nitrogen compounds, along with the desired hydrogen (Figure 5.8). This implies that before the hydrogen can be utilised effectively for various applications, extensive purification steps are required to meet stringent purity standards (Luberti and Ahn, 2022). These purification processes often demand considerable energy and resources, potentially offsetting the efficiency gains achieved during the initial hydrogen production phase. Therefore, while THAI presents an intriguing avenue for on-site hydrogen generation, the substantial purification requirements should be carefully considered in assessing its overall viability for large-scale hydrogen production. Future research should focus on optimising purification techniques to minimise energy consumption and costs, ultimately enhancing the feasibility of using THAI-derived hydrogen as a reliable and sustainable energy source.

## 5.6 Conclusions

This study focused on three main targets: 1) incorporating hydrogen reactions into the THAI model to analyse their interaction, 2) investigating the impact of these reactions on the history match, highlighting the importance of the reaction scheme choice during in-situ combustion (ISC) processes, and 3) how (1) and (2) impact the practicality and technical performance of the process. The reservoir simulation model successfully incorporated hydrogen reactions and was calibrated and validated using field data from the KP2 well. Sensitivity analyses were conducted to assess the influence of various parameters on the performance of the ISC process. Grid independence analysis indicated that the cell length of 1.2 m in the i direction adequately captured the important flow dynamics in the reservoir, without significant impact from further refinement. The history matching of the KP2 well showed a good agreement between the model predictions and field data, with minor discrepancies observed during combustion

initiation and stable production periods. These discrepancies may be attributed to uncertainties in reservoir characterisation or operational factors not explicitly accounted for in the model. Nevertheless, the overall agreement suggests that the developed reservoir simulation model provides valuable insights into ISC process performance.

The analysis of hydrogen reactions revealed interesting outcomes. The inclusion of coke gasification reactions resulted in hydrogen production. However, it also led to reduced oil rates due to decreased temperature and increased gas saturation resulting in decreased oil relative permeability. The forward water-gas shift (FWGS) reaction demonstrated negligible impact on the oil production as it does not rely on hydrocarbon base reactants, decreasing the competition with cracking and oxidation reactions. The combined effect of coke gasification and FWGS resulted in higher hydrogen production and slightly reduced oil rates compared to the base case. In contrast, the reverse water-gas shift (RWGS) reaction had minimal impact on the hydrogen fraction, suggesting that its inclusion may not significantly alter the overall ISC process performance in terms of hydrogen generation. However, further investigations are needed to evaluate the impacts of RWGS in more complex reservoir scenarios.

Overall, this study emphasises the importance of including hydrogen reactions in the THAI model to understand their interaction and assess their impact on ISC processes. The model and sensitivity analyses provide valuable insights for decision-making in optimising the design and operation of ISC projects. Furthermore, the study highlights the significance of choosing an appropriate reaction scheme during history matching, as different schemes can influence the match and ultimately the accuracy of the model predictions. By considering these two main targets, this research contributes to a better understanding of ISC processes in heavy oil reservoirs. It underscores the role of

reservoir simulation in evaluating and optimising ISC techniques, leading to more efficient and sustainable heavy oil recovery operations. Future research should focus on refining the model by incorporating detailed reservoir characterisation, addressing uncertainties in input parameters, and exploring additional factors that may affect ISC process performance.

# CHAPTER 6. CONCLUSIONS

## 6.1 Laboratory-scale modelling

Overall, the study's broader findings underscored the promise of continuous steam injection for enhanced oil quality and production rates. Additionally, while hydrogen injection exhibited initial potential, its long-term influence on upgrading processes within THAI-CAPRI scenarios suggested a nuanced interplay between injected and in-situ-generated hydrogen, impacting oil production and quality in diverse ways.

### 6.1.1 Modelling and Validation of THAI-CAPRI Processes

The exploration of THAI and THAI-CAPRI processes through simulation provided insights into their reaction kinetics and operational aspects. Utilising in-situ generated hydrogen within the THAI-CAPRI framework hinted at enhanced heavy oil upgrading capabilities. Validated models aligned well with experimental data, showcasing promising matches through visual comparisons and statistical analyses.

### 6.1.2 Steaming Protocols and Process Impact

The study investigated various steaming protocols on THAI and THAI-CAPRI processes, emphasising their influence on oil quality and cumulative production. Continuous steam injection exhibited promising outcomes, leading to high-quality oil and increased production rates. THAI-CAPRI consistently demonstrated advantages in API upgrading regardless of the steaming protocol, especially with continuous steam injection, showcasing substantial API improvements and enhanced oil viscosity reduction.

### 6.1.3 Hydrogen Injection and Its Role in Upgrading

Exploring the addition of hydrogen alongside oxygen in the THAI-CAPRI process revealed complexities in fuel availability, temperatures, and oil production. While models incorporating hydrogen injection showed potential overestimation of cumulative oil

production, they emphasised the importance of hydrogen's influence on upgraded oil production. However, the actual impact of injected hydrogen on the long-term upgrading process was observed to diminish over time, indicating a saturation point in its effectiveness.

The research highlighted the intricate relationship between hydrogen injection and oil upgrading, showcasing varied models displaying rapid API increases followed by declines or continuous acceleration reaching a plateau. Moreover, considering catalytic hydrogen addition without minimum activation temperatures offered insights into more accurate density distributions, providing avenues for enhancing catalytic upgrading at THAI process temperatures.

## 6.2 Field-scale modelling

This study underscores the significance of incorporating hydrogen reactions in THAI models to understand their interactions and evaluate their impact on ISC processes. The findings and sensitivity analyses provide valuable insights for optimising ISC project design and operation decisions. Emphasising the importance of appropriate reaction schemes during history matching contributes to a better understanding of ISC processes in heavy oil reservoirs. Future research should focus on refining the model by incorporating detailed reservoir characterisation and addressing uncertainties to further enhance ISC process evaluations.

### 6.2.1 Incorporating Hydrogen Reactions and History Matching

This study aimed to integrate hydrogen reactions into the THAI model, focusing on their interactions and assessing their impact on ISC processes. The reservoir simulation model successfully incorporated these reactions and underwent calibration and validation against field data from the KP2 well. Sensitivity analyses evaluated various parameters'

influences on ISC process performance, highlighting an optimal cell length capturing critical flow dynamics without significant refinement impact.

### 6.2.2 History Match Insights and Discrepancies

The history match of the KP2 well revealed an overall agreement between model predictions and field data, with minor discrepancies during combustion initiation and stable production periods. These discrepancies, attributed to reservoir characterisation uncertainties or unaccounted operational factors, underscore the model's usefulness in providing insights into ISC process performance despite minor deviations.

### 6.2.3 Impact Analysis of Hydrogen Reactions

Examining hydrogen reactions, coke gasification resulted in hydrogen production but reduced oil rates due to temperature decrease and increased gas saturation impacting oil relative permeability. Forward water-gas shift (FWGS) showed negligible impact on oil production, reducing competition with other reactions. The combined effect of coke gasification and FWGS heightened hydrogen production but slightly reduced oil rates. Conversely, the reverse water-gas shift (RWGS) demonstrated minimal influence on hydrogen fraction, indicating negligible impact on ISC process performance in hydrogen generation.

## 6.3 Future recommendations

- The refinement of reservoir characterisation via the exploration of advanced laboratory techniques such as high-resolution imaging, microfluidics, and core analysis to capture detailed reservoir properties. Utilise state-of-the-art technologies to reduce uncertainties in porosity, permeability, rock-fluid interactions, and other critical parameters. This approach will enhance the

accuracy of laboratory-scale and field-scale simulations, providing more representative data for model development.

- Optimisation of the reaction scheme choices through conducting controlled experiments in laboratory setups to simulate different reaction schemes under varying temperature, pressure, and composition conditions. Use real-time monitoring tools to observe and analyse the reaction kinetics, identifying the most effective schemes for hydrogen generation, oil upgrading, and overall ISC performance. These findings will refine the choice of reaction schemes for future field-scale simulations.
- Expand laboratory-based sensitivity analyses by systematically varying a wider spectrum of parameters, including hydrocarbon composition, injection rates, catalyst types, and reaction scheme and kinetics. Utilise advanced data analytics and statistical methods to comprehensively understand the impact of these parameters on THAI and THAI-CAPRI processes at a smaller scale. This approach will contribute to a more nuanced understanding of how variations influence THAI performance.
- Utilise field-scale simulations to evaluate the economic feasibility of various reaction schemes and operational scenarios for ISC projects. Consider factors such as catalyst cost, oil recovery rates, and potential hydrogen production. Integrate economic models with reservoir simulations to identify the most cost-effective strategies for implementing THAI and THAI-CAPRI in real oil fields.
- Implement field-scale simulations to assess the impact of injecting downhole catalytic species or using fixed-bed catalysts on hydrogen generation and upgrading processes during ISC and THAI in heavy oil reservoirs. Model different types of catalytic materials, their distribution, and activation potential in the

reservoir. Analyse their catalytic effects on hydrogen generation and oil upgrading, considering factors like temperature gradients, reservoir heterogeneity, and long-term performance under field conditions.

## REFERENCES


ADO, M. R. 2020a. A detailed approach to up-scaling of the Toe-to-Heel Air Injection (THAI) In-Situ Combustion enhanced heavy oil recovery process. *Journal of Petroleum Science and Engineering,* **187,** 106740.

ADO, M. R. 2020b. Impacts of kinetics scheme used to simulate toe-to-heel air injection (THAI) in situ combustion method for heavy oil upgrading and production. *ACS omega,* **5,** 1938-1948.

ADO, M. R. 2020c. Predictive capability of field scale kinetics for simulating toe-to-heel air injection heavy oil and bitumen upgrading and production technology. *Journal of Petroleum Science and Engineering,* **187,** 106843.

ADO, M. R. 2021a. Improving oil recovery rates in THAI in situ combustion process using pure oxygen. *Upstream Oil and Gas Technology,* **6,** 100032.

ADO, M. R. 2021b. Understanding the mobilised oil drainage dynamics inside laboratory-scale and field-scale reservoirs for more accurate THAI process design and operation procedures. *Journal of Petroleum Exploration and Production Technology,* **11,** 4147-4162.

ADO, M. R. 2022. Comparisons of predictive ability of THAI in situ combustion process models with pre-defined fuel against that having fuel deposited based on Arrhenius kinetics parameters. *Journal of Petroleum Science and Engineering,* **208,** 109716.

ADO, M. R., GREAVES, M. & RIGBY, S. P. 2018. Effect of pre-ignition heating cycle method, air injection flux, and reservoir viscosity on the THAI heavy oil recovery process. *Journal of Petroleum Science and Engineering,* **166,** 94-103.

ADO, M. R., GREAVES, M. & RIGBY, S. P. 2019. Numerical simulation of the impact of geological heterogeneity on performance and safety of THAI heavy oil production process. *Journal of Petroleum Science and Engineering,* **173,** 1130-1148.

ADO, M. R., GREAVES, M. & RIGBY, S. P. 2022a. Effect of operating pressure on the performance of THAI-CAPRI in situ combustion and in situ catalytic process for simultaneous thermal and catalytic upgrading of heavy oils and bitumen. *Petroleum Research,* **7,** 155-164.

ADO, M. R., GREAVES, M. & RIGBY, S. P. 2022b. Simulation of catalytic upgrading in CAPRI, an add-on process to novel in-situ combustion, THAI. *Petroleum Research,* **7,** 297-307.

AFANASEV, P., POPOV, E., CHEREMISIN, A., BERENBLYUM, R., MIKITIN, E., SOROKIN, E., BORISENKO, A., DARISHCHEV, V., SHCHEKOLDIN, K. & SLAVKINA, O. 2021. An experimental study of the possibility of in situ hydrogen generation within gas reservoirs. *Energies,* **14,** 5121.

AHLBRANDT, T. S. 2002. Future petroleum energy resources of the world. *International Geology Review,* **44,** 1092-1104.

AKKUTLU, I. Y. & YORTSOS, Y. C. 2003. The dynamics of in-situ combustion fronts in porous media. *Combustion and Flame,* **134,** 229-247.

ALVAREZ, G., POTEAU, S., ARGILLIER, J.-F., LANGEVIN, D. & SALAGER, J.-L. 2009. Heavy oil− water interfacial properties and emulsion stability: Influence of dilution. *Energy & Fuels,* **23,** 294-299.

ANBARI, H., ROBINSON, J. P., GREAVES, M. & RIGBY, S. P. 2023. Field performance and numerical simulation study on the toe to heel air injection (THAI) process in a heavy oil reservoir with bottom water. *Journal of Petroleum Science and Engineering,* **220,** 111202.

AYASSE, C., BLOOMER, C., LYNGBERG, E., BODDY, W., DONNELLY, J. & GREAVES, M. 2005. First Field Pilot of the THAI Process.
BAI, B., GUO, Q., LI, Y., HU, X. & MA, J. 2018. Catalytic gasification of crushed coke and changes of structural characteristics. *Energy & Fuels,* **32,** 3356-3367.
BHUTTO, A. W., BAZMI, A. A. & ZAHEDI, G. 2013. Underground coal gasification: From fundamentals to applications. *Progress in Energy and Combustion Science,* **39,** 189-214.
BRANDT, A. R., MASNADI, M. S., ENGLANDER, J. G., KOOMEY, J. & GORDON, D. 2018. Climate-wise choices in a world of oil abundance. *Environmental Research Letters,* **13,** 044027.
BURCH, R., GOGUET, A. & MEUNIER, F. C. 2011. A critical analysis of the experimental evidence for and against a formate mechanism for high activity water-gas shift catalysts. *Applied Catalysis A: General,* **409,** 3-12.
CAO, E., GREAVES, M. & RIGBY, S. P. Phase Properties of Mobile Oil Zone in the THAI-CAPRI Process. Canadian International Petroleum Conference, 2009. OnePetro.
CHAO, K., CHEN, Y., LI, J., ZHANG, X. & DONG, B. 2012. Upgrading and visbreaking of super-heavy oil by catalytic aquathermolysis with aromatic sulfonic copper. *Fuel Processing Technology,* **104,** 174-180.
CHEN, W.-H., BISWAS, P. P., ONG, H. C., NGUYEN, T.-B. & DONG, C.-D. 2023. A critical and systematic review of sustainable hydrogen production from ethanol/bioethanol: Steam reforming, partial oxidation, and autothermal reforming. *Fuel,* **333,** 126526.
CHEN, W.-H. & CHEN, C.-Y. 2020. Water gas shift reaction for hydrogen production and carbon dioxide capture: A review. *Applied Energy,* **258,** 114078.
CHIANESE, S., LOIPERSBÖCK, J., MALITS, M., RAUCH, R., HOFBAUER, H., MOLINO, A. & MUSMARRA, D. 2015. Hydrogen from the high temperature water gas shift reaction with an industrial Fe/Cr catalyst using biomass gasification tar rich synthesis gas. *Fuel Processing Technology,* **132,** 39-48.
COATES, R. & ZHAO, L. Numerical Evaluation of THAI Prcess. Canadian International Petroleum Conference, 2001. OnePetro.
DAI, C. & ZHAO, F. 2019. *Oilfield chemistry*, Springer.
DAZA, Y. A. & KUHN, J. N. 2016. CO 2 conversion by reverse water gas shift catalysis: comparison of catalysts, mechanisms and their consequences for CO 2 conversion to liquid fuels. *RSC advances,* **6,** 49675-49691.
DELUGA, G., SALGE, J., SCHMIDT, L. & VERYKIOS, X. 2004. Renewable hydrogen from ethanol by autothermal reforming. *Science,* **303,** 993-997.
DEMIRBAŞ, A. & ÇAĞLAR, A. 1998. Catalytic steam reforming of biomass and heavy oil residues to hydrogen. *Energy, Education Science and Technology,* **11,** 45-52.
DRAČÍNSKÝ, M., ČECHOVÁ, L., HODGKINSON, P., PROCHÁZKOVÁ, E. & JANEBA, Z. 2015. Resonance-assisted stabilisation of hydrogen bonds probed by NMR spectroscopy and path integral molecular dynamics. *Chemical Communications,* **51,** 13986-13989.
DUDLEY, B. 2018. BP statistical review of world energy 2018. *Energy economic, Centre for energy economics research and policy. British Petroleum, Available via https://www. bp. com/en/global/corporate/energy-economics/statistical-review-of-world-energy/electricity. html,* **5**.
DUTTA, N. C., BACHRACH, R. & MUKERJI, T. 2021. *Quantitative analysis of geopressure for geoscientists and engineers*, Cambridge University Press.
ESCOBAR, J., BARRERA, M. C., SANTES, V. & TERRAZAS, J. E. 2017. Naphthalene hydrogenation over Mg-doped Pt/Al2O3. *Catalysis Today,* **296,** 197-204.

FERDOUS, D., DALAI, A. K. & ADJAYE, J. 2006. Hydrodenitrogenation and hydrodesulfurization of heavy gas oil using NiMo/Al2O3 catalyst containing boron: Experimental and kinetic studies. *Industrial & engineering chemistry research,* **45,** 544-552.

FERMOSO, J., ARIAS, B., GIL, M. V., PLAZA, M., PEVIDA, C., PIS, J. & RUBIERA, F. 2010. Co-gasification of different rank coals with biomass and petroleum coke in a high-pressure reactor for H2-rich gas production. *Bioresource technology,* **101,** 3230-3235.

FERMOSO, J., ARIAS, B., PLAZA, M., PEVIDA, C., RUBIERA, F., PIS, J., GARCÍA-PEÑA, F. & CASERO, P. 2009. High-pressure co-gasification of coal with biomass and petroleum coke. *Fuel Processing Technology,* **90,** 926-932.

FERRARI, M., BOSMANS, S., MAGGI, R., DELMON, B. & GRANGE, P. 2001. CoMo/carbon hydrodeoxygenation catalysts: influence of the hydrogen sulfide partial pressure and of the sulfidation temperature. *Catalysis Today,* **65,** 257-264.

FISHTIK, I., ALEXANDER, A., DATTA, R. & GEANA, D. 2000. A thermodynamic analysis of hydrogen production by steam reforming of ethanol via response reactions. *International Journal of Hydrogen Energy,* **25,** 31-45.

FLAHERTY, D. W., YU, W.-Y., POZUN, Z. D., HENKELMAN, G. & MULLINS, C. B. 2011. Mechanism for the water–gas shift reaction on monofunctional platinum and cause of catalyst deactivation. *Journal of catalysis,* **282,** 278-288.

FORZATTI, P. & LIETTI, L. 1999. Catalyst deactivation. *Catalysis today,* **52,** 165-181.

GRABOWSKI, J. W., VINSOME, P. K., LIN, R. C., BEHIE, G. & RUBIN, B. A fully implicit general purpose finite-difference thermal model for in situ combustion and steam. SPE Annual Technical Conference and Exhibition?, 1979. SPE, SPE-8396-MS.

GREAVES, M., DONG, L. & RIGBY, S. 2011a. Upscaling THAI: Experiment to pilot. *Society of Petroleum Engineers - Canadian Unconventional Resources Conference 2011, CURC 2011,* **2**.

GREAVES, M., DONG, L. & RIGBY, S. 2012a. Simulation study of the toe-to-heel air injection three-dimensional combustion cell experiment and effects in the mobile oil zone. *Energy & Fuels,* **26,** 1656-1669.

GREAVES, M., DONG, L. L. & RIGBY, S. Upscaling THAI: experiment to pilot. Canadian Unconventional Resources Conference, 2011b. OnePetro.

GREAVES, M., DONG, L. L. & RIGBY, S. Determination of Limits to Production in THAI. SPE Canada Heavy Oil Conference, 2012b. SPE, SPE-157817-MS.

GREAVES, M., DONG, L. L. & RIGBY, S. P. Upscaling THAI: experiment to pilot. 2011c. OnePetro.

GREAVES, M. & XIA, T. CAPRI-Downhole catalytic process for upgrading heavy oil: Produced oil properties and composition. 2001. OnePetro.

GREAVES, M. & XIA, T. Simulation studies of THAI process. Canadian International Petroleum Conference, 2000a. OnePetro.

GREAVES, M. & XIA, T. CAPRI-Downhole catalytic process for upgrading heavy oil: Produced oil properties and composition. Canadian international petroleum conference, 2001a. OnePetro.

GREAVES, M. & XIA, T. 2004. Downhole upgrading of Wolf Lake oil using THAI–CAPRI processes-tracer tests. *Preprints of Papers-American Chemical Society, Division of Fuel Chemistry,* **49,** 69-72.

GREAVES, M., XIA, T., IMBUS, S. & NERO, V. THAI-CAPRI process: tracing downhole upgrading of heavy oil. Canadian international petroleum conference, 2004a. OnePetro.

GREAVES, M., XIA, T. & TURTA, A. 2008a. Stability of THAI™ process-Theoretical and experimental observations. *Journal of Canadian Petroleum Technology,* **47**.
GREAVES, M. & XIA, T. X. 2000b. Simulation Studies of THAI Process.
GREAVES, M. & XIA, T. X. Simulation studies of THAI process. 2000c. OnePetro.
GREAVES, M. & XIA, T. X. 2001b. CAPRI-Downhole Catalytic Process for Upgrading Heavy Oil: Produced Oil Properties and Composition. *Journal of Canadian Petroleum Technology,* **43**.
GREAVES, M., XIA, T. X., IMBUS, S. & NERO, V. 2004b. THAI-CAPRI Process: Tracing Downhole Upgrading of Heavy Oil.
GREAVES, M., XIA, T. X., IMBUS, S. & NERO, V. THAI-CAPRI process: tracing downhole upgrading of heavy oil. 2004c. OnePetro.
GREAVES, M., XIA, T. X. & TURTA, A. T. 2008b. Stability of THAI™ process-Theoretical and experimental observations. *Journal of Canadian Petroleum Technology,* **47**.
GREAVES, M., XIA, T. X., TURTA, A. T. & AYASSE, C. Recent laboratory results of THAI and its comparison with other IOR processes. 2000a. OnePetro.
GREAVES, M., XIA, T. X., TURTA, A. T. & AYASSE, C. 2000b. Recent Laboratory Results of THAI and Its Comparison with Other IOR Processes.
GRIGORE, M., SAKUROVS, R., FRENCH, D. & SAHAJWALLA, V. 2009. Coke gasification: the influence and behavior of inherent catalytic mineral matter. *Energy & Fuels,* **23,** 2075-2085.
HAJDO, L., HALLAM, R. & VORNDRAN, L. Hydrogen generation during in-situ combustion. Spe California regional meeting, 1985. OnePetro.
HART, A. 2014a. The novel THAI–CAPRI technology and its comparison to other thermal methods for heavy oil recovery and upgrading. *Journal of Petroleum Exploration and Production Technology,* **4,** 427-437.
HART, A. 2014b. The novel THAI–CAPRI technology and its comparison to other thermal methods for heavy oil recovery and upgrading. *Journal of Petroleum Exploration and Production Technology,* **4,** 427-437.
HART, A., LEEKE, G., GREAVES, M. & WOOD, J. Down-hole catalytic upgrading of heavy oil and bitumen to meet tomorrow's energy needs: the THAI–CAPRI process. Proceeding of the third North Am Symp Chem React Eng March, 2013. 17-20.
HART, A., LEEKE, G., GREAVES, M. & WOOD, J. 2014. Down-hole heavy crude oil upgrading by CAPRI: Effect of hydrogen and methane gases upon upgrading and coke formation. *Fuel,* **119,** 226-235.
HART, A. & WOOD, J. 2018. In situ catalytic upgrading of heavy crude with CAPRI: influence of hydrogen on catalyst pore plugging and deactivation due to coke. *Energies,* **11,** 636.
HART, A., WOOD, J. & GREAVES, M. 2017. In situ catalytic upgrading of heavy oil using a pelletized Ni-Mo/Al2O3 catalyst in the THAI process. *Journal of Petroleum Science and Engineering,* **156,** 958-965.
HASAN, M. & RIGBY, S. 2019a. Enhanced Recovery of Heavy Oil Using A Catalytic Process. *IOP Conference Series: Materials Science and Engineering,* **579,** 012030.
HASAN, M. M. & RIGBY, S. P. Enhanced recovery of heavy oil using a catalytic process. 2019b. IOP Publishing, 012030.
HEAD, I. M., JONES, D. M. & LARTER, S. R. 2003. Biological activity in the deep subsurface and the origin of heavy oil. *Nature,* **426,** 344-352.
HEIN, F. J. 2006. Heavy oil and oil (tar) sands in North America: An overview & summary of contributions. *Natural Resources Research,* **15,** 67-84.

HEIN, F. J. 2017. Geology of bitumen and heavy oil: An overview. *Journal of Petroleum Science and Engineering,* **154,** 551-563.
HELFENSTEYN, S., TOLLET, H., DEGRÈVE, J. & CREEMERS, C. 2003. LEIS-surface analysis of commercial sulfided oxide catalysts. *Applied Catalysis A: General,* **239,** 221-228.
HILL, P. 2017. Hydrocarbon distribution in the Mannville Waseca Member, Edam oil field, west-central Saskatchewan. *Saskatchewan Geological Survey,* **1,** 21.
HINKLE, A. & BATZLE, M. 2006. Heavy oils: A worldwide overview. *The Leading Edge,* **25,** 742-749.
HOBBS, M., RADULOVIC, P. & SMOOT, D. L. 1993. Combustion and gasification of coals in fixed-beds. *Progress in Energy and Combustion Science,* **19,** 505-586.
KAPADIA, P. R., KALLOS, M. S. & GATES, I. D. 2011. Potential for hydrogen generation from in situ combustion of Athabasca bitumen. *Fuel,* **90,** 2254-2265.
KAPADIA, P. R., WANG, J. J., KALLOS, M. S. & GATES, I. D. 2013. Practical process design for in situ gasification of bitumen. *Applied energy,* **107,** 281-296.
KARIMI, A. & GRAY, M. R. 2011. Effectiveness and mobility of catalysts for gasification of bitumen coke. *Fuel,* **90,** 120-125.
KARIMI, A., SEMAGINA, N. & GRAY, M. R. 2011. Kinetics of catalytic steam gasification of bitumen coke. *Fuel,* **90,** 1285-1291.
KARIMOV, T., LAMAN, M. & ABBUZARLI, U. 2018. IMPACT OF OIL ON INTERNATIONAL TRADE. *Managerial Challenges of the Contemporary Society. Proceedings,* **11,** 64.
KILIAN, L. & ZHOU, X. 2020. Does drawing down the US Strategic Petroleum Reserve help stabilize oil prices? *Journal of Applied Econometrics,* **35,** 673-691.
KOTHARI, R., BUDDHI, D. & SAWHNEY, R. 2008. Comparison of environmental and economic aspects of various hydrogen production methods. *Renewable and Sustainable Energy Reviews,* **12,** 553-563.
KULKARNI, M. M. & RAO, D. N. 2004. *Analysis of the novel Toe-To-Heel Air Injection (THAI) process using simple analytical models*, American Institute of Chemical Engineers.
LI, Y., WANG, Z., HU, Z., XU, B., LI, Y., PU, W. & ZHAO, J. 2021. A review of in situ upgrading technology for heavy crude oil. *Petroleum,* **7,** 117-122.
LOPEMAN, T., ANBARI, H., LEEKE, G. & WOOD, J. 2022. Numerical Modeling of Toe-to-Heel Air Injection and Its Catalytic Variant (CAPRI) under Varying Steam Conditions. *Energy & Fuels: an American Chemical Society Journal,* **37,** 237-250.
LUBERTI, M. & AHN, H. 2022. Review of Polybed pressure swing adsorption for hydrogen purification. *International Journal of Hydrogen Energy,* **47,** 10911-10933.
MARAFI, A., HAUSER, A. & STANISLAUS, A. 2006. Atmospheric residue desulfurization process for residual oil upgrading: An investigation of the effect of catalyst type and operating severity on product oil quality. *Energy & fuels,* **20,** 1145-1149.
MARAFI, A., HAUSER, A. & STANISLAUS, A. 2007. Deactivation patterns of Mo/Al2O3, Ni–Mo/Al2O3 and Ni–MoP/Al2O3 catalysts in atmospheric residue hydrodesulphurization. *Catalysis today,* **125,** 192-202.
MARTIN, W. L., ALEXANDER, J. D. & DEW, J. N. 1958. Process variables of in situ combustion. *Transactions of the AIME,* **213,** 28-35.
MENG, X., XU, C., GAO, J. & LIU, Z. 2008. Influence of feed properties and reaction conditions on catalytic pyrolysis of gas oils and heavy oils. *Fuel,* **87,** 2463-2468.
MEYER, R. F. & ATTANASI, E. D. 2003. Heavy oil and natural bitumen-strategic petroleum resources. *World,* **434,** 650-7.
MEYER, R. F., ATTANASI, E. D. & FREEMAN, P. A. 2007. Heavy oil and natural bitumen resources in geological basins of the world: Map showing klemme basin

classification of sedimentary provinces reporting heavy oil or natural bitumen. *US Geol. Surv. Open-File Rep,* **2007,** 1084.
MOORE, L. M. 1996. The basic practice of statistics. Taylor & Francis.
MORROW, A. W., MUKHAMETSHINA, A., ALEKSANDROV, D. & HASCAKIR, B. Environmental impact of bitumen extraction with thermal recovery. SPE Heavy Oil Conference-Canada, 2014. OnePetro.
MURTHY, B. N., SAWARKAR, A. N., DESHMUKH, N. A., MATHEW, T. & JOSHI, J. B. 2014. Petroleum coke gasification: a review. *The Canadian Journal of Chemical Engineering,* **92,** 441-468.
NIKOLAIDIS, P. & POULLIKKAS, A. 2017. A comparative overview of hydrogen production processes. *Renewable and sustainable energy reviews,* **67,** 597-611.
NURMI, P. & OY 2021. *Preliminary evaluation of the Estonian geoenergy potential and overview of available technologies, expert opinion for using those technologies in the Estonian geological conditions, suggestions for possible further actions and examples of case studies*.
OKOLIE, J. A., PATRA, B. R., MUKHERJEE, A., NANDA, S., DALAI, A. K. & KOZINSKI, J. A. 2021. Futuristic applications of hydrogen in energy, biorefining, aerospace, pharmaceuticals and metallurgy. *International journal of hydrogen energy,* **46,** 8885-8905.
PAL, D., CHAND, R., UPADHYAY, S. & MISHRA, P. 2018. Performance of water gas shift reaction catalysts: A review. *Renewable and Sustainable Energy Reviews,* **93,** 549-565.
PEI, H., ZHANG, G., GE, J., ZHANG, J., ZHANG, Q. & FU, L. Investigation of nanoparticle and surfactant stabilized emulsion to enhance oil recovery in waterflooded heavy oil reservoirs. SPE Canada heavy oil technical conference, 2015. OnePetro.
PHILLIPS, C. R., HAIDAR, N. I. & POON, Y. C. 1985. Kinetic models for the thermal cracking of athabasca bitumen: the effect of the sand matrix. *Fuel,* **64,** 678-691.
RABIU ADO, M. 2017. *Numerical simulation of heavy oil and bitumen recovery and upgrading techniques.* University of Nottingham.
REEVE, J., MAHMUD, T., TWIGG, M. V. & DUPONT, V. 2022. The kinetics of acetic acid steam reforming on Ni/Ca-Al2O3 catalyst. *International Journal of Hydrogen Energy,* **47,** 35709-35722.
REN, Y., FREITAG, N. & MAHINPEY, N. A Simple Kinetic Model for Coke CombustionDuring an In Situ Combustion (ISC) Process. PETSOC Canadian International Petroleum Conference, 2005. PETSOC, PETSOC-2005-110.
RIERA, J. A., LIMA, R. M. & KNIO, O. M. 2023. A review of hydrogen production and supply chain modeling and optimization. *International Journal of Hydrogen Energy*.
RODDY, D. J. 2013. A syngas network for reducing industrial carbon footprint and energy use. *Applied Thermal Engineering,* **53,** 299-304.
ROSA, L., DAVIS, K. F., RULLI, M. C. & D'ODORICO, P. 2017. Environmental consequences of oil production from oil sands. *Earth's Future,* **5,** 158-170.
ROSTRUP-NIELSEN, J. R. & ROSTRUP-NIELSEN, T. 2002. Large-scale hydrogen production. *Cattech,* **6,** 150-159.
SANCHEZ, N., RUIZ, R., HACKER, V. & COBO, M. 2020. Impact of bioethanol impurities on steam reforming for hydrogen production: A review. *International Journal of Hydrogen Energy,* **45,** 11923-11942.
SANTOS, R., LOH, W., BANNWART, A. & TREVISAN, O. 2014. An overview of heavy oil properties and its recovery and transportation methods. *Brazilian Journal of Chemical Engineering,* **31,** 571-590.

SATO, S., LIN, S.-Y., SUZUKI, Y. & HATANO, H. 2003. Hydrogen production from heavy oil in the presence of calcium hydroxide☆. *Fuel,* **82,** 561-567.

SCHRÖDER, V. & HOLTAPPELS, K. 2005. Explosion characteristics of hydrogen-air and hydrogen-oxygen mixtures at elevated pressures.

SHAH, A., FISHWICK, R., WOOD, J., LEEKE, G., RIGBY, S. & GREAVES, M. 2010. A review of novel techniques for heavy oil and bitumen extraction and upgrading. *Energy & Environmental Science,* **3,** 700-714.

SHAH, A. A., FISHWICK, R. P., LEEKE, G. A., WOOD, J., RIGBY, S. P. & GREAVES, M. 2011. Experimental optimization of catalytic process in situ for heavy-oil and bitumen upgrading. *Journal of Canadian Petroleum Technology,* **50,** 33-47.

SHAKIRULLAH, M., AHMAD, I., KHAN, M. A., SHAH, A. A. & ISHAQ, M. 2008. Conversion of asphalt into distillate products. *Energy conversion and management,* **49,** 107-112.

SINGH, A., MATHEWES, T., DALAWAT, K., AGARWAL, J. & SHAH, M. 2019a. *THAI-CAPRI Technology for Heavy Crudes*.

SINGH, A., MATHEWS, T. A., DALAWAT, K., AGARWAL, J. & SHAH, M. THAI-CAPRI Technology for Heavy Crude Reserves. ICTEA: International Conference on Thermal Engineering, 2019b.

SMITH, B., LOGANATHAN, M. & SHANTHA, M. S. 2010. A review of the water gas shift reaction kinetics. *International Journal of Chemical Reactor Engineering,* **8**.

SOIKET, M. I., ONI, A., GEMECHU, E. & KUMAR, A. 2019. Life cycle assessment of greenhouse gas emissions of upgrading and refining bitumen from the solvent extraction process. *Applied Energy,* **240,** 236-250.

SPEIGHT, J. G. 2019. *Heavy oil recovery and upgrading*, Gulf Professional Publishing.

TARE, T. & GREAVES, M. 2002. 3D Physical Model Studies of Downhole Catalytic Upgrading ofWolf Lake Heavy Oil Using THAI. *Journal of Canadian Petroleum Technology,* **41**.

TIBILETTI, D., GOGUET, A., MEUNIER, F. C., BREEN, J. P. & BURCH, R. 2004. On the importance of steady-state isotopic techniques for the investigation of the mechanism of the reverse water-gas-shift reaction. *Chemical communications*, 1636-1637.

TIJINK, P. & COTTIER, J. 2019. The description and quantification of the truncation errors produced by local-grid refinement in reservoir simulation. *SPE Reservoir Evaluation & Engineering,* **22,** 660-672.

TRIMM, D. 1983. Catalyst design for reduced coking. *Applied Catalysis,* **5,** 263-290.

TROMMER, D., NOEMBRINI, F., FASCIANA, M., RODRIGUEZ, D., MORALES, A., ROMERO, M. & STEINFELD, A. 2005. Hydrogen production by steam-gasification of petroleum coke using concentrated solar power—I. Thermodynamic and kinetic analyses. *International Journal of Hydrogen Energy,* **30,** 605-618.

TURTA, A., GREAVES, M. & GRABOVSKI, J. 2018. Comprehensive Assessment of Toe-To-Heel Air Injection (THAI) Process. Guidelines for Development of Future Generations of In-Situ Combustion Processes. *Report Issued by AT EOR Consultancy, Calgary, January 2018.*

TURTA, A., KAPADIA, P. & GADELLE, C. 2020. THAI process: Determination of the quality of burning from gas composition taking into account the coke gasification and water-gas shift reactions. *Journal of Petroleum Science and Engineering,* **187,** 106638.

TURTA, A., SINGHAL, A., SIERRA, R., GREAVES, M. & ISLAM, M. Evaluation of the First Field Piloting of the THAI Process: Athabasca Pilot. SPE Canadian Energy Technology Conference, 2023. SPE, D021S017R001.

TZANETIS, K., MARTAVALTZI, C. & LEMONIDOU, A. 2012. Comparative exergy analysis of sorption enhanced and conventional methane steam reforming. *International Journal of Hydrogen Energy,* **37,** 16308-16320.
WEI, W., WANG, J., AFSHORDI, S. & GATES, I. D. 2020. Detailed analysis of Toe-to-Heel Air Injection for heavy oil production. *Journal of Petroleum Science and Engineering,* **186,** 106704.
WIKEL, K. & KENDALL, R. 2012. 4D Study of Secondary Recovery Utilizing THAI from a Saskatchewan Heavy Oil Reservoir. *Search and Discovery Article*.
XIA, T., GREAVES, B., WERFILLI, M. & RATHBONE, R. THAI process-effect of oil layer thickness on heavy oil recovery. Canadian international petroleum conference, 2002a. OnePetro.
XIA, T., GREAVES, B., WERFILLI, M. S. & RATHBONE, R. R. 2002b. THAI Process-Effect of Oil Layer Thickness on Heavy Oil Recovery.
XIA, T., GREAVES, M., TURTA, A. & AYASSE, C. 2003a. THAI—A 'short-distance displacement'in situ combustion process for the recovery and upgrading of heavy oil. *Chemical Engineering Research and Design,* **81,** 295-304.
XIA, T., GREAVES, M., WERFILLI, W. & RATHBONE, R. 2002c. Downhole Conversion of Lloydminster Heavy Oil Using THAI-CAPRI Process.
XIA, T., GREAVES, M., WERFILLI, W. & RATHBONE, R. Downhole conversion of Lloydminster heavy oil using THAI-CAPRI process. SPE International Thermal Operations and Heavy Oil Symposium and International Horizontal Well Technology Conference, 2002d. OnePetro.
XIA, T. X., GREAVES, M. & TURTA, A. 2003b. *Main Mechanism for Stability of THAI- "Toe-to-Heel Air Injection"*.
XIA, T. X., GREAVES, M. & TURTA, A. Main mechanism for stability of THAI-Toe-to-Heel Air Injection. 2003c. OnePetro.
XIA, T. X., GREAVES, M., WERFILLI, W. S. & RATHBONE, R. R. Downhole conversion of Lloydminster heavy oil using THAI-CAPRI process. 2002e. OnePetro.
YANG, S., HUANG, S., JIANG, Q., YU, C. & ZHOU, X. 2022. Experimental study of hydrogen generation from in-situ heavy oil gasification. *Fuel,* **313,** 122640.
YI, H., LI, C. & WANG, X. 2002. Research and development of CEP-1 catalyst for catalytic pyrolysis and its application. *Shiyou Lianzhi yu Huagong,* **33,** 38-42.
YUE, M., LAMBERT, H., PAHON, E., ROCHE, R., JEMEI, S. & HISSEL, D. 2021. Hydrogen energy systems: A critical review of technologies, applications, trends and challenges. *Renewable and Sustainable Energy Reviews,* **146,** 111180.
ZHU, H., CHEN, Z., PASTOR-PEREZ, L., LONG, X. & MILLAN, M. 2023. How syngas composition affects catalytic steam reforming of tars: An analysis using toluene as model compound. *International Journal of Hydrogen Energy,* **48,** 1290-1303.

## APPENDIX 1 – EXAMPLE INPUT FILE FOR LABORATORY-SCALE THAI MODEL

```
TITLE1 'SIMULATION OF TOE-TO-HEEL AIR INJECTION'
** ====================== INPUT/OUTPUT
CONTROL=========================
INTERRUPT STOP
INUNIT LAB
OUTUNIT LAB
OUTPRN ITER NEWTON
OUTPRN GRID OBHLOSS PRES SG SO SOLCONC SW TEMP VISO VISW X Y

OUTPRN WELL ALL
WRST 400
WPRN GRID 300
WPRN ITER 300
OUTSRF GRID CCHLOSS CMPDENO CMPDENW CMPVISG CMPVISO CMPVISW FLUXRC
FLUXSC FPOROS KRG KRO
      KRW KVALYW KVALYX MASDENG MASDENO MASDENW OBHLOSS PCOG PCOW
PERMI PERMJ
      PERMK PRES SG SO MASS SOLCONC SW TEMP VISG VISO VISW VPOROS
      W X Y
OUTSRF WELL MASS COMPONENT ALL
OUTSRF WELL MOLE COMPONENT ALL
OUTSRF SPECIAL MAXVAR MASDENO
        MAXVAR VISO
        MAXVAR PRES
        MAXVAR MASS SOLCONC 'COKE'
        MAXVAR TEMP
        MINVAR MASDENO
        MINVAR VISO
        MINVAR PRES
        MINVAR MASS SOLCONC 'COKE'
        MINVAR TEMP
        AVGVAR MASDENO
        AVGVAR VISO
        AVGVAR PRES
        AVGVAR MASS SOLCONC 'COKE'
        AVGVAR TEMP
        MOLEFRAC  'Producer' 'CO2' GAS
        MOLEFRAC  'Producer' 'CO' GAS
        MOLEFRAC  'Producer' 'N2' GAS
        MOLEFRAC  'Producer' 'O2' GAS
        MOLEFRAC  'Producer' 'H2O' GAS
        MOLEFRAC  'Producer' 'LO' OIL
        MOLEFRAC  'Producer' 'HO' OIL
        MATBAL  GASEOUS 'H2O'
        MATBAL  AQUEOUS 'H2O'
        MATBAL  GASEOUS 'LO'
        MATBAL  GASEOUS 'HO'
```

```
        MATBAL  OLEIC 'LO'
        MATBAL  OLEIC 'HO'
        MATBAL  CURRENT 'COKE'
        MATBAL  CURRENT 'O2'
        MATBAL  CURRENT 'CO2'
        MATBAL  CURRENT 'N2'
        MATBAL  CURRENT 'CO'
        MATBAL  CURRENT 'LO'
        MATBAL  CURRENT 'HO'
        MATBAL  REACTION 'H2O'
        MATBAL  REACTION 'CO2'
        MATBAL  REACTION 'CO'
        MATBAL  REACTION 'O2'
        MATBAL  REACTION 'LO'
        MATBAL  REACTION 'HO'
        MATBAL  REACTION 'COKE'
        DELP  'Injector' 'Producer'
        OBHLOSSCUM
        CCHLOSSCUM
        OBHLOSSRATE
        CCHLOSSRATE
OUTSRF WELL LAYER ALL
OUTSRF WELL DOWNHOLE
OUTSRF *FLUX_SECTOR *ALL *RC *SUM
REWIND 150
INTERRUPT RESTART-STOP
**  Distance units: cm
RESULTS XOFFSET         0.0000
RESULTS YOFFSET         0.0000
RESULTS ROTATION        0.0000  **  (DEGREES)
RESULTS AXES-DIRECTIONS 1.0 -1.0 1.0
** ************************************************************************
** Definition of fundamental cartesian grid
** ************************************************************************
GRID VARI 30 19 7
KDIR DOWN
DI IVAR
30*2
DJ JVAR
19*2.10526
DK ALL
3420*1.466667 570*1.2
DTOP
570*0
NULL CON 1
POR CON 0.34
PERMI CON 11500
PERMJ CON 11500
PERMK CON 3450
```

```
PINCHOUTARRAY CON 1
*end-grid
ROCKTYPE 1
ROCKCP 0.753
THCONR 5.0
THCONW 0.34
THCONO 0.2
THCONG 0.065
THCONS 3.12

THCONMIX COMPLEX
HLOSSPROP OVERBUR 0.095020147 0.0950829
UNDERBUR 0.095020147 0.0950829
ROCKTYPE 2
ROCKCP 0.753
THCONR 5.0
THCONW 0.34
THCONO 0.2
THCONG 0.065
THCONS 3.12
THCONMIX SIMPLE
THTYPE CON 1
** ================== FLUID DEFINITIONS ====================
** Model and number of components
MODEL 8 7 3 1
COMPNAME 'H2O' 'HO' 'LO' 'CO2' 'CO' 'N2' 'O2' 'COKE'
CMM
0.018 0.878 0.1719 0.04401 0.02801 0.028013 0.031999 0.013
PCRIT
22048 1031.29 2305.95 7376 3496 3394 5046
TCRIT
374.25 780 425.16 31.05 -140.25 -146.95 -118.55
KV1
1.1860e+7 0 0
KV2
0 0 0
KV3
0 0 0
KV4
-3816.44 0 0
KV5
-227.02 0 0
KVTABLIM 100 2000 10 990
**$ Gas-liquid K Value tables
** Gas-liquid K Value tables
KVTABLE 'HO'
**
4.53768E-12  2.26884E-13
1.30069E-08  6.50346E-10
```

2.67699E-06  1.33849E-07
1.21436E-04  6.07182E-06
2.13399E-03  1.06699E-04
1.98966E-02  9.94832E-04
1.18938E-01  5.94688E-03
5.14333E-01  2.57166E-02
1.74413E+00  8.72063E-02
4.90460E+00  2.45230E-01
1.19039E+01  5.95193E-01
2.56792E+01  1.28396E+00
5.03332E+01  2.51666E+00
9.11663E+01  4.55832E+00
1.54604E+02  7.73020E+00
**$ Gas-liquid K Value tables
** Gas-liquid K Value tables
KVTABLE 'LO'
**
1.40504E-05  7.02519E-07
1.26714E-03  6.33571E-05
2.57692E-02  1.28846E-03
2.22829E-01  1.11415E-02
1.12703E+00  5.63515E-02
3.98328E+00  1.99164E-01
1.09490E+01  5.47452E-01
2.50607E+01  1.25304E+00
4.99919E+01  2.49959E+00
8.97067E+01  4.48533E+00
1.48112E+02  7.40562E+00
2.28775E+02  1.14388E+01
3.34727E+02  1.67364E+01
4.68359E+02  2.34180E+01
6.31390E+02  3.15695E+01
CPG1
38.182 -34.081 -7.913 19.795 30.869 31.15 28.106
CPG2
-0.0175 4.1375 0.9609 7.34E-02 -1.29E-02 -1.36E-02 -3.68E-06
CPG3
5e-05 -2.279e-3 -5.288e-4 5.60E-05 2.79E-05 2.68E-05 1.75E-05
CPG4
-3e-08 4.8365e-6 1.131e-7 1.72E-08 -1.27E-08 -1.17E-08 -1.07E-08
HVR
4820. 9999. 6220.
EV
0.38 0.38 0.38
SOLID_DEN 'COKE' 0.00138 0 0
SOLID_CP 'COKE' 12 0.0
MASSDEN
0.000999 0.0011075037 0.0009038
CP

5.8e-7 2.03E-07 6.91E-07
CT1
-1.9095e-3 1.08E-05 2.02E-05
CT2
7.296e-6 4.58E-07 1.58E-06
AVG
1.7e-5 7.565e-6 4.174e-6 4.098e-6 4.098e-6 4.098e-6 4.232e-6
BVG
1.116 1.102 0.943 0.702 0.702 0.702 0.702
GVISCOR
VISCTABLE
** temp
20 0.000E+00 5.8025E+06 4.3000E+02
30.256 0.000E+00 7.6980E+05 3.2900E+02
40.513 0.000E+00 3.3123E+05 2.4900E+02
50.025 0.000E+00 7.2396E+04 8.5000E+01
60.026 0.000E+00 1.9738E+04 5.2000E+01
70.025 0.000E+00 6.7097E+03 3.9000E+01
80.025 0.000E+00 2.8739E+03 2.9900E+01
90.025 0.000E+00 1.5462E+03 2.1000E+01
100.025 0.000E+00 7.9864E+02 1.2700E+01
110.025 0.000E+00 3.8726E+02 8.4600E+00
120.025 0.000E+00 2.0609E+02 6.8800E+00
130.025 0.000E+00 1.1565E+02 5.9300E+00
140.025 0.000E+00 7.0158E+01 5.3000E+00
150.025 0.000E+00 5.0774E+01 4.7000E+00
160.025 0.000E+00 2.1336E+01 3.6300E+00
180.025 0.000E+00 1.3269E+01 3.1300E+00
200.025 0.000E+00 6.5473E+00 2.1500E+00
220.025 0.000E+00 4.1458E+00 1.9600E+00
240.025 0.000E+00 3.1049E+00 1.6800E+00
265 0.000E+00 2.3659E+00 1.4135E+00
280 0.000E+00 2.0213E+00 1.0689E+00
295 0.000E+00 1.7544E+00 8.2704E-01
310 0.000E+00 1.4931E+00 6.9224E-01
325 0.000E+00 1.2761E+00 5.9821E-01
340 0.000E+00 1.1178E+00 5.1269E-01
355 0.000E+00 9.5799E-01 4.7073E-01
370 0.000E+00 8.4324E-01 4.2410E-01
385 0.000E+00 7.5386E-01 3.8119E-01
400 0.000E+00 6.8147E-01 3.4360E-01
415 0.000E+00 6.2907E-01 3.0464E-01
430 0.000E+00 5.8398E-01 2.7235E-01
445 0.000E+00 5.4485E-01 2.4535E-01
460 0.000E+00 5.1071E-01 2.2254E-01
475 0.000E+00 4.8072E-01 2.0311E-01
490 0.000E+00 4.5422E-01 1.8645E-01
505 0.000E+00 4.3067E-01 1.7206E-01
520 0.000E+00 4.0967E-01 1.5955E-01

535  0.000E+00  3.9082E-01  1.4861E-01
900  0.000E+00  1.9226E-01  6.5111E-02
PRSR 101.325
TEMR 25.0
** Reaction specification
STOREAC
0 1 0 0 0 0 0 0
STOPROD
0 0 1 0 0 0 0 54.3153846154
FREQFAC 1.50E9
EACT 0.99e5
RENTH 0.0
** Reaction specification
STOREAC
0 1 0 0 0 0 80.0325 0
STOPROD
26.72 0 0 0 105.605 0 0 0
FREQFAC 1.812e11
RENTH 5.913e5
EACT 1.38e5
** Reaction specification
STOREAC
0 0 1 0 0 0 18.59 0
STOPROD
14.5 0 0 0 18.0565 0 0 0
FREQFAC 1.812e12
RENTH 4.913e5
EACT 1.38e5
** Reaction specification
STOREAC
0 0 0 0 0 0 1.22 1
STOPROD
0.5 0 0 0 1.5365505 0 0 0
FREQFAC 8.6e7
RENTH 4.18032e5
** ============== Rock-FLUID PROPERTIES
EACT 0.123e5
RTEMLOWR 499.85
RTEMUPR 999.85
ROCKFLUID
RPT 1 WATWET
SWT
**$ Sw krw krow
0.1 0.0 0.9
0.25 0.004 0.6
0.44 0.024 0.28
0.56 0.072 0.144
0.672 0.168 0.048
0.752 0.256 0.0

```
SLT
**$ Sl krg krog
0.10 0.9 0.000
0.1200 0.5650 0.0100
0.2500 0.4100 0.0520
0.4720 0.2880 0.1000
0.5800 0.1560 0.2100
0.6800 0.0670 0.3400
0.7200 0.0340 0.4100
0.8320 0.0120 0.6200
0.9500 0.0060 0.8200
0.9900 0.0000 0.9000
RPT 2
SWT
**$ Sw krw krow
0.0 0.0 1.0
1.0 1.0 0.0
SLT
**$ Sl krg krog
0.0 1.0 0.000
1.0 0.0 1.0
KRTYPE CON 1
INITIAL
VERTICAL OFF

INITREGION 1
PRES CON 290
TEMP CON 27
SW CON 0.15
SO IJK 1:30 1:19 1:7 0.85
5:30 10 6 0
SG IJK 5:30 10 6 1.0
MFRAC_OIL 'LO' CON      0.5275
MFRAC_OIL 'HO' CON      0.4725
MFRAC_GAS 'O2' CON          0
MFRAC_GAS 'N2' CON          0
MFRAC_GAS 'H2O' CON          0
MFRAC_GAS 'CO2' CON          0
MFRAC_GAS 'CO' CON          0
CONC_SLD 'COKE' CON          0

NUMERICAL
NUMERICAL
NORM PRESS 2000
DTMIN 1e-12
MAXSTEPS 100000000
MATBALTOL 1e-6
NEWTONCYC 30
NORTH 150
```

```
ITERMAX 250

SOLVER PARASOL
DPLANES 12
PNTHRDS 8
PPATTERN AUTOPSLAB 4

MINPRES 100.0
MAXTEMP 1220.0
NCUTS 15
MAXPRES 10000.0



RUN
DATE 2019 1 30.0000
DTWELL 0.01
**
WELL  'Producer'
PRODUCER 'Producer'
OPERATE  MIN  BHP  170.0  CONT REPEAT
OPERATE  MAX  STL  25.0  CONT REPEAT
MONITOR  MAX  TEMP  1200.0  STOP
**        rad  geofac  wfrac  skin
GEOMETRY  i  0.2  0.2488  1.0  0.0
    PERF     GEOA  'Producer'
** UBA            ff        Status  Connection
   30 10 6      12.5  OPEN    FLOW-TO  'SURFACE'  REFLAYER
   29 10 6       1.0  OPEN    FLOW-TO  1
   28 10 6       1.0  OPEN    FLOW-TO  2
   27 10 6       1.0  OPEN    FLOW-TO  3
   26 10 6       1.0  OPEN    FLOW-TO  4
   25 10 6       1.0  OPEN    FLOW-TO  5
   24 10 6       1.0  OPEN    FLOW-TO  6
   23 10 6       1.0  OPEN    FLOW-TO  7
   22 10 6       1.0  OPEN    FLOW-TO  8
   21 10 6       1.0  OPEN    FLOW-TO  9
   20 10 6       1.0  OPEN    FLOW-TO  10
   19 10 6       1.0  OPEN    FLOW-TO  11
   18 10 6       1.0  OPEN    FLOW-TO  12
   17 10 6       1.0  OPEN    FLOW-TO  13
   16 10 6       1.0  OPEN    FLOW-TO  14
   15 10 6       1.0  OPEN    FLOW-TO  15
   14 10 6       1.0  OPEN    FLOW-TO  16
   13 10 6       1.0  OPEN    FLOW-TO  17
   12 10 6       1.0  OPEN    FLOW-TO  18
   11 10 6       1.0  OPEN    FLOW-TO  19
   10 10 6       1.0  OPEN    FLOW-TO  20
    9 10 6       1.0  OPEN    FLOW-TO  21
```

```
   8 10 6       1.0  OPEN   FLOW-TO  22
   7 10 6       1.0  OPEN   FLOW-TO  23
   6 10 6       1.0  OPEN   FLOW-TO  24
   5 10 6       1.0  OPEN   FLOW-TO  25
LAYERXYZ  'Producer'
** perf geometric data: UBA, block entry(x,y,z) block exit(x,y,z), length
   30 10 6  59.000000  19.999969  7.333335  59.000000  19.999969  8.800002
1.466667
   29 10 6  58.000000  19.999969  8.066669  56.000000  19.999969  8.066669
2.000000
   28 10 6  56.000000  19.999969  8.066669  54.000000  19.999969  8.066669
2.000000
   27 10 6  54.000000  19.999969  8.066669  52.000000  19.999969  8.066669
2.000000
   26 10 6  52.000000  19.999969  8.066669  50.000000  19.999969  8.066669
2.000000
   25 10 6  50.000000  19.999969  8.066669  48.000000  19.999969  8.066669
2.000000
   24 10 6  48.000000  19.999969  8.066669  46.000000  19.999969  8.066669
2.000000
   23 10 6  46.000000  19.999969  8.066669  44.000000  19.999969  8.066669
2.000000
   22 10 6  44.000000  19.999969  8.066669  42.000000  19.999969  8.066669
2.000000
   21 10 6  42.000000  19.999969  8.066669  40.000000  19.999969  8.066669
2.000000
   20 10 6  40.000000  19.999969  8.066669  38.000000  19.999969  8.066669
2.000000
   19 10 6  38.000000  19.999969  8.066669  36.000000  19.999969  8.066669
2.000000
   18 10 6  36.000000  19.999969  8.066669  34.000000  19.999969  8.066669
2.000000
   17 10 6  34.000000  19.999969  8.066669  32.000000  19.999969  8.066669
2.000000
   16 10 6  32.000000  19.999969  8.066669  30.000000  19.999969  8.066669
2.000000
   15 10 6  30.000000  19.999969  8.066669  28.000000  19.999969  8.066669
2.000000
   14 10 6  28.000000  19.999969  8.066669  26.000000  19.999969  8.066669
2.000000
   13 10 6  26.000000  19.999969  8.066669  24.000000  19.999969  8.066669
2.000000
   12 10 6  24.000000  19.999969  8.066669  22.000000  19.999969  8.066669
2.000000
   11 10 6  22.000000  19.999969  8.066669  20.000000  19.999969  8.066669
2.000000
   10 10 6  20.000000  19.999969  8.066669  18.000000  19.999969  8.066669
2.000000
```

```
   9 10 6   18.000000  19.999969  8.066669  16.000000  19.999969  8.066669
2.000000
   8 10 6   16.000000  19.999969  8.066669  14.000000  19.999969  8.066669
2.000000
   7 10 6   14.000000  19.999969  8.066669  12.000000  19.999969  8.066669
2.000000
   6 10 6   12.000000  19.999969  8.066669  10.000000  19.999969  8.066669
2.000000
   5 10 6   10.000000  19.999969  8.066669  9.000000  19.999969  8.066669  1.000000

HEATR IJK
2:2    2:18    1:1  2000

DATE 2019 1 30.00694
OUTSRF GRID FLUXRC PRES SG SO SOLCONC SW TEMP W X Y

DATE 2019 1 30.0138888

DATE 2019 1 30.0208333


WELL 'Injector'
INJECTOR UNWEIGHT 'Injector'
INCOMP  GAS  0.0  0.0  0.0  0.0  0.0  0.79  0.21
TINJW  25.0
OPERATE  MAX  STG  8000.0  CONT REPEAT
OPERATE  MAX  BHP  1900.0  CONT REPEAT
GEOMETRY J 0.2 0.2488 1.0 0
**$ UBA wi Status Connection
** UBA wi Status Connection
     PERF       WI  'Injector'
** UBA           wi        Status  Connection
   2 18 1      1.25  OPEN    FLOW-FROM  'SURFACE'  REFLAYER
   2 17 1      1.25  OPEN    FLOW-FROM  1
   2 16 1      1.25  OPEN    FLOW-FROM  2
   2 15 1      1.25  OPEN    FLOW-FROM  3
   2 14 1      1.25  OPEN    FLOW-FROM  4
   2 13 1      1.25  OPEN    FLOW-FROM  5
   2 12 1      1.25  OPEN    FLOW-FROM  6
   2 11 1      1.25  OPEN    FLOW-FROM  7
   2 10 1      1.25  OPEN    FLOW-FROM  8
   2 9 1       1.25  OPEN    FLOW-FROM  9
   2 8 1       1.25  OPEN    FLOW-FROM  10
   2 7 1       1.25  OPEN    FLOW-FROM  11
   2 6 1       1.25  OPEN    FLOW-FROM  12
   2 5 1       1.25  OPEN    FLOW-FROM  13
   2 4 1       1.25  OPEN    FLOW-FROM  14
   2 3 1       1.25  OPEN    FLOW-FROM  15
   2 2 1       1.25  OPEN    FLOW-FROM  16
```

```
HEATR CON 0

DATE 2019 1 30.02778

DATE 2019 1 30.03472

DATE 2019 1 30.04167

DATE 2019 1 30.04861

DATE 2019 1 30.05556

DATE 2019 1 30.06250

DATE 2019 1 30.06944

DATE 2019 1 30.07639

DATE 2019 1 30.08333

DATE 2019 1 30.09028

DATE 2019 1 30.09722

DATE 2019 1 30.10417

DATE 2019 1 30.11111

DATE 2019 1 30.11806

DATE 2019 1 30.12500

DATE 2019 1 30.13194

**
**
WELL  'Injector'
INJECTOR UNWEIGHT 'Injector'
INCOMP  GAS  0.0  0.0  0.0  0.0  0.0  0.79  0.21
TINJW  25.0
OPERATE  MAX  BHP  1900.0  CONT REPEAT
OPERATE  MAX  STG  8000.0  CONT REPEAT
**$        rad  geofac  wfrac  skin
GEOMETRY  J  0.2  0.2488  1.  0.
    PERF      WI  'Injector'
** UBA           wi        Status  Connection
   2 18 1       1.25  OPEN    FLOW-FROM  'SURFACE'  REFLAYER
   2 17 1       1.25  OPEN    FLOW-FROM  1
```

```
  2 16 1      1.25  OPEN   FLOW-FROM  2
  2 15 1      1.25  OPEN   FLOW-FROM  3
  2 14 1      1.25  OPEN   FLOW-FROM  4
  2 13 1      1.25  OPEN   FLOW-FROM  5
  2 12 1      1.25  OPEN   FLOW-FROM  6
  2 11 1      1.25  OPEN   FLOW-FROM  7
  2 10 1      1.25  OPEN   FLOW-FROM  8
  2 9 1      1.25  OPEN   FLOW-FROM  9
  2 8 1      1.25  OPEN   FLOW-FROM  10
  2 7 1      1.25  OPEN   FLOW-FROM  11
  2 6 1      1.25  OPEN   FLOW-FROM  12
  2 5 1      1.25  OPEN   FLOW-FROM  13
  2 4 1      1.25  OPEN   FLOW-FROM  14
  2 3 1      1.25  OPEN   FLOW-FROM  15
  2 2 1      1.25  OPEN   FLOW-FROM  16

DATE 2019 1 30.13889

DATE 2019 1 30.14583

DATE 2019 1 30.15278

DATE 2019 1 30.15972

DATE 2019 1 30.16667

DATE 2019 1 30.17361

DATE 2019 1 30.18056

DATE 2019 1 30.18750

DATE 2019 1 30.19444

DATE 2019 1 30.20139

DATE 2019 1 30.20833

DATE 2019 1 30.21528

DATE 2019 1 30.22222
DATE 2019 1 30.54167
STOP
```

## APPENDIX 2 – EXAMPLE INPUT FILE FOR LAB-SCALE THAI-CAPRI MODEL

```
TITLE1 'SIMULATION OF TOE-TO-HEEL AIR INJECTION'
** ====================== INPUT/OUTPUT
CONTROL=========================
INTERRUPT STOP
INUNIT LAB
OUTUNIT LAB
OUTPRN ITER NEWTON
OUTPRN GRID OBHLOSS PRES SG SO SOLCONC SW TEMP VISO VISW X Y

OUTPRN WELL ALL
WRST 400
WPRN GRID 300
WPRN ITER 300
WSRF SECTOR 1
OUTSRF GRID CCHLOSS CMPDENO CMPDENW CMPVISG CMPVISO CMPVISW FLUXRC
FLUXSC FPOROS KRG KRO
      KRW KVALYW KVALYX MASDENG MASDENO MASDENW OBHLOSS PCOG PCOW
PERMI PERMJ
      PERMK PRES SG SO MASS SOLCONC SW TEMP VISG VISO VISW VPOROS
      W X Y
OUTSRF WELL MASS COMPONENT ALL
OUTSRF WELL MOLE COMPONENT ALL
OUTSRF SPECIAL MAXVAR MASDENO
        MAXVAR VISO
        MAXVAR PRES
        MAXVAR MASS SOLCONC 'COKE'
        MAXVAR TEMP
        MINVAR MASDENO
        MINVAR VISO
        MINVAR PRES
        MINVAR MASS SOLCONC 'COKE'
        MINVAR TEMP
        AVGVAR MASDENO
        AVGVAR VISO
        AVGVAR PRES
        AVGVAR MASS SOLCONC 'COKE'
        AVGVAR TEMP
        MOLEFRAC  'Producer' 'CO2' GAS
        MOLEFRAC  'Producer' 'CO' GAS
        MOLEFRAC  'Producer' 'N2' GAS
        MOLEFRAC  'Producer' 'O2' GAS
        MOLEFRAC  'Producer' 'H2O' GAS
        MOLEFRAC  'Producer' 'MC' OIL
        MOLEFRAC  'Producer' 'HC' OIL
        MATBAL  GASEOUS 'H2O'
        MATBAL  AQUEOUS 'H2O'
        MATBAL  GASEOUS 'MC'
```

```
        MATBAL  GASEOUS 'HC'
        MATBAL  GASEOUS 'UHC'
        MATBAL  OLEIC 'MC'
        MATBAL  OLEIC 'HC'
        MATBAL  OLEIC 'UHC'
        MATBAL  CURRENT 'COKE'
        MATBAL  CURRENT 'O2'
        MATBAL  CURRENT 'CO2'
        MATBAL  CURRENT 'N2'
        MATBAL  CURRENT 'CO'
        MATBAL  CURRENT 'MC'
        MATBAL  CURRENT 'HC'
        MATBAL  CURRENT 'UHC'
        MATBAL  REACTION 'H2O'
        MATBAL  REACTION 'CO2'
        MATBAL  REACTION 'CO'
        MATBAL  REACTION 'O2'
        MATBAL  REACTION 'MC'
        MATBAL  REACTION 'HC'
        MATBAL  REACTION 'UHC'
        MATBAL  REACTION 'COKE'
        DELP  'Injector' 'Producer'
        OBHLOSSCUM
        CCHLOSSCUM
        OBHLOSSRATE
        CCHLOSSRATE
OUTSRF WELL LAYER ALL
OUTSRF WELL DOWNHOLE
REWIND 150
INTERRUPT RESTART-STOP
**  Distance units: cm
RESULTS XOFFSET         0.0000
RESULTS YOFFSET         0.0000
RESULTS ROTATION        0.0000  **  (DEGREES)
RESULTS AXES-DIRECTIONS 1.0 -1.0 1.0
** ************************************************************************
** Definition of fundamental cartesian grid
** ************************************************************************
GRID VARI 30 19 7
KDIR DOWN
DI IVAR
30*2
DJ JVAR
19*2.10526
DK ALL
3420*1.466667 570*1.2
DTOP
570*0
**  0 = null block, 1 = active block
```

```
NULL CON          1
POR CON        0.34
PERMI CON       11500
PERMJ CON       11500
PERMK CON        3450
**  0 = pinched block, 1 = active block
PINCHOUTARRAY CON          1
*end-grid
ROCKTYPE 1
ROCKCP 0.753
THCONR 5.0
THCONW 0.34
THCONO 0.2
THCONG 0.065
THCONS 3.12

THCONMIX COMPLEX
HLOSSPROP OVERBUR 0.095020147 0.0950829
UNDERBUR 0.095020147 0.0950829
ROCKTYPE 2
ROCKCP 0.753
THCONR 5.0
THCONW 0.34
THCONO 0.2
THCONG 0.065
THCONS 3.12
THCONMIX SIMPLE
THTYPE CON          1
** ================== FLUID DEFINITIONS ====================
** Model and number of components
MODEL 11 9 4 1
COMPNAME 'H2O' 'HC' 'MC' 'UHC' 'CO2' 'CO' 'N2' 'O2' 'H2' 'COKE' 'CAT'
CMM
0.018 0.878 0.1719 0.2525 0.04401 0.02801 0.028013 0.031999 0.002016 0.013
0.10473
PCRIT
22048 1031.29 2305.95 1523.46 7376 3496 3394 5046 1015.5
TCRIT
374.25 780 425.16 1048.5 31.05 -140.25 -146.95 -118.55 -239.95
KV1
1.1860e+7 0 0 0
KV2
0 0 0 0
KV3
0 0 0 0
KV4
-3816.44 0 0 0
KV5
-227.02 0 0 0
```

KVTABLIM 100 4000 10 990
**$ Gas-liquid K Value tables
** Gas-liquid K Value tables
KVTABLE 'HC'
**
4.53768E-12  2.26884E-13
1.30069E-08  6.50346E-10
2.67699E-06  1.33849E-07
1.21436E-04  6.07182E-06
2.13399E-03  1.06699E-04
1.98966E-02  9.94832E-04
1.18938E-01  5.94688E-03
5.14333E-01  2.57166E-02
1.74413E+00  8.72063E-02
4.90460E+00  2.45230E-01
1.19039E+01  5.95193E-01
2.56792E+01  1.28396E+00
5.03332E+01  2.51666E+00
9.11663E+01  4.55832E+00
1.54604E+02  7.73020E+00
**$ Gas-liquid K Value tables
** Gas-liquid K Value tables
KVTABLE 'MC'
**
1.40504E-05  7.02519E-07
1.26714E-03  6.33571E-05
2.57692E-02  1.28846E-03
2.22829E-01  1.11415E-02
1.12703E+00  5.63515E-02
3.98328E+00  1.99164E-01
1.09490E+01  5.47452E-01
2.50607E+01  1.25304E+00
4.99919E+01  2.49959E+00
8.97067E+01  4.48533E+00
1.48112E+02  7.40562E+00
2.28775E+02  1.14388E+01
3.34727E+02  1.67364E+01
4.68359E+02  2.34180E+01
6.31390E+02  3.15695E+01
** Gas-liquid K Value tables
KVTABLE 'UHC'
**
1.961E-06  1.961E-08
2.780E-04  2.780E-06
7.650E-03  7.650E-05
8.215E-02  8.215E-04
4.889E-01  4.889E-03
1.962E+00  1.962E-02
5.969E+00  5.969E-02

1.485E+01  1.485E-01
3.174E+01  3.174E-01
6.040E+01  6.040E-01
1.049E+02  1.049E+00
1.692E+02  1.692E+00
2.572E+02  2.572E+00
3.723E+02  3.723E+00
5.172E+02  5.172E+00
CPG1
38.182 -34.081 -7.913 -34.081 19.795 30.869 31.15 28.106 27.804
CPG2
0 4.1375 0.9609 4.1375 7.34E-02 -1.29E-02 -1.36E-02 -3.68E-06 0
CPG3
5e-05 -2.279e-3 -5.288e-4 -2.279e-3 5.60E-05 2.79E-05 2.68E-05 1.75E-05 0
CPG4
-3e-08 4.8365e-6 1.131e-7 4.8365e-6 1.72E-08 -1.27E-08 -1.17E-08 -1.07E-08 0
HVR
4820. 9999. 6220. 9999.
EV
0.38 0.38 0.38 0.38
SOLID_DEN 'COKE' 0.00138 0 0
SOLID_DEN 'CAT' 0.0010531 0 0
SOLID_CP 'COKE' 12 0.0
SOLID_CP 'CAT' 74.8835 0
MASSDEN
0.000999 0.0011075037 0.0008928 0.000800481
CP
5.8e-7 2.03E-07 6.91E-07 2.03E-07
CT1
-1.9095e-3 1.08E-05 2.02E-05 1.08E-05
CT2
7.296e-6 4.58E-07 1.58E-06 4.58E-07
AVG
1.7e-5 7.565e-6 4.174e-6 7.565e-6 4.098e-6 4.098e-6 4.232e-6 4.098e-6 4.098e-6
BVG
1.116 1.102 0.943 1.102 0.702 0.702 0.702 0.702 0.702
GVISCOR
VISCTABLE
**  temp
20  0.000E+00  5.8025E+06  4.3000E+02  7.6485E+02
30.256  0.000E+00  7.6980E+05  3.2900E+02  3.6388E+02
40.513  0.000E+00  3.3123E+05  2.4900E+02  6.8866E+01
50.025  0.000E+00  7.2396E+04  8.5000E+01  3.3227E+01
60.026  0.000E+00  1.9738E+04  5.2000E+01  7.9493E+00
70.025  0.000E+00  6.7097E+03  3.9000E+01  2.5532E+00
80.025  0.000E+00  2.8739E+03  2.9900E+01  1.0190E+00
90.025  0.000E+00  1.5462E+03  2.1000E+01  4.9113E-01
100.025  0.000E+00  7.9864E+02  1.2700E+01  2.7890E-01
110.025  0.000E+00  3.8726E+02  8.4600E+00  1.4874E-01

120.025 0.000E+00 2.0609E+02 6.8800E+00 7.6921E-02
130.025 0.000E+00 1.1565E+02 5.9300E+00 4.4610E-02
140.025 0.000E+00 7.0158E+01 5.3000E+00 2.7310E-02
150.025 0.000E+00 5.0774E+01 4.7000E+00 1.7921E-02
160.025 0.000E+00 2.1336E+01 3.6300E+00 6.4253E-03
180.025 0.000E+00 1.3269E+01 3.1300E+00 4.2698E-03
200.025 0.000E+00 6.5473E+00 2.1500E+00 2.2529E-03
220.025 0.000E+00 4.1458E+00 1.9600E+00 1.5360E-03
240.025 0.000E+00 3.1049E+00 1.6800E+00 1.1822E-03
265 0.000E+00 2.3659E+00 1.4135E+00 9.1913E-04
280 0.000E+00 2.0213E+00 1.0689E+00 7.6606E-04
295 0.000E+00 1.7544E+00 8.2704E-01 6.4961E-04
310 0.000E+00 1.4931E+00 6.9224E-01 5.5100E-04
325 0.000E+00 1.2761E+00 5.9821E-01 4.7196E-04
340 0.000E+00 1.1178E+00 5.1269E-01 4.1159E-04
355 0.000E+00 9.5799E-01 4.7073E-01 3.5771E-04
370 0.000E+00 8.4324E-01 4.2410E-01 3.1636E-04
385 0.000E+00 7.5386E-01 3.8119E-01 2.8313E-04
400 0.000E+00 6.8147E-01 3.4360E-01 2.5579E-04
415 0.000E+00 6.2907E-01 3.0464E-01 2.3420E-04
430 0.000E+00 5.8398E-01 2.7235E-01 2.1576E-04
445 0.000E+00 5.4485E-01 2.4535E-01 1.9988E-04
460 0.000E+00 5.1071E-01 2.2254E-01 1.7409E-04
475 0.000E+00 4.8072E-01 2.0311E-01 1.6353E-04
490 0.000E+00 4.5422E-01 1.8645E-01 1.5421E-04
505 0.000E+00 4.3067E-01 1.7206E-01 1.4593E-04
520 0.000E+00 4.0967E-01 1.5955E-01 1.3854E-04
535 0.000E+00 3.9082E-01 1.4861E-01 1.1631E-04
900 0.000E+00 1.9226E-01 6.5111E-02 5.8815E-05
PRSR 101.325
TEMR 25.0
** Reaction specification
STOREAC
0 1 0 0 0 0 0 0 0 0 0
STOPROD
0 0 1 0 0 0 0 0 0 54.3153846154 0
FREQFAC 1.50E9
EACT 0.99e5
RENTH 0.0
** Reaction specification
STOREAC
0 1 0 0 0 0 0 80.0325 0 0 0
STOPROD
26.72 0 0 0 0 105.605 0 0 0 0 0
FREQFAC 1.812e12
RENTH 5.913e5
EACT 1.38e5
** Reaction specification
STOREAC

0 0 1 0 0 0 0 18.59 0 0 0
STOPROD
14.5 0 0 0 0 18.0565 0 0 0 0 0
FREQFAC 1.812e11
RENTH 4.913e5
EACT 1.38e5
** Reaction specification
STOREAC
0 0 0 0 0 0 0 1.22 0 1 0
STOPROD
0.5 0 0 0 0 1.5365505 0 0 0 0 0
FREQFAC 8.6e7
RENTH 4.18032e5
** ========== Rock-FLUID PROPERTIES
EACT 0.123e5
RTEMLOWR 499.85
RTEMUPR 999.85
** Reaction specification
STOREAC
1.00089 0 0 0 0 1 0 0 0 0 0
STOPROD
0 0 0 0 1 0 0 0 1 0 0
FREQFAC 5e9
RENTH 41.3e3
EACT 1.49e5
** Reaction specification
STOREAC
1 0 0 0 0 0 0 0 0 0.92508 0
STOPROD
0 0 0 0 0 1 0 0 1 0 0
FREQFAC 2.117e15
RENTH 0.00
EACT 9.2e3
** Reaction specification
STOREAC
0 0 0 0 1 0 0 0 0 0.92385 0
STOPROD
0 0 0 0 0 2 0 0 0 0 0
FREQFAC 2.592e8
RENTH 0.00
EACT 5.3e3
** Reaction specification
STOREAC
0 1 0 0 0 0 0 0 10 0 1
STOPROD
0 0 0 3.55706930693 0 0 0 0 0 0 1
RORDER
0 1.5 0 0 0 0 0 0 1.1 0 1
FREQFAC 8.5e18

```
RENTH 0.0
EACT 9.9e4
** Reaction specification
STOREAC
0 0 0 0 1 0 0 0 1 0 0
STOPROD
1.00089 0 0 0 0 1 0 0 0 0 0
FREQFAC 5e7
EACT 1.9e5
RENTH -41.3e3
ROCKFLUID
RPT 1 WATWET
SWT
**$ Sw krw krow
0.1 0.0 0.9
0.25 0.004 0.6
0.44 0.024 0.28
0.56 0.072 0.144
0.672 0.168 0.048
0.752 0.256 0.0
SLT
**$ Sl krg krog
0.10 0.9 0.000
0.1200 0.5650 0.0100
0.2500 0.4100 0.0520
0.4720 0.2880 0.1000
0.5800 0.1560 0.2100
0.6800 0.0670 0.3400
0.7200 0.0340 0.4100
0.8320 0.0120 0.6200
0.9500 0.0060 0.8200
0.9900 0.0000 0.9000
RPT 2
SWT
**$ Sw krw krow
0.0 0.0 1.0
1.0 1.0 0.0
SLT
**$ Sl krg krog
0.0 1.0 0.000
1.0 0.0 1.0
KRTYPE CON          1
INITIAL
VERTICAL OFF

INITREGION 1
PRES CON        290
TEMP CON         27
SW CON       0.15
```

```
SO IJK 1:30 1:19 1:7 0.85
5:30 10 6 0.01
SG IJK 5:30 10 6 0.99
MFRAC_OIL 'MC' CON       0.545
MFRAC_OIL 'HC' CON       0.455
MFRAC_GAS 'O2' CON          0
MFRAC_GAS 'N2' CON          0
MFRAC_GAS 'H2O' CON          0
MFRAC_GAS 'CO2' CON          0
MFRAC_GAS 'CO' CON          0
CONC_SLD 'CAT' CON          0
*MOD
4:30 10 6 = 0.05
NUMERICAL
NORM PRESS 4000
MFRAC_GAS 'CO2' CON          0
CONVERGE TOTRES LOOSE
NUMERICAL
DTMIN 1e-12
MAXSTEPS 100000000
MATBALTOL 1e-6
NEWTONCYC 30
NORTH 150
ITERMAX 250
SOLVER PARASOL
DPLANES 12
PNTHRDS 8
PPATTERN AUTOPSLAB 4
MINPRES 100.0
MAXTEMP 1220.0
NCUTS 15
MAXPRES 10000.0



RUN
DATE 2019 1 30.0000
DTWELL 0.01
**
WELL  'Producer'
PRODUCER 'Producer'
OPERATE  MIN  BHP  1000.0  CONT REPEAT
OPERATE  MAX  STL  25.0  CONT REPEAT
MONITOR  MAX  TEMP  1200.0  STOP
**        rad  geofac  wfrac  skin
GEOMETRY  i  0.2  0.2488  1.0  0.0
    PERF     GEOA  'Producer'
** UBA            ff        Status  Connection
   30 10 6       12.5  OPEN    FLOW-TO  'SURFACE'  REFLAYER
```

```
  29 10 6      1.0  OPEN   FLOW-TO  1
  28 10 6      1.0  OPEN   FLOW-TO  2
  27 10 6      1.0  OPEN   FLOW-TO  3
  26 10 6      1.0  OPEN   FLOW-TO  4
  25 10 6      1.0  OPEN   FLOW-TO  5
  24 10 6      1.0  OPEN   FLOW-TO  6
  23 10 6      1.0  OPEN   FLOW-TO  7
  22 10 6      1.0  OPEN   FLOW-TO  8
  21 10 6      1.0  OPEN   FLOW-TO  9
  20 10 6      1.0  OPEN   FLOW-TO  10
  19 10 6      1.0  OPEN   FLOW-TO  11
  18 10 6      1.0  OPEN   FLOW-TO  12
  17 10 6      1.0  OPEN   FLOW-TO  13
  16 10 6      1.0  OPEN   FLOW-TO  14
  15 10 6      1.0  OPEN   FLOW-TO  15
  14 10 6      1.0  OPEN   FLOW-TO  16
  13 10 6      1.0  OPEN   FLOW-TO  17
  12 10 6      1.0  OPEN   FLOW-TO  18
  11 10 6      1.0  OPEN   FLOW-TO  19
  10 10 6      1.0  OPEN   FLOW-TO  20
   9 10 6      1.0  OPEN   FLOW-TO  21
   8 10 6      1.0  OPEN   FLOW-TO  22
   7 10 6      1.0  OPEN   FLOW-TO  23
   6 10 6      1.0  OPEN   FLOW-TO  24
   5 10 6      1.0  OPEN   FLOW-TO  25
LAYERXYZ  'Producer'
** perf geometric data: UBA, block entry(x,y,z) block exit(x,y,z), length
  30 10 6  59.000000  19.999969  7.333335  59.000000  19.999969  8.800002
1.466667
  29 10 6  58.000000  19.999969  8.066669  56.000000  19.999969  8.066669
2.000000
  28 10 6  56.000000  19.999969  8.066669  54.000000  19.999969  8.066669
2.000000
  27 10 6  54.000000  19.999969  8.066669  52.000000  19.999969  8.066669
2.000000
  26 10 6  52.000000  19.999969  8.066669  50.000000  19.999969  8.066669
2.000000
  25 10 6  50.000000  19.999969  8.066669  48.000000  19.999969  8.066669
2.000000
  24 10 6  48.000000  19.999969  8.066669  46.000000  19.999969  8.066669
2.000000
  23 10 6  46.000000  19.999969  8.066669  44.000000  19.999969  8.066669
2.000000
  22 10 6  44.000000  19.999969  8.066669  42.000000  19.999969  8.066669
2.000000
  21 10 6  42.000000  19.999969  8.066669  40.000000  19.999969  8.066669
2.000000
  20 10 6  40.000000  19.999969  8.066669  38.000000  19.999969  8.066669
2.000000
```

```
   19 10 6  38.000000  19.999969  8.066669  36.000000  19.999969  8.066669
2.000000
   18 10 6  36.000000  19.999969  8.066669  34.000000  19.999969  8.066669
2.000000
   17 10 6  34.000000  19.999969  8.066669  32.000000  19.999969  8.066669
2.000000
   16 10 6  32.000000  19.999969  8.066669  30.000000  19.999969  8.066669
2.000000
   15 10 6  30.000000  19.999969  8.066669  28.000000  19.999969  8.066669
2.000000
   14 10 6  28.000000  19.999969  8.066669  26.000000  19.999969  8.066669
2.000000
   13 10 6  26.000000  19.999969  8.066669  24.000000  19.999969  8.066669
2.000000
   12 10 6  24.000000  19.999969  8.066669  22.000000  19.999969  8.066669
2.000000
   11 10 6  22.000000  19.999969  8.066669  20.000000  19.999969  8.066669
2.000000
   10 10 6  20.000000  19.999969  8.066669  18.000000  19.999969  8.066669
2.000000
    9 10 6   18.000000  19.999969  8.066669  16.000000  19.999969  8.066669
2.000000
    8 10 6   16.000000  19.999969  8.066669  14.000000  19.999969  8.066669
2.000000
    7 10 6   14.000000  19.999969  8.066669  12.000000  19.999969  8.066669
2.000000
    6 10 6   12.000000  19.999969  8.066669  10.000000  19.999969  8.066669
2.000000
    5 10 6   10.000000  19.999969  8.066669  9.000000  19.999969  8.066669  1.000000

WELL 'Injector'
INJECTOR UNWEIGHT 'Injector'
INCOMP  GAS  1.0  0.0  0.0  0.0  0.0  0.0  0.0  0.0  0.0
TINJW  273.0
QUAL  0.8
PINJW  700.0
OPERATE  MAX  STG  400.0  CONT REPEAT
GEOMETRY J 0.2 0.2488 1.0 0
**$ UBA wi Status Connection
** UBA wi Status Connection
     PERF       WI  'Injector'
** UBA           wi        Status  Connection
    2 18 1       1.25  OPEN    FLOW-FROM  'SURFACE'  REFLAYER
    2 17 1       1.25  OPEN    FLOW-FROM  1
    2 16 1       1.25  OPEN    FLOW-FROM  2
    2 15 1       1.25  OPEN    FLOW-FROM  3
    2 14 1       1.25  OPEN    FLOW-FROM  4
    2 13 1       1.25  OPEN    FLOW-FROM  5
    2 12 1       1.25  OPEN    FLOW-FROM  6
```

```
   2 11 1      1.25  OPEN    FLOW-FROM  7
   2 10 1      1.25  OPEN    FLOW-FROM  8
   2 9 1       1.25  OPEN    FLOW-FROM  9
   2 8 1       1.25  OPEN    FLOW-FROM  10
   2 7 1       1.25  OPEN    FLOW-FROM  11
   2 6 1       1.25  OPEN    FLOW-FROM  12
   2 5 1       1.25  OPEN    FLOW-FROM  13
   2 4 1       1.25  OPEN    FLOW-FROM  14
   2 3 1       1.25  OPEN    FLOW-FROM  15
   2 2 1       1.25  OPEN    FLOW-FROM  16

HEATR IJK
2:2 2:18 1:1 2115

DATE 2019 1 30.00694
OUTSRF GRID FLUXRC PRES SG SO SOLCONC SW TEMP W X Y
TIME 20
OUTSRF GRID REMOVE
TIME 30
OUTSRF GRID REMOVE

WELL 'Injector'
INJECTOR UNWEIGHT 'Injector'
INCOMP  GAS  1.00010476e-06  0.0  0.0  0.0  0.0  0.0  0.787878  0.212121  0.0
TINJW  273.0
QUAL  0.8
PINJW  700.0
OPERATE  MAX  STG  12200.0  CONT REPEAT
OPERATE  MAX  BHP  1900.0  CONT REPEAT
GEOMETRY J 0.2 0.2488 1.0 0
**$ UBA wi Status Connection
** UBA wi Status Connection
     PERF      WI  'Injector'
** UBA           wi        Status  Connection
   2 18 1      1.25  OPEN    FLOW-FROM  'SURFACE'  REFLAYER
   2 17 1      1.25  OPEN    FLOW-FROM  1
   2 16 1      1.25  OPEN    FLOW-FROM  2
   2 15 1      1.25  OPEN    FLOW-FROM  3
   2 14 1      1.25  OPEN    FLOW-FROM  4
   2 13 1      1.25  OPEN    FLOW-FROM  5
   2 12 1      1.25  OPEN    FLOW-FROM  6
   2 11 1      1.25  OPEN    FLOW-FROM  7
   2 10 1      1.25  OPEN    FLOW-FROM  8
   2 9 1       1.25  OPEN    FLOW-FROM  9
   2 8 1       1.25  OPEN    FLOW-FROM  10
   2 7 1       1.25  OPEN    FLOW-FROM  11
   2 6 1       1.25  OPEN    FLOW-FROM  12
   2 5 1       1.25  OPEN    FLOW-FROM  13
   2 4 1       1.25  OPEN    FLOW-FROM  14
```

```
   2 3 1       1.25  OPEN    FLOW-FROM  15
   2 2 1       1.25  OPEN    FLOW-FROM  16

HEATR CON 0

DATE 2019 1 30.02778

DATE 2019 1 30.03472

DATE 2019 1 30.04167

DATE 2019 1 30.04861

DATE 2019 1 30.05556

DATE 2019 1 30.06250

DATE 2019 1 30.06944

WELL 'Injector'
INJECTOR UNWEIGHT 'Injector'
INCOMP  GAS  0.34  0.0  0.0  0.0  0.0  0.0  0.52  0.14  0.0
TINJW  273.0
QUAL  0.8
PINJW  700.0
OPERATE  MAX  STG  12200.0  CONT REPEAT
OPERATE  MAX  BHP  1900.0  CONT REPEAT
GEOMETRY J 0.2 0.2488 1.0 0
**$ UBA wi Status Connection
** UBA wi Status Connection
     PERF       WI  'Injector'
** UBA           wi        Status  Connection
   2 18 1      1.25  OPEN    FLOW-FROM  'SURFACE'  REFLAYER
   2 17 1      1.25  OPEN    FLOW-FROM  1
   2 16 1      1.25  OPEN    FLOW-FROM  2
   2 15 1      1.25  OPEN    FLOW-FROM  3
   2 14 1      1.25  OPEN    FLOW-FROM  4
   2 13 1      1.25  OPEN    FLOW-FROM  5
   2 12 1      1.25  OPEN    FLOW-FROM  6
   2 11 1      1.25  OPEN    FLOW-FROM  7
   2 10 1      1.25  OPEN    FLOW-FROM  8
   2 9 1       1.25  OPEN    FLOW-FROM  9
   2 8 1       1.25  OPEN    FLOW-FROM  10
   2 7 1       1.25  OPEN    FLOW-FROM  11
   2 6 1       1.25  OPEN    FLOW-FROM  12
   2 5 1       1.25  OPEN    FLOW-FROM  13
   2 4 1       1.25  OPEN    FLOW-FROM  14
   2 3 1       1.25  OPEN    FLOW-FROM  15
   2 2 1       1.25  OPEN    FLOW-FROM  16
```

```
DATE 2019 1 30.07639

DATE 2019 1 30.08333

DATE 2019 1 30.09028

DATE 2019 1 30.09722

DATE 2019 1 30.10417

DATE 2019 1 30.11111

DATE 2019 1 30.11806

DATE 2019 1 30.12500

DATE 2019 1 30.13194

**
**


DATE 2019 1 30.13889

DATE 2019 1 30.14583

DATE 2019 1 30.15278

DATE 2019 1 30.15972

WELL 'Injector'
INJECTOR UNWEIGHT 'Injector'
INCOMP GAS 0.141630912 0.0 0.0 0.0 0.0 0.0 0.676290796 0.182078291 0.0
TINJW 273.0
QUAL 0.8
PINJW 700.0
OPERATE MAX BHP 1900.0 CONT REPEAT
OPERATE MAX STG 9300.0 CONT REPEAT
**$       rad geofac wfrac skin
GEOMETRY J 0.2 0.2488 1. 0.
   PERF      WI 'Injector'
** UBA          wi       Status Connection
  2 18 1      1.25 OPEN   FLOW-FROM 'SURFACE' REFLAYER
  2 17 1      1.25 OPEN   FLOW-FROM 1
  2 16 1      1.25 OPEN   FLOW-FROM 2
  2 15 1      1.25 OPEN   FLOW-FROM 3
  2 14 1      1.25 OPEN   FLOW-FROM 4
  2 13 1      1.25 OPEN   FLOW-FROM 5
```

```
   2 12 1      1.25  OPEN   FLOW-FROM  6
   2 11 1      1.25  OPEN   FLOW-FROM  7
   2 10 1      1.25  OPEN   FLOW-FROM  8
   2 9 1       1.25  OPEN   FLOW-FROM  9
   2 8 1       1.25  OPEN   FLOW-FROM  10
   2 7 1       1.25  OPEN   FLOW-FROM  11
   2 6 1       1.25  OPEN   FLOW-FROM  12
   2 5 1       1.25  OPEN   FLOW-FROM  13
   2 4 1       1.25  OPEN   FLOW-FROM  14
   2 3 1       1.25  OPEN   FLOW-FROM  15
   2 2 1       1.25  OPEN   FLOW-FROM  16

DATE 2019 1 30.17361

DATE 2019 1 30.18056

DATE 2019 1 30.18750

DATE 2019 1 30.19444

DATE 2019 1 30.20139
DATE 2019 1 30.20833

WELL  'Injector'
INJECTOR UNWEIGHT 'Injector'
INCOMP  GAS  1.00010476e-06  0.0  0.0  0.0  0.0  0.0  0.787878  0.212121  0.0
TINJW  273.0
QUAL  0.8
PINJW  700.0
OPERATE  MAX  BHP  1900.0  CONT REPEAT
OPERATE  MAX  STG  8000.0  CONT REPEAT
**$        rad  geofac  wfrac  skin
GEOMETRY  J  0.2  0.2488  1.  0.
    PERF      WI  'Injector'
** UBA           wi        Status  Connection
   2 18 1      1.25  OPEN   FLOW-FROM  'SURFACE'  REFLAYER
   2 17 1      1.25  OPEN   FLOW-FROM  1
   2 16 1      1.25  OPEN   FLOW-FROM  2
   2 15 1      1.25  OPEN   FLOW-FROM  3
   2 14 1      1.25  OPEN   FLOW-FROM  4
   2 13 1      1.25  OPEN   FLOW-FROM  5
   2 12 1      1.25  OPEN   FLOW-FROM  6
   2 11 1      1.25  OPEN   FLOW-FROM  7
   2 10 1      1.25  OPEN   FLOW-FROM  8
   2 9 1       1.25  OPEN   FLOW-FROM  9
   2 8 1       1.25  OPEN   FLOW-FROM  10
   2 7 1       1.25  OPEN   FLOW-FROM  11
   2 6 1       1.25  OPEN   FLOW-FROM  12
   2 5 1       1.25  OPEN   FLOW-FROM  13
```

```
  2 4 1      1.25  OPEN   FLOW-FROM  14
  2 3 1      1.25  OPEN   FLOW-FROM  15
  2 2 1      1.25  OPEN   FLOW-FROM  16

DATE 2019 1 30.21528

DATE 2019 1 30.22222
DATE 2019 1 30.27778

WELL  'Injector'
INJECTOR UNWEIGHT 'Injector'
INCOMP  GAS  0.500062891  0.0  0.0  0.0  0.0  0.0  0.394950316  0.104986793  0.0
TINJW  273.0
QUAL  0.8
PINJW  700.0
OPERATE  MAX  BHP  1900.0  CONT REPEAT
OPERATE  MAX  STG  16000.0  CONT REPEAT
**$        rad  geofac  wfrac  skin
GEOMETRY  J  0.2  0.2488  1.  0.
    PERF      WI  'Injector'
** UBA           wi        Status  Connection
  2 18 1      1.25  OPEN   FLOW-FROM  'SURFACE'  REFLAYER
  2 17 1      1.25  OPEN   FLOW-FROM  1
  2 16 1      1.25  OPEN   FLOW-FROM  2
  2 15 1      1.25  OPEN   FLOW-FROM  3
  2 14 1      1.25  OPEN   FLOW-FROM  4
  2 13 1      1.25  OPEN   FLOW-FROM  5
  2 12 1      1.25  OPEN   FLOW-FROM  6
  2 11 1      1.25  OPEN   FLOW-FROM  7
  2 10 1      1.25  OPEN   FLOW-FROM  8
  2 9 1      1.25  OPEN   FLOW-FROM  9
  2 8 1      1.25  OPEN   FLOW-FROM  10
  2 7 1      1.25  OPEN   FLOW-FROM  11
  2 6 1      1.25  OPEN   FLOW-FROM  12
  2 5 1      1.25  OPEN   FLOW-FROM  13
  2 4 1      1.25  OPEN   FLOW-FROM  14
  2 3 1      1.25  OPEN   FLOW-FROM  15
  2 2 1      1.25  OPEN   FLOW-FROM  16

DATE 2019 1 30.33333
STOP
```

## APPENDIX 3 – EXAMPLE INPUT FILE FOR FIELD-SCALE THAI MODEL

```
TITLE1 'SIMULATION OF TOE-TO-HEEL AIR INJECTION'
** ====================== INPUT/OUTPUT CONTROL
========================
INTERRUPT STOP
INUNIT LAB
OUTUNIT LAB
OUTPRN ITER NEWTON
OUTPRN GRID OBHLOSS PRES SG SO SOLCONC SW TEMP VISO VISW X Y

OUTPRN WELL ALL
WRST 400
WPRN GRID 300
WPRN ITER 300
OUTSRF GRID CCHLOSS CMPDENO CMPDENW CMPVISG CMPVISO CMPVISW FLUXRC
FLUXSC FPOROS KRG KRO
      KRW KVALYW KVALYX MASDENG MASDENO MASDENW OBHLOSS PCOG PCOW
PERMI PERMJ
      PERMK PRES SG SO MASS SOLCONC SW TEMP VISG VISO VISW VPOROS
      W X Y
OUTSRF WELL MASS COMPONENT ALL
OUTSRF WELL MOLE COMPONENT ALL
OUTSRF SPECIAL MAXVAR MASDENO
        MAXVAR VISO
        MAXVAR PRES
        MAXVAR MASS SOLCONC 'COKE'
        MAXVAR TEMP
        MINVAR MASDENO
        MINVAR VISO
        MINVAR PRES
        MINVAR MASS SOLCONC 'COKE'
        MINVAR TEMP
        AVGVAR MASDENO
        AVGVAR VISO
        AVGVAR PRES
        AVGVAR MASS SOLCONC 'COKE'
        AVGVAR TEMP
        MOLEFRAC  'Producer' 'CO2' GAS
        MOLEFRAC  'Producer' 'CO' GAS
        MOLEFRAC  'Producer' 'N2' GAS
        MOLEFRAC  'Producer' 'H2O' GAS
        MOLEFRAC  'Producer' 'LO' OIL
        MOLEFRAC  'Producer' 'HO' OIL
        MATBAL  GASEOUS 'H2O'
        MATBAL  AQUEOUS 'H2O'
        MATBAL  GASEOUS 'LO'
        MATBAL  GASEOUS 'HO'
        MATBAL  OLEIC 'LO'
```

```
        MATBAL  OLEIC 'HO'
        MATBAL  CURRENT 'COKE'
        MATBAL  CURRENT 'CO2'
        MATBAL  CURRENT 'N2'
        MATBAL  CURRENT 'CO'
        MATBAL  CURRENT 'LO'
        MATBAL  CURRENT 'HO'
        MATBAL  REACTION 'H2O'
        MATBAL  REACTION 'CO2'
        MATBAL  REACTION 'CO'
        MATBAL  REACTION 'LO'
        MATBAL  REACTION 'HO'
        MATBAL  REACTION 'COKE'
        DELP  'Injector 1' 'Producer'
        DELP  'Injector 3' 'Producer'
**OBHLOSSCUM
**CCHLOSSCUM
**OBHLOSSRATE
**CCHLOSSRATE
OUTSRF WELL LAYER ALL
OUTSRF WELL DOWNHOLE
REWIND 150
INTERRUPT RESTART-STOP
**  Distance units: cm
RESULTS XOFFSET         0.0000
RESULTS YOFFSET         0.0000
RESULTS ROTATION         0.0000  **  (DEGREES)
RESULTS AXES-DIRECTIONS 1.0 -1.0 1.0
** ************************************************************************
** Definition of fundamental cartesian grid
** ************************************************************************
GRID VARI 45 19 7
KDIR DOWN
DI IVAR
45*490
DJ JVAR
19*511.5789
DK ALL
5985*356.4
DTOP
855*0
**  0 = null block, 1 = active block
NULL CON          1
POR CON        0.32
PERMI CON        4948
PERMJ CON        4948
PERMK CON        3793
**  0 = pinched block, 1 = active block
PINCHOUTARRAY CON          1
```

```
*end-grid

ROCKTYPE 1
ROCKCP 0.753
THCONR 5.0
THCONW 0.34
THCONO 0.2
THCONG 0.065
THCONS 3.12
THCONMIX COMPLEX
HLOSSPROP OVERBUR 0.095020147 0.0950829
UNDERBUR 0.095020147 0.0950829


ROCKTYPE 2
ROCKCP 0.753
THCONR 5.0
THCONW 0.34
THCONO 0.2
THCONG 0.065
THCONS 3.12
THCONMIX SIMPLE
THTYPE CON          1
** ================== FLUID DEFINITIONS ====================
** Model and number of components
MODEL 9 8 3 1
COMPNAME 'H2O' 'HO' 'LO' 'CO2' 'CO' 'N2' 'H2' 'O2' 'COKE'
CMM
0.018 0.878 0.1719 0.04401 0.02801 0.028013 0.002016 0.031999 0.013
PCRIT
22048 1031.29 2305.95 7376 3496 3394 1315.200000 5046
TCRIT
374.25 780 425.16 31.05 -140.25 -146.95 -239.95 -118.55
KV1
1.1860e+7 0 0
KV2
0 0 0
KV3
0 0 0
KV4
-3816.44 0 0
KV5
-227.02 0 0
KVTABLIM 100 10000 10 990
**$ Gas-liquid K Value tables
**$
**$ Gas-liquid K Value tables
** Gas-liquid K Value tables
**
```

KVTABLE 'HO'
4.53768E-12  2.26884E-13
1.30069E-08  6.50346E-10
2.67699E-06  1.33849E-07
1.21436E-04  6.07182E-06
2.13399E-03  1.06699E-04
1.98966E-02  9.94832E-04
1.18938E-01  5.94688E-03
5.14333E-01  2.57166E-02
1.74413E+00  8.72063E-02
4.90460E+00  2.45230E-01
1.19039E+01  5.95193E-01
2.56792E+01  1.28396E+00
5.03332E+01  2.51666E+00
9.11663E+01  4.55832E+00
1.54604E+02  7.73020E+00
**$ Gas-liquid K Value tables
**$
**$ Gas-liquid K Value tables
** Gas-liquid K Value tables
**
KVTABLE 'LO'
1.40504E-05  7.02519E-07
1.26714E-03  6.33571E-05
2.57692E-02  1.28846E-03
2.22829E-01  1.11415E-02
1.12703E+00  5.63515E-02
3.98328E+00  1.99164E-01
1.09490E+01  5.47452E-01
2.50607E+01  1.25304E+00
4.99919E+01  2.49959E+00
8.97067E+01  4.48533E+00
1.48112E+02  7.40562E+00
2.28775E+02  1.14388E+01
3.34727E+02  1.67364E+01
4.68359E+02  2.34180E+01
6.31390E+02  3.15695E+01
CPG1
38.182 -34.081 -7.913 19.795 30.869 31.15 2.699E+01 28.106
CPG2
-0.0175 4.1375 0.9609 7.34E-02 -1.29E-02 -1.36E-02 1.193E-02 -3.68E-06
CPG3
5e-05 -2.279e-3 -5.288e-4 5.60E-05 2.79E-05 2.68E-05 -2.406E-05 1.75E-05
CPG4
-3e-08 4.8365e-6 1.131e-7 1.72E-08 -1.27E-08 -1.17E-08 2.145E-08 -1.07E-08
HVR
4820. 9999. 6220.
EV
0.38 0.38 0.38

SOLID_DEN 'COKE' 0.00138 0 0
SOLID_CP 'COKE' 12 0.0
MASSDEN
0.000999 0.0011075037 0.0009038
CP
5.8e-7 2.03E-07 6.91E-07
CT1
-1.9095e-3 1.08E-05 2.02E-05
CT2
7.296e-6 4.58E-07 1.58E-06
AVG
1.7e-5 7.565e-6 4.174e-6 4.098e-6 4.098e-6 4.098e-6 2.321E-04 4.232e-6
BVG
1.116 1.102 0.943 0.702 0.702 0.702 6.192E-01 0.702
GVISCOR
VISCTABLE
** temp
20 0.000E+00 5.8025E+06 4.3000E+02
30.256 0.000E+00 7.6980E+05 3.2900E+02
40.513 0.000E+00 3.3123E+05 2.4900E+02
50.025 0.000E+00 7.2396E+04 8.5000E+01
60.026 0.000E+00 1.9738E+04 5.2000E+01
70.025 0.000E+00 6.7097E+03 3.9000E+01
80.025 0.000E+00 2.8739E+03 2.9900E+01
90.025 0.000E+00 1.5462E+03 2.1000E+01
100.025 0.000E+00 7.9864E+02 1.2700E+01
110.025 0.000E+00 3.8726E+02 8.4600E+00
120.025 0.000E+00 2.0609E+02 6.8800E+00
130.025 0.000E+00 1.1565E+02 5.9300E+00
140.025 0.000E+00 7.0158E+01 5.3000E+00
150.025 0.000E+00 5.0774E+01 4.7000E+00
160.025 0.000E+00 2.1336E+01 3.6300E+00
180.025 0.000E+00 1.3269E+01 3.1300E+00
200.025 0.000E+00 6.5473E+00 2.1500E+00
220.025 0.000E+00 4.1458E+00 1.9600E+00
240.025 0.000E+00 3.1049E+00 1.6800E+00
265 0.000E+00 2.3659E+00 1.4135E+00
280 0.000E+00 2.0213E+00 1.0689E+00
295 0.000E+00 1.7544E+00 8.2704E-01
310 0.000E+00 1.4931E+00 6.9224E-01
325 0.000E+00 1.2761E+00 5.9821E-01
340 0.000E+00 1.1178E+00 5.1269E-01
355 0.000E+00 9.5799E-01 4.7073E-01
370 0.000E+00 8.4324E-01 4.2410E-01
385 0.000E+00 7.5386E-01 3.8119E-01
400 0.000E+00 6.8147E-01 3.4360E-01
415 0.000E+00 6.2907E-01 3.0464E-01
430 0.000E+00 5.8398E-01 2.7235E-01
445 0.000E+00 5.4485E-01 2.4535E-01

460  0.000E+00  5.1071E-01  2.2254E-01
475  0.000E+00  4.8072E-01  2.0311E-01
490  0.000E+00  4.5422E-01  1.8645E-01
505  0.000E+00  4.3067E-01  1.7206E-01
520  0.000E+00  4.0967E-01  1.5955E-01
535  0.000E+00  3.9082E-01  1.4861E-01
900  0.000E+00  1.9226E-01  6.5111E-02
PRSR 101.325
TEMR 15
** Reaction specification
STOREAC
0 1 0 0 0 0 0 0 0
STOPROD
0 0 1 0 0 0 0 0 54.3153846154
FREQFAC 2e9
EACT 1.15e5
RENTH 0.0
RTEMUPR 700
** Reaction specification
STOREAC
0 1 0 0 0 0 0 80.0325 0
STOPROD
48.03122827 0 0 51.89555891 10.37037883 0 0 0 0
FREQFAC 3.069e7
RENTH 4.00e7
EACT 1.38e5
** Reaction specification
STOREAC
0 0 1 0 0 0 0 18.59 0
STOPROD
10.70919483 0 0 11.57079823 2.312212521 0 0 0 0
FREQFAC 3.069e6
RENTH 1.600e7
EACT 1.38e5
** Reaction specification
STOREAC
0 0 0 0 0 0 0 1.22 1
STOPROD
0.72681466 0 0 0.785290204 0.156925893 0 0 0 0
FREQFAC 5e3
RENTH 3.90e5
** ============== Rock-FLUID PROPERTIES
EACT 1.23e5
RTEMLOWR 450
RTEMUPR 505

** ============== Rock-FLUID PROPERTIES
==============================
**ROCKFLUID**
RPT 1 WATWET
** Sw krw krow
SWT
SMOOTHEND QUAD
0.100000 0.00000 0.993821
0.120000 5.333333E-04 0.952838
0.140000 1.066667E-03 0.911856
0.160000 1.600000E-03 0.870874
0.180000 2.133333E-03 0.829892
0.200000 2.666667E-03 0.788909
0.220000 3.200000E-03 0.747927
0.240000 3.733333E-03 0.706945
0.260000 5.376560E-03 0.669804
0.280000 8.129680E-03 0.636506
0.300000 1.088280E-02 0.603208
0.320000 1.363592E-02 0.569910
0.340000 1.638904E-02 0.536612
0.360000 1.914216E-02 0.503314
0.380000 2.189528E-02 0.470016
0.400000 2.464840E-02 0.436718
0.420000 2.740152E-02 0.403420
0.440000 3.015464E-02 0.370121
0.460000 3.923969E-02 0.340238
0.480000 4.832474E-02 0.310356
0.500000 5.740979E-02 0.280473
0.520000 6.649485E-02 0.250590
0.540000 7.557990E-02 0.220707
0.560000 8.466495E-02 0.190824
0.580000 0.103304 0.170927
0.600000 0.121944 0.151031
0.620000 0.140584 0.131134
0.640000 0.159223 0.111238
0.660000 0.177863 9.134113E-02
0.680000 0.204721 7.466463E-02
0.700000 0.243906 6.281818E-02
0.720000 0.283091 5.097173E-02
0.740000 0.322277 3.912529E-02
0.760000 0.363157 2.966948E-02
0.780000 0.406578 2.379962E-02
0.800000 0.450000 1.792976E-02
0.820000 0.498000 1.434380E-02
0.840000 0.546000 1.075785E-02
0.860000 0.594000 7.171902E-03
0.880000 0.642000 3.585951E-03
0.900000 0.690000 0.00000
** Sl krg krog

SLT
SMOOTHEND QUAD

| | | |
|---|---|---|
| 0.100000 | 0.992530 | 0.00000 |
| 0.119778 | 0.915285 | 3.663058E-03 |
| 0.139556 | 0.870060 | 8.729871E-03 |
| 0.159333 | 0.825199 | 1.381264E-02 |
| 0.179111 | 0.780337 | 1.889540E-02 |
| 0.198889 | 0.735476 | 2.397817E-02 |
| 0.218667 | 0.690614 | 2.906093E-02 |
| 0.238444 | 0.645753 | 3.414370E-02 |
| 0.258222 | 0.606003 | 4.029210E-02 |
| 0.278000 | 0.573436 | 4.793814E-02 |
| 0.297778 | 0.540870 | 5.558419E-02 |
| 0.317556 | 0.508304 | 6.323024E-02 |
| 0.337333 | 0.475738 | 7.087629E-02 |
| 0.357111 | 0.443172 | 7.852234E-02 |
| 0.376889 | 0.410605 | 8.616838E-02 |
| 0.396667 | 0.378039 | 9.381443E-02 |
| 0.416444 | 0.345473 | 0.101460 |
| 0.436222 | 0.312907 | 0.109107 |
| 0.456000 | 0.280341 | 0.116753 |
| 0.475778 | 0.250639 | 0.126153 |
| 0.495556 | 0.233068 | 0.142984 |
| 0.515333 | 0.215497 | 0.159814 |
| 0.535111 | 0.197926 | 0.176645 |
| 0.554889 | 0.180356 | 0.193475 |
| 0.574667 | 0.162785 | 0.210306 |
| 0.594444 | 0.147881 | 0.233750 |
| 0.614222 | 0.133961 | 0.259635 |
| 0.634000 | 0.120041 | 0.285521 |
| 0.653778 | 0.106122 | 0.311407 |
| 0.673556 | 9.220205E-02 | 0.337292 |
| 0.693333 | 8.108117E-02 | 0.367952 |
| 0.713111 | 7.131302E-02 | 0.400920 |
| 0.732889 | 6.289835E-02 | 0.436293 |
| 0.752667 | 5.520710E-02 | 0.472952 |
| 0.772444 | 4.751585E-02 | 0.509611 |
| 0.792222 | 3.982459E-02 | 0.546270 |
| 0.812000 | 3.213334E-02 | 0.582929 |
| 0.831778 | 2.444209E-02 | 0.619588 |
| 0.851556 | 2.131368E-02 | 0.661788 |
| 0.871333 | 1.823711E-02 | 0.704052 |
| 0.891111 | 1.516055E-02 | 0.746315 |
| 0.910889 | 1.208399E-02 | 0.788578 |
| 0.930667 | 9.007426E-03 | 0.830841 |
| 0.950444 | 5.933333E-03 | 0.873506 |
| 0.970222 | 2.966667E-03 | 0.933664 |
| 0.990000 | 0.00000 | 0.993821 |

```
RPT 2

SWT
**$       Sw      krw     krow
0.0      0.0      1.0
1.0      1.0      0.0

SLT
**$       Sl      krg     krog
0.0      1.0    0.000
1.0      0.0    1.0
KRTYPE CON          1

** ============== INITIAL CONDITIONS
====================================
INITIAL
VERTICAL OFF

INITREGION 1
PRES CON        3000
TEMP CON          25
SW CON        0.24
SO CON        0.76
MFRAC_OIL 'LO' CON        0.53
MFRAC_OIL 'HO' CON        0.47
MFRAC_GAS 'N2' CON          0
MFRAC_GAS 'H2O' CON          0
MFRAC_GAS 'CO2' CON          0
MFRAC_GAS 'CO' CON          0
CONC_SLD 'COKE' CON          0
** ============== NUMERICAL CONTROL
====================================
NUMERICAL
AUTOTUNE ON
DTMIN 1e-16
MAXSTEPS 100000000
NORM PRESS 10000

CONVERGE TOTRES TIGHTER
MATBALTOL 1e-6
NEWTONCYC 30
NORTH 180
NCUTS 15
ITERMAX 280
SOLVER PARASOL
DPLANES 12
PNTHRDS 8
PPATTERN AUTOPSLAB 4
**MINPRES 100.0
```

```
**MAXTEMP 946.85
**MAXPRES 9800.0

RUN
TIME 0
DTWELL 0.1

WELL  'Producer'
PRODUCER 'Producer'
OPERATE  MIN  BHP  2800.0  CONT REPEAT
OPERATE  MAX  STO  15278.0  CONT REPEAT
**        rad  geofac  wfrac  skin
GEOMETRY  i  8.9  0.2488  1.0  0.0
    PERF     GEOA  'Producer'
** UBA            ff        Status  Connection
   44 10 5       1.0  OPEN    FLOW-TO  'SURFACE'  REFLAYER
   40 10 5       1.0  OPEN    FLOW-TO  1
   37 10 5       1.0  OPEN    FLOW-TO  2
   34 10 5       1.0  OPEN    FLOW-TO  3
   31 10 5       1.0  OPEN    FLOW-TO  4
   28 10 5       1.0  OPEN    FLOW-TO  5
   25 10 5       1.0  OPEN    FLOW-TO  6
   22 10 5       1.0  OPEN    FLOW-TO  7
   19 10 5       1.0  OPEN    FLOW-TO  8
   16 10 5       1.0  OPEN    FLOW-TO  9
   13 10 5       1.0  OPEN    FLOW-TO  10
   10 10 5       1.0  OPEN    FLOW-TO  11
   7 10 5        1.0  OPEN    FLOW-TO  12
LAYERXYZ  'Producer'
** perf geometric data: UBA, block entry(x,y,z) block exit(x,y,z), length
   44 10 5  21559.999995  4859.999435  1603.800000  21070.000005  4859.999435
1603.800000  490.000000
   40 10 5  19599.999995  4859.999435  1603.800000  19110.000005  4859.999435
1603.800000  490.000000
   37 10 5  18129.999995  4859.999435  1603.800000  17640.000005  4859.999435
1603.800000  490.000000
   34 10 5  16659.999995  4859.999435  1603.800000  16170.000005  4859.999435
1603.800000  490.000000
   31 10 5  15189.999995  4859.999435  1603.800000  14700.000005  4859.999435
1603.800000  490.000000
   28 10 5  13719.999995  4859.999435  1603.800000  13230.000005  4859.999435
1603.800000  490.000000
   25 10 5  12249.999995  4859.999435  1603.800000  11760.000005  4859.999435
1603.800000  490.000000
   22 10 5  10779.999995  4859.999435  1603.800000  10290.000005  4859.999435
1603.800000  490.000000
   19 10 5  9309.999995  4859.999435  1603.800000  8820.000005  4859.999435
1603.800000  490.000000
```

```
  16 10 5  7839.999995  4859.999435  1603.800000  7350.000005  4859.999435
1603.800000  490.000000
  13 10 5  6369.999995  4859.999435  1603.800000  5880.000005  4859.999435
1603.800000  490.000000
  10 10 5  4899.999995  4859.999435  1603.800000  4410.000005  4859.999435
1603.800000  490.000000
   7 10 5   3429.999995  4859.999435  1603.800000  2940.000005  4859.999435
1603.800000  490.000000
**
WELL  'Injector 1'
INJECTOR MOBWEIGHT IMPLICIT 'Injector 1'
INCOMP  GAS  0.0  0.0  0.0  0.0  0.0  0.79  0.0  0.21
TINJW  25.0
PINJW  3500.0
OPERATE  MAX  STG  20833333.0  CONT REPEAT
**        rad  geofac  wfrac  skin
GEOMETRY  K  8.9  0.2488  1.0  0.0
    PERF     GEOA  'Injector 1'
** UBA           ff        Status  Connection
  2 10 1       1.0  OPEN    FLOW-FROM  'SURFACE'
SHUTIN 'Injector 1'
**
**
WELL  'Injector 2'
INJECTOR MOBWEIGHT IMPLICIT 'Injector 2'
INCOMP  WATER  1.0  0.0  0.0
TINJW  250.0
QUAL  1.0
OPERATE  MAX  BHP  9500.0  CONT
**        rad  geofac  wfrac  skin
GEOMETRY  K  8.9  0.2488  1.0  0.0
    PERF     GEOA  'Injector 2'
** UBA           ff        Status  Connection
  2 10 1       1.0  OPEN    FLOW-FROM  'SURFACE'
HEATR IJK
2 10 1 1000000
2 9 1 1000000
2 11 1 1000000
2 10 2 1000000
2 9 2 1000000
2 11 2 1000000
2 10 3 1000000
2 9 3 1000000
2 11 3 1000000
OUTSRF GRID REMOVE
**
WSRF GRID TNEXT
TIME  43200.0
**
```

```
**
WELL  'Injector 1'
INJECTOR MOBWEIGHT IMPLICIT 'Injector 1'
INCOMP  GAS  0.0  0.0  0.0  0.0  0.0  0.79  0.0  0.21
TINJW  25.0
PINJW  3500.0
OPERATE  MAX  STG  20000000.0  CONT REPEAT
OPEN 'Injector 1'
**
WELL  'Injector 2'
INJECTOR MOBWEIGHT IMPLICIT 'Injector 2'
INCOMP  WATER  1.0  0.0  0.0
TINJW  250.0
QUAL  1.0
OPERATE  MAX  STG  180000.0  CONT REPEAT
SHUTIN 'Injector 2'
**
TIME 86400.0
**
HEATR IJK
2 10 1 0
2 9 1 0
2 11 1 0
2 10 2 0
2 9 2 0
2 11 2 0
2 10 3 0
2 9 3 0
2 11 3 0
**
TIME 151200.0
TIME 161280.0
TIME 171360.0
TIME 181440.0
TIME 191520.0

TIME 200000
WSRF GRID TNEXT
TIME 201600.0
TIME 211680.0
TIME 221760.0

TIME 230000
WSRF GRID TNEXT
OUTSRF GRID REMOVE
TIME 231840.0
TIME 241920.0
TIME 252000.0
```

```
TIME 259200.0
**
WELL  'Injector 1'
INJECTOR MOBWEIGHT IMPLICIT 'Injector 1'
INCOMP  GAS  0.0  0.0  0.0  0.0  0.0  0.79  0.0  0.21
TINJW  25.0
PINJW  3500.0
OPERATE  MAX  STG  10000000.0  CONT REPEAT
OPEN 'Injector 1'
TIME 262080.0
TIME 272160.0
TIME 282240.0
TIME 292320.0
TIME 300000
WSRF GRID TNEXT
OUTSRF GRID REMOVE
TIME 302400.0
TIME 312480.0
TIME 322560.0
TIME 324000.0
TIME 332640.0
TIME 342720.0
TIME 352800.0
TIME 362880.0
TIME 372960.0
TIME 383040.0
TIME 393120.0
TIME 400000
WSRF GRID TNEXT
OUTSRF GRID REMOVE
TIME 403200.0
TIME 413280.0
TIME 423360.0
TIME 433440.0
TIME 443520.0
TIME 453600.0
TIME 463680.0
TIME 473760.0
TIME 483840.0
TIME 493920.0
TIME 500000
WSRF GRID TNEXT
OUTSRF GRID REMOVE
TIME 504000.0
TIME 514080.0
TIME 524160.0
TIME 600000
WSRF GRID TNEXT
OUTSRF GRID REMOVE
```

TIME 700000
WSRF GRID TNEXT
OUTSRF GRID REMOVE
TIME 800000
WSRF GRID TNEXT
OUTSRF GRID REMOVE
TIME 900000
WSRF GRID TNEXT
OUTSRF GRID REMOVE
TIME 1000000
WSRF GRID TNEXT
OUTSRF GRID REMOVE
TIME 1037270
DTWELL 1000
WSRF GRID TNEXT
OUTSRF GRID REMOVE
TIME 1060000
DTWELL 1000
OUTSRF GRID REMOVE
TIME 1080000
DTWELL 1000
WSRF GRID TNEXT
OUTSRF GRID REMOVE
TIME 1100000
DTWELL 1000
OUTSRF GRID REMOVE
TIME 1101600.0
TIME 1130000
**STOP**
DTWELL 1000
OUTSRF GRID REMOVE
TIME 1132703
DTWELL 1000
WSRF GRID TNEXT
OUTSRF GRID REMOVE
TIME 1170000
OUTSRF GRID REMOVE
DTWELL 1000
WSRF GRID TNEXT
TIME 1576800.0
WSRF GRID TNEXT
TIME 1622880.0
WSRF GRID TNEXT
TIME 1664640.0
WSRF GRID TNEXT
TIME 1709280.0
WSRF GRID TNEXT
TIME 1752480.0
WSRF GRID TNEXT

TIME 1797120.0
WSRF GRID TNEXT
TIME 1840320.0
WSRF GRID TNEXT
TIME 1884960.0
WSRF GRID TNEXT
TIME 1929600.0
WSRF GRID TNEXT
TIME 1972800.0
WSRF GRID TNEXT
TIME 2017440.0
WSRF GRID TNEXT
TIME 2060640.0
WSRF GRID TNEXT
TIME 2105280.0
WSRF GRID TNEXT
TIME 2149920.0
WSRF GRID TNEXT
TIME 2190240.0
WSRF GRID TNEXT
TIME 2234880.0
WSRF GRID TNEXT
TIME 2278080.0
WSRF GRID TNEXT
TIME 2322720.0
WSRF GRID TNEXT
TIME 2365920.0
WSRF GRID TNEXT
TIME 2410560.0
WSRF GRID TNEXT
TIME 2455200.0
WSRF GRID TNEXT
TIME 2498400.0
WSRF GRID TNEXT
TIME 2543040.0
WSRF GRID TNEXT
TIME 2586240.0
WSRF GRID TNEXT
TIME 2630880.0
WSRF GRID TNEXT
TIME 2675520.0
WSRF GRID TNEXT
TIME 2715840.0
WSRF GRID TNEXT
TIME 2760480.0
WSRF GRID TNEXT
TIME 2803680.0
WSRF GRID TNEXT
TIME 2848320.0

STOP